



HAL
open science

Thermoplastic Vulcanizates Based on Hydrogenated Natural Rubber/Polypropylene Blends

Korn Taksapattanakul

► **To cite this version:**

Korn Taksapattanakul. Thermoplastic Vulcanizates Based on Hydrogenated Natural Rubber/Polypropylene Blends. Food and Nutrition. Le Mans Université; Prince of Songkla University, 2016. English. NNT: 2016LEMA1028 . tel-01954357

HAL Id: tel-01954357

<https://theses.hal.science/tel-01954357>

Submitted on 13 Dec 2018

HAL is a multi-disciplinary open access archive for the deposit and dissemination of scientific research documents, whether they are published or not. The documents may come from teaching and research institutions in France or abroad, or from public or private research centers.

L'archive ouverte pluridisciplinaire **HAL**, est destinée au dépôt et à la diffusion de documents scientifiques de niveau recherche, publiés ou non, émanant des établissements d'enseignement et de recherche français ou étrangers, des laboratoires publics ou privés.



IMMM
Institut des Molécules
et Matériaux du Mans



Thèse de Doctorat

Korn TAKSAPATTANAKUL

*Mémoire présenté en vue de l'obtention du
grade de Docteur de l'Université du Maine
sous le sceau de l'Université Bretagne Loire
en cotutelle avec Prince of Songkla University*

École doctorale : MATIERE, MOLECULES, MATERIAUX EN PAYS DE LOIRE

Discipline : PHYSIQUE

Spécialité : (7)

Unité de recherche : Institut des Molécules et Matériaux du Mans, IMMM –UMR-
CNRS 6283 and Rubber Technology and Polymer Science department, Chemistry
Division of Science department, Faculty of Science and Technology, Prince of
Songkla University, Pattani campus

Soutenu le 15 décembre 2016

Thèse N° : (10)

Thermoplastic vulcanizates based on hydrogenated natural rubber/polypropylene blends

JURY

Rapporteurs :	Mme SOPHIE BISTAC, PROFESSEUR, Université de Haute-Alsace M. TAWEECHAI AMORNSAKCHAI, PROFESSEUR, Université de Mahidol
Examineurs :	M. POLPHAT RUAMCHAROEN, PROFESSEUR, Université de Songkhla Rajabhat M. PHILIPPE DANIEL, PROFESSEUR, Université du Maine M. TULYAPONG TULYAPITAK, PROFESSEUR, Université de Prince of Songkla M. PRANEE PHINYOCHEEP, PROFESSEUR, Université de Mahidol Mme JAREERAT SAMRAN-RUAMCHAROEN, PROFESSEUR, Université de Prince of Songkla
Directeur de Thèse :	M. PHILIPPE DANIEL, PROFESSEUR, Université du Maine M. TULYAPONG TULYAPITAK, PROFESSEUR, Université de Prince of Songkla
Co-directeur de Thèse :	M. PRANEE PHINYOCHEEP, PROFESSEUR, Université de Mahidol M. POLPHAT RUAMCHAROEN, PROFESSEUR, Université de Songkhla Rajabhat



**Thermoplastic Vulcanizates based on Hydrogenated Natural Rubber/
Polypropylene Blends**

Korn Taksapattanakul

A Thesis Submitted in Partial Fulfillment of the Requirements for the Degree of

Doctor of Philosophy in Polymer Technology

Prince of Songkla University

Pattani, Thailand

and

Le Grade de Docteur de l'Université du Maine

(Physique)

Faculté des Sciences et Techniques

Université du Maine

Le Mans, France

2017

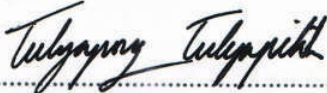
Copyright of Prince of Songkla University

Thesis Title Thermoplastic Vulcanizates based on Hydrogenated
Natural Rubber/Polypropylene Blends

Author Mr. Korn Taksapattanakul

Major Program Polymer Technology (PSU)
Physique (Université du Maine)

Major Advisor:


.....
(Asst. Prof. Dr. Tulyapong Tulyapitak)

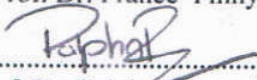
Examining Committee:

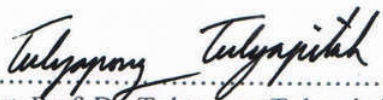

.....Chairperson
(Asst. Prof. Dr. Jareerat Ruamcharoen)

Co-advisor:


.....
(Prof. Dr. Philippe Daniel)

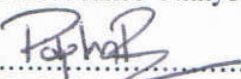

.....
(Assoc. Prof. Dr. Pranee Phinyocheep)

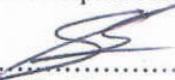

.....
(Asst. Prof. Dr. Polphat Ruamcharoen)


.....
(Asst. Prof. Dr. Tulyapong Tulyapitak)


.....
(Prof. Dr. Philippe Daniel)

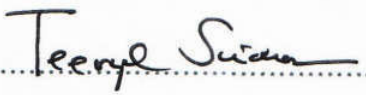

.....
(Assoc. Prof. Dr. Pranee Phinyocheep)


.....
(Asst. Prof. Dr. Polphat Ruamcharoen)


.....
(Prof. Dr. Sophie Bistac)


.....
(Assoc. Prof. Dr. Taweekchai Amornsakchai)

The Graduate School, Prince of Songkla University, Thailand and Faculté des Sciences et techniques, Université du Maine, Le Mans, France, have approved this thesis as partial fulfillment of the requirements for the Doctor of Philosophy (Polymer Technology) and Le Grade de Docteur de l'Université du Maine (Physique).


.....
(Assoc. Prof. Dr. Teerapol Srichana)
Dean of Graduate School

This is to certify that the work here submitted is the result of the candidate's own investigations. Due acknowledgement has been made of any assistance received.

Tulyapong Tulyapitak.....Signature

(Asst. Prof. Dr. Tulyapong Tulyapitak)

Major Advisor

Korn Taksapattanakul.....Signature

(Mr. Korn Taksapattanakul)

Candidate

I hereby certify that this work has not been accepted in substance for any degree, and is not being currently submitted in candidature for any degree.

Korn Taksapattanakul.....Signature

(Mr. Korn Taksapattanakul)

Candidate

Thesis Title Thermoplastic Vulcanizates Based on Hydrogenated Natural Rubber/Polypropylene Blends

Author Mr. Korn Taksapattanakul

Major Program Polymer Technology (PSU)
Physique (Université du Maine)

Academic Year 2016

ABSTRACT

The non-catalytic hydrogenation of natural rubber latex (NRL) was carried out by using diimide generated *in situ* from the reaction between hydrazine (N_2H_4) and hydrogen peroxide (H_2O_2). The effects of mole ratios of $[\text{C}=\text{C}]:[\text{N}_2\text{H}_4]:[\text{H}_2\text{O}_2]$, reaction conditions, solvent types, solvent volumes and reaction scale-up on the hydrogenation levels were investigated. Nuclear magnetic resonance (NMR), Fourier transform infrared (FTIR), and Raman spectroscopic techniques were employed to investigate the chemical structure of the hydrogenated natural rubber (HNRs) and to quantify the hydrogenation levels. It was found that variations in moles of N_2H_4 and H_2O_2 in the range of 1.0-2.0 moles resulted in degrees of hydrogenation in the range of 10-18%. Little improvement in hydrogenation levels of HNRs was obtained when NRL particles were swollen in solvents by which toluene yielded better results than hexane. The increase in toluene volume resulted in the increase in hydrogenation levels up to 42 %. TEM micrographs revealed that swelling mainly occurred at the surface of NRL particles, implying that hydrogenation reaction confined largely at the surface of NRL particles. After removal of toluene, particle size and particle size distribution of partially hydrogenated NRL remained unchanged. To further improve degrees of hydrogenation, the reaction volume was extended and 65% hydrogenation levels were obtained. Therefore, 14%HNR, 33%HNR, and 65%HNR were successfully prepared under suitable reaction conditions. However, crosslinking and *cis-trans* isomerization were side-reactions occurring during hydrogenation. Gel and *trans* contents increased with increasing hydrogenation levels, leading to the increase in hardness of HNRs. Mooney viscosities of HNRs increased with increasing degrees of hydrogenation due to the increased gel contents. Mooney torque relaxation of NR and HNRs were similar. Thermogravimetric analysis revealed that

HNRs had greater thermal stability than NR and thermal stability increased with increasing degrees of hydrogenation. HNR vulcanizates were much better resistant to ozone and UV than cured NR. Sulfur-vulcanized rubbers had greater ozone resistance than peroxide-cure rubbers due to less amounts of carbon-carbon double bonds present in rubbers. In addition, modulus at low strain and tensile strength of sulfur-cured rubbers were higher than those of peroxide-cured rubbers, but lower elongation due to higher crosslink densities. Also, modulus at low strain and tensile strength increased with increasing hydrogenation levels of HNRs, in contrast to strain at break. Thermoplastic vulcanizates (TPVs) from blends of HNR and Polypropylene (PP) were prepared via dynamic vulcanization using peroxide and sulfur as curing agents. The effects of blend ratios on mechanical properties of TPVs were investigated. Tensile strength increased with increasing PP portions, but breaking strain decreased. Morphology of TPVs was characterized with Raman mapping and scanning electron microscope (SEM). The phase sizes of crosslinked rubber obtained from both techniques were correlated well.

Key words: Non-catalytic hydrogenation, Hydrogenated natural rubber, Raman spectroscopy, Thermoplastic vulcanizates

ชื่อวิทยานิพนธ์	เทอร์โมพลาสติกวัลคาไนซ์จากยางธรรมชาติไฮโดรจินเนตเบลนค์กับพอลิโพรพิลีน
ผู้เขียน	นายกร ทักขพัฒน์กุล
สาขาวิชา	เทคโนโลยีพอลิเมอร์ (PSU) ฟิสิกส์ (Université du Maine)
ปีการศึกษา	2559

บทคัดย่อ

ปฏิกิริยาการเติมไฮโดรเจนแบบไม่ใช้ตัวเร่งของน้ำยางธรรมชาติ (NRL) ใช้ไดอิมิดซึ่งเกิดจากปฏิกิริยาระหว่างไฮดราซีน (N_2H_4) และไฮโดรเจนเปอร์ออกไซด์ (H_2O_2)

ไฮโดรจินเนตเตรียมผ่านปฏิกิริยาไฮโดรจินเนชันแบบไม่ใช้ตัวเร่ง ซึ่งอาศัยไดอิมิดที่เกิดจากปฏิกิริยาออกซิเดชันของไฮดราซีนด้วยไฮโดรเจนเปอร์ออกไซด์ ศึกษาผลของอัตราส่วนโดยโมลของ $[C=C]:[N_2H_4]:[H_2O_2]$ สภาวะการเตรียมปฏิกิริยา ประเภทตัวทำละลาย ปริมาตรของตัวทำละลายและการขยายขนาดการเตรียมปฏิกิริยา โครงสร้างทางเคมีของยางธรรมชาติไฮโดรจินเนตและการคำนวณเปอร์เซ็นต์ของการเกิดไฮโดรจินเนชัน ได้วิเคราะห์โดยใช้เทคนิคนิวเคลียร์แมกเนติกเรโซแนนซ์ อินฟราเรดสเปกโตรสโคปีและรามาน

จากการแปรอัตราส่วนโดยโมลของไฮดราซีนและไฮโดรเจนเปอร์ออกไซด์ในช่วง 1.0-2.0 โมล พบว่า เปอร์เซ็นต์การเกิดไฮโดรจินเนชันของน้ำยางธรรมชาติอยู่ในช่วงประมาณ 10-18% นอกจากนี้สามารถเพิ่มเปอร์เซ็นต์การเกิดไฮโดรจินเนชันของน้ำยางธรรมชาติด้วยวิธีการทำให้อุณหภูมิของน้ำยางธรรมชาติเกิดการบวมพองที่ผิวด้วยตัวทำละลาย พบว่า เปอร์เซ็นต์การเกิดไฮโดรจินเนชันของน้ำยางธรรมชาติด้วยตัวทำละลายโทลูอินเพิ่มขึ้นมากกว่าตัวทำละลายเฮกเซน จากการเพิ่มปริมาตรของตัวทำละลายโทลูอิน พบว่า เปอร์เซ็นต์การเกิดไฮโดรจินเนชันของน้ำยางธรรมชาติเพิ่มขึ้นถึง 42% และเปอร์เซ็นต์การเกิดไฮโดรจินเนชันของน้ำยางธรรมชาติเพิ่มขึ้นถึง 65 % โดยการขยายขนาดของการเตรียมปฏิกิริยา นอกจากนี้พบว่า ปฏิกิริยาไฮโดรจินเนชันทำให้เกิดปฏิกิริยาข้างเคียง เช่น การเกิดเจลและการเกิดไอโซเมอร์ไรเซชันแบบซิส-ทรานส์

จากการศึกษาสัณฐานวิทยาของอนุภาคน้ำยางธรรมชาติไฮโดรจินเนตด้วยกล้องจุลทรรศน์อิเล็กตรอนแบบส่องผ่าน พบว่า ปฏิกิริยาไฮโดรจินเนชันเกิดที่บริเวณผิวของอนุภาคน้ำยางธรรมชาติ และเมื่อระเหยตัวทำละลายโทลูอิน พบว่า ขนาดอนุภาคและการกระจายตัวของน้ำยางธรรมชาติไฮโดรจินเนตไม่มีการเปลี่ยนแปลง

จากการศึกษาสมบัติทางความร้อนพบว่า ยางธรรมชาติไฮโดรจินเนตมีความเสถียรต่อความร้อนสูงกว่ายางธรรมชาติ และความเสถียรต่อความร้อนเพิ่มขึ้นเมื่อเปอร์เซ็นต์ของการเกิดไฮโดรจินเนชันของยางธรรมชาติเพิ่มขึ้น ยางธรรมชาติไฮโดรจินเนตวัลคาไนซ์ มีความเสถียรต่อการสลายตัวด้วยไอโซนและยูวีดีกว่ายางธรรมชาติวัลคาไนซ์ นอกจากนี้พบว่า ระบบการวัลคาไนซ์ด้วยซัลเฟอร์ของยางธรรมชาติมีความเสถียรต่อการสลายตัวด้วยไอโซนและยูวีดีกว่าการวัลคาไนซ์ด้วยเปอร์ออกไซด์ เนื่องจากปริมาณของพันธะคู่ของยางธรรมชาติลดลง เพราะระบบการวัลคาไนซ์ด้วยซัลเฟอร์จะเกิดปฏิกิริยาที่พันธะคู่ของยางธรรมชาติ

จากการศึกษาสมบัติทางกายภาพของยางธรรมชาติไฮโดรจินเนต พบว่า ยางธรรมชาติไฮโดรจินเนตมีความแข็งที่เพิ่มขึ้น ซึ่งเป็นผลจากการเกิดเจลและไอโซเมอร์ไรเซชันแบบทรานส์ ค่าความหนืดมูนี้เพิ่มขึ้นเมื่อเปอร์เซ็นต์ของการเกิดไฮโดรจินเนชันของยางธรรมชาติเพิ่มขึ้น เนื่องจากการเกิดเจลที่เพิ่มขึ้น ในขณะที่การคลายความเค้นแบบมูนี้ของยางธรรมชาติและยางธรรมชาติไฮโดรจินเนตมีค่าที่ใกล้เคียงกัน ค่ามอดูลัสที่ค่าความเครียดต่ำและความต้านทานแรงดึงสูงสุดเพิ่มขึ้น เมื่อเปอร์เซ็นต์ของการเกิดไฮโดรจินเนชันของยางธรรมชาติเพิ่มขึ้น ในขณะที่ระยะยืด ณ จุดแตกหัก ลดลง

จากการเตรียมเทอร์โมพลาสติกวัลคาไนซ์จากยางธรรมชาติไฮโดรจินเนตเบลนด์กับพอลิโพรพิลีนผ่านกระบวนการที่เรียกว่า ไดนามิกวัลคาไนเซชัน ด้วยระบบการวัลคาไนซ์ทั้งซัลเฟอร์และเปอร์ออกไซด์ พบว่า ความต้านทานแรงดึงสูงสุดเพิ่มขึ้น เมื่อสัดส่วนของพอลิโพรพิลีนเพิ่มขึ้น ในขณะที่ระยะยืด ณ จุดแตกหัก ลดลง สันฐานวิทยาของเทอร์โมพลาสติกวัลคาไนซ์ วิเคราะห์โดยใช้เทคนิค แผนภาพรามาน และ กล้องอิเล็กตรอนชนิดส่องกราด พบว่า เทคนิคแผนภาพรามานสามารถคำนวณหาสัดส่วนของเฟสยางและเฟสพลาสติกและขนาดของเฟสยางและลักษณะการกระจายตัวของเฟสยางในเฟสพลาสติกของเทอร์โมพลาสติกวัลคาไนซ์

คำสำคัญ: ปฏิกริยาไฮโดรจินเนชันแบบไม่ใช้ตัวเร่ง ยางธรรมชาติไฮโดรจินเนต รามานสเปกโตรสโคปี
เทอร์โมพลาสติกวัลคาไนซ์

ACKNOWLEDGEMENTS

Completely of the doctoral thesis is not finish without the support and assistance from all people. I would like to thank them.

I would like to take my sincere gratitude to my doctoral thesis advisor, Asst. Prof. Dr. Tulyapong Tulyapitak, Assoc. Prof. Dr. Pranee Phinyocheep, Asst. Prof. Dr. Polphat Ruamcharoen, Asst. Prof. Dr. Jareerat Ruamcharoen and Prof. Dr. Philippe Daniel for teaching, suggestion, English editing and proof reading of manuscript and thesis.

I am grateful to all lecturers, technical staff and my friends of Rubber Technology and Polymer Science department, Chemistry Division of Science department, Faculty of Science and Technology, Prince of Songkla University, Pattani campus, Rubber and Polymer Technology program, Faculty of Science and Technology, Songkhla Rajabhat University, Department of Chemistry, Faculty of Science, Mahidol University, Thailand and Institut des Molécules et Matériaux du Mans, IMMM –UMR-CNRS 6283, Université du Maine, France. Especial thank to Prof. Dr. Lazhar Benyahia, Dr. Fabienne Lagarde and Dr. Mathieu Edely of Faculté des Sciences et techniques, Université du Maine, France for technical help and practical advices.

I would like to extend my sincerest thanks to thesis committee, Prof. Dr. Sophie Bistac and Assoc. Prof. Dr. Taweechai Amornsakchai for comments and reviewing this thesis.

Thanks to the financial support from human resource development in science project (Science Achievement Scholarship of Thailand, SAST) and the financial support from Prince of Songkla University graduate thesis grant for Ph.D. research.

I also thank my family for support everything during as a Ph.D student.

Korn Taksapattanakul

CONTENTS

	Page
ABSTRACT (ENGLISH)	v
ABSTRACT (THAI)	vii
ACKNOWLEDGEMENTS	ix
CONTENTS	x
LIST OF TABLES	xv
LIST OF FIGURES	xvii
LIST OF ABBREVIATIONS	xxiv
CHAPTER 1 INTRODUCTION	1
CHAPTER 2 LITERATURE REVIEW	4
2.1 Hydrogenation of natural rubber	4
2.2 Characterization of hydrogenated natural rubber	8
2.2.1 Nuclear magnetic resonance spectroscopy	8
2.2.1.1 ¹ H-NMR of NR and HNRs	11
2.2.1.2 ¹³ C-NMR of NR and HNRs	12
2.2.2 Infrared spectroscopy	12
2.2.2.1 Infrared spectrum	15
2.2.2.2 Raman spectroscopy	16
2.2.3 Infrared and Raman spectra of NR and HNRs	19
2.3 Vulcanization of hydrogenated natural rubber	19
2.3.1 Peroxide vulcanization	20
2.3.2 Sulfur vulcanization	20
2.4 Thermoplastic vulcanizates	24
2.5 Characterization of thermoplastic vulcanizates	26
2.5.1 Raman imaging	27
2.5.2 Imaging methods	29
2.5.2.1 Point mapping	30
2.5.2.2 Line scanning	30

CONTENTS (continued)

	Page
2.5.2.3 Global mapping	31
CHAPTER 3 MATERIALS AND METHODS	33
3.1 Materials and Equipments	33
3.1.1 Materials	33
3.1.2 Equipment and Apparatus	34
3.2 Preparation of hydrogenated natural rubbers	35
3.2.1 Non-catalytic hydrogenation of natural rubber latex	35
3.2.2 Characterization of NR and HNRs	37
3.2.2.1 Chemical structure	37
3.2.2.2 Hydrogenation levels	37
3.2.2.3 <i>cis</i> and <i>trans</i> Isomerization	38
3.2.2.4 Morphology of latex by transmission electron microscopy	38
3.2.2.5 Glass transition temperature (T_g) by differential scanning calorimetry	39
3.2.2.6 Particle size and particle size distribution	39
3.2.2.7 Hardness	39
3.2.2.8 Rheological properties	40
3.2.2.9 Gel content	40
3.2.2.10 Thermogravimetric analysis	40
3.3 Properties of NR and HNR compounds and vulcanizates	41
3.3.1 Preparation of HNR compounds	41
3.3.2 Cure properties and preparation of vulcanized rubber sheet	41
3.3.3 Characterization of NR and HNR vulcanizates	43
3.3.3.1 Ozone and Ultraviolet (UV) resistance test	43
3.3.3.2 Raman spectroscopy	43

CONTENTS (continued)

	Page
3.3.3.3 Tensile properties	44
3.3.3.4 Crosslink density	45
3.4 Thermoplastic vulcanizates (TPVs) based on blends of HNRs and PP	45
3.4.1 Preparation of TPVs	45
3.4.2 Characterization of TPVs	46
3.4.2.1 Mixing behavior and dynamic vulcanization	46
3.4.2.2 Raman mapping	46
3.4.2.3 Phase size analysis	47
3.4.2.4 Scanning electron microscopy	47
3.4.2.5 Dynamic mechanical analysis	47
CHAPTER 4 RESULTS AND DISCUSSION	49
4.1 Preparation and characterization of hydrogenated natural rubbers	49
4.1.1 Non-catalytic hydrogenation of natural rubber latex	49
4.1.1.1 Chemical structure characterization of HNRs by ¹ H-NMR	49
4.1.1.2 Effect of hydrazine	50
4.1.1.3 Effect of hydrogen peroxide	51
4.1.1.4 Effects of reaction temperature and time	52
4.1.2 Improvement of hydrogenation levels of NRL	54
4.1.2.1 Effect of solvent types	54
4.1.2.2 Effect of solvent volume	55
4.1.2.3 Effect of reaction scale-up	56
4.1.2.4 <i>cis-trans</i> isomerization	61
4.1.2.5 Particle size of NRL and HNRL	63
4.2 Properties of HNRs	64

CONTENTS (continued)

	Page
4.2.1 Appearance	64
4.2.2 Gel content	65
4.2.3 Hardness	66
4.2.4 Glass transition temperature (T_g)	67
4.2.5 Rheological properties of NR and HNRs	68
4.2.5.1 Apparent shear stress and viscosity	68
4.2.5.2 Mooney Viscosity and Mooney Stress Relaxation	70
4.2.6 Thermal properties	73
4.2.6.1 Decomposition properties	73
4.3 Vulcanization and physical properties of HNRs	76
4.3.1 Vulcanization properties of HNR compounds	76
4.3.2 Ozone and UV resistance	78
4.3.3 Crosslink densities of HNR vulcanizates	86
4.3.4 Tensile properties of HNR vulcanizates	87
4.4 Thermoplastic vulcanizates based on dynamically vulcanized HNR and PP blends	88
4.4.1 Mixing of TPVs	88
4.4.2 Morphological characterization of TPVs by Raman mapping	91
4.4.3 Phase size analysis by Raman mapping technique	95
4.4.4 Determination of blend ratio by Raman spectroscopy	97
4.4.5 Dynamic mechanical behavior of TPVs	99
4.4.6 Tensile properties of TPVs	101
4.4.7 Fractured surface of TPVs	102
CHAPTER 5 CONCLUSIONS	104

CONTENTS (continued)

	Page
REFERENCES	106
APPENDICES	114
CURRICULUM VITAE	145

LIST OF TABLES

Table	Page
2.1 Classification of accelerators and their vulcanization speed	20
2.2 Sulfur vulcanization systems	23
3.1 Experimental runs to study the effects of mole ratios of hydrogenation degrees of NRL at $50\pm 3^\circ\text{C}$ for 24 hrs	36
3.2 Formulations of rubber compounds	42
3.3 Cure time ($t_{c,90}$) for each rubber compounds	42
4.1 Effects of reaction scale-up on degrees of hydrogenation of NRL	57
4.2 Hydrogenation levels of HNRs calculated from $^1\text{H-NMR}$ and Raman spectra	61
4.3 Average particle size of NRL and HNRL	64
4.4 Power law index (n) and flow consistency (K)	69
4.5 Mooney viscosity and relaxation rate of NR and HNRs	71
4.6 Decomposition temperatures of NR, HNRs and EPDM 4725P	74
4.7 Cure properties of peroxide-vulcanized rubber compounds at various temperatures	78
4.8 Cure properties of sulfur-vulcanized rubber compounds at various temperatures	78
4.9 Characteristic peak frequency of unvulcanized and vulcanized HNRs	83
4.10 Integral intensity of C=C bond stretching, $I_{\text{C=C}}$, at 1664 cm^{-1} of NR and HNRs vulcanized by peroxide and sulfur	84
4.11 Difference integral intensity (ΔI_{P}) peak, $I_{\text{C=C}}$, at 1664 cm^{-1} of NR and HNRs vulcanized by peroxide and sulfur before and after ozone exposure	85
4.12 Difference integral intensity (ΔI_{P}) peak, $I_{\text{C=C}}$, at 1664 cm^{-1} of NR and HNRs vulcanized by peroxide and sulfur before and after UV exposure	86

LIST OF TABLES (continued)

Table	Page
4.13 The content of each component of TPVs based on NR/PP and 65 %HNR/PP blends	98

LIST OF FIGURES

Figure	Page
2.1 Chemical structure of <i>cis</i> -1,4-polyisoprene	4
2.2 The magnetic field generated by nuclei spins (a) random orientation of these dipoles in the absence of an applied field, (b) the dipole aligned with the applied magnetic field, (c) the average alignment at a small angle to the applied field caused by thermal motion, and (d) precession of magnetic moment around the magnetic field at Larmor frequency	9
2.3 Quantized energy of nuclei in the applied field	10
2.4 Energy levels for a molecule, (A) pure rotational Transitions, (B) rotational- vibrational transitions, and (C) rotational-vibrational-electronic transitions	13
2.5 Model of a harmonic oscillator (a) mass m bound to a spring with force constant k and (b) masses m_1 and m_2 connected by the spring with the same force constant	14
2.6 Jablonski diagram illustrating quantum energy for Rayleigh and Raman scattering	17
2.7 Polarization of the molecule induced by the electric field of the incident light	18
2.8 Mechanisms of NR vulcanization by dicumyl peroxide	21
2.9 Possible crosslink structures of peroxide-cured NR	22
2.10 Possible scission reaction in ethylene-propylene rubber	22
2.11 Reaction pathway for accelerated sulfur vulcanization	24
2.12 Torque-time characteristics of a dynamic vulcanization process in an internal mixer for peroxide-vulcanized PP/EPR (40/60) blend	26

LIST OF FIGURES (continued)

Figure	Page
2.13 Schematic of morphology transformation during the dynamic vulcanization of polymer blends	27
2.14 Schematic diagrams from bright field imaging to Raman mapping. The hypercube is a collection of Raman intensities as a function of $I(x, y, \nu)$. At a fixed position (x_i, y_i) , it is a localized Raman spectrum. At a fixed wave number ν_k , it is a Raman intensity map	28
2.15 Schematic diagrams describing (a) point mapping, (b) line scanning, and (c) global mapping. The top row illustrates the illumination pattern on the sample and the bottom row shows the image onto the Detector	29
4.1 ¹ H-NMR spectra of (a) 0 % HNR, (b) 11 %HNR and (d) 18 %HNR	49
4.2 Effect of moles of hydrazine on degrees of hydrogenation of NRL (mole ratio of [C=C]:[H ₂ O ₂] is 1:1)	51
4.3 Effect of moles of hydrogen peroxide on degrees of hydrogenation of NRL (mole ratio of [C=C]:[N ₂ H ₄] = 1:1)	52
4.4 Effect of reaction temperature and reaction time on degrees of hydrogenation of NRL (mole ratio of [C=C]:[N ₂ H ₄]:[H ₂ O ₂] is 1:1.5:1 and volume ratio of toluene to NRL is 0.1)	53
4.5 ¹ H-NMR spectra of (a) NR, (b) 14 %HNR prepared by swelling NRL with hexane, and (c) 16 %HNR prepared by swelling NRL with toluene (volume ration of solvent to NRL is 0.1)	54
4.6 ¹ H-NMR spectra of NR and HNRs at various toluene/NRL volume ratios; (a) NR, (b) 18 %HNR (no toluene), (c) 21%HNR (volume ratio = 0.1), (d) 29 %HNR (volume ratio = 0.4), (e) 33 %HNR (volume ratio = 0.7), and (f) 42 %HNR (volume ratio = 0.1)	55

LIST OF FIGURES (continued)

Figure	Page
4.7 Effects of toluene /NRL volume ratios on degrees of hydrogenation of NRL	56
4.8 TEM images at 40k magnification of (a) unswollen NRL particle, (b) NRL particle swollen by 10% volume of toluene, and (c) NRL particle swollen by 100% volume of toluene	57
4.9 Effects of increased reaction volume on collision of reacting particles due to high pressure build-up	58
4.10 ¹ H-NMR spectra of (a) NR, (b) 14 %HNR, (c) 33 %HNR and (d) 65 %HNR	59
4.11 Raman spectra of (a) NR, (b) 14 %HNR, (c) 33 %HNR, and (d) 65%HNR	59
4.12 FT-IR spectra of (a) NR, (b) 14 %HNR, (c) 33 %HNR, and (d) 65 %HNR	60
4.13 Correlation between degrees of hydrogenation calculated from Raman and ¹ H NMR spectra	61
4.14 ¹ H-NMR spectra of (a) NR, (b) 14%HNR, (c) 33%HNR, and 65 %HNR	62
4.15 <i>cis</i> and <i>trans</i> contents as a function of hydrogenation levels of HNRs	63
4.16 The mechanism of <i>cis-trans</i> isomerization	63
4.17 Particle size distributions of various latices; NRL, 14%HNRL, 33%HNRL, and 65%HNRL	64
4.18 Appearance of (a) NR, (b) 14%HNR, (c) 33%HNR and (d) 65%HNR	65
4.19 Gel contents as a function of hydrogenation levels of HNRs	66
4.20 Crosslinking reaction initiated by hydroxyl radical ([•] OH)	66
4.21 Effect of degree of hydrogenation on hardness of HNRs	67
4.22 DSC thermograms of NR, 14%HNR, 33%HNR, and 65 %HNR	68

LIST OF FIGURES (continued)

Figure	Page
4.23 Apparent shear stresses and viscosities of NR and HNRs as a function of shear rate	69
4.24 Schematic of structural orientation of polymers under shear field	70
4.25 Time-dependent Mooney viscosities of NR, 14%HNR, 33%HNR and 65 %HNR	71
4.26 Mooney stress relaxation of NR, 14% HNR, 33% HNR and 65% HNR	72
4.27 TGA curves of NR, 14 %HNR, 33 %HNR, 65 %HNR and EPDM (heating rate of 20°C/min under oxygen atmosphere)	73
4.28 Derivatives of TGA curves of NR, 14 %HNR, 33 %HNR, 65 %HNR and EPDM (heating rate of 20°C/min under oxygen atmosphere)	74
4.29 Raman spectra of (a) NR, (b) 65 %HNR and (c) EPDM 4725P	75
4.30 FT-IR spectra of (a) NR, (b) 65 %HNR and (c) EPDM 4725P	75
4.31 ODR curves of NR and HNR compounds vulcanized by dicumyl peroxide (left column) and sulfur (right column) at 150°C (a, b), 180°C (c, d), and 200°C (e, f)	77
4.32 Optical photographs of cracks on surfaces of rubbers vulcanized by peroxide after ozone exposure; (a) NR, (b) 14%HNR, (c) 33%HNR, and (d) 65%HNR	79
4.33 Optical photographs of cracks on surfaces of rubber vulcanized by sulfur after ozone exposure; (a) NR, (b) 14%HNR, (c) 33%HNR, and (d) 65%HNR	80
4.34 Optical photographs of cracks on surfaces of rubber vulcanized by peroxide after UV exposure; (a) NR, (b) 14%HNR, (c) 33%HNR, and (d) 65%HNR	81
4.35 Optical photographs of cracks on surfaces of rubber vulcanized by sulfur after UV exposure; (a) NR, (b) 14 %HNR, (c) 33 %HNR, and (d) 65 %HNR	82

LIST OF FIGURES (continued)

Figure	Page
4.36 Mechanisms of ozone degradation in diene rubbers	82
4.37 Raman spectra of 65 %HNR; (U) unvulcanized, (P) peroxide-vulcanized, and (S) sulfur-vulcanized	83
4.38 Raman spectra of peroxide-cured 65%HNR before (black line) and after (red line) ozone exposure	85
4.39 Crosslink densities versus degree of hydrogenation by peroxide and sulfur cure	86
4.40 True stress - true strain curves of NR and HNRs vulcanized by peroxide	87
4.41 True stress - true strain curves of NR and HNRs vulcanized by sulfur	88
4.42 Mixing torque-time profiles of TPVs prepared from blends of NR/PP and 65 %HNR/PP at blend ratios 70/30 and 50/50 vulcanized with peroxide (left column) and sulfur (right column)	89
4.43 Mixing torque-time profiles of TPVs prepared from blends of 65 %HNR/PP at blend ratio 70/30 and 50/50 vulcanized with peroxide	90
4.44 Morphology of simple blends; (a) NR/PP and (b) 65%HNR/PP at blend ratio of 50/50 (wt/wt%); Raman optical micrograph (left): rubber phase (white), PP phase (dark); Raman spectra (middle); and Raman mapping (right): PP phase (blue) and rubber phase (red)	92
4.45 Morphology of TPVs prepared from dynamically vulcanized blends of (a) NR/PP and (b) 65%HNR/PP at 50/50 blend ratio vulcanized by peroxide; Raman optical micrograph (left), rubber phase (white) and PP phase (dark); Raman spectra (middle); and Raman mapping (right), PP phase (blue) and rubber phase (red)	93

LIST OF FIGURES (continued)

Figure	Page
4.46 Morphology of TPVs prepared from dynamically vulcanized blends of (a) NR/PP and (b) 65%HNR/PP at 50/50 blend ratio vulcanized by sulfur; Raman optical micrograph (left), rubber phase (white) and PP phase (dark); Raman spectra (middle); and Raman mapping (right), PP phase (blue) and rubber phase (red)	94
4.47 Raman maps of TPVs based on 50/50 of 65 %HNR/PP dynamically vulcanized blends cured by peroxide, revealing crosslinked rubber particles (red) dispersed in matrix PP (blue)	95
4.48 SEM micrograph of TPVs based on 50/50 of 65 %HNR/PP dynamically vulcanized blends cured by peroxide, revealing crosslinked rubber particles (dark hole) dispersed in PP matrix (magnification 4,500x)	96
4.49 Correlation between of particle sizes of crosslinked rubber phase of TPVs measured by Raman mapping and SEM methods (50/50 of 65%HNR/PP blend)	96
4.50 Raman spectra of TPVs based on 65 %HNR/PP blends cured by peroxide at blend ratios of (a) 70/30, (b) 60/40, (c) 50/50, (d) 40/60	97
4.51 Raman maps of TPVs based on 65 %HNR/PP blends cured by peroxide with blend ratio (a) 70/30 and (b) 40/60 (PP phase (blue) and rubber phase (red))	98
4.52 Strain-dependent storage modulus of 65 %HNR vulcanizates and TPVs based on 65%HNR/PP blends vulcanized by peroxide at 70/30 and 50/50 blend ratios	100
4.53 Strain-dependent storage modulus of 65 %HNR vulcanizates and TPVs based on 65 %HNR/PP blends vulcanized by sulfur at 70/30 and 50/50 blend ratios	100

LIST OF FIGURES (continued)

Figure		Page
4.54	True stress-true strain curves of HNR vulcanizate and peroxide-cured TPVs based on 65%HNR/PP blends at various blend ratios	101
4.55	Tensile properties of peroxide-cured TPVs based on 65 %HNR/PP blends as a function of rubber contents	102
4.56	The fractured surfaces of peroxide-cured TPVs based on 65%HNR/PP blends at blend ratio of (a) 70/30 and (b) 50/50	103

LIST OF ABBREVIATIONS

NR	Natural rubber
NRL	Natural rubber latex
HNRs	Hydrogenated natural rubbers
EPR	Ethylene propylene rubber
EPDM	Ethylene propylene diene monomer rubber
TMS	Tetramethylsilane
TPVs	Thermoplastic vulcanizates
NMR	Nuclear magnetic resonance
PP	Polypropylene
UV	Ultraviolet
¹ H-NMR	Proton nuclear magnetic resonance
¹³ C-NMR	Carbon nuclear magnetic resonance
DSC	Differential scanning calorimetry
PSD	Particle size and particle size distributions
PIDS	Polarization intensity differential scattering
TGA	Thermogravimetric analysis
DCP	Dicumyl peroxide
TMTD	Tetramethylthiuram disulfide
MBT	2-Mercaptobenzothiazole
TAC	Triallyl cyanurate
CV	Conventional vulcanization
EV	Efficient vulcanization
SEV	Semi-efficient vulcanization
IR	Infrared
SEM	Scanning electron microscope
AFM	Atomic force microscopy
TEM	Transmission electron microscopy

LIST OF ABBREVIATIONS (continued)

DMA	Dynamic mechanical analysis
DRC	Dry rubber content
KAS	Kissinger-Akahira-Sunose
1D	One-dimensional
TS	Tensile strength
I	Nuclear spin number
H_o	Magnetic field
γ	Magnetogyric ratio
μ	Magnetic moment
$Ih/2\pi$	Angular momentum
ΔE	Energy level
h	Planck's constant
μ_o	Thermal equilibrium magnetization
N_1	Number of spins per unit volume
k	Boltzmann's constant
T	Absolute temperature
χ_o	Static magnetic susceptibility
λ	Wave length
ν	Frequency
$\bar{\nu}$	Wave number
c	Speed of light
n	Refractive index
E_p	Photons of the energy
E_{rot}	Rotational energy
E_{vib}	Vibrational energy
E_{el}	Electronic energy
m	Mass

LIST OF ABBREVIATIONS (continued)

k	Spring force constant
F	Force
x	Distance
ν	Vibrational frequency
ϕ	Phase angle
A	Absorbance
I_0	Intensity in the background spectrum
I	Intensity in the sample spectrum
ε	Absorptivity
b	Path length
c	Concentration
$\%T$	Percent transmission
P	Polarization
α	Polarizability
E	Electric field
t	Time
ν_j	A characteristic frequency for the j^{th} normal mode
α_0	Inherent polarizability
$\eta_{\text{EPR}} / \eta_{\text{PP}}$	Viscosity ratio
X	Hydrogenation levels
T_g	Glass transition temperature
W	Weight
T_i	Initial decomposition temperature
k_0	A constant
E_a	Activation energy
R	Gas constant
$g(\alpha)$	Kinetic model

LIST OF ABBREVIATIONS (continued)

α	Fraction of reactant remaining
β	Heating rate
T_z	Decomposition temperature
M_L	Minimum torque
M_H	Maximum torque
t_{s1}	Scorch time
$T_{c,90}$	Cure time
A	A true cross-sectional area
A_o	An original cross-sectional area
l_o	An original length
l	A deformed length
ε_t	True strain
σ_{ib}	Tensile strength
F_b	Force at break.
ε_b	Elongation at break or ultimate strain
l_b	Specimen length at fracture
ϕ_r	Volume fraction of the rubber
ρ_s	Density of toluene
ρ_r	Density of rubber
ν	Crosslink density
\bar{V}_s	Molar volume of toluene
χ_1	Polymer-solvent interaction parameter

CHAPTER 1

INTRODUCTION

1.1 Background and rational

Natural rubber (NR) is an important material widely used in rubber industry because of its excellent mechanical properties. Chemical structure of NR consists of *cis*-1,4-polyisoprene. However, unsaturation of the backbone makes NR susceptible to degradation when exposed to oxygen, ozone, and sunlight. In addition, heat resistance of NR is also poor. Attempts have been made to improve these drawbacks. One is to chemically modify chemical structure of NR by turning unsaturated units into saturated ones which can be achieved via epoxidation, maleinization, halogenations, hydrogenation, and so on. Hydrogenation of NR involved addition of hydrogen molecules to double bonds of isoprene units in the backbone chains. The products obtained can be either partially or fully hydrogenated natural rubbers (HNRs) whose thermal and degradation properties will be improved. HNRs are expected as potential replacements for ethylene propylene (EPR) and ethylene propylene diene monomer (EPDM) rubbers.

Hydrogenation of NR can be carried out by both catalytic and non-catalytic processes. In catalytic processes, homogeneous and heterogeneous catalysts can be used. The dominant homogeneous catalysts are complexes of group VIII transition metals in the second row of the periodic table, such as rhodium, ruthenium, and palladium. Heterogeneous catalysts rely on insoluble transition metal catalysts such as Pd/Al₂O₃, Pd/CaCO₃, and Pd/BaSO₄. Generally, homogeneous hydrogenation results in low conversion and scission of polymer backbone. In addition, the catalysts are difficult to be removed from the system. Heterogeneous catalysts yield high conversions, do not cause chain scission, and can be easily removed. However, catalytic hydrogenation processes are normally carried out at high temperatures and pressures, which are difficult to handle, and some systems are poisonous.

Non-catalytic processes employ hydrogenation reagents generated from various types of reactions, such as decarboxylation of potassium azodicarboxylate, photochemical irradiation of 1-thia-3,4-diazolidine-2,5-dione,

thermolysis of arylsulfonylhydrazide, the thermal decomposition of *p*-toluenesulfonyl hydrazide (*p*-TSH) and the oxidation of hydrazine by hydrogen peroxide.

Complete hydrogenation of NR would provide an alternating EPR with better thermal, oxidative, and chemical resistance than the original NR. However, it is not easily to achieve. The unsaturated isoprene units can be only partially hydrogenated. The advantage of the partially HNRs is that they possess the elastic character of unsaturated part and the plastic behaviors of saturated part.

Thermoplastic vulcanizates (TPVs) have become potential materials in rubber industry. TPVs can be prepared via dynamic vulcanization, in which an elastomer is vulcanized under dynamic shear to generate finely dispersed cross-linked rubber particles distributed in the continuous thermoplastic matrix. Important commercial TPVs are based on blends of EPDM and polypropylene (PP), for example, Santoprene, which are used as substitutes for thermoset EPDM in windshield rubber seal applications. Due to its high melting point and high crystallinity, PP provides TPVs good mechanical properties even at elevated temperatures. EPDM is used because it is stable against ozone and high temperatures, thus giving the corresponding TPVs good heat and ozone resistance. However, there has not been yet reported on TPVs based on HNR/PP blends. It is expected that HNR/PP blends when dynamically cured would give TPVs with good mechanical properties and ozone and heat resistance as well as those based on EPDM/PP blends.

In this research, hydrogenation of NR is carried out by using a non-catalytic process employing oxidation of hydrazine by hydrogen peroxide. Nuclear magnetic resonance (NMR) and Raman spectroscopic techniques are employed to investigate the chemical structure of the HNRs and to quantify the degree of hydrogenation. The thermoplastic vulcanizates (TPVs) will be prepared from blends of HNR and PP via dynamic vulcanization using peroxide and sulfur as curing agents. Thermal, mechanical and morphological properties of TPVs will be investigated.

1.2 Objectives

- 1.2.1 To prepare HNRs with various degrees of hydrogenation using diimide generated *in situ* from the reaction of hydrazine and hydrogen peroxide.
- 1.2.2 To prepare TPVs based on blends of HNR and PP.

1.3 Expected advantages

- 1.3.1 Realization of the techniques for preparation of HNR by using hydrazine and hydrogen peroxide and for preparation of TPVs based on blends of HNR and PP.
- 1.3.2 To obtain HNRs and TPVs with better thermal and mechanical properties for a wide range of applications.

CHAPTER 2

LITERATURE REVIEW

Natural rubber (NR) is produced from the latex of the *Heavea brasiliensis* tree. The chemical structure of NR is *cis*-1,4-polyisoprene (Fig. 2.1). It is widely used in rubber industries, for example, tire, rubber parts in automotive industries, and etc., due to its good mechanical and dynamic properties. However, the presence of carbon–carbon double bonds in the backbone makes NR prone to degrade by thermal-oxidation, ozone, and ultraviolet (UV) radiation. In addition, hydrocarbon nature of NR results in its low resistance to many types of organic solvents, fuel, and gasoline. These drawbacks lead to limit use of NR in many applications. Improvement of these disadvantages can be achieved by a number of ways, i.e., careful selection of cure systems, use of suitable antidegradants in compound formulations, blending with other polymers with good degradation properties, and structural modification by chemical means.

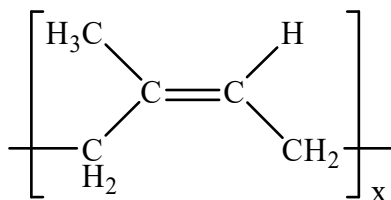


Figure 2.1 Chemical structure of *cis*-1,4-polyisoprene (Nagdi, 1993)

2.1 Hydrogenation of natural rubber

Chemical modification of NR continues to be an active research field for the improvement of properties of the rubber. This is because double bonds in rubber chains are very active and susceptible to various chemical reactions, such as epoxidation, halogenation, maleinization and hydrogenation. Hydrogenation is an important method for improving and modifying properties of unsaturated polymers to provide greater stability against thermal, oxidative, (Phinyocheep *et al.*, 2002; Samran *et al.*, 2004a; Hinchiranan *et al.*, 2006a; Hinchiranan *et al.*, 2009) and radiation-

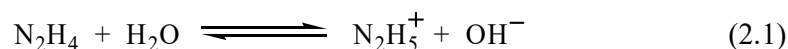
induced degradation (Mahittikul *et al.*, 2007a; Mahittikul *et al.*, 2007b). Hydrogenation of NR involves the addition of hydrogen molecules into unsaturated isoprene units to give saturated moieties (Hudlicky, 1984; Rylander, 1985).

Hydrogenation of diene-based polymers can be brought about by catalytic and non-catalytic processes. For catalytic processes, homogeneous and heterogeneous catalysts can be employed. Homogeneous catalysts are based on rhodium, ruthenium, and palladium complexes (Hinchiranan *et al.*, 2006a; Hinchiranan *et al.*, 2006b), while heterogeneous ones are dominated by insoluble transition metal catalysts such as kieselguhr-supported nickel (Rachapudy *et al.*, 1979; Singha *et al.*, 1997), and calcium carbonate-supported palladium (Rachapudy *et al.*, 1979). Since the reaction rates of the heterogeneous reaction are usually slower than those of homogeneous hydrogenation (Neon *et al.*, 1996), therefore, homogeneous catalysts are more favorable than heterogeneous catalysts (Hinchiranan *et al.*, 2006a; Hinchiranan *et al.*, 2006b). However, catalytic processes need careful operation due to requirement of high pressure of hydrogen, difficulty in catalyst removal, and toxicity of some catalyst systems (Singha *et al.*, 1997).

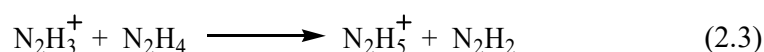
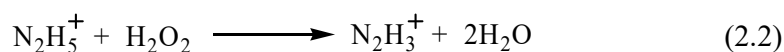
Non-catalytic processes utilize organic molecules which can generate hydrogenation agents such as diimide (N_2H_2). Diimide can provide a hydrogen molecule to the carbon-carbon double bonds without using a catalyst. Diimide hydrogenation can be easily performed at atmospheric pressure with simpler devices and processes, therefore, it is more convenient than catalytic hydrogenation (Samran *et al.*, 2004a; Samran *et al.*, 2004b). Diimide can be produced by various methods, such as the oxidation of hydrazine, the thermal decomposition of arenesulfonylhydrazides, the thermal decomposition of *p*-toluenesulfonylhydrazide (*p*-TSH), and the photochemical irradiation of 1-thia-3,4-diazolidine-2,5-dione (Harwood *et al.*, 1973; De Sarkar *et al.*, 2000; Samran *et al.*, 2004b; Lin, 2005; Arayaprane and Rempel, 2009; Simma *et al.*, 2009; Mahittikul *et al.*, 2007a).

However, hydrogenation of unsaturated elastomers using diimide generated *in situ* from the thermal decomposition of *p*-toluenesulfonyl hydrazide (*p*-TSH) resulted in side reactions. Catalytic oxidation of hydrazine by hydrogen peroxide had also some drawbacks, i.e., difficulty in catalyst removal, catalyst toxicity, and undesired reactions (Xie *et al.*, 2003; Lin, 2005). Thus, the non-catalytic

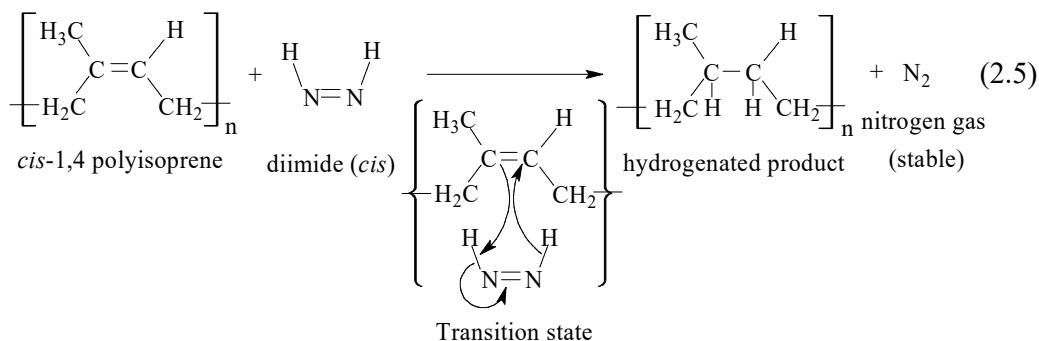
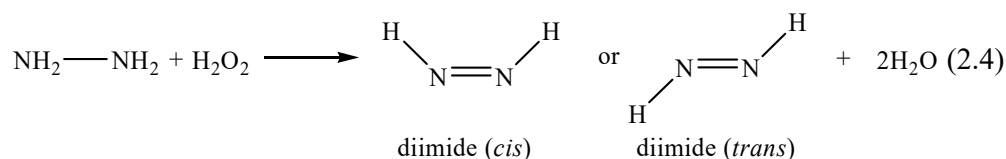
process utilizing diimide *in situ* generated from reaction between hydrazine (N_2H_4) and hydrogen peroxide (H_2O_2) is more interesting approach because it can be easily carried out under mild condition with less limitation. The reactions between N_2O_4 and H_2O_2 to form diimide are redox reactions. The reaction between hydrazine and water is represented by the following equilibrium and is postulated to form a protonated intermediate, hydrazonium ion ($N_2H_5^+$), (De Sarkar *et al.*, 1997).



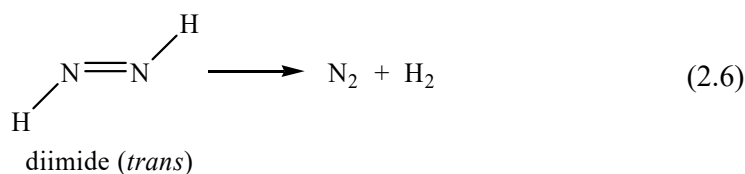
Hydrazonium ion ($N_2H_5^+$) is further oxidized by H_2O_2 to form diimide as follows

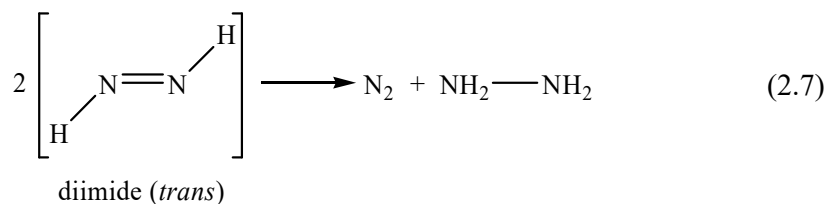


Diimide may exist as *cis-trans* isomers (eq. (2.4)); only the *cis* isomer serves as a reducing agent for NR (eq. (2.5)) (Hudlicky, 1984).



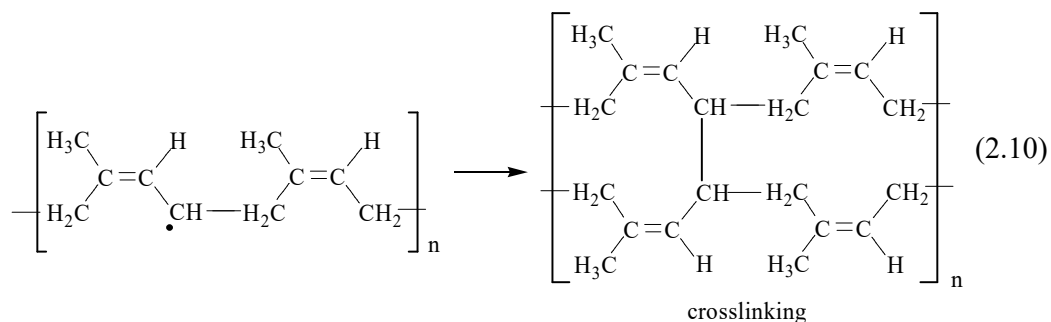
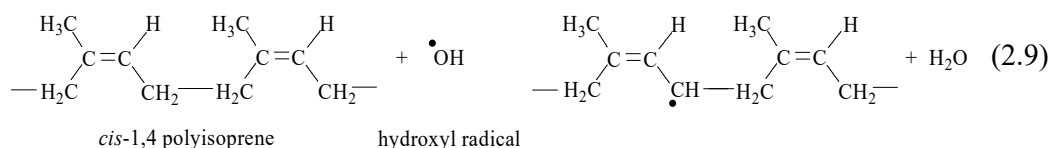
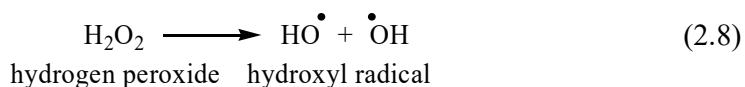
The *trans* isomer will lead to decomposition reactions of diimide as shown in eq. (2.6) and (2.7), respectively.





The *trans* isomer is slightly more stable than the *cis* isomer (Handt *et al.*, 2006). Although these species are stable at very low temperature (-196°C), they can undergo disproportionation to hydrazine and nitrogen at higher temperature (-180°C) (Pasto and Taylor, 1991).

It was found that redox reactions between N_2H_4 and H_2O_2 and decomposition of H_2O_2 also produced radicals. This suggested that excessive amounts of H_2O_2 would lead to an increase in the dissociation of H_2O_2 to form active hydroxyl radicals ($\cdot\text{OH}$) (Jones, 1999; Yves and Fontanille, 2008) as shown in eq. (2.8). Therefore, crosslinking reaction can be occurred through the formation of rubber radical (eq. 2.9) and then rubber radicals react to form the gel formation (eq. 2.10) (Xie *et al.*, 2003).



2.2 Characterization of hydrogenated natural rubber

NR and HNRs can be characterized by various methods such as proton nuclear magnetic resonance ($^1\text{H-NMR}$) (Phinyocheep *et al.*, 2002; Samran *et al.*, 2004c; Mahittikul *et al.*, 2007b), infrared (Samran *et al.*, 2004c; Hinchiranan *et al.*, 2006b; Mahittikul *et al.*, 2007b) and Raman spectroscopy (Jackson *et al.*, 1990; Hendra *et al.*, 1994; Xue, 1997; Samran *et al.*, 2004a). These techniques give the details of chemical structures of NR and HNRs.

2.2.1 Nuclear magnetic resonance (NMR) Spectroscopy

NMR techniques can be employed to molecules containing atomic nuclei possessing spins as described by the nuclear spin number (I). The nuclear spin can generate a small magnetic field. These dipoles assume random orientation in the absence of an applied magnetic field (Figure 2.2 (a)). In NMR, a constant external magnetic field (H_o) is applied to the nuclei causing them to align in the direction of the applied field (Figure 2.2 (b)). However, due to angular momentum and thermal motion of the nuclei, the magnetic moments will not completely align with the direction of the field (Figure 2.2 (c)). The torque from the applied field forces the magnetic moment to precess around the direction of the field at a characteristic angular frequency known as *Larmor frequency*, ω_o , which is proportional to H_o and given by

$$\omega_o \text{ (rad/s)} = \gamma H_o \quad (2.11)$$

or

$$\nu_o \text{ (MHz)} = \left(\frac{\gamma}{2\pi} \right) H_o \quad (2.12)$$

where γ is the magnetogyric ratio or the ratio of magnetic moment (μ) and angular momentum ($Ih/2\pi$).

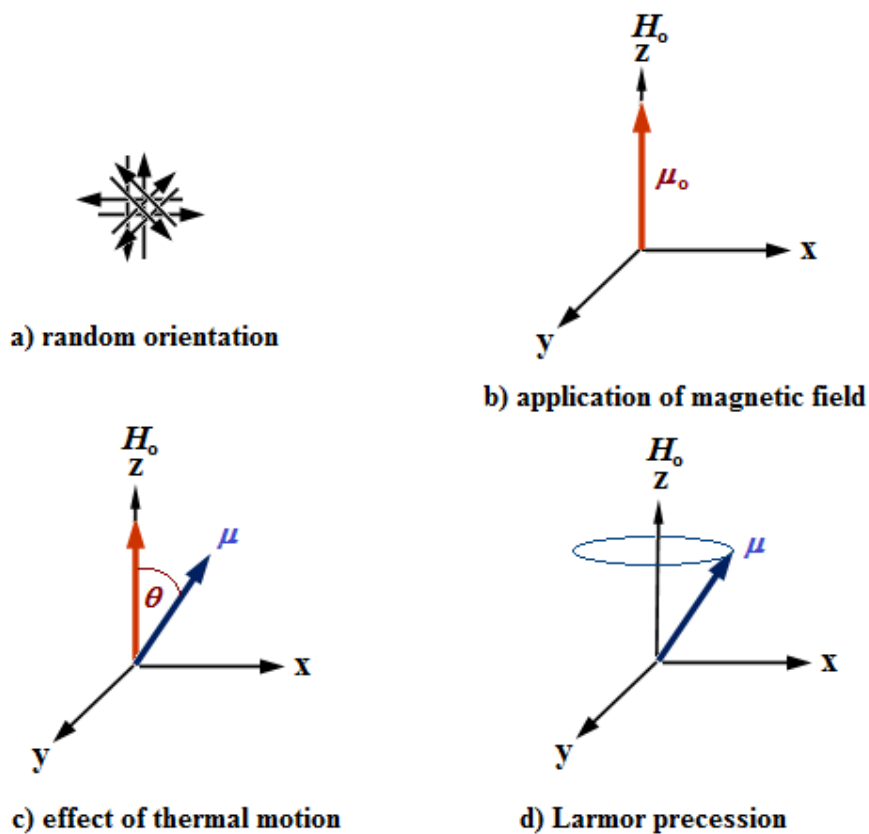


Figure 2.2 The magnetic field generated by nuclei spins (a) random orientation of these dipoles in the absence of an applied field, (b) the dipole aligned with the applied magnetic field, (c) the average alignment at a small angle to the applied field caused by thermal motion, and (d) precession of magnetic moment around the magnetic field at Larmor frequency (Koenig, 1999)

The nuclei with a spin number of 1/2 assume two energy states; aligned with the field (lower energy) and aligned against the field (higher energy) as shown in Figure 2.3.

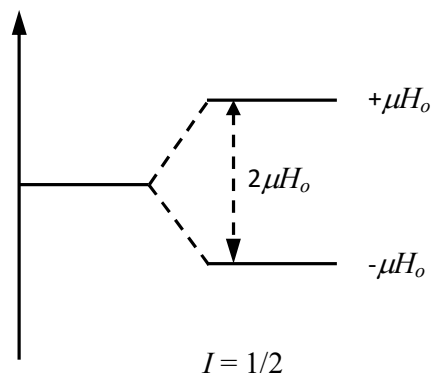


Figure 2.3 Quantized energy of nuclei in the applied field

The energy level (ΔE) is given by

$$\Delta E = \gamma \left(\frac{h}{2\pi} \right) H_o = \gamma \hbar H_o \quad (2.13)$$

where h is Planck's constant. At equilibrium, the spins are distributed between these two quantum energy levels according to Boltzmann distribution. Due to thermal motion and interactions between the molecules the magnetic moments of the protons are randomly oriented. The average magnetization is, however, preferentially aligned along the magnetic field. This average magnetic moment is called the thermal equilibrium magnetization, μ_o , which is given by

$$\mu_o = \left(\frac{N_1}{3kT} \right) \gamma^2 \hbar^2 I(I+1) H_o = \chi_o H_o \quad (2.14)$$

where N_1 is the number of spins per unit volume, k is Boltzmann's constant, T is the absolute temperature, χ_o is the static magnetic susceptibility, and H_o is the applied magnetic field. The average magnetization is approximately 1.4 ppm meaning that there are 1.4 excess aligned protons per million protons. The intensity of NMR signal is proportional to μ_o and directly related to H_o . The vector sum along H_o of the individual spin moments is called the macroscopic nuclear magnetization, μ (Figure

2.2 (d)). The small difference in size of the two opposing populations results in a net magnetization vector, μ , in the direction of H_o . For the proton with spins of 1/2, this equilibrium magnetization increases with field strength H_o and inversely proportional to T . As the spins are randomly oriented along the direction of H_o , the z-axis, which is perpendicular to the xy-plane, thus, no net magnetization is in that plane.

If a second, less intense magnetic field H_1 , for example, radio-frequency electromagnetic field tuned to the Larmor frequency, is applied along the x-axis, the spins will start to precess about the x-axis at a frequency given by

$$\Delta E_o = h\nu_o \quad (2.15)$$

In terms of the applied magnetic field, the frequency of the radio-frequency field is

$$\nu_o = \gamma H_o \quad (2.16)$$

This equation explains the resonance condition for the NMR experiment and the resonant radio-frequency corresponds to the Larmor frequency for the applied magnetic field. In a given applied magnetic field, different nuclei resonate at widely different frequencies, due to difference in γ for each nuclear isotope. For example in a magnetic field of 1T, the frequency of ^1H is 42.576 MHz, where as that of ^{13}C is 10.705 MHz.

If the short radio-frequency pulse at the Larmor frequency is applied, all spins are precessed together about the x-axis as a coherent packet. It is possible to rotate μ at any given angle by adjusting the duration, t_p , of the radio-frequency pulse. In usual NMR measurement, a 90° radio-frequency pulse is applied along the x-axis to flip μ over the z-axis to the y-axis where it can be detected.

2.2.1.1 ^1H -NMR of NR and HNRs

^1H -NMR analysis of NR revealed three main characteristic peaks at 5.12, 2.03, and 1.67 ppm, corresponding to proton adjacent to C=C bond, methylene, and methyl protons of unsaturated unit, respectively. For HNR samples, the intensity of the peak at 5.12 and 1.67 ppm was reported to decrease with increasing hydrogenation time. The increase in the intensity of the methyl and methylene proton peaks at 0.84 and 1.1-1.3 ppm, respectively, with hydrogenation time was due to transformation of unsaturated double bonds into saturated single bonds. It was also

reported that the degrees of hydrogenation could be determined by comparison of the integrals of signal at 5.12 ppm with those for proton signal of saturated units (Samran *et al.*, 2004c).

2.2.1.2 ^{13}C -NMR of NR and HNRs

In the case of NR, ^{13}C -NMR results showed the strong carbon signals of C=C bond of *cis*-isoprene at 135.2 and 125.5 ppm. Three peaks corresponding to methyl and two methylene carbons of unsaturated unit were at 23.4, 26.4, and 32.2 ppm, respectively. After hydrogenation, the appearance of the peaks at 19.5, 33.0, and 37.1 ppm assigning for the methyl, methane, and methylene carbon of saturated moieties was observed. Their intensity increased with increasing hydrogenation time. ^{13}C -NMR analysis revealed that *cis-trans* isomerization of isoprene units also took place as evidenced by the peaks at 134.9 and 124.7 ppm corresponding to olefinic carbons of *trans*-polyisoprene of HNRs (Samran *et al.*, 2004c).

2.2.2 Infrared (IR) spectroscopy

Infrared spectroscopy is the most common spectroscopic technique used for characterizing polymeric materials. It is used to elucidate the details of molecular structures and intermolecular interactions of polymers. IR spectroscopy probes the oscillation of atoms in molecules. IR light is an electromagnetic radiation consisting of alternating electric and magnetic fields which can be described by a continuous sinusoidal wave like motion. For IR and Raman spectroscopy, only the electric field is considered. The important parameters are the wave length (λ), frequency (ν), and wave number ($\bar{\nu}$), which are related by

$$\bar{\nu} = \frac{\nu}{(c/n)} = \frac{1}{\lambda} \quad (2.17)$$

where c is the speed of light and n is the refractive index of the medium through which the light passes. The IR radiation is emitted from the source with the photons of the energy (E_p) given by

$$E_p = h\nu \quad (2.18)$$

where h is Planck's constant. Photons of specific energy may be absorbed or emitted by a molecule leading to energy transfer. If the molecule absorbs the energy, it is

raised from ground to the excited state (Figure 2.4). The rotational (E_{rot}), vibrational (E_{vib}), or electronic (E_{el}) energy is changed by ΔE ,

$$\Delta E = h\nu = \frac{hc}{\lambda} \quad (2.19)$$

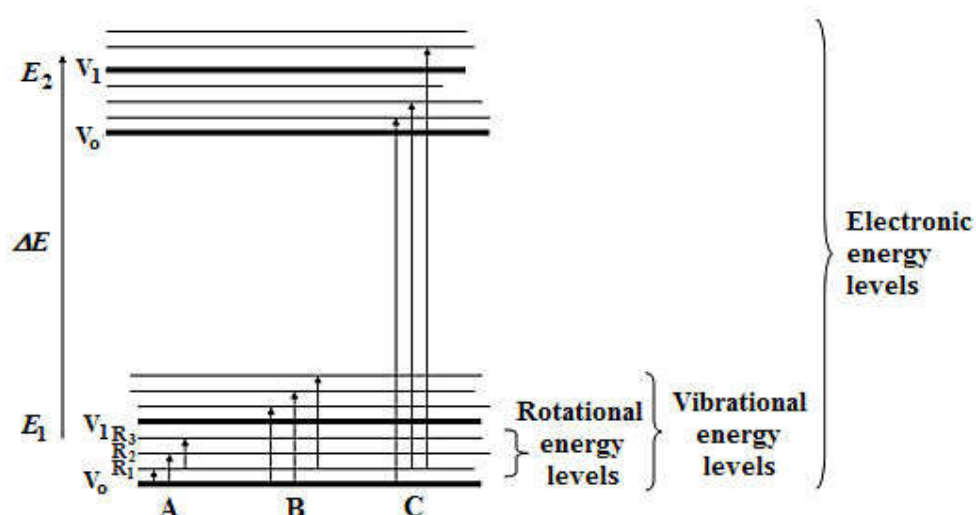


Figure 2.4 Energy levels for a molecule, (A) pure rotational transitions, (B) rotational-vibrational transitions, and (C) rotational-vibrational-electronic transitions

Each atom has three degrees of freedom so that it can move independently along each axes of the Cartesian coordinate system. For a molecule consisted of N atoms, there will be $3N$ degrees of motional freedom. Three are involved the simultaneous moving of all atoms in the same direction parallel to the axes of the Cartesian coordinate system or translational motions. Another three degrees of freedom do not change the distance between atoms. They are involved with rotational motions about the axes of inertial ellipsoid of the molecule. The remaining $3N - 6$ degrees are motions that cause the change in the distance between atoms, the length of chemical bonds, and the bond angles. All vibrational motions of the molecule are caused by superposition of $3N - 6$ non-interacting normal vibrations.

A simple model describing the vibrating molecule consists of an atom of mass m bound to a large mass by the weightless spring with the force constant k

(Figure 2.5 (a)). The force F necessary for moving the atom by a distance x from an equilibrium position is given by

$$F = -kx \quad (2.20)$$

The negative sign indicates that this force is in opposite direction to elongation.

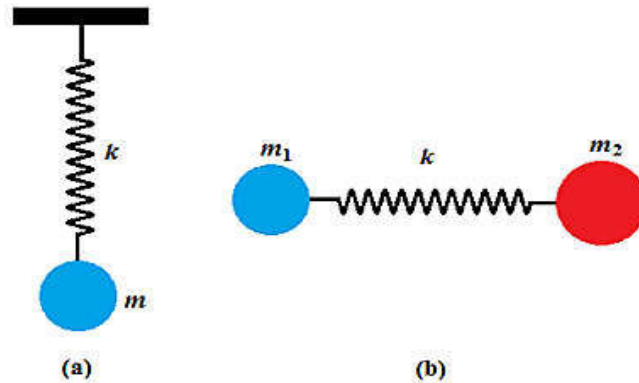


Figure 2.5 Model of a harmonic oscillator (a) mass m bound to a spring with force constant k and (b) masses m_1 and m_2 connected by the spring with the same force constant

According to Newton's law, the force is also proportional to the mass m and the acceleration;

$$F = m \frac{d^2x}{dt^2} \quad (2.21)$$

Combination of equations (2.20) and (2.21) gives rise to

$$m \frac{d^2x}{dt^2} = -kx \quad (2.22)$$

For harmonic oscillation,

$$x = x_o \cos (2\pi\nu t + \phi) \quad (2.23)$$

where ν is the vibrational frequency and ϕ is the phase angle. The second derivative of x with respect to t is given by

$$\frac{d^2x}{dt^2} = -4\pi^2\nu^2 x_o \cos (2\pi\nu t + \phi) = -4\pi^2\nu^2 x \quad (2.24)$$

Inserting equation (2.24) into (2.22) yields

$$\nu = \frac{1}{2\pi} \sqrt{\frac{k}{m}} \quad (2.25)$$

For a diatomic molecule (Figure 2.5 (a)), the mass m or reduced mass can be obtained from

$$\frac{1}{m} = \frac{1}{m_1} + \frac{1}{m_2} \quad (2.26)$$

Therefore, the frequency of vibration of diatomic molecule is given by

$$\nu = \frac{1}{2\pi} \sqrt{\left(\frac{1}{m_1} + \frac{1}{m_2}\right)k} \quad (2.27)$$

In vibrational spectroscopy, the frequency is commonly measured in wavenumber, $\bar{\nu}$. If atomic mass units are employed and the spring constant is measured in N/cm, the wave number of diatomic vibration is given by (Colthup *et al.*, 1975)

$$\bar{\nu} (cm^{-1}) = 1303 \sqrt{\left(\frac{1}{m_1} + \frac{1}{m_2}\right)k} \quad (2.28)$$

A C-H group of atomic masses of 12 and 1 units, respectively, with the force constant of the bond of 5 N/cm will have the wavenumber of 3033 cm^{-1}

For polyatomic molecules, the bonds will experience various types of vibrations and rotations. Therefore, atoms continuously fluctuate over times. Vibrational motions for diatomic or triatomic molecules are easily defined as stretching and bending. However, this is not the case for large molecules which experience several vibrational motions and interactions. When the vibration causes the interatomic distance along the axis of the bond between two atoms to change, this process is called bond stretching. If the vibration results in the change in the bond angle, this process is termed bending. Four bending vibrations, namely, wagging, twisting, rocking, and scissoring do exist.

2.2.2.1 Infrared spectrum (Smith, 2011)

Infrared spectrum is a plot of measured infrared intensity against wave number, which is always plotted in absorbance units implying amount of infrared light absorbed by a sample. The absorbance spectrum is calculated from

$$A = \log \left(\frac{I_0}{I} \right) \quad (2.29)$$

where A is the absorbance, I_0 is the intensity in the background spectrum, and I is the intensity in the sample spectrum.

Absorbance can be related to the concentration of molecules through Beer's law;

$$A = \varepsilon bc \quad (2.30)$$

where ε is absorptivity, b is path length, and c is concentration. The area or height of a peak in absorption spectrum is proportional to concentration of molecules. Infrared spectrum can be plotted in terms of percent transmission ($\%T$) against wave number. $\%T$ can be calculated from

$$\%T = \left(\frac{I}{I_0} \right) \times 100 \quad (2.31)$$

2.2.2.2 Raman spectroscopy (Colthup *et al.*, 1975; McCreery, 2000)

When the light of energy $h\nu$ irradiated a molecule, the energy may be absorbed, transmitted, or scattered. In Rayleigh scattering, the molecules scatter light with no change in individual photon wavelength. Rayleigh scattering can be considered as an elastic collision between the molecule and the incident photon. Because the energy for molecular vibration and rotation is unchanged in the elastic collision, therefore, the energy and the frequency of the scattered photons are the same as those of the incident photons (Figure 2.6). The Raman effect can be considered as an inelastic collision between the incident photon and the molecule resulting in the change in the energy and the frequency of the scattered photon. The scattered photon has an energy of $h\nu_j$, corresponding to a vibrational transition, which is different from the energy ($h\nu$) of the incident photon by the amount ΔE_j

$$\Delta E_j = h\nu - h\nu_j \quad (2.32)$$

At ambient temperature, most molecules are in their vibrational ground state and much smaller number of molecules is in the virtual excited state which is not necessarily a true quantum state of the molecule. The virtual state can be considered

as a very short lived distortion of the electron cloud caused by the oscillating electric field of the light. The electron cloud of the molecule can also be perturbed by molecular vibration. It is possible that optical oscillation and molecular vibration can interact, resulting in Raman scattering.

When the molecule is collided by the oscillating electric field of the incident light, a polarization of the molecule is induced (Figure 2.7). This induced dipole irradiates the scattered light with or without exchanging energy with vibrations of the molecule. The strength of polarization (P) is given by

$$P = \alpha E \quad (2.33)$$

where α is the polarizability and E is the electric field. The classical Raman scattering is based on the effects of molecular vibrations on the polarizability. Consider the laser light of the electric field E which is given by

$$E = E_0 \cos 2\pi\nu t \quad (2.34)$$

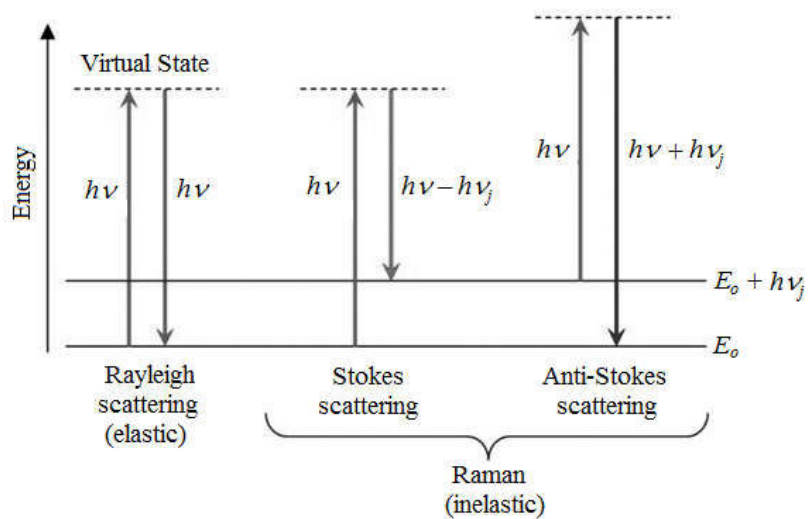


Figure 2.6 Jablonski diagram illustrating quantum energy for Rayleigh and Raman scattering

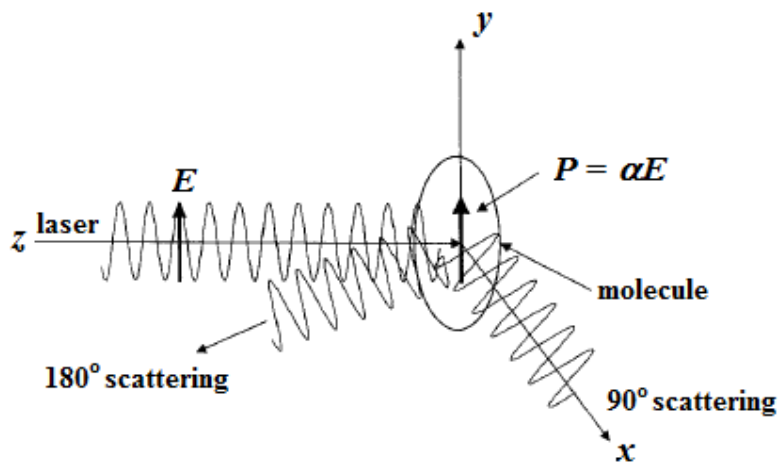


Figure 2.7 Polarization of the molecule induced by the electric field of the incident light (McCreery, 2000)

where t is time and ν is the frequency of the laser light. Normally, molecular vibrations are considered to be composed of normal modes, Q_j , of which there are $3N-6$ (or $3N-5$ for a linear molecule) in a molecule with N atoms. Q_j is given by

$$Q_j = Q_j^o \cos 2\pi\nu_j t \quad (2.35)$$

where ν_j is a characteristic frequency for the j^{th} normal mode. The polarizability of the molecule will be modulated by the molecular vibration so that

$$\alpha = \alpha_o + \left(\frac{\partial \alpha}{\partial Q_j} \right) Q_j + \dots \quad (2.36)$$

Combination of equations (2.33) and (2.34) together with ignoring the higher order terms of equation (2.36) results in

$$P = \alpha_o E_o \cos 2\pi\nu t + E_o \left(\frac{\partial \alpha}{\partial Q_j} \right) Q_j^o \cos 2\pi\nu t \cos 2\pi\nu_j t \quad (2.37)$$

By noting that $\cos a \cos b = [\cos(a-b) + \cos(a+b)]/2$, equation (2.37) can be rewritten as

$$P = \alpha_o E_o \cos 2\pi\nu t + E_o \left(\frac{\partial \alpha}{\partial Q_j} \right) Q_j^o \frac{\cos 2\pi(\nu - \nu_j)t}{2} + E_o \left(\frac{\partial \alpha}{\partial Q_j} \right) Q_j^o \frac{\cos 2\pi(\nu + \nu_j)t}{2} \quad (2.38)$$

Equation (2.38) implies that the light will be scattered at three frequencies. The first term corresponds to Rayleigh scattering, for which the scattered light will have the same frequency as the laser, and its magnitude is proportional to the inherent polarizability (α_o) of the molecule. The second term is Stokes scattering which occurs at $\nu - \nu_j$ and the third term is Anti-Stokes scattering at $\nu + \nu_j$ (Figure 2.6). ν_j is the same frequency which would be observed in IR absorption for a given vibration mode. Although equation (2.38) is incomplete, it, however, does provide some useful insights. First, polarization and scattering intensities (both Rayleigh and Raman) are linear with laser intensity. Second, Raman scattering results only from vibrations that change the polarizability. Third, Raman shifts can be both positive and negative. Fourth, variation of $(\partial\alpha/\partial Q_j)$ due to different molecules and different vibrational modes in a given molecule leads to wide variations in Raman scattering intensity. Fifth, since $(\partial\alpha/\partial Q_j)$ is much smaller than α_o , therefore, Rayleigh scattering is much stronger than Raman scattering.

2.2.3 Infrared and Raman spectra of NR and HNRs

It was reported for NR of IR absorption occurred at 1665 cm^{-1} and 836 cm^{-1} corresponding to the C=C stretching mode and the C-H out of plane deformation of the trisubstituted carbon-carbon double bond of isoprene unit, respectively (Samran *et al.*, 2004c) can be observed. With increasing hydrogenation time, the intensity of the peaks at 1665 cm^{-1} and 836 cm^{-1} gradually decreased with the appearance of the peaks at 735 cm^{-1} assigning to $-\text{CH}_2-$ groups of HNRs.

Raman spectra of NR showed strong intensity at 1664 cm^{-1} which represented C=C stretching (Samran *et al.*, 2004a). The intensity of this peak decreased with increasing degrees of hydrogenation.

2.3 Vulcanization of hydrogenated natural rubber

Partially hydrogenated natural rubbers (HNRs) can be vulcanized by using peroxide and sulfur. The reactions between peroxide and rubber can take place either at saturated ethylene-propylene segment or at allylic position of isoprene units while those of sulfur and rubber occurs mainly at unsaturated units (Loan, 1972; Akiba and Hashim, 1997).

2.3.1 Peroxide vulcanization

The mechanisms of peroxide crosslinking for NR using dicumyl peroxide (DCP) are shown in Figures 2.8. DCP first undergoes thermal decomposition to form cumyloxy radicals followed by abstraction of allylic hydrogens by cumyloxy radicals to form polymeric radicals. Then, polymeric radicals are coupled to form crosslinks whose possible structures are shown in Figure 2.9. In the case of saturated rubbers such as EPR, chain scission may also occur (Figure 2.10).

2.3.2 Sulfur vulcanization

Sulfur is widely used to vulcanize NR and other diene rubbers. It must be used in combination with activators and accelerators. Many types of accelerators are available and their classification in terms of chemical compositions and vulcanization speed is shown in Table 2.1. Metal oxide and fatty acid are the most commonly used activators, of which ZnO 3-5 phr and stearic acid 1-3 phr are in general.

Table 2.1 Classification of accelerators and their vulcanization speed

Types	Examples	Speed of vulcanization
Dithiocarbamates	ZDMC, ZDEC, ZDBC	Very fast
Thiurams	TMTM, TMTD, DPTTS	Very fast
Thiazole	MBT, MBTS, ZMBT	Moderate
Sulfenamides	CBS, MBS, TBBS	Fast
Thiophosphates	DIPDIS	Semi-fast
Guanidines	DPG	Slow

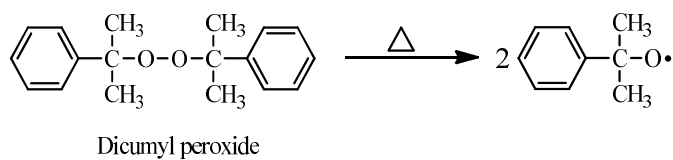
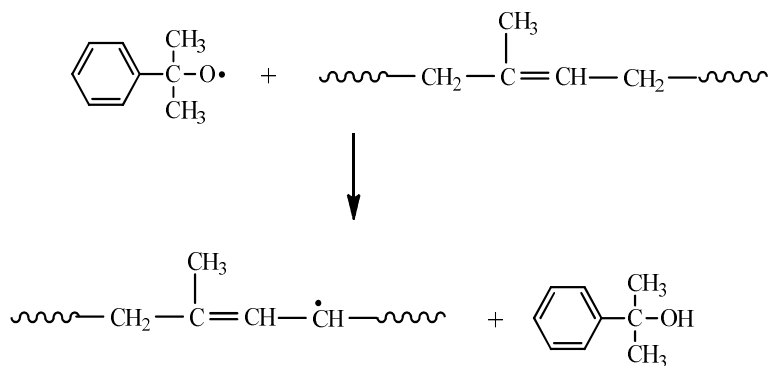
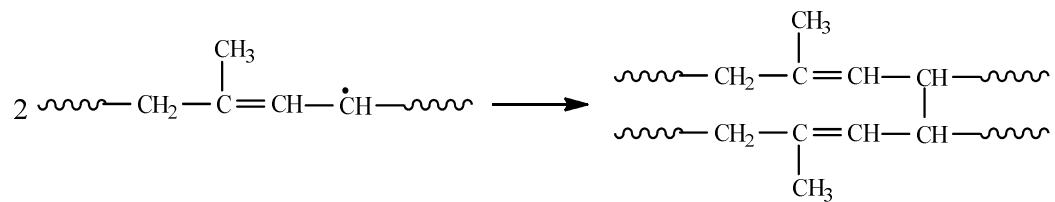
DCP decomposition**Hydrogen abstraction****Coupling of macroradicals**

Figure 2.8 Mechanisms of NR vulcanization by dicumyl peroxide (Loan, 1972; Akiba and Hashim, 1997)

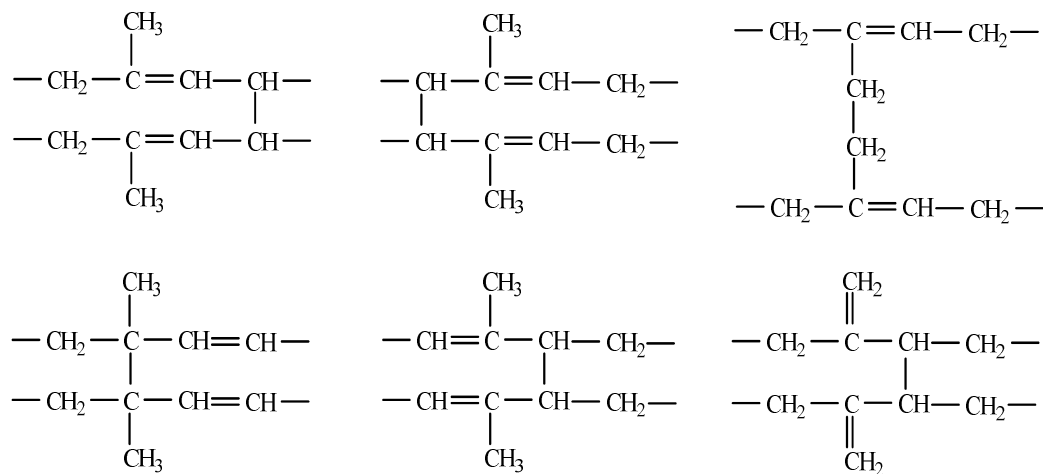


Figure 2.9 Possible crosslink structures of peroxide-cured NR (Loan, 1972; Akiba and Hashim, 1997)

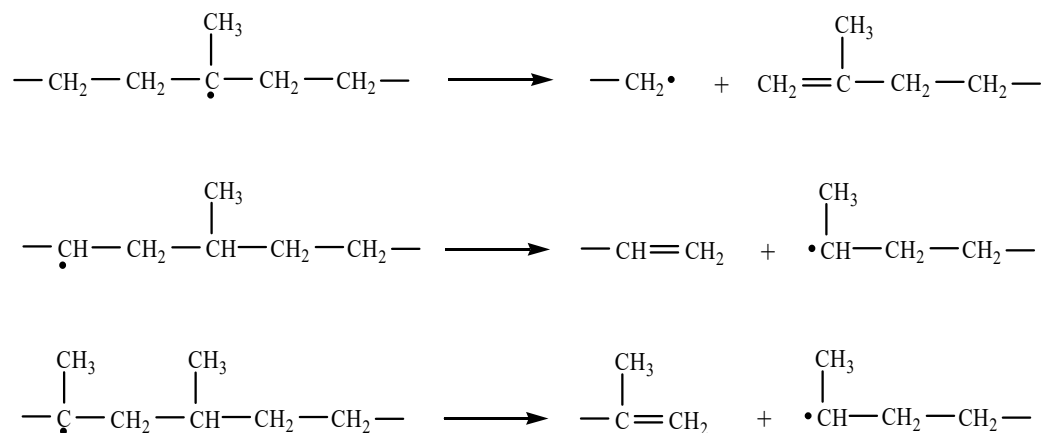


Figure 2.10 Possible scission reaction in ethylene-propylene rubber (Loan, 1972; Akiba and Hashim, 1997)

The ratio of amounts of sulfur to accelerator determines vulcanization systems which are conventional (CV), efficient (EV), and semi-efficient (SEV) vulcanization (Table 2.2).

Table 2.2 Sulfur vulcanization systems

Vulcanization Systems	Sulfur (S, phr)	Accelerator (A, phr)	A/S ratio
Conventional (CV)	2.0-3.5	1.2-0.4	0.1-0.6
Semi-efficient (SEV)	1.0-1.7	2.5-1.2	0.7-2.5
Efficient (EV)	0.4-0.8	5.0-2.0	2.5-12.0

CV system employs high sulfur to accelerator ratios. Thus, crosslinks formed in rubber vulcanizates are mainly polysulfidic which provide better flex and dynamic properties but poor heat and reversion resistance to rubber.

In EV system, low levels of sulfur and high levels of accelerator are employed. In some particular cases, sulfur donors are used instead of sulfur. The crosslink types occurred in rubbers are mostly mono- and disulfidic. Therefore, rubbers cured by EV systems are dominant in low compression set and high heat and reversion resistance.

To obtain optimum mechanical and dynamic properties with intermediate heat and reversion resistance SEV system is employed. SEV system utilizes intermediate amounts of sulfur and accelerator.

Although sulfur vulcanization of NR was discovered more than 170 years, its mechanism is still not completely understood. Unaccelerated sulfur vulcanization has been proposed to proceed via free radical or ionic intermediates or both. However, mechanisms of accelerated sulfur vulcanization are more complicated and involved many steps as shown in Figure 2.11.

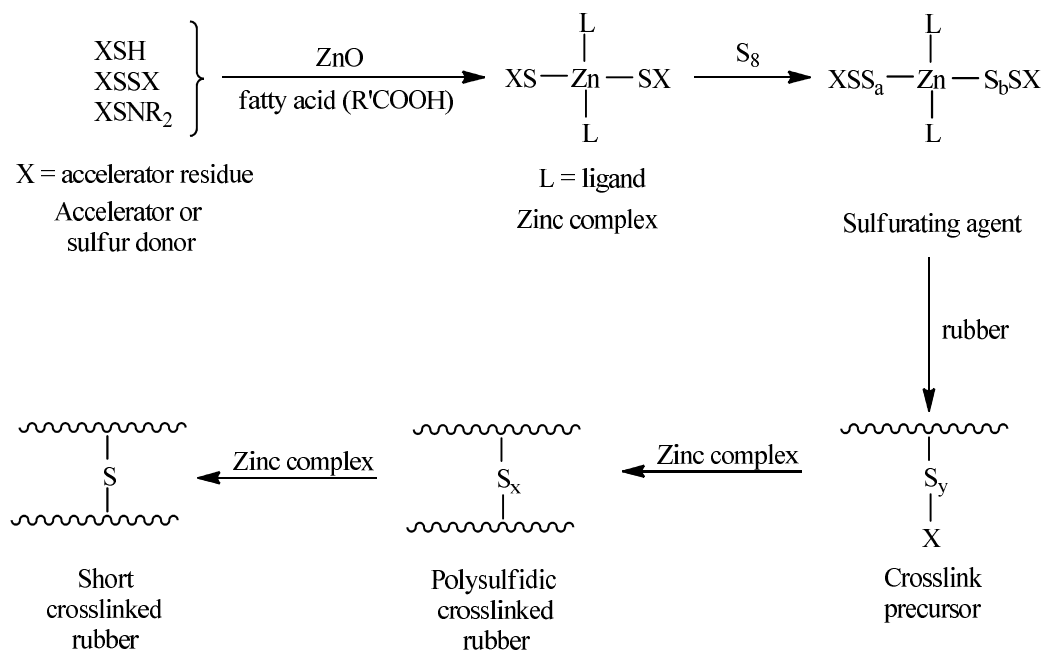


Figure 2.11 Reaction pathway for accelerated sulfur vulcanization (Loan, 1972; Akiba and Hashim, 1997)

2.4 Thermoplastic vulcanizates

Thermoplastic vulcanizates (TPVs) are composed of both rubber and thermoplastic phases and considered as a special class of thermoplastic elastomers (TPEs). TPVs are produced by dynamic vulcanization process in which vulcanized rubber particles are uniformly dispersed in a continuous thermoplastic matrix. Generally, TPVs contain relatively high amounts of crosslinked rubber particles (50–70 wt%). During dynamic vulcanization, the increased viscosity of the elastomer phase affects the phase continuity by promoting phase inversion, which enables the crosslinked elastomer to become the dispersed phase. In most case, the sizes of crosslinked rubber particles are of 0.1–2.0 μm in diameter (Van Duin and Machado, 2005; Vennemann *et al.*, 2006; Costa *et al.*, 2008; Prut *et al.*, 2008; Goharpey *et al.*, 2008). Such a morphological feature results in soft and high elastic products (l’Abee *et al.*, 2009). Although the rubber phase is already vulcanized, the continuous thermoplastic matrix enables TPVs to be melt-processed using common thermoplastic

processing machines such as extrusion, blow molding, and injection molding (Boyce *et al.*, 2001).

Thermoplastic vulcanizates can be prepared by using batch or discontinuous mixing, when relatively short cycles are required and polymer melts require heavy machinery to achieve satisfactory mixing. Batch mixing is frequently done in a specified volume of a mixing device such as an internal mixer (Drobny, 2007), in which the typical stages of the dynamic vulcanization can be notified. Figure 2.12 illustrates the torque-time profile of the production of a dynamic vulcanizate based on polypropylene (PP) and ethylene-propylene rubber (EPR). The blend consisted of 40 wt% PP and 60 wt% EPR with viscosity ratio ($\eta_{\text{EPR}} / \eta_{\text{PP}}$) of 1.5 were prepared using a laboratory internal mixer (Radusch, 2005). PP was first plasticized (first peak) followed by the addition of the uncrosslinked EPR rubber (second peak). A polymer blend was then produced as reflected by slightly decreasing torque or blend viscosity, which was caused by thermo-mechanical breakdown of polymer molecules. In this stage, a co-continuous phase was formed. At a specified time, the crosslinking agent was added. The progress of crosslinking reaction resulted in the increasing torque, which is then followed by the breakup of the highly deformed rubber threads in the co-continuous phase. Crosslinking and dispersion of the rubber component simultaneously and rapidly occurred. The amounts of crosslinking agent would determine the duration of this process. After the crosslinking process was completed (expressed by the third peak) the highly viscous rubber particles are only distributed in the low viscosity thermoplastic matrix (Radusch, 2005).

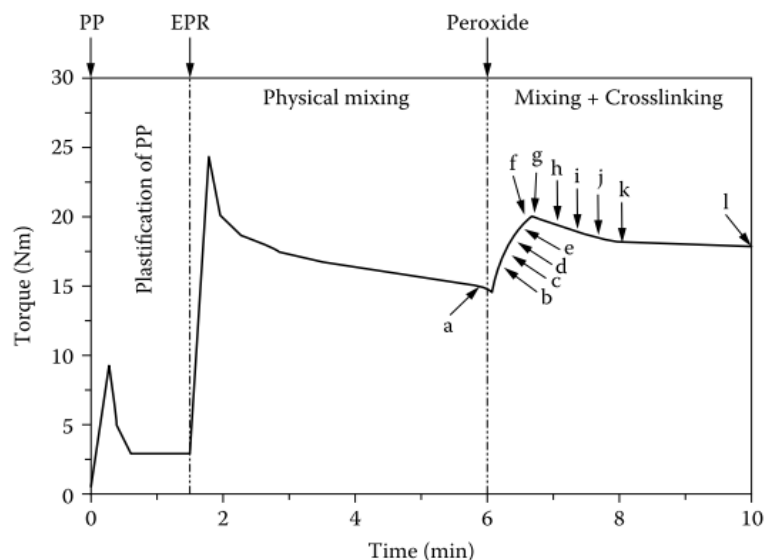


Figure 2.12 Torque-time characteristics of a dynamic vulcanization process in an internal mixer for peroxide-vulcanized PP/EPR (40/60) blend (Radusch, 2005)

Morphological transformation during the dynamic vulcanization of polymer blends can be explained as shown in Figure 2.13. In the initial stage, a mixture of the molten thermoplastic and the uncrosslinked rubber co-exist in co-continuous phases. As the curing agent is added and crosslinking takes place, the rubber phase becomes elongated until highly deformed stage is reached and then it breaks into small particles (Figure 2.13). This process is called phase inversion, in which the lower portion thermoplastic phase becomes the only continuous phase throughout which the crosslinked rubber particles are uniformly dispersed (Nicolini *et al.*, 2008).

2.5 Characterization of thermoplastic vulcanizates

Morphological characterization of TPVs can be done by many methods such as scanning electron microscope (SEM) (Han *et al.*, 1998; Li and Kontopoulou, 2009), atomic force microscopy (AFM) (Prut *et al.*, 2008; Le *et al.*, 2010) and transmission electron microscopy (TEM) (Van Duin and Machado, 2005; l'Abee *et al.*, 2009). Raman imaging is an excellent method for acquiring information about the spatial distribution of molecular species (Turrell and Corset, 1996; Ferraro, 2003;

Esmonde-White and Morris, 2010; Lee, 2012). It combines Raman spectroscopy and imaging techniques and may be used to characterize the distribution of polymeric components in multiphase polymer blends.

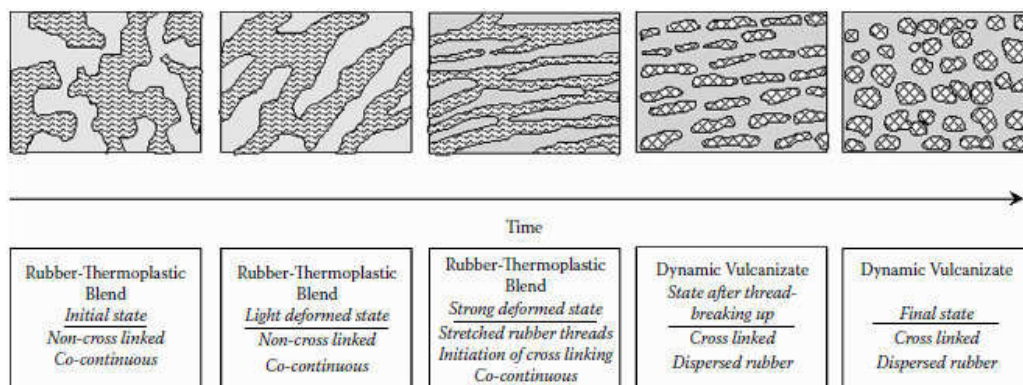


Figure 2.13 Schematic of morphology transformation during the dynamic vulcanization of polymer blends (Radusch, 2005)

2.5.1 Raman Imaging

The general principle of Raman imaging consists of mapping the spatial arrangement of one constituent of an inhomogeneous sample by isolating from the Raman scattered photons which originate from a characteristic Raman line of the specific compound (Barbillat, 1996). A complete spectrum is collected at each and every pixel of the image, and then examined to generate false color images based on material composition and structure. Raman peak provides images of material concentration and distribution. The position of Raman peak gives images of molecular structure and phase and the peak width yields images of crystallinity and phase. Due to the inherent weakness of Raman scattering, two- and three-dimensional Raman imaging is not simple. However, modern technology makes possible for recording higher resolution images. Hyperspectral imaging is referred to any spectral imaging whose spectral quality is comparable to that of traditionally recorded spectra. Therefore, Raman hyperspectral imaging is referred to as a method for recording a Raman hypercube whose spectral quality is comparable to that of traditionally collected Raman spectra. The Raman hypercube is a set of intensity data made of $I(x, y, \nu)$, where x and y are coordinates of the image pixels and ν is the wave number.

Raman hyperspectral imaging is performed using a high spatial resolution Raman microscope to collect numerous Raman spectra from different locations of the sample. The conventional experiment scheme from bright field imaging to Raman imaging is shown in Figure 2.14. Bright field imaging is useful for visualizing the sample topology and morphology and identifying the region of interest for analysis, while Raman imaging is for visualizing the local chemistry, morphology, and spatial distribution of chemical ingredients.

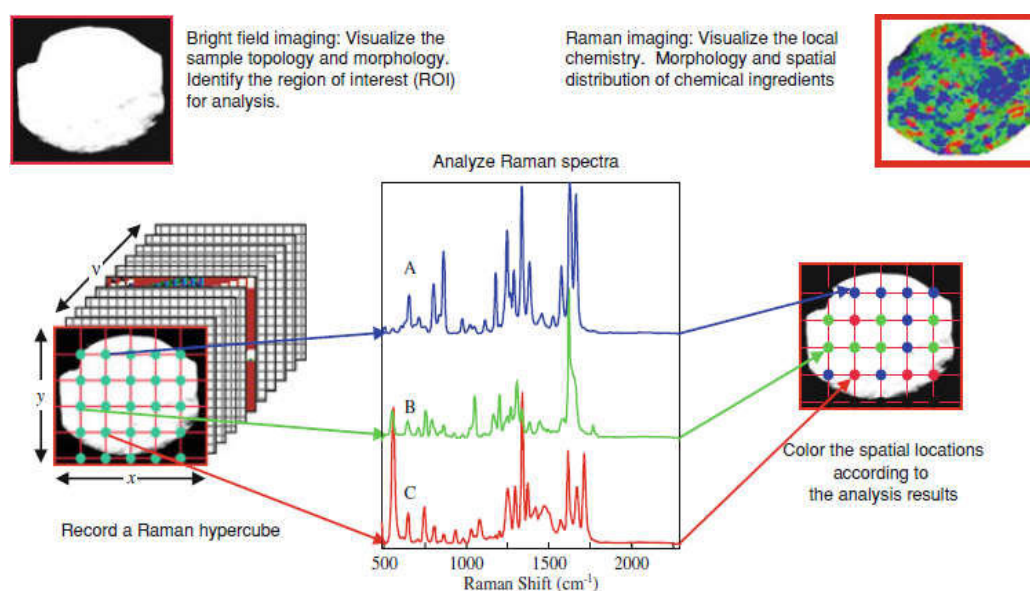


Figure 2.14 Schematic diagrams from bright field imaging to Raman mapping. The hypercube is a collection of Raman intensities as a function of $I(x, y, \nu)$. At a fixed position (x_i, y_i) , it is a localized Raman spectrum. At a fixed wave number ν_k , it is a Raman intensity map (Lee, 2012)

Raman hyperspectral imaging requires multivariate analysis due to a number of reasons. First, spectral features would be mixed at varying degrees with contributions from multiple chemical/spectral species depending on the local concentration and intrinsic Raman scattering cross section of each ingredient. Second, crystallinity, orientation, or domain size of each ingredient can affect relative and overall intensities. Third, there would be additional interference from fluorescence background, scattering and noise. And forth, there will be large volume of data and

information in the hypercube. Therefore, Raman signals can be separated from varying sources and ingredients by multivariate analysis.

2.5.2 Imaging Methods

Raman imaging methods can be carried out by point mapping, line scanning and global mapping. Schematic diagrams of these methods are shown in Figure 2.15.

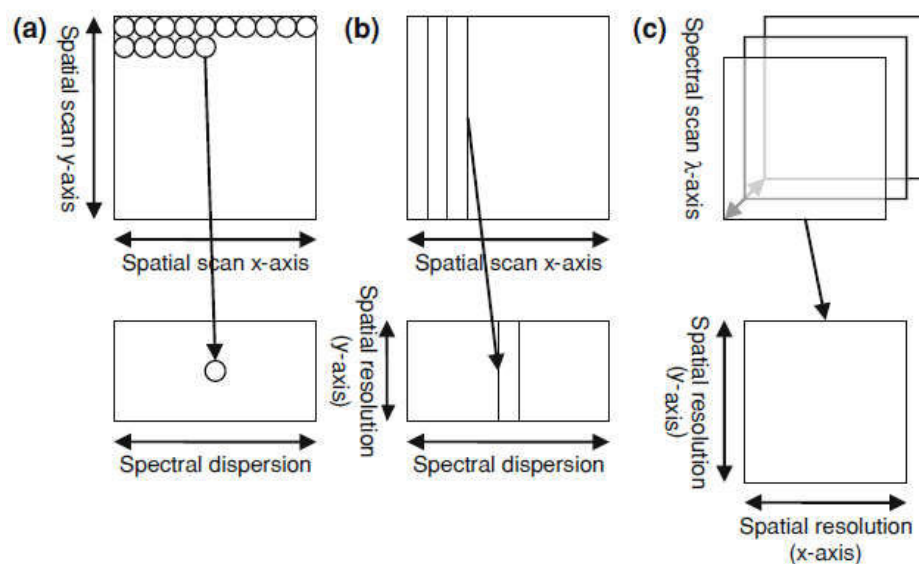


Figure 2.15 Schematic diagrams describing (a) point mapping, (b) line scanning, and (c) global mapping. The top row illustrates the illumination pattern on the sample and the bottom row shows the image onto the detector (Lee, 2012)

2.5.2.1 Point mapping

This is the simplest method used for recording Raman hypercubes of high spectral and spatial resolutions. The operator can specify the mapping area and measured locations, usually in a rectangular shape and grid pattern. A Raman spectrum is collected at each point, and a mapping stage is used to move from point-to-point on the sample. Scanning along the x - and y -axes is required. If desired, any experiment conditions controlled by the computer can be programmed. This is, so far, the most flexible and popular Raman hyperspectral imaging method employed.

It is possible to scan the laser. This can be done by placing mirrors in the optical path which both incident and scattering beams pass. Mirrors can be precisely moved at a high speed. When the mirrors are moved at a high speed, a predetermined area of the sample is illuminated uniformly and the signal returns instantaneously. Since the scattering and incident beam paths are coincident, the result is an averaged Raman spectrum of the illuminated area. The main advantage of this method is that large area of the sample with a few numbers of measurements can be made. It is suitable for a sample with large particles or agglomerates, or finding a small sample on a large substrate. The mirrors can be moved in a stop-and-go fashion to excite individual points, therefore, measurements at a very fine grid, which is useful to map a small sample, can be carried out. We follow this method in our work.

2.5.2.2 Line scanning

In this method, the sample is illuminated in a line, which is imaged onto the entrance slit of the spectrograph, and then onto the detector along the y -axis (column). Raman signal along the line is dispersed along the x -axis (row) of the detector for spectral resolution. A correlation between rows of the detector and points in the illuminated line provides the spatial resolution along the illuminated line. To map an area, the sample is moved along only one spatial axis which is orthogonal to the line illumination. The objective lens and the size of the detector will limit the height of mapping area.

When compared to the point mapping, the advantage of line scanning is the speed. To map 25x 25 points, point mapping requires 625 measurements, while 25 measurements are for line scanning. Furthermore, line scanning can reduce the heat-induced damage by spreading the laser beam over the illuminated line. However, the main disadvantage of the line scanning is the spatial resolution. Since the propagation of the signal from the sample to the detector is in a line shape, a confocal hole cannot be used to reject out-of-focus signal. Therefore, line scanning cannot be truly confocal though the entrance slit offers a measure of confocality. In addition, non-uniform illumination may occur, especially, between the edges and the center of the illuminated line.

2.5.2.3 Global mapping

In this method, a finite area of the sample is illuminated and then imaged onto the detector. Resolution of spectra is achieved with a liquid crystal tunable filter (LCTF) or a combination of LCTFs. Global imaging performs Raman multi-spectra imaging by recording Raman peak intensity images at a few predetermined wavelengths, which takes a much shorter time than recording a full Raman hypercube. However, the authenticity of “Raman” image cannot be verified without a full range spectrum. For recording a full spectrum, filters must be tuned at a series of wavelengths. The speed of the measurement is determined by the number of points along the spectral axis and the speed of tuning from one wavelength to the next. The spectra resolution is limited by the filters.

Raman imaging has been employed for characterizing polypropylene (PP)-polyethylene (PE) blends (Schmidt *et al.*, 2002; Furukawa *et al.*, 2006), tertiary blends of polystyrene (PS), polypropylene and poly(styrene-ethylene/propylene) diblock copolymer (Lee *et al.*, 2011), multilayered thin film consisting of chlorinated PP, ethylene-propylene rubber (EPR) and PP blend (Morris *et al.*, 1999). Raman mapping images of polyethylene (PE) and polypropylene (PP) blends were reported to be greatly affected by melt flow index (MFI) ratios of PE and PP (Furukawa *et al.*, 2006).

However, morphological studies of thermoplastic vulcanizates based on HNR/PP blends using Raman mapping have not yet been reported up to our knowledge.

CHAPTER 3

MATERIALS AND METHODS

3.1 Materials and Equipments

3.1.1 Materials

- 3.1.1.1 High ammonia natural rubber latex (*cis*-1,4 polyisoprene) with 60% dry rubber content (DRC) was a product of Yala Latex Co., Yala, Thailand
- 3.1.1.2 Hydrazine monohydrate ($\text{N}_2\text{H}_4\cdot\text{H}_2\text{O}$) with 35% assay, a commercial grade, was supplied by Kaiser-Wilhelm-Allee, Lanxess Deutschland Gmbh, Germany.
- 3.1.1.3 Hydrogen peroxide (H_2O_2), a commercial grade of 50% assay, was a product of Thai Peroxide Co., Ltd., Thailand.
- 3.1.1.4 Toluene (C_7H_8), 90% assay, a commercial grade, was supplied by Boss Optical Limited Partnership, Thailand.
- 3.1.1.5 Sulfur (S_8), a vulcanizing agent, was yellow powder with specific gravity of 2.0. It was a product of Siam Chemicals Co., Ltd., Samutprakarn, Thailand.
- 3.1.1.6 Stearic acid ($\text{C}_{18}\text{H}_{36}\text{O}_2$), a cure activator, is white solid with specific gravity of 0.85. It was supplied by Imperial Chemical Co., Ltd., Pathumthani, Thailand.
- 3.1.1.7 Zinc oxide, a cure activator, is white powder. Its specific gravity was 5.6. It was supplied by Global Chemical Co., Ltd., Samutprakarn, Thailand.
- 3.1.1.8 Tetramethylthiuram disulfide (TMTD, $\text{C}_6\text{H}_{12}\text{S}_4\text{N}_2$) is an accelerator and a sulfur donor. Its specific gravity is 1.30. It was supplied by Flexsys Co., Ltd., Belgium.
- 3.1.1.9 2-Mercaptobenzothiazole (MBT, $\text{C}_7\text{H}_5\text{S}_2\text{N}$), specific gravity of 1.42, is an accelerator for sulfur vulcanization. It was a product of Flexsys America LP Co., Ltd., United States.

- 3.1.1.10 Dicumyl peroxide (DCP, $C_{18}H_{22}O_2$) is a vulcanizing agent. It is 98% assay with specific gravity of 1.56. Its half-life is 1 min at 180°C, 1 hr at 135°C, and 10 hr at 116°C. It was supplied by Wuzhou International Co., Ltd., China.
- 3.1.1.11 Triallyl cyanurate (TAC, $C_{12}H_{15}N_3O_3$) is a coagent for peroxide vulcanization. It has specific gravity of 1.11 and contains 98-99% of active functional group. It was a product of Fluka Chemie GmbH, Switzerland.
- 3.1.1.12 Polypropylene (PP), HP500N, a general purpose grade for injection molding, was supplied by Lyondell Basell Co., USA.
- 3.1.1.13 Ethylene propylene diene monomer (EPDM) rubber, IP4725 grade, contains 70 mass% of ethylene, 25 mass% of propylene, and 5 mass% of ethylidene norbornene (ENB). It was the product of Dow Chemical Co., United States.

3.1.2 Equipment and Apparatus

- 3.1.2.1 1L- and 2L-Three-necked round bottom flask
- 3.1.2.2 Condenser
- 3.1.2.3 Dropping funnel
- 3.1.2.4 Mechanical stirrer
- 3.1.2.5 1H -NMR (VARIAN NMR, Unity Inova 500)
- 3.1.2.6 Raman spectrometer (Xplora-Horiba)
- 3.1.2.7 Fourier transform infrared spectroscopy (A225/Q Platinum ATR, Multiple Crystals Diamond Tensor 27 Bruker spectrometer)
- 3.1.2.8 Transmission electron microscopy (JEM 2010, JEOL: TEM)
- 3.1.2.9 Differential scanning calorimeter (Q100 V9.8 Build 296 TA Instrument)

- 3.1.2.10 Laser particle size analyzer (Coulter, LS-230, small volume module (model: liquid module))
- 3.1.2.11 Durometer (Digital hardness tester, toyoseiki Co. Ltd, Japan)
- 3.1.2.12 Capillary rheometer (Goettfert-Rheograph 20)
- 3.1.2.13 Mooney viscometer (model VISCAL, Tech Pro Co., Ltd, USA)
- 3.1.2.14 Thermogravimetric analysis (Perkin-Elmer, STA 6000)
- 3.1.2.15 Internal mixer (Brabender Plastic-Corder PL-2000)
- 3.1.2.16 Oscillating disk rheometer (ODR 2000, Monsanto)
- 3.1.2.17 Ozone chamber (Model Rev. 2.0, Korea)
- 3.1.2.18 UV test chamber (QUV accelerated weathering tester, Model QUV spray, American)
- 3.1.2.19 Tensile testing machine (Model H 10KS, Hounsfield test equipment, Tinius Olsen Ltd, UK)
- 3.1.2.20 Scanning electron microscopy (JEOL, JSM-6510LV)
- 3.1.2.21 Rheometrics solids analyzer instrument (RSA 2)

3.2 Preparation of hydrogenated natural rubbers (HNRS)

3.2.1 Non-catalytic hydrogenation of natural rubber latex (NRL)

Concentrated NRL was diluted to 20% DRC and then added to a 1-L three-necked round bottom flask equipped with a condenser and a dropping funnel under constant stirring speed and at specified temperature. A specified volume of hydrazine was added dropwise and then hydrogen peroxide was slowly introduced into the reactor by dropping funnel. Hydrogenated NRL samples were collected at specified period of time, coagulated by methanol, sheeted, and then washed several times with water before drying in vacuum oven at 50°C.

The effects of mole ratios of [C=C]:[N₂H₄]:[H₂O₂] on hydrogenation degrees of NRL were studied using the values shown in Table 3.1. In this case, the hydrogenation reactions were carried out at 50°C for 24 hrs.

Table 3.1 Experimental runs to study the effects of mole ratios of hydrogenation degrees of NRL at $50\pm 3^\circ\text{C}$ for 24 hrs.

Run	Molar ratio of		
	[C=C]	[N ₂ H ₄]	[H ₂ O ₂]
1	1.0	0.5	1.0
2	1.0	1.0	1.0
3	1.0	1.5	1.0
4	1.0	2.0	1.0
5	1.0	1.0	0.5
6	1.0	1.0	1.5
7	1.0	1.0	2.0

The effects of reaction temperatures and times on hydrogenation levels of NRL were studied by fixing the mole ratio of [C=C]:[N₂H₄]:[H₂O₂] at 1:1.5:1. Reaction temperatures were varied from 30°C to 60°C and reaction times were varied from 2 to 24 hrs.

Hydrogenation of NRL was also carried out in the swollen state at 50°C for 24 hrs. Two types of solvents, toluene and hexane, were used. The effects of swelling degrees on degrees of hydrogenation were studied by varying the volume ratios of solvent to latex. After reaction, the solvent was removed from HNR lattices before being coagulated by methanol, sheeted, washed with water, and dried in vacuum oven at 50°C.

The effects of reaction scale-up on the degrees of hydrogenation of NRL were also investigated. In this case, the 2-L reactor was used, and the volumes of NRL were scaled up from 250 mL to 650 mL. To achieve the designed degrees of hydrogenation, the typical mole ratios of [C=C]:[N₂H₄]:[H₂O₂] and toluene volume were chosen.

3.2.2 Characterization of NR and HNRs

3.2.2.1 Chemical structure

The structures of rubbers were characterized by $^1\text{H-NMR}$, Raman and FT-IR spectroscopy. $^1\text{H-NMR}$ spectra were obtained using a Varian Unity Inova 500 MHz NMR spectrometer. The rubbers were dissolved in deuterated chloroform (CDCl_3) using tetramethylsilane (TMS) as an internal reference. The measurements were performed with 90° pulses and an acquisition time of 1 s.

Raman spectra of rubbers were recorded with a Xplora-Horiba Raman spectrometer at room temperature under a microscope with a magnification $\times 50$. The simple spectrograph was adjusted with a $600 \text{ lines}\cdot\text{mm}^{-1}$ grating. Rubbers were illuminated with a He-Ne laser source selecting the red line at 785 nm. The Raman spectra of rubbers were collected in the range of $500\text{-}3500 \text{ cm}^{-1}$ with 50 accumulations and an acquisition time of 2s. The best resolution was obtained by setting both the entrance slit and the confocal pinhole at the same value of $300 \mu\text{m}$.

FT-IR spectra of rubbers were obtained using an A225/Q Platinum ATR, Multiple Crystals Diamond Tensor 27 Bruker spectrometer. The spectra were acquired at wavenumber of $500\text{-}3500 \text{ cm}^{-1}$.

3.2.2.2 Hydrogenation levels

The hydrogenation levels (X) of HNRs can be determined from $^1\text{H NMR}$ and Raman spectra (Samran *et al.*, 2004c). For $^1\text{H NMR}$ spectra, X was calculated from the areas under assigned characteristic peaks of $^1\text{H-NMR}$ according to equation (3.1),

$$X = \left(\frac{A_{0.8}}{A_{0.8} + 3A_{5.2}} \right) \times 100 \quad (3.1)$$

where $A_{0.8}$ and $A_{5.2}$ are the integrated areas of methyl proton signals of HNR and proton signals adjacent to C=C bond, respectively.

The degrees of hydrogenation of HNRs were also determined from the ratio of integrated area of Raman peak at 1665 cm^{-1} , corresponding to C=C bonds stretching, to that at 1434 cm^{-1} , corresponding to the CH_2 bending (Samran *et al.*, 2004a);

$$X = \left(\frac{K - 2\alpha}{K + \alpha} \right) \times 100 \quad (3.2)$$

where K and α were the ratios of the integrated area of the C=C peak to CH₂ vibration peak of starting NR and HNRs, respectively.

3.2.2.3 *cis* and *trans* Isomerization

The *cis* and *trans* isomerization of HNRs was investigated by ¹H-NMR. The percentages of *cis* and *trans* configurations were calculated from the integrated areas of ¹H-NMR characteristic peaks according to equations (3.3) and (3.4) (Samran *et al.*, 2004c),

$$cis (\%) = \left(\frac{A_{1.67}}{A_{1.64} + A_{1.67}} \right) \times 100 \quad (3.3)$$

$$trans (\%) = \left(\frac{A_{1.64}}{A_{1.64} + A_{1.67}} \right) \times 100 \quad (3.4)$$

$A_{1.64}$ and $A_{1.67}$ are the integrated areas of the proton signals of methyl groups corresponding to *trans* and *cis* configurations, respectively.

3.2.2.4 Morphology of latex by transmission electron microscopy

The morphology of unswollen and swollen NRLs was studied using JEOL JEM 2010 TEM. The latex was first diluted to approximately one four hundredth of its original concentration with distilled water. An aqueous solution (2 wt %) of OsO₄ was added to stain NR molecules. The stained latex was then placed on a 400 mesh grid, and dried overnight in desiccators before characterization.

3.2.2.5 Glass transition temperature (T_g) by differential scanning calorimetry

Thermal properties of NR and HNRs were characterized using differential scanning calorimeter model DSC Q100 V9.8 Build 296 of TA Instrument. The measurement was performed in the temperature range from -80°C to 150°C with cooling and heating rates of $10^{\circ}\text{C}/\text{min}$. The sample was first equilibrated at 25°C for 5 min and then heated to 150°C with the rate of $10^{\circ}\text{C}/\text{min}$. The sample was held at 150°C for 1 min before ramping down to -80°C with the rate of $10^{\circ}\text{C}/\text{min}$. The sample was held at -80°C for 1 min and then ramped up to 150°C . The thermogram of the sample was automatically recorded by computer. The glass transition temperature (T_g) was determined from the midpoint of the base line shift of DSC thermograms.

3.2.2.6 Particle size and particle size distribution

Particle size and particle size distributions (PSD) of HNR latices were measured using Coulter LS-230 particle size analyzer (liquid module) operating with a 750 nm laser beam. The laser light from the source was passed through a chamber containing the latex sample. The scattered light was then detected by a photo-detector array. The intensity of scattered light on each detector was then converted to PSD plot calculated using mathematical algorithms. Beckman Coulter LS230 uses 126 detectors in its diffraction arrays and the polarization intensity differential scattering (PIDS) system to measure particles from 0.04 to 2000 μm in a single scan.

About 10 mL of a 20 %DRC latex sample (NR or HNR) was diluted to 10% DRC latex in a beaker. Then, 4-10 drops of dilute surfactant solution (2-5 wt%) were added and mixed with the latex sample before analysis. Particle size and PSD of the latex sample were calculated by Coulter software.

3.2.2.7 Hardness

Shore A hardness of NR and HNRs was measured according to ASTM D2240 using Shore A Durometer, digital hardness tester of Toyoseiki Co. Ltd, Japan. The measurement was done on a sample of at least 6.0 mm thick and at

$26 \pm 2^\circ\text{C}$. Hardness was measured from three different positions on the specimen and recorded in Shore A after 30 sec of indentation.

3.2.2.8 Rheological properties

Rheological properties of NR and HNRs were studied using Goettfert-Rheograph 20 capillary rheometer. The experiment was carried over a shear rate range from 10 to 1500 s^{-1} at 180°C . The capillary die of 2 mm in diameter and 32 mm in length was used.

Mooney viscosities of NR and HNRs were measured according to ASTM D1646 by using a VISCAL Mooney viscometer of Tech Pro Co., Ltd. A large rotor was used with the speed of 2 rpm. The test was carried out at 125°C . The sample was first pre-heated for 1 min and then tested for 4 min. Also, stress relaxation of rubbers was measured for another 3 min after immediate stop of the rotor.

3.2.2.9 Gel content

About 0.35 g (W_1) of rubbers was immersed in 25 mL of toluene at room temperature for 168 hrs. The swollen samples were then taken out and excessive toluene was rapidly removed by blotting with filter paper. The samples were dried at 50°C for 48 hrs and weighed (W_2). The gel content was determined from equation (3.5),

$$gel (\%) = \frac{W_2}{W_1} \times 100 \quad (3.5)$$

3.2.2.10 Thermogravimetric analysis

Thermogravimetric analysis (TGA) of NR and HNRs was performed on a Perkin-Elmer STA 6000. The temperature of the sample was ramped from 30°C to 600°C at a heating rate of 5, 10, 15, and $20^\circ\text{C}/\text{min}$ under an oxygen atmosphere. The initial decomposition temperature (T_i) was obtained from the intersection of two tangents at the initial stages of the decomposition. The kinetics of decomposition were analyzed to estimate the activation energy by using Kissinger-Akahira-Sunose (KAS) equation (Aboulkas and El Harfi, 2008; Slopicka *et al.*, 2011; Blaine and Kissinger, 2012),

$$\ln \frac{\beta}{T_z^2} = \ln \frac{k_0 R}{E_a g(\alpha)} - \frac{E_a}{RT_z} \quad (3.6)$$

where k_0 is a constant, E_a is the activation energy, R is gas constant, $g(\alpha)$ is the kinetic model or the “some-function-of α ”, α is the fraction of reactant remaining, β is heating rate, and T_z is the decomposition temperature. The plot of $\ln (\beta/T_z^2)$ versus $1/T_z$ will give a straight line with a slope from which the activation energy can be calculated.

3.3 Properties of NR and HNR compounds and vulcanizates

3.3.1 Preparation of HNR Compounds

The formulations used for preparing NR and HNR compounds were shown in Table 3.2. Rubber compounds were prepared using a 60 mL internal mixer, Brabender Plasticorder PL-2000, with fill factor of 0.8. The mixing was performed at 30°C and a rotor speed of 60 rpm. The rubber was first masticated for 2 min. Then, vulcanizing agents were added and mixed with the rubber for 8 min. The rubber compound was taken out and then sheeted using a two roll mill. The compound sheet was kept at room temperature for 24 hr before its cure properties being measured.

3.3.2 Cure Properties and Preparation of Vulcanized Rubber Sheet

The cure properties of rubber compounds, such as minimum torque (M_L), maximum torque (M_H), scorch time ($t_{s,1}$), and cure time ($t_{c,90}$) were measured by using an oscillating disk rheometer, ODR 2000, at 180°C for 30 minutes. The biconical disk rotor was oscillated at amplitude of 1° and frequency of 1.67 Hz. M_L , M_H , $t_{s,1}$, and $t_{c,90}$ can be determined from the rheograph, a plot of torque versus time. Scorch time, $t_{s,1}$, is referred to as the time when the torque rises above M_L for 1 dN.m. The cure time, $t_{c,90}$, is the time to reach 90% of torque increase (M_{90})

$$M_{90} = M_L + \frac{90}{100}(M_H - M_L) \quad (3.7)$$

Vulcanized rubber sheets, about 1 mm thick, were prepared using a compression molding at 180°C and a pressure of 12.5 MPa. The rubber compounds were vulcanized according to their $t_{c,90}$ (Table 3.3). The vulcanized sheets were kept at room temperature for 24 hr before testing their physical properties.

Table 3.2 Formulations of rubber compounds

Ingredients	Vulcanization systems	
	Peroxide (phr)	Sulfur (phr)
Rubber (NR or HNRs)	100	100
DCP	1.0	-
TAC	0.6	-
Sulfur	-	1.50
TMTD	-	0.65
MBT	-	0.40
Zinc oxide	-	5.00
Stearic acid	-	1.00

phr - parts per hundred of rubber

Table 3.3 Cure time ($t_{c,90}$) for each rubber compounds

Rubbers	Cure time ($t_{c,90}$), min	
	Peroxide cure	Sulfur cure
NR	4.07	1.43
14 %HNR	4.15	1.55
33 %HNR	4.30	2.02
65 %HNR	4.00	1.60

3.3.3 Characterization of NR and HNR Vulcanizates

3.3.3.1 Ozone and Ultraviolet (UV) resistance test

A specimen of 1 mm thick and 3 mm wide was stretched to 30% deformation using a specimen holder before being placed in the ozone chamber. The specimen was exposed to ozone atmosphere of 50 ± 5 pphm at 40°C for 168 hr. After that it was removed from the chamber and kept at room temperature for a week before analyzing with Raman spectroscopy.

UV resistance test of rubber vulcanizates was conducted according to ASTM D1148 in a QUV accelerated weathering tester (Model QUV spray) at 50°C . The UV irradiance level was set to $0.77 \text{ W/m}^2 \cdot \text{nm}$ at 340 nm. A rectangular specimen, $62 \times 12 \text{ mm}^2$, was exposed to UV for 168 hr. After exposure, it was removed from the chamber and kept at room temperature for 1 week before characterizing with Raman spectroscopy.

The cracks on the surface and the change in chemical structures of rubber vulcanizates after ozone and UV aging were examined by using Raman spectroscopy which provides Raman spectra and the image of the cracks at the same time.

3.3.3.2 Raman Spectroscopy

Raman spectra of the surface cracks of NR, HNR and EPDM vulcanizates, before and after exposure to ozone and UV, were recorded with an Xplora-Horiba spectrometer adjusting the spectrograph configuration with a $1200 \text{ lines mm}^{-1}$ grating. Samples were illuminated with a He-Ne laser source selecting the red line at 785 nm. The Raman shift range was selected between $500 - 3500 \text{ cm}^{-1}$ with 50 accumulations and each acquisition time of 2 s. The slit and pinhole were set to 100 and $500 \mu\text{m}$, respectively.

The normalized peak integral intensities of C=C bonds from degree of hydrogenation and vulcanization system was determined while the change of peak intensity area which relates to the deleterious effect from ozone calculated by the subtraction of peak intensities of double bond signal of isoprene units after exposure by those before exposure (Overman and Thomas, 1999; Rich and Breton, 2002; Yu *et al.*, 2008).

The cracks on the surface of rubber vulcanizates were also investigated by using Raman spectroscopy with a microscope magnification x10 of objective lens in one-dimensional (1D) modes.

3.3.3.3 Tensile properties

The dumbbell test pieces were cut from a 1 mm thick vulcanized rubber sheet using die D according to ASTM D412. The tensile testing machine, model H10KS Hounsfield test equipment, was used to stretch the specimen with the cross head speed of 50 ± 5 mm/min. The narrow section of the specimen was marked with two pieces of reflective tape between which the distance was 10.0 mm. The deformation of the specimen was monitored by laser extensometer. Tensile properties of rubber vulcanizates, such as elongation at break, and tensile strength were calculated from all measured quantities. At least 3 specimens were tested.

A true stress (σ_t) can be calculated from

$$\sigma_t = \frac{F}{A} \quad (3.8)$$

where F is a force used to stretch the rubber and A is a true cross-sectional area. Rubbery materials are considered to be incompressible, i.e., there is no volume change upon deformation. Therefore, A can be approximated by Al_o/l and σ_t is given by

$$\sigma_t = \frac{Fl}{A_o l_o} \quad (3.9)$$

where A_o is an original cross-sectional area, l_o is an original length, and l is a deformed length.

A true strain (ε_t) was calculated from

$$\varepsilon = \ln \frac{l}{l_o} = \ln \frac{A}{A_o} \quad (3.10)$$

The tensile strength (TS, σ_{tb}) can be calculated from

$$\sigma_{tb} = \frac{F_b l}{A_o l} \quad (3.11)$$

where F_b is the force at break.

The elongation at break or ultimate strain (ε_b) is given by

$$\varepsilon_b = \frac{l_b - l_o}{l_o} \quad (3.12)$$

where l_b is the specimen length at fracture.

3.3.3.4 Crosslink density

The crosslink density of rubber vulcanizates was determined by equilibrium swelling measurements (Flory, 1953; Treloar, 1973; Sperling, 2005). A sample was weighed in the range of 0.38-0.40 g and immersed in toluene in a closed vial to reach swelling equilibrium. Then the sample was removed from the vial and the excess amount of solvent on the rubber surface was wiped out by paper. The sample was quickly weighed (w_1) and dried at 50°C for 168 h and weighed again (w_2). The volume fraction (ϕ_r) of the rubber in the swollen gel was calculated by Equation (3.13)

$$\phi_r = \frac{(w_2 / \rho_r)}{((w_1 - w_2) / \rho_s) + (w_2 / \rho_r)} \quad (3.13)$$

where ρ_s is the density of toluene (0.88 g/cm³) and ρ_r is the density of rubber. The crosslink density (ν), number of moles of network chains per unit volume, of the sample could be calculated from

$$\nu = -\frac{1}{\bar{V}_s} \frac{[\ln(1 - \phi_r) + \phi_r + \chi_1 \phi_r^2]}{\left(\phi_r^{1/3} - \frac{\phi_r}{2}\right)} \quad (3.14)$$

where \bar{V}_s is the molar volume of toluene (106.2 cm³/mol for toluene) and χ_1 is the polymer-solvent interaction parameter (0.42 for NR-toluene system).

3.4 Thermoplastic vulcanizates (TPVs) based on blends of HNRs and PP

3.4.1 Preparation of TPVs

The TPVs from blends of HNR and PP at various blends ratios, i.e., 70/30, 60/40, 50/50, 40/60 were prepared via dynamic vulcanization using peroxide and sulfur as vulcanizing agents. A 50 cm³ laboratory internal mixer, Brabender Plasticorder PL-2000, was employed to prepare all TPVs. The TPVs were mixed using fill factor of 0.8 at a constant rotor speed of 80 rpm and initial temperature of

180°C. Firstly, PP was melted for 3 min in the mixer. Then, a rubber compound prepared using the recipe in Table 3.2 according to method in 3.3.1 was added and mixed with PP until the constant torque was reached. The mixing for each batch took 10 min. After complete mixing, the TPV was removed from the mixer, sheeted on the two-roll mill, and kept at room temperature for 24 hr before investigating their physical properties.

TPV sheets were prepared by compression molding at 190°C and pressure of 12.5 MPa for 10 min, cooled down under pressure to room temperature, and stored at room temperature for 24 hr before their physical properties being tested.

3.4.2 Characterization of TPVs

3.4.2.1 Mixing Behavior and Dynamic Vulcanization

The mixing behavior and dynamic vulcanization of HNR-PP blends were analyzed from torque-time profiles obtained from Brabender Plasticorder PL-2000.

3.4.2.2 Raman mapping

The morphology of TPVs was investigated by using Raman spectroscopy with a microscope magnification $\times 10$ of objective lens. The samples were cut from frozen in liquid nitrogen.

Raman spectra of the blends were recorded with an Xplora-Horiba spectrometer. The experiment was performed at room temperature under microscope (Olympus BX 40) using a long distance work objective with a magnification $\times 50$. The simple spectrograph was adjusted with a 1200 lines per mm grating. The samples were illuminated with a laser light at 785 nm. The frequency range studied was 400-1800 cm^{-1} with 50 accumulations and an acquisition time of 2s per spectrum. The lateral resolution is dependent on the entrance slit, the selected objective, and the grating. In this case, the 100 μm entrance slit was used. Raman mapping was recorded by means of scanning a sample surface ($10 \times 10 \mu\text{m}^2$) by step size of 0.9 μm in both X- and Y-axes (point to point), which is lower than the lateral resolution in these conditions. The confocal pinhole conjugated to microscope was adjusted to 500 μm in this experiment and gives the depth resolution which can be

estimated in these conditions to $1\mu\text{m}$. Labspec 6 software was used to operate the mapping system, record spectra, and analyze the data.

The contents of TPV components can be calculated using the equations (3.15) and (3.16),

$$PP (\%) = \left(\frac{I_{(813-846)}}{I_{(813-846)} + I_{(1434-1664)}} \right) \times 100 \quad (3.15)$$

$$NR \text{ or } HNR (\%) = \left(\frac{I_{(1434-1664)}}{I_{(813-846)} + I_{(1434-1664)}} \right) \times 100 \quad (3.16)$$

where $I_{(813-846)}$ and $I_{(1434-1664)}$ are integrated peak intensities of PP phase in the range of 813 to 846 cm^{-1} and NR or HNR phase in the range of 1434-1664 cm^{-1} , respectively.

3.4.2.3 Phase size analysis

The sizes of cross-linked rubber particles dispersed in the thermoplastic matrix of TPVs were determined from Raman maps in comparison with electron micrograph from SEM. For Raman mapping, Image J software (an open source image processing program designed for scientific multidimensional images) was used to calculate the phase size (Igathinathane *et al.*, 2008; Greaves *et al.*, 2008).

3.4.2.4 Scanning electron microscopy

The fracture surfaces of TPVs were studied using Jeol (JSM-6510LV) scanning electron microscopy with an applied voltage of 15 kV. The dumbbell specimens were frozen in liquid nitrogen and fractured. The samples were then immersed in toluene at room temperature together with stirring for 120 hr to extract dispersed rubber. The samples were dried and surface-coated with gold before characterization.

3.4.2.5 Dynamic mechanical analysis

Dynamic mechanical analysis (DMA) of rubber vulcanizates and TPVs was carried out using a Rheometrics RSA 2 analyzer. A strip specimen of 20 mm long, 4 mm wide, and 1 mm thick is used. The test was carried out in tension

mode. All tests were conducted at room temperature. Dynamic strain sweep test was carried out in range of 0.01 to 1 % at the frequency of 1 rad/s.

CHAPTER 4

RESULTS AND DISCUSSION

4.1 Preparation and characterization of hydrogenated natural rubbers

4.1.1 Non-catalytic hydrogenation of natural rubber latex

4.1.1.1 Chemical structure characterization of HNRs by ^1H -NMR

Hydrogenated natural rubbers (HNRs) were prepared by non-catalytic hydrogenation of NRL using diimide as hydrogenation reagent. Diimide was generated *in-situ* via reaction of hydrazine and hydrogen peroxide. The chemical structures of NR and HNRs were characterized using ^1H -NMR (Figure 4.1).

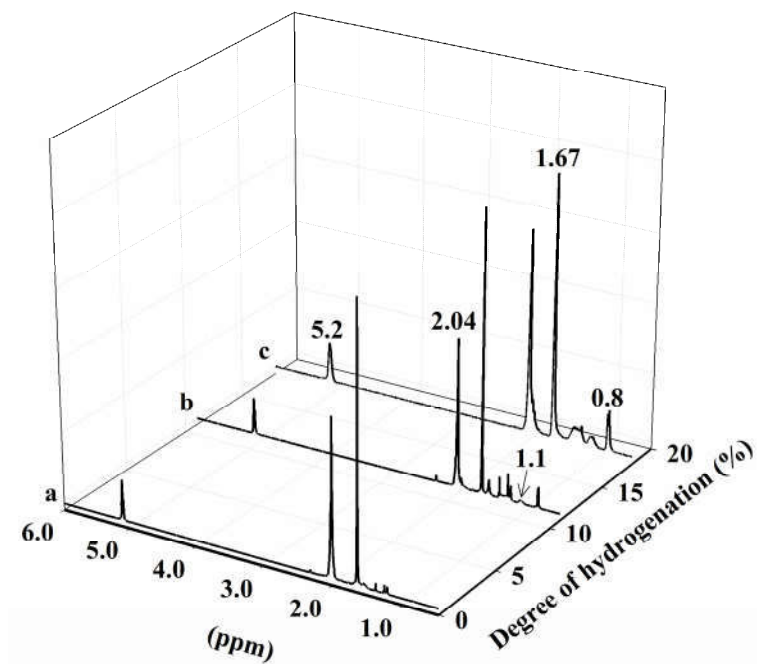
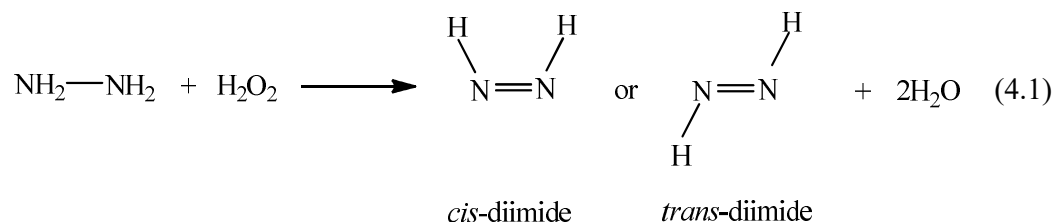


Figure 4.1 ^1H -NMR spectra of (a) 0 %HNR, (b) 11 %HNR and (c) 18 %HNR

The three main characteristic peaks of NR are at 1.67, 2.04, and 5.2 ppm, corresponding to proton signals of methyl and methylene groups of isoprene unit, and that adjacent to C=C bond, respectively (Samran *et al.*, 2004a). For HNRs, a decrease in the peak intensity at 5.2 ppm was observed together with appearance of methyl and methylene proton signals at 0.8 and 1.1 ppm, respectively, indicating the conversion of unsaturated double bonds to saturated units.

4.1.1.2 Effect of hydrazine

The effects of hydrazine concentrations on hydrogenation percentages were investigated by fixing the mole ratio of [C=C] to [H₂O₂] at 1:1. The amounts of hydrazine were varied from 0.5 to 2.0 moles. It was found that the degrees of hydrogenation increased with increasing moles of hydrazine from 0.5 to 1.5 (Figure 4.2) because of the increased amounts of diimide generated *in situ* (Xie *et al.*, 2003). Two forms of diimide, *cis*- and *trans*-configurations (equation (4.1)) can be generated (Paquette, 1991). However, only *cis*-diimide is an effective hydrogenation agent; *trans*-diimide is ineffective and easily decomposes to yield nitrogen and hydrogen gases (Hudlicky, 1984; Handt *et al.*, 2006). The maximum degree of hydrogenation was about 18%. Further increase in hydrazine concentrations caused a slight decrease in degree of hydrogenation possibly due to disproportionation of diimide to form hydrazine and nitrogen gas (Hudlicky, 1984).



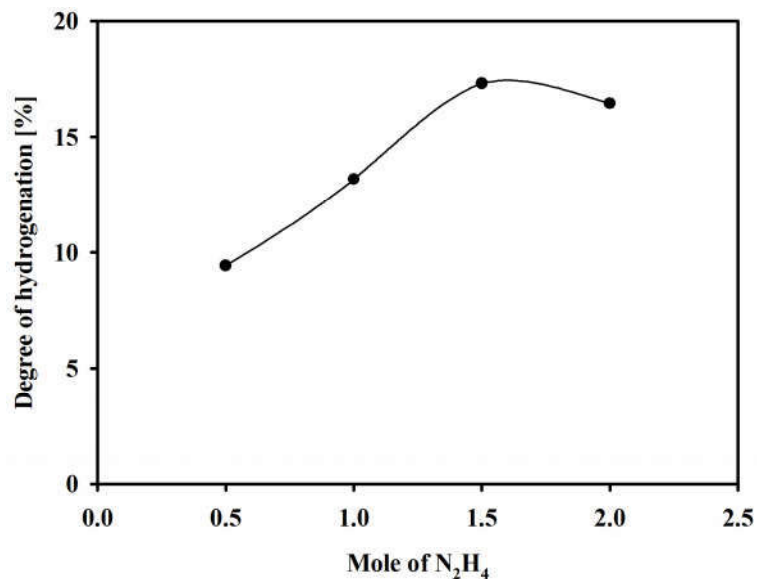
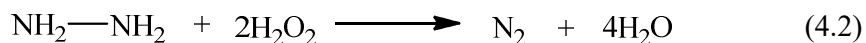


Figure 4.2 Effect of moles of hydrazine on degrees of hydrogenation of NRL (mole ratio of [C=C]:[H₂O₂] is 1:1)

4.1.1.3 Effect of hydrogen peroxide

The effects of hydrogen peroxide concentrations on hydrogenation levels were studied by fixing the molar ratio of [C=C] to [N₂H₄] at 1:1, and the hydrogenation reaction was carried out at 50 ± 3 °C for 24 hrs. It was found that degrees of hydrogenation increased with increasing moles of hydrogen peroxide up to 1.5, then slightly decreased (Figure 4.3). At lower moles (<1.5) of hydrogen peroxide the hydrogenation percentages increased due to the increase in concentrations of diimide generated *in situ*. The maximum hydrogenation level was about 15 %. At higher concentrations (>1.5 moles), the excessive hydrogen peroxide may react with hydrazine to form nitrogen gas and water (equation (4.2)) resulting in lower amounts of diimide, hence, lower degrees of hydrogenation (Xie *et al.*, 2003).



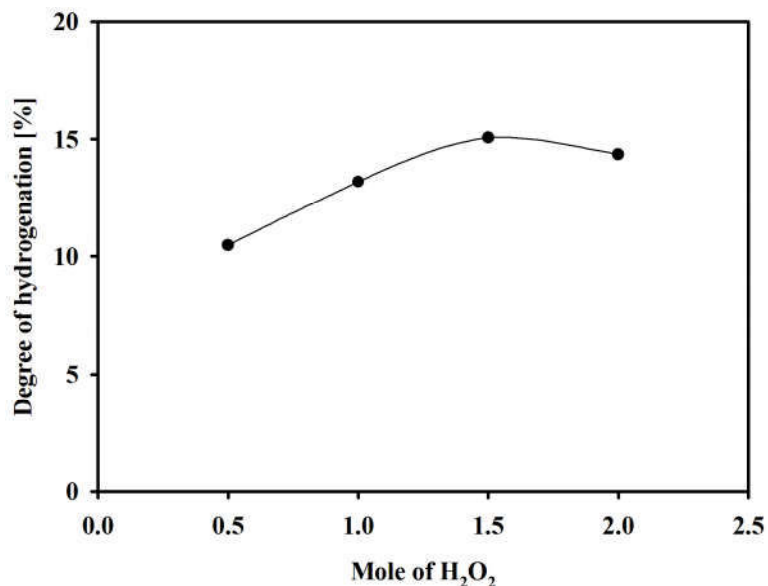


Figure 4.3 Effect of moles of hydrogen peroxide on degrees of hydrogenation of NRL (mole ratio of [C=C]:[N₂H₄] = 1:1)

Furthermore, redox reaction between hydrogen peroxide and hydrazine together with thermal decomposition of hydrogen peroxide can generate hydroxyl radicals which cause crosslinking between rubber molecules to form gel (Xie *et al.*, 2003).

From the results above, it can be seen that variation in moles of hydrazine and hydrogen peroxide was insufficient to obtain high degrees of hydrogenation of NRL. The maximum hydrogenation levels of NRL were about 15-18 %.

4.1.1.4 Effects of reaction temperature and time

The effects of reaction temperature and reaction time on the degrees of hydrogenation were studied by using the molar ratio of [C=C]:[N₂H₄]:[H₂O₂] at 1:1.5:1 and volume ratio of toluene to NRL at 0.1. Small amount of toluene was used with the expectation that degrees of hydrogenation of NRL could be improved. The range of temperature was 30-60 °C and time period was 2-24 hrs. The degrees of hydrogenation increased with increasing reaction temperature (Figure 4.4). The activity of reacting species is low at low temperature.

As reaction temperature was increased, the activity and collision of reacting species increased, enhancing the hydrogenation percentages of the product. However, hydrogenation reaction is strongly exothermic. At 60 °C small amounts of natural rubber latex coagulated due to less stability, and the reaction was difficult to control due to formation of gas bubbles during addition of hydrogen peroxide. From these reasons, the suitable reaction temperature was at 50 °C. The degrees of hydrogenation also increased with increasing reaction time (Figure 4.4) since reacting species had more chances to collide with each other.

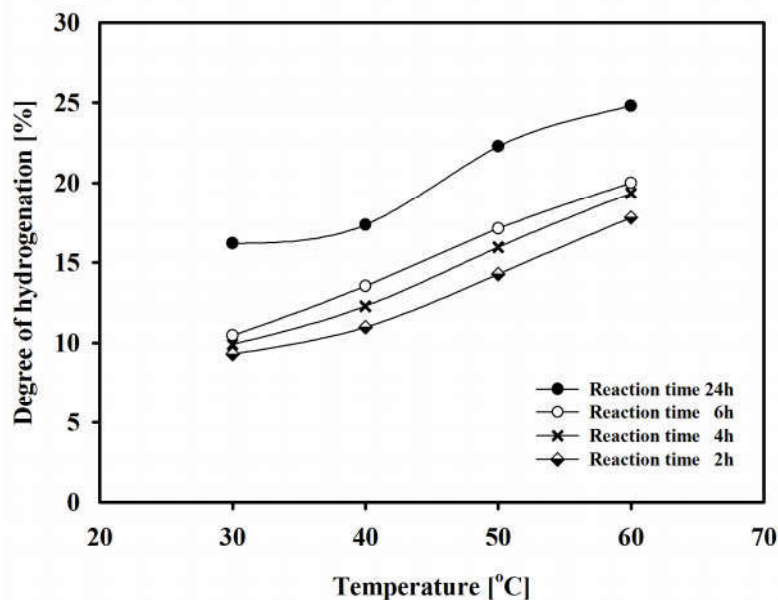


Figure 4.4 Effect of reaction temperature and reaction time on degrees of hydrogenation of NRL (mole ratio of $[C=C]:[N_2H_4]:[H_2O_2]$ is 1:1.5:1 and volume ratio of toluene to NRL is 0.1)

4.1.2 Improvement of hydrogenation levels of NRL

Non-catalytic hydrogenation of NRL seemed not to yield high hydrogenation levels possibly due to confinement of hydrogenation agents only at the surface of the latex particle. To improve hydrogenation degrees of NRL, solvents like hexane and toluene were used to swell rubber particles aiming that hydrogenation agents could diffuse into inside rubber particles and have more chances to react with unsaturated sites.

4.1.2.1 Effect of solvent types

Effects of toluene and hexane on ^1H -NMR of hydrogenated NRs were shown in Figure 4.5.

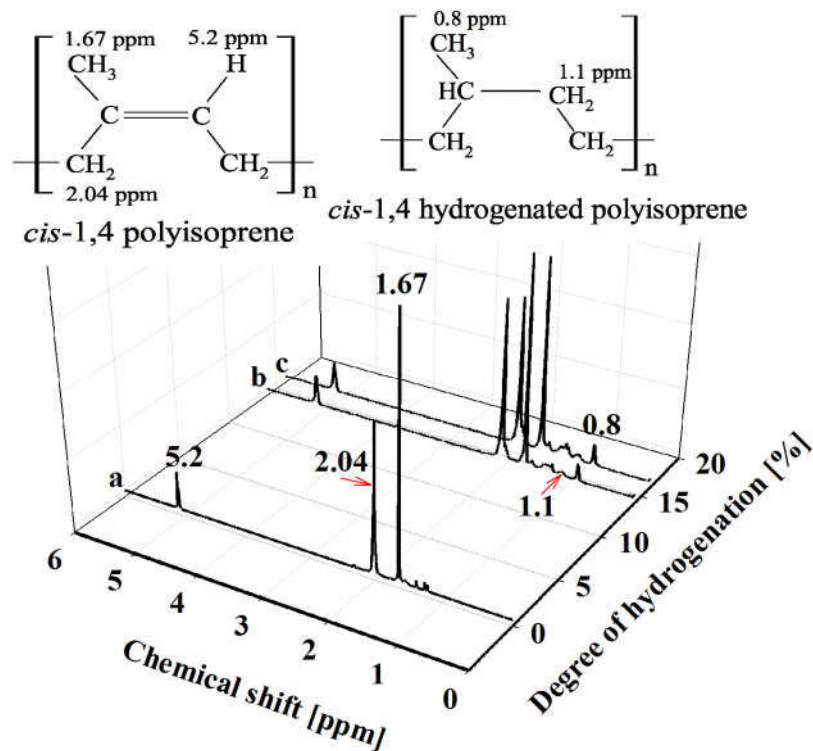


Figure 4.5 ^1H -NMR spectra of (a) NR, (b) 14 %HNR prepared by swelling NRL with hexane, and (c) 16 %HNR prepared by swelling NRL with toluene (volume ratio of solvent to NRL is 0.1)

In both cases, the intensity of the proton signals of isoprene units (1.67, 2.04, and 5.2 ppm corresponding to protons of methyl, methylene groups and that adjacent to C=C bond, respectively) decreased when compared to those of NR. The conversion of double bonds to saturated moiety was evidenced by appearance of the signals at 0.8 and 1.1 ppm, corresponding to methyl and methylene protons of saturated units, respectively. However, toluene resulted in 16 %HNR which was slightly higher than hexane (14 %HNR). Therefore, toluene was chosen for investigating the effect of volume of solvent on degree of hydrogenation.

4.1.2.2 Effect of solvent volume

Effects of volume ratios of toluene to NRL on $^1\text{H-NMR}$ and degrees of hydrogenation of hydrogenated NRs were shown in Figure 4.6 and 4.7, respectively.

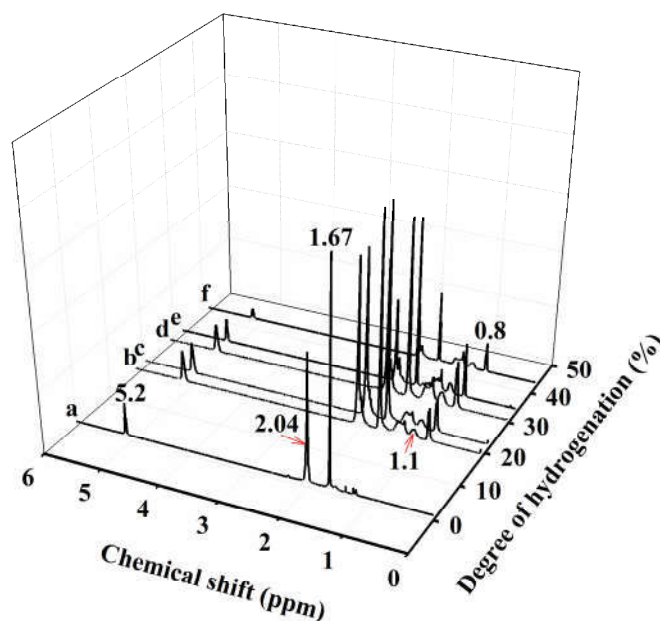


Figure 4.6 $^1\text{H-NMR}$ spectra of NR and HNRs at various toluene/NRL volume ratios; (a) NR, (b) 18 %HNR (no toluene), (c) 21 %HNR (volume ratio = 0.1), (d) 29 %HNR (volume ratio = 0.4), (e) 33 %HNR (volume ratio = 0.7), and (f) 42 %HNR (volume ratio = 0.1)

The increase in volumes of toluene resulted in the decrease in peak intensities of unsaturated units (1.67, 2.04, and 5.2 ppm, respectively) together with the increase in peak intensities of hydrogenated isoprene units (0.8 and 1.1 ppm, respectively) indicating the increase in hydrogenation levels. The maximum degree of hydrogenation was 42 %. The increased volumes of toluene caused more surface swelling of rubber particles (Figure 4.8). Therefore, more diimide could diffuse into the particles and react with unsaturated isoprene units to form hydrogenated products. However, hydrogenation apparently confined only at the swollen surface of the rubber particles.

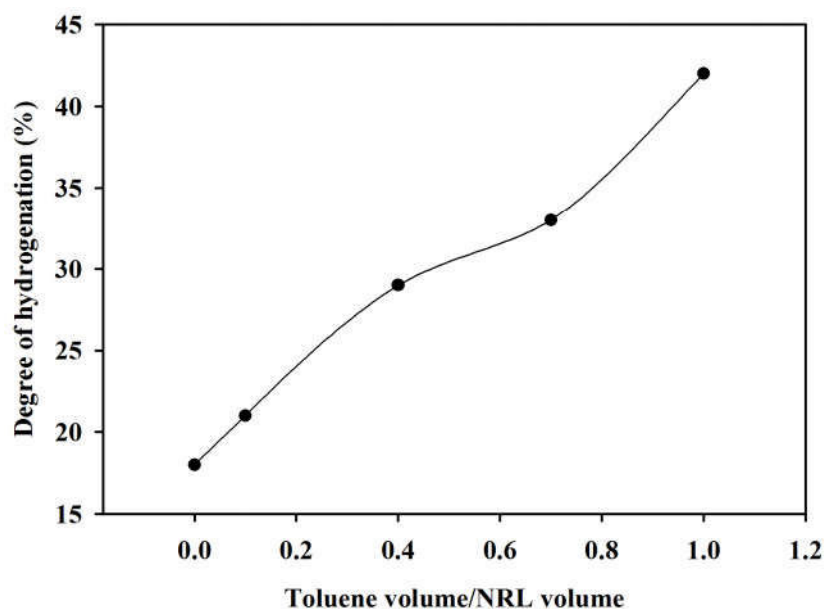


Figure 4.7 Effects of toluene /NRL volume ratios on degrees of hydrogenation of NRL

4.1.2.3 Effect of reaction scale-up

To further improve hydrogenation degrees of NRL, the effects of reaction scale-up were investigated. In this case, the reaction volume was increased from 250 mL to 650 mL using 2L reactor. The effects of reaction scale-up on hydrogenation levels of NRL were shown in Table 4.1. It was found that hydrogenation levels of NRL increased with reaction scale-up. The hydrogenation

level of 65 % was obtained. The increase in reaction volume resulted in the decreased volume of the space above the surface of the reaction mass in the reactor. As mentioned above hydrazine can react with hydrogen peroxide to form diimide or nitrogen gas. Furthermore, *trans*-diimide generated may decompose to yield nitrogen and hydrogen gases. Therefore, it was expected that there would be larger pressure build-up for the system with larger reaction volume. The pressure build-up would increase the opportunity for reacting species to react each other, resulting in higher degrees of hydrogenation (Figure 4.9).

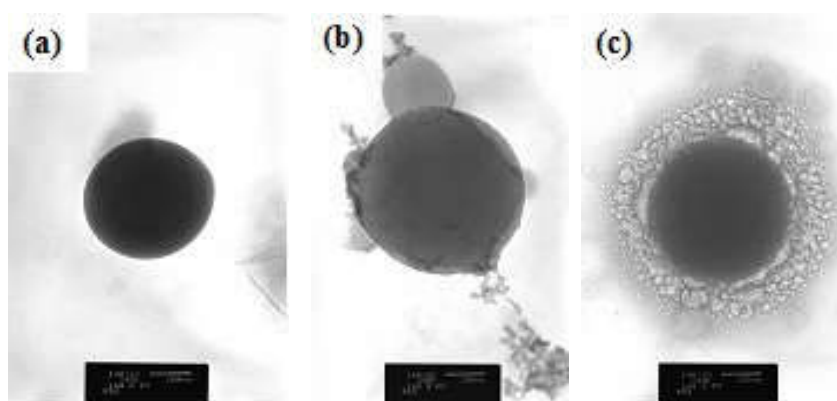


Figure 4.8 TEM images at 40k magnification of (a) unswollen NRL particle, (b) NRL particle swollen by 10 % volume of toluene, and (c) NRL particle swollen by 100 % volume of toluene

Table 4.1 Effects of reaction scale-up on degrees of hydrogenation of NRL

Mole ratios of [C=C]:[N ₂ H ₄]:[H ₂ O ₂]	Volume ratios of toluene to NRL	Degrees of hydrogenation (%) at different reaction volumes	
		250 mL	650 mL
1:0:0	0.0	0	0
1:1:0.5	0.0	10	14
1:1.5:1	0.1	21	33
1:1.5:1	1.0	42	65

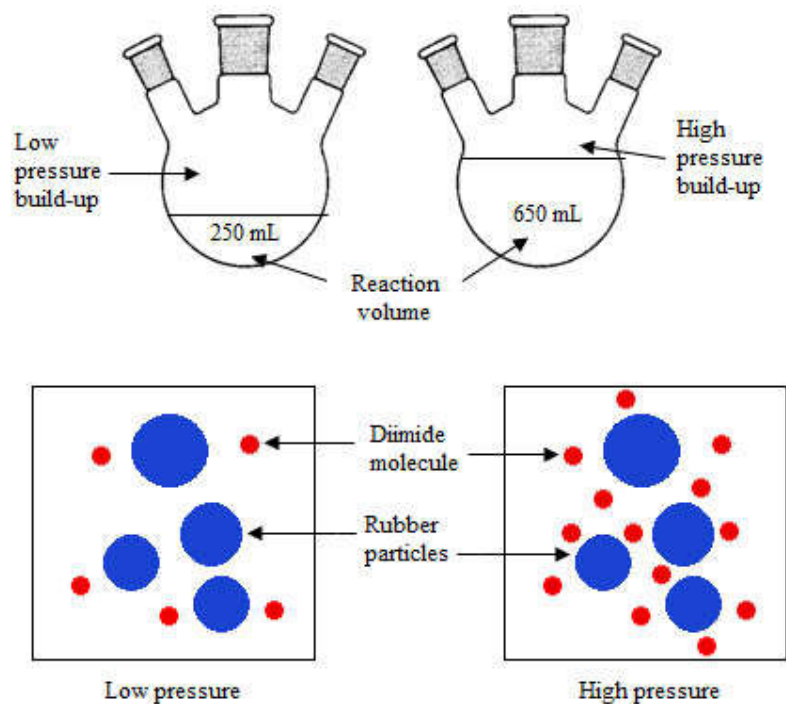


Figure 4.9 Possibility effects of increased reaction volume on collision of reacting particles due to high pressure build-up

$^1\text{H-NMR}$, Raman and FT-IR spectra of NR and HNRs prepared by reaction scale-up were shown in Figures 4.10, 4.11, and 4.12, respectively. The increase in hydrogenation degrees was evidenced by the decrease in intensities of the characteristic peaks of unsaturated parts at 1.67, 2.04, and 5.2 ppm, respectively, and the increase in peak intensities of saturated parts at 0.8 and 1.1 ppm

Raman spectra of NR and HNRs presented in Figure 4.11 revealed the decrease in the peak intensity at 1000 cm^{-1} , 1309 cm^{-1} and 1665 cm^{-1} , corresponding to frequencies of C-CH₂ stretching, -CH₃ wagging, and C=C bond, respectively (Jackson *et al.*, 1990; Bunce *et al.*, 1993; Hendra and Jackson, 1994; Healey *et al.*, 1996; Samran *et al.*, 2004a). The increase in peak intensities at 817 cm^{-1} (-CH wagging), 1434 cm^{-1} (-CH₂- symmetric stretching) and 2966 cm^{-1} (-CH₃ asymmetric stretching) with increasing degrees of hydrogenation was also observed.

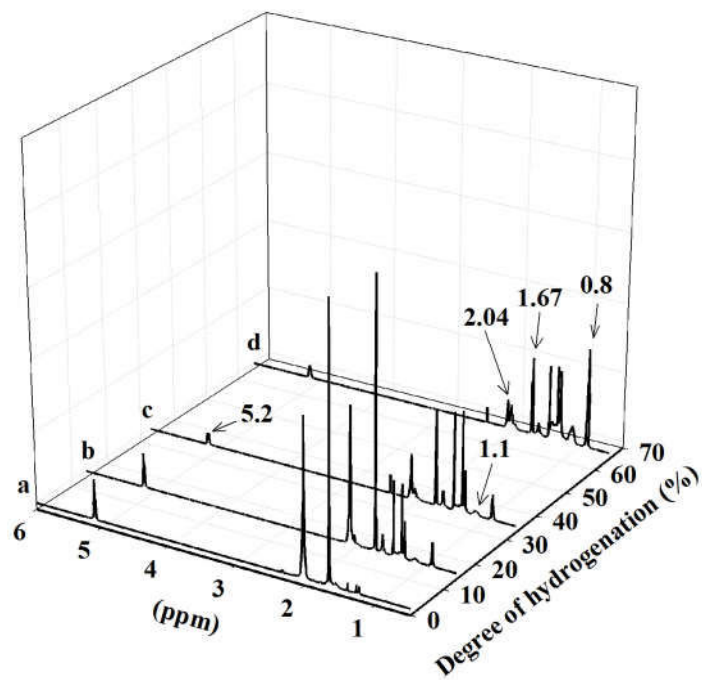


Figure 4.10 $^1\text{H-NMR}$ spectra of (a) NR, (b) 14 %HNR, (c) 33 %HNR and (d) 65 %HNR

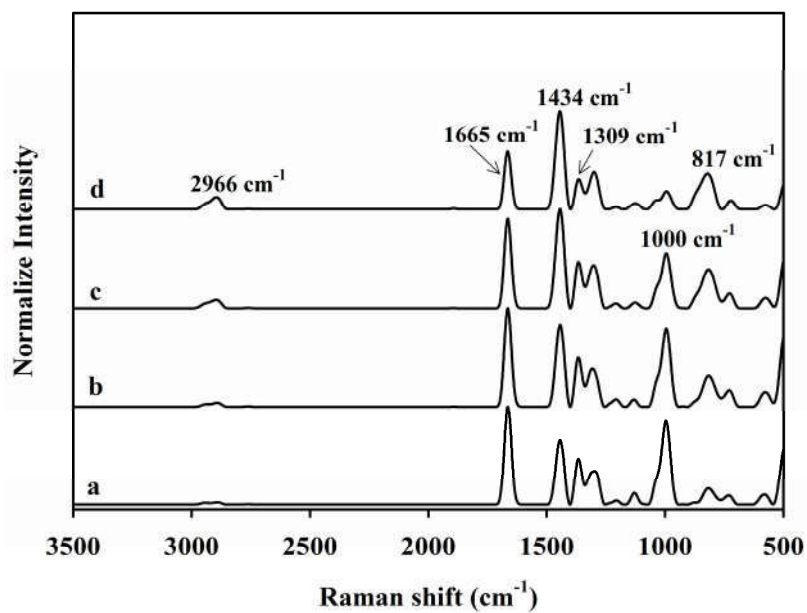


Figure 4.11 Raman spectra of (a) NR, (b) 14 %HNR, (c) 33 %HNR, and (d) 65%HNR

The FT-IR spectra of NR and HNRs were shown in Figure 4.12. The increasing hydrogenation levels resulted in the decrease in peak intensities at 575 cm^{-1} , 836 cm^{-1} , 1374 cm^{-1} , 1456 cm^{-1} , 1664 cm^{-1} , 2856 cm^{-1} , and 2962 cm^{-1} peaks, corresponding to frequencies of C–H out of plane bending, C–H bending, $-\text{CH}_3$ bending, $-\text{CH}_2-$ scissoring, C=C bond stretching, $-\text{CH}_3$ symmetric stretching, and $-\text{CH}_3$ asymmetric stretching, respectively. In contrast, the intensity of the peak at 739 cm^{-1} ($-\text{CH}_2-$ rocking) and 2924 cm^{-1} ($-\text{CH}_2-$ asymmetric stretching) increased with increasing degrees of hydrogenation.

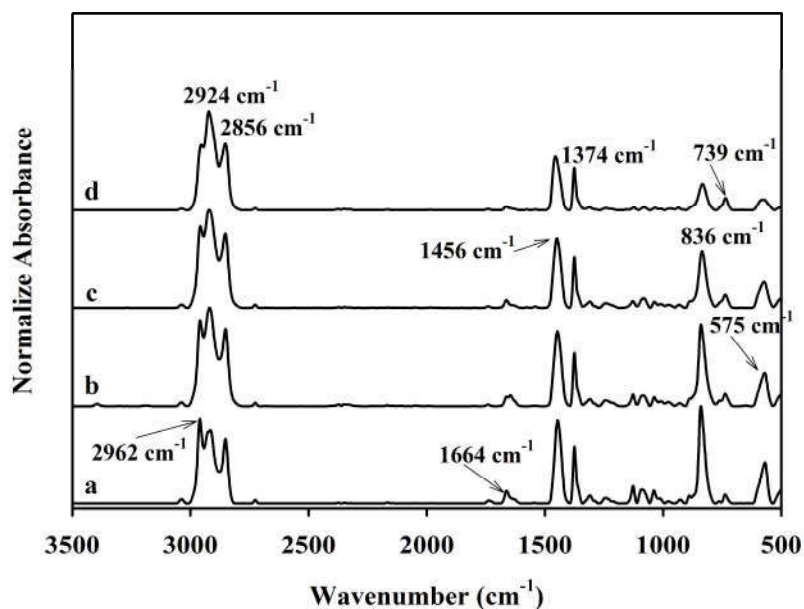


Figure 4.12 FT-IR spectra of (a) NR, (b) 14 %HNR, (c) 33 %HNR, and (d) 65 %HNR

The degrees of hydrogenation of HNRs calculated from Raman spectra (shown in Table 4.2) were correlated well with those calculated from ^1H -NMR spectra (Figure 4.13).

Table 4.2 Hydrogenation levels of HNRs calculated from ^1H -NMR and Raman spectra

Mole ratios of [C=C]:[N ₂ H ₄]:[H ₂ O ₂]	Volume ratios of toluene to NRL	Degrees of hydrogenation (%) at reaction volume of 650 mL	
		^1H -NMR	Raman
1:0:0	0.0	0	0
1:1:0.5	0.0	14	16
1:1.5:1	0.1	33	32
1:1.5:1	1.0	65	63

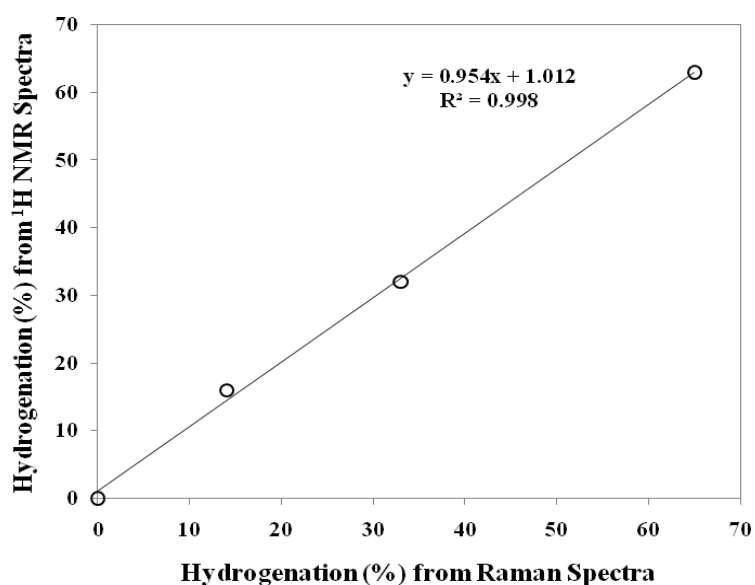


Figure 4.13 Correlation between degrees of hydrogenation calculated from Raman and ^1H NMR spectra

4.1.2.4 *cis-trans* isomerization

During the progress of hydrogenation reaction, *cis-trans* isomerization of isoprene unit also occurred. Figure 4.14 showed ^1H -NMR spectra of NR and HNRs in the range of 1.60 - 1.70 ppm. The characteristic peak at 1.67 ppm corresponded to the methyl proton of *cis*-isoprene unit. The intensity of this peak apparently decreased with increasing hydrogenation degrees of HNRs. However, a new characteristic peak at 1.64 ppm, corresponding to the methyl proton of *trans*-isoprene unit, was observed. The intensity of this peak tended to increase with increasing hydrogenation levels of HNRs.

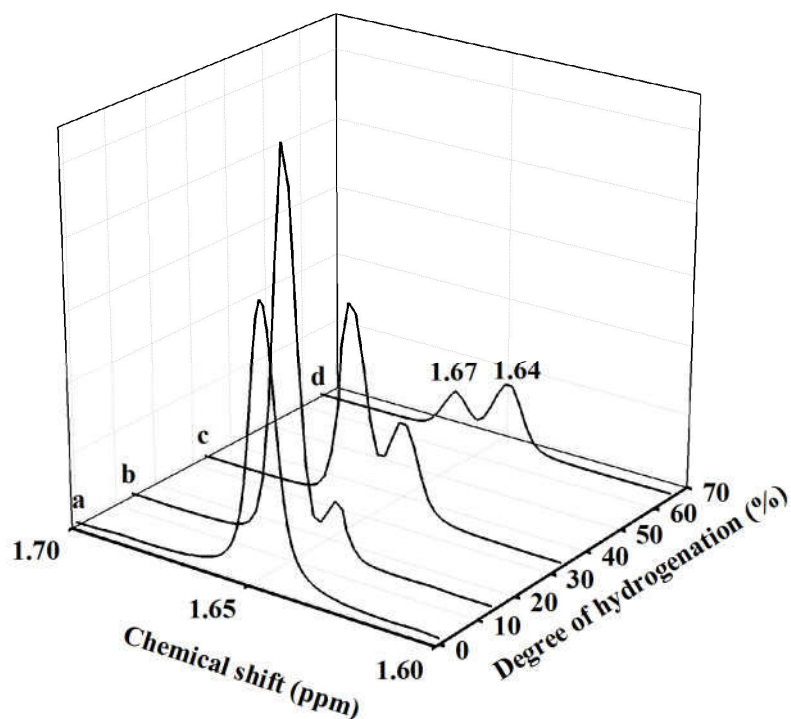


Figure 4.14 ¹H-NMR spectra of (a) NR, (b) 14 %HNR, (c) 33 %HNR, and 65 %HNR

Variation in *cis* and *trans* contents with hydrogenation degrees of HNRs was shown in Figure 4.15. The amounts of *cis* structure decreased with increasing hydrogenation degrees in contrast to *trans* structure. Hydrogenation of NR required hydrogen atoms released from diimide molecules to react with carbon-carbon double bonds of isoprene units. The intermediates were unstable and *cis-trans* isomerization could be taken place through rotation of the weak double bond as shown in Figure 4.16 (Samran, 2005). *Cis* structure in the backbone chain resulted in flexible and elastic material while *trans* structure made rubber hard and less elastic (Daniel *et al.*, 2010).

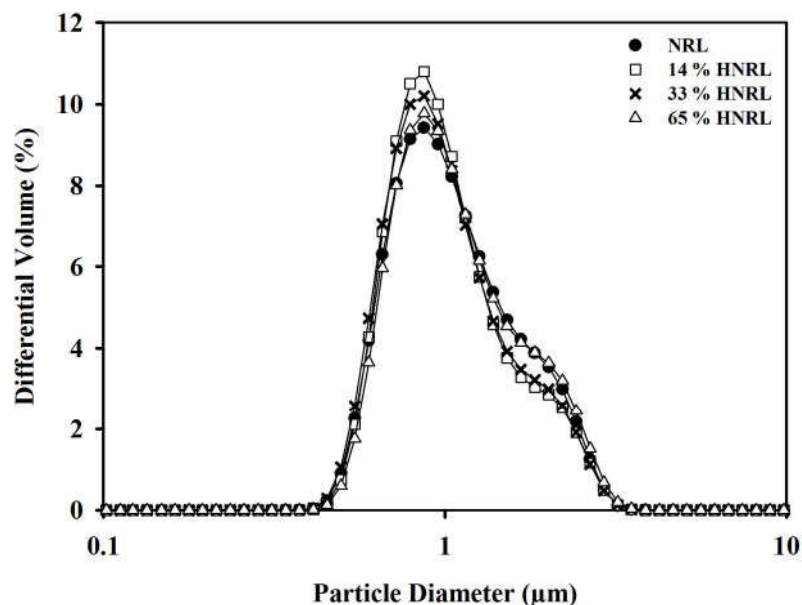


Figure 4.17 Particle size distributions of various lattices; NRL, 14%HNRL, 33%HNRL, and 65%HNRL

Table 4.3 Average particle size of NRL and HNRL

Latices	Particle size range (μm)	Mean particle size (μm)	S.D. (μm)
NRL	0.342 - 4.240	1.215	0.538
14 % HNRL	0.375 - 4.655	1.165	0.518
33 % HNRL	0.342 - 4.240	1.165	0.524
65 % HNRL	0.375 - 4.655	1.239	0.557

4.2 Properties of HNRs

4.2.1 Appearance

Appearance of dried solid NR and HNRs was shown in Figure 4.18. It was seen that the color of the rubber turned from amber-like for NR into more white with increasing hydrogenation contents. This may be due to transformation of carbon-carbon double bonds to carbon-carbon single bonds and *cis-trans* isomerization.

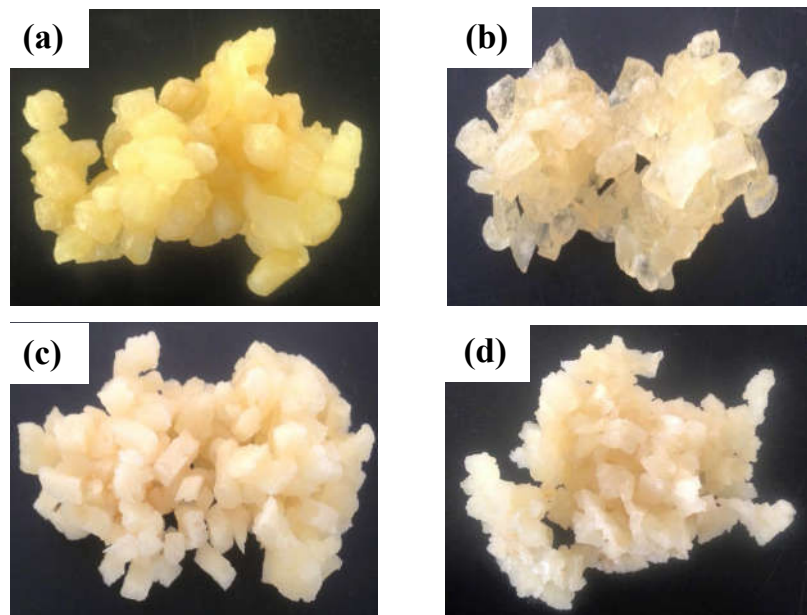


Figure 4.18 Appearance of (a) NR, (b) 14 %HNR, (c) 33 %HNR and (d) 65 %HNR

4.2.2 Gel content

HNRs prepared by non-catalytic hydrogenation contained significant amounts of gel. Apparently, gel contents increased with increasing hydrogenation degrees of HNRs (Figure 4.19), indicating that crosslinking reaction also took place during hydrogenation. This was due possibly to hydroxyl radicals generated from the thermal decomposition of H_2O_2 could initiate crosslinking (Figure 4.20).

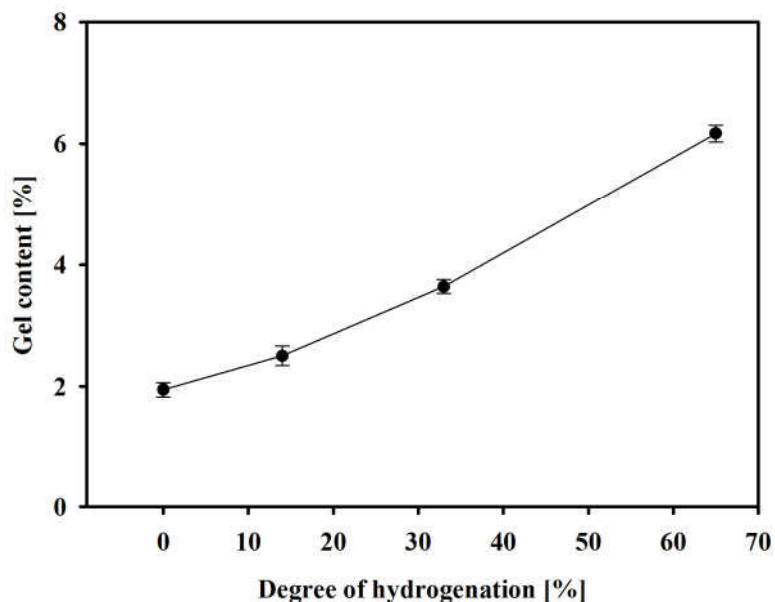


Figure 4.19 Gel content as a function of hydrogenation levels of HNRs

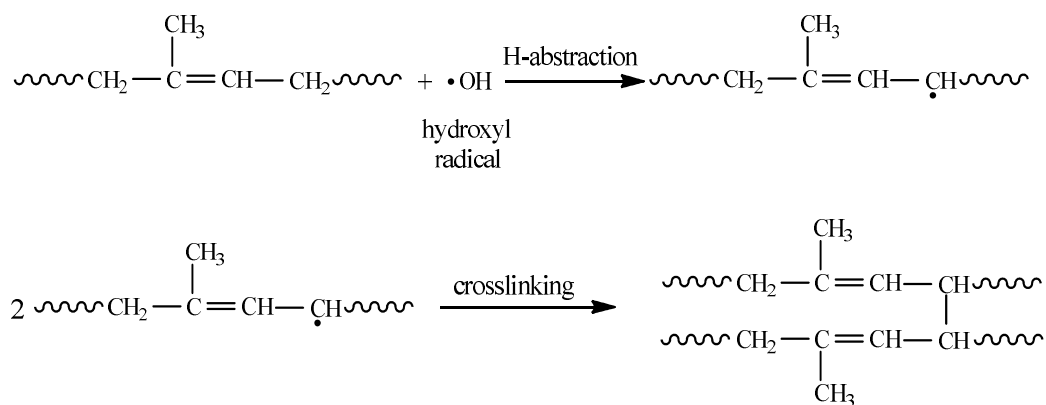


Figure 4.20 Crosslinking reaction initiated by hydroxyl radical ($\cdot\text{OH}$)

4.2.3 Hardness

The effect of hydrogenation levels on hardness of HNRs was shown in Figure 4.21. It was notably that hardness of HNRs increased with increasing degrees of hydrogenation. The increase in the amounts of saturated unit and *trans* structure during hydrogenation resulted in stiffer chain molecules and hence hardness of the rubbers.

4.2.4 Glass transition temperature (T_g)

DSC thermograms of NR and HNRs were shown in Figure 4.22. It was seen that T_{gs} of NR and HNRs were similar and T_g of HNRs were not affected by the increase in degrees of hydrogenation. These results were similar to those reported by Hinchiranan *et al.* (2006b) and Mahittikul *et al.* (2007a). As mentioned previously hydrogenation reaction confined largely at the surface of rubber particles, thus, the core of the rubber particle was still mainly NR. This was probably the reason why T_g of HNRs was independent of hydrogenation levels.

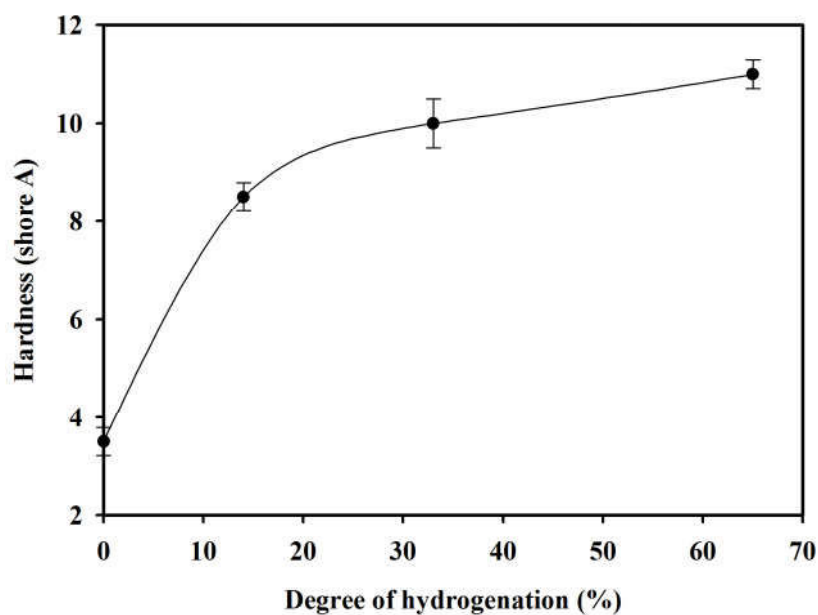


Figure 4.21 Effect of degree of hydrogenation on hardness of HNRs

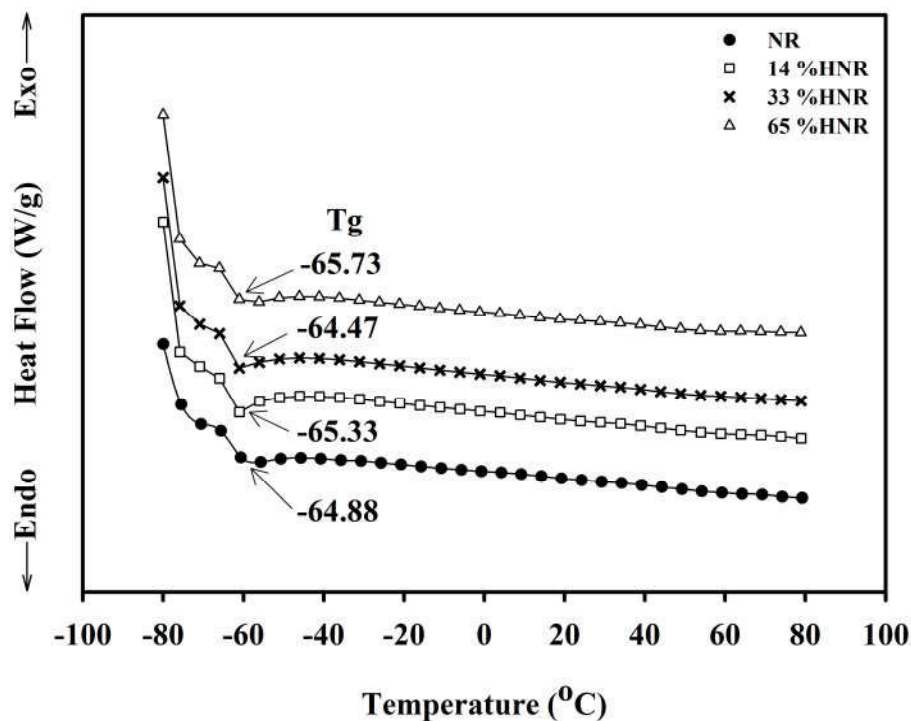


Figure 4.22 DSC thermograms of NR, 14 %HNR, 33 %HNR, and 65 %HNR

4.2.5 Rheological properties of NR and HNRs

4.2.5.1 Apparent shear stress and viscosity

Rheological properties of NR and HNRs were measured using capillary rheometer. Apparent shear stresses and viscosities of NR and HNRs as a function of shear rate were shown in Fig. 4.23. The apparent shear stresses of NR and HNRs increased with increasing apparent shear rates, while the apparent shear viscosities decreased, indicating shear thinning behavior. The power law indices (n) of NR (0.28) and HNRs (0.14 - 0.22) were less than 1 as shown in Table 4.4. For HNRs, the power law indices slightly decreased with increasing degrees of hydrogenation, suggesting that materials were more slightly difficult to flow. This was probably due to larger gel contents present in HNRs with higher degrees of hydrogenation. At low shear rates, shear stresses and viscosities of HNRs increased with increasing hydrogenation degrees due to gel present in the rubbers and structural changes from unsaturation to saturation.

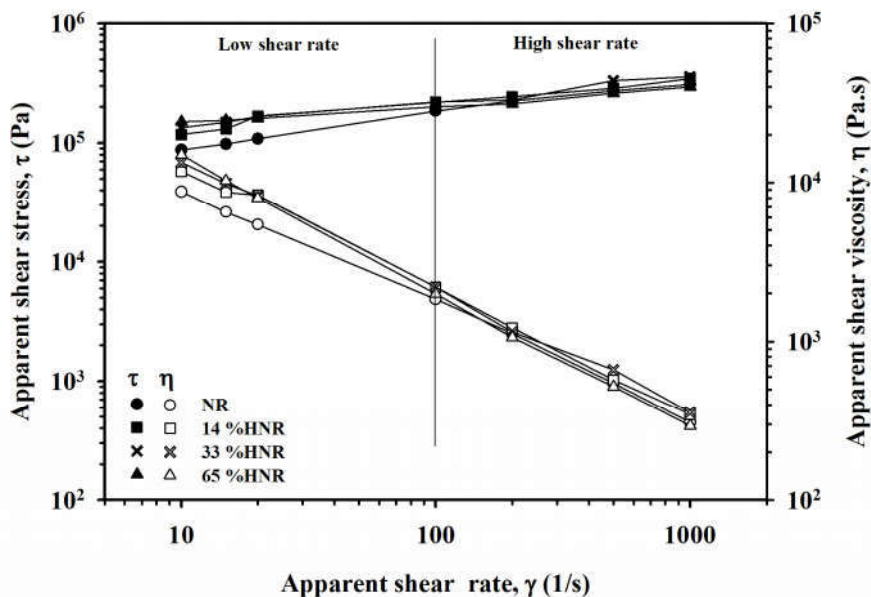


Figure 4.23 Apparent shear stresses and viscosities of NR and HNRs as a function of shear rate

Table 4.4 Power law index (n) and flow consistency (K)

Rubbers	Low shear rate at $10\text{-}100\text{ s}^{-1}$		High shear rate at $100\text{-}1000\text{ s}^{-1}$		All shear rate at $10\text{-}1000\text{ s}^{-1}$	
	K^* (kPa)	n	K (kPa)	n	K (kPa)	n
NR	40.73	0.33	67.61	0.22	46.68	0.28
14 %HNR	66.07	0.26	87.10	0.20	76.42	0.22
33 %HNR	85.11	0.21	70.79	0.24	84.20	0.21
65 %HNR	110.15	0.13	87.09	0.17	104.40	0.14

*The higher K the more 'viscous' (Tanner, 2000)

However, at high shear rates the shear stresses, viscosities and flow consistency (K) of HNRs were less dependent on degrees of hydrogenation and gel present in the rubbers. As the shear rates were increased, rubber molecules oriented and aligned along the shear field, and disentangled. Break-up of physical and chemical crosslinks by high shear force was also possible (Figure 4.24). These resulted in the increase in shear stress and the decrease in viscosity (Tanner, 2000).

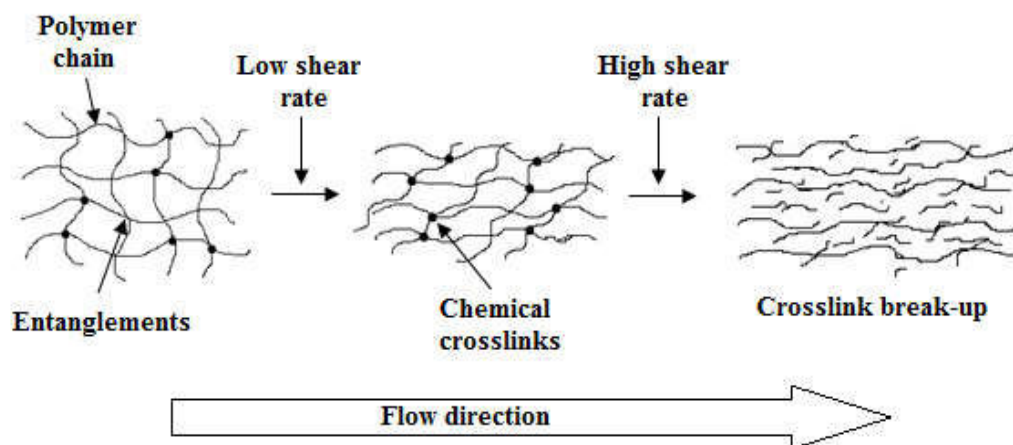


Figure 4.24 Schematic of structural orientation of polymers under shear field

4.2.5.2 Mooney Viscosity and Mooney Stress Relaxation

The changes in Mooney torques with time of NR and HNRs were shown in Figure 4.25. Apparently, Mooney torque of NR was nearly constant with time, while those for HNRs largely decreased with time in the initial stage (zone A) indicating thixotropic behavior. This was presumably due to the movement of ethylene-propylene segments present in HNRs. After that (zone B) Mooney torques slightly increased with time due to gel present in HNRs. Mooney viscosities, reported as $ML(1+4) @ 125\text{ }^{\circ}\text{C}$ (Table 4.5), of HNRs increased with increasing hydrogenation levels because of the increased gel contents present in the rubbers.

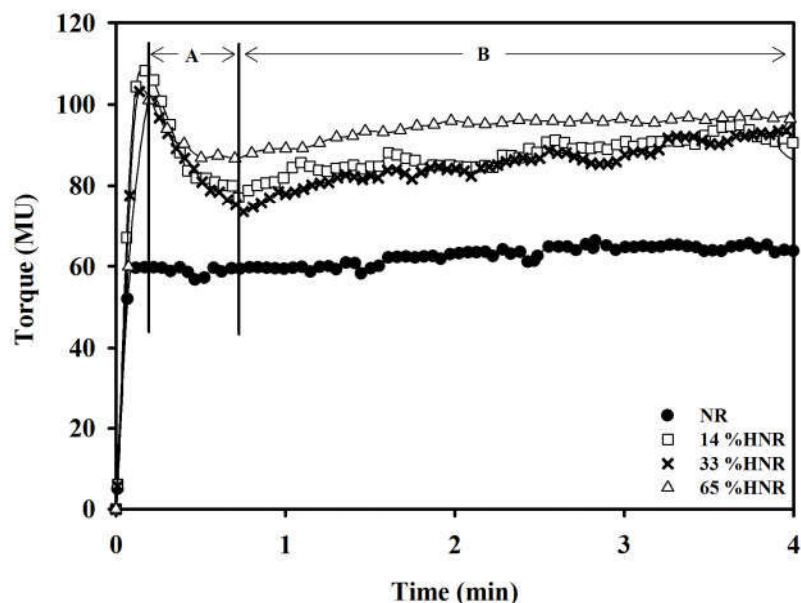


Figure 4.25 Time-dependent Mooney viscosities of NR, 14 %HNR, 33 %HNR and 65 %HNR

Table 4.5 Mooney viscosity and relaxation rate of NR and HNRs

Rubbers	ML(1+4) @ 125°C	<i>a</i>
NR	63.7	- 0.150
14%HNR	90.4	- 0.168
33%HNR	93.9	- 0.156
65%HNR	96.6	- 0.144

Mooney relaxation behavior of NR and HNRs was investigated immediately after rotor stop. The Mooney relaxation can be approximated by power law model;

$$\log M = a \log t + \log k$$

where M is Mooney torque during relaxation test, t is relaxation time, k is Mooney torque 1 s after the rotor stopped, and a is relaxation rate. The rubber with larger value of a , a steeper slope, will have higher viscoelastic to elastic ratio and lower elastic quality than rubber with flatter slope. Therefore, it will be easier to flow and process.

Mooney stress relaxation of NR and HNRs was illustrated in Figure 4.26 and relaxation rates were shown in Table 4.5. It was found that relaxation rates of NR and HNRs were similar. Although the increase in hydrogenation degrees resulted in the increase in ethylene-propylene segments, the gel contents were also increased (Figure 4.19). The former would enhance flow of HNRs, while the latter made HNRs more elastic. Therefore, relaxation behavior of NR and HNRs was balanced by presence of ethylene-propylene segments and gel.

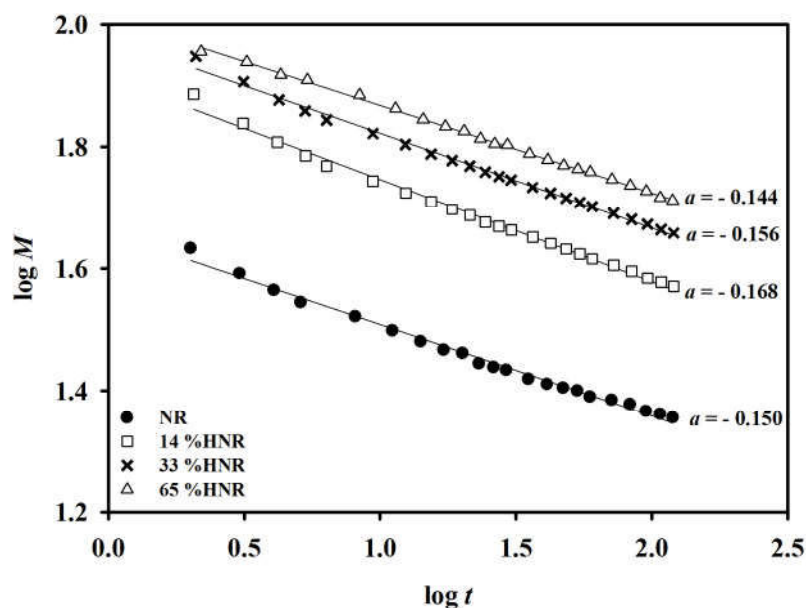


Figure 4.26 Mooney stress relaxation of NR, 14 %HNR, 33 %HNR and 65 %HNR

For HNRs, however, relaxation rate tended to slightly decreased with increasing hydrogenation levels due to the presence of gel, which made the rubber become more elastic.

4.2.6 Thermal properties

4.2.6.1 Decomposition properties

Decomposition temperatures (T_d) of NR, HNRs and EPDM were investigated using thermogravimetric analyzer (TGA). TGA thermograms, plots of weight loss (%) against temperature, of rubbers were shown in Figure 4.27 and derivatives of TGA curves were shown in Figure 4.28.

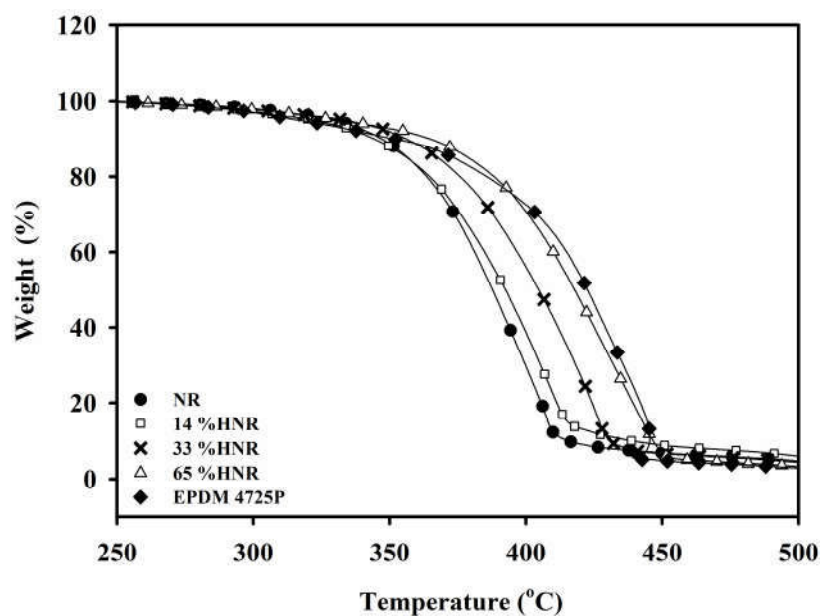


Figure 4.27 TGA curves of NR, 14 %HNR, 33 %HNR, 65 %HNR and EPDM (heating rate of 20°C/min under oxygen atmosphere)

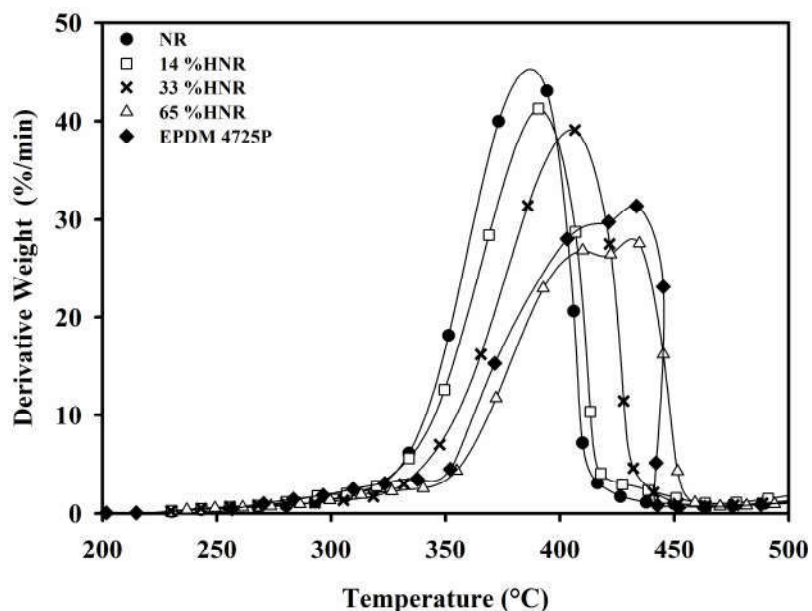


Figure 4.28 Derivatives of TGA curves of NR, 14 %HNR, 33 %HNR, 65 %HNR and EPDM (heating rate of 20°C/min under oxygen atmosphere)

Table 4.6 Decomposition temperatures of NR, HNRs and EPDM 4725P

Rubbers	T_d (°C)
NR	385.9
14 %HNR	390.8
33 %HNR	404.5
65 %HNR	431.1
EPDM 4725P	433.0

It was found that T_d of HNRs were higher than that of NR, but lower than that of EPDM (Table 4.6). For HNRs, the increase in degrees of hydrogenation shifted T_d to higher temperatures. NR contains carbon-carbon double bonds which are susceptible to oxidation. Hydrogenation of NR resulted in the increase in saturated carbon-carbon single bonds which were less susceptible to oxidation.

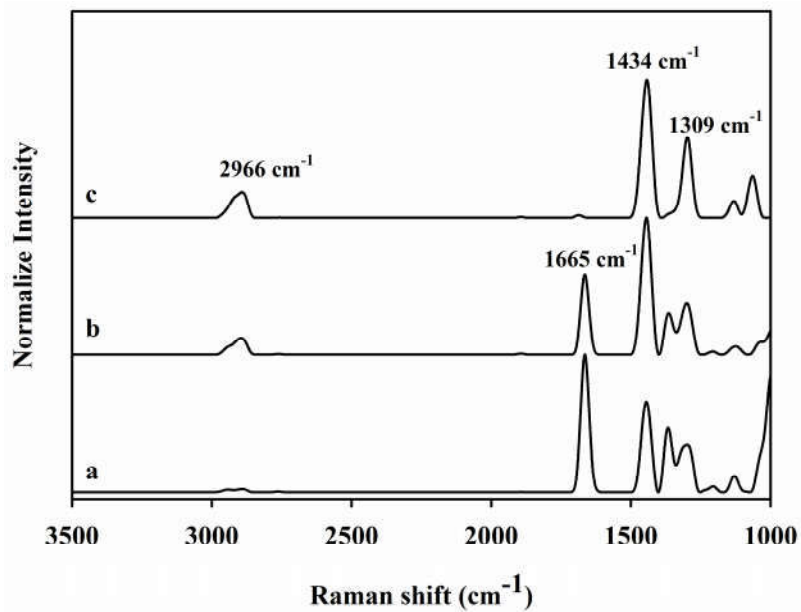


Figure 4.29 Raman spectra of (a) NR, (b) 65 %HNR and (c) EPDM 4725P

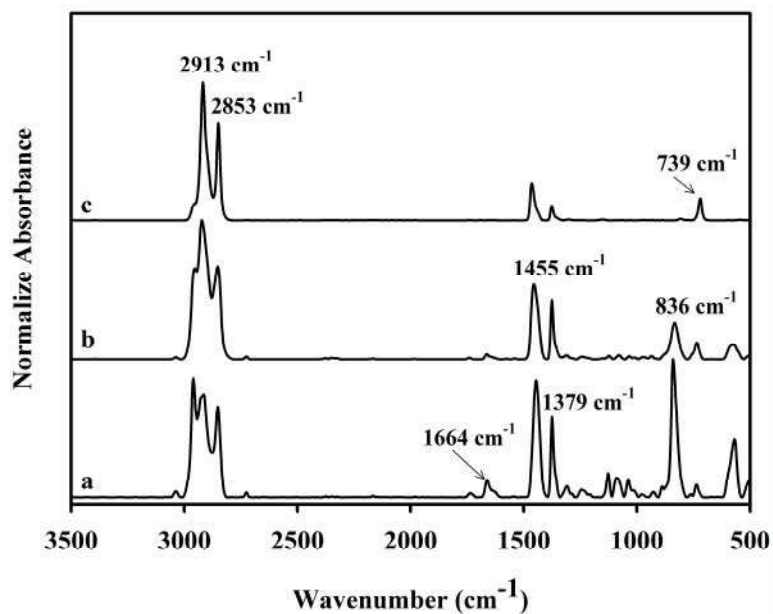


Figure 4.30 FT-IR spectra of (a) NR, (b) 65 %HNR and (c) EPDM 4725P

Therefore, thermal stability of HNRs was much improved when compared to NR. Thermal stability of HNRs increased with increasing hydrogenation levels. Thermal stability of 65 %HNR was comparable to that of EPDM because their chemical structure were very similar as confirmed by Raman and FT-IR spectra shown in Figures 4.29 and 4.30, respectively.

4.3 Vulcanization and physical properties of HNRs

4.3.1 Vulcanization properties of HNR compounds

ODR curves of NR and HNRs vulcanized by dicumyl peroxide (DCP) and sulfur at various temperatures were shown in Figure 4.31 and cure properties were shown in Tables 4.7 and 4.8.

For peroxide-cured rubbers, cure properties such as scorch time (t_{s1}) and cure time ($t_{c,90}$) decreased with increasing temperatures. At 150 °C, the rate of vulcanization was very slow due to decomposition of peroxide was not complete leading to small amounts free radicals that could initiate crosslinking. Therefore, torque rose slowly. At higher temperatures, peroxide easily decomposed and radicals generated could effectively initiate crosslinking, leading to rapid increase in torque. Although the rate of vulcanization at 180 °C was greater than that at 150 °C, slight reversion and smaller maximum torque was observed. This was due to thermal degradation of polymer chains under shear. For peroxide vulcanization, the optimum cure temperature was 180 °C. Apparently cure rates of HNR compounds were independent of degrees of hydrogenation.

For sulfur-vulcanized rubber compounds, t_{s1} and $t_{c,90}$ also decreased while vulcanization rate increased with increasing temperatures. However, reversion, thermal degradation of crosslink under dynamic shear, was pronounced at high temperatures.

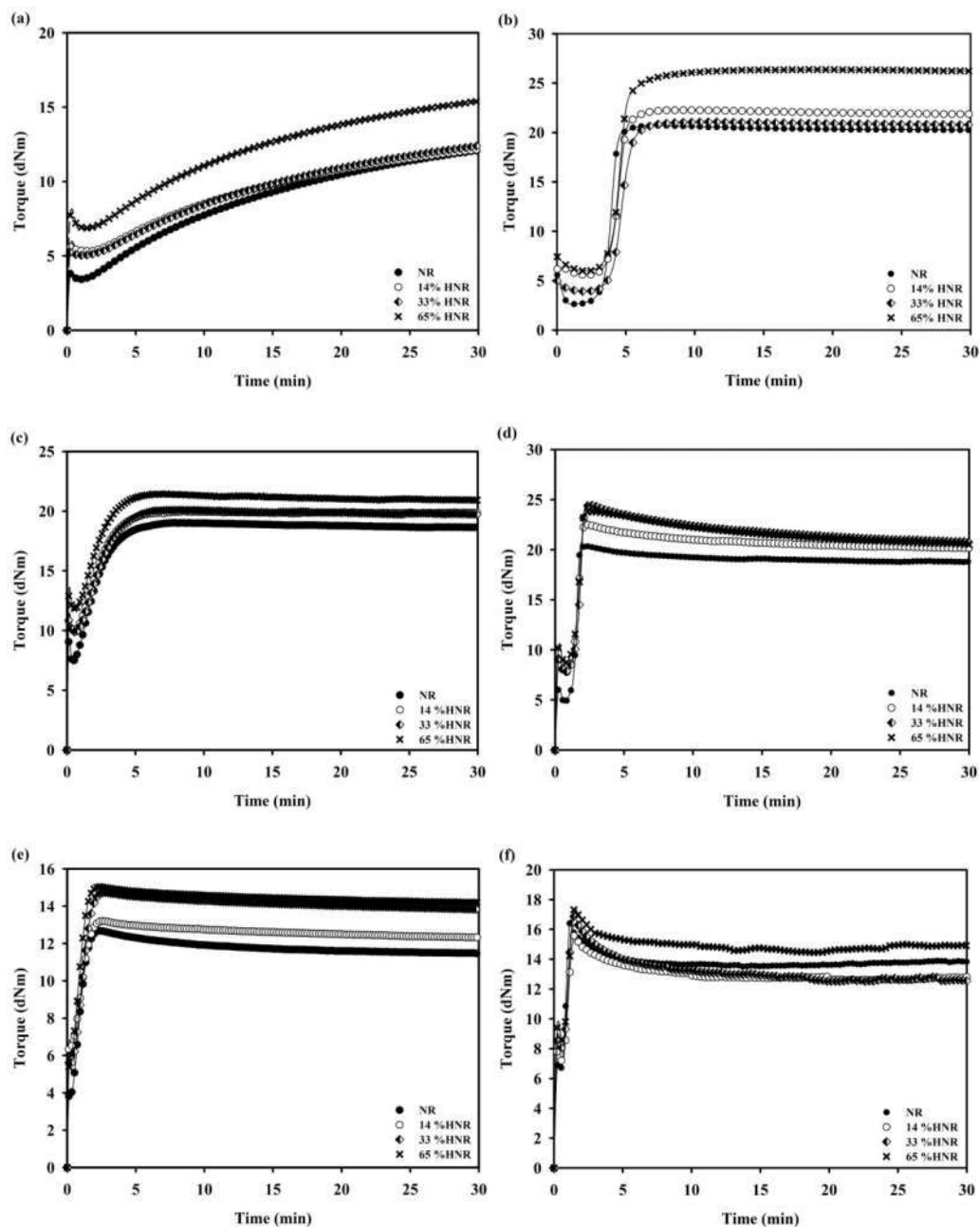


Figure 4.31 ODR curves of NR and HNR compounds vulcanized by dicumyl peroxide (left column) and sulfur (right column) at 150 °C (a, b), 180 °C (c, d), and 200 °C (e, f)

Table 4.7 Cure properties of peroxide-vulcanized rubber compounds at various temperatures

Rubbers	Cure properties											
	150 °C				180 °C				200 °C			
	M_H	M_L	T_{s1}	T_{c90}	M_H	M_L	T_{s1}	T_{c90}	M_H	M_L	T_{s1}	T_{c90}
NR	12.11	3.42	3.09	11.24	19.03	7.46	0.51	4.07	12.68	3.82	0.29	1.33
14 %HNR	12.18	5.32	4.20	11.50	20.00	9.96	1.03	4.15	13.20	6.34	0.36	1.45
33 %HNR	12.40	5.03	4.07	11.66	20.13	9.89	1.08	4.30	14.73	5.49	0.35	1.49
65 %HNR	15.42	6.87	3.40	14.56	21.45	11.86	1.06	4.01	15.05	5.60	0.25	1.30

Table 4.8 Cure properties of sulfur-vulcanized rubber compounds at various temperatures

Rubbers	Cure properties											
	150 °C				180 °C				200 °C			
	M_H	M_L	t_{s1}	$t_{c,90}$	M_H	M_L	t_{s1}	$t_{c,90}$	M_H	M_L	t_{s1}	$t_{c,90}$
NR	20.68	2.58	2.56	4.27	20.38	4.83	1.07	1.43	16.40	6.02	0.33	1.00
14 %HNR	22.26	5.60	3.28	5.11	22.49	7.72	1.09	1.55	15.58	7.14	0.45	1.13
33 %HNR	21.07	3.91	3.37	5.38	24.46	7.81	1.13	2.02	16.91	7.90	0.45	1.13
65 %HNR	26.38	5.99	3.26	5.34	23.81	8.71	1.10	1.57	17.32	8.60	0.48	1.15

4.3.2 Ozone and UV Resistance

Raman optical photographs of cracks on surfaces rubber vulcanized by peroxide and sulfur after exposure to ozone and UV were shown in Figures 4.32-4.35. The larger number of cracks was observed for NR vulcanizates, and cracks spread when compared to HNR vulcanizates due to larger amounts of C=C bonds in rubber molecules. Ozone cracking involved the attack of ozone on C=C bonds to form ozonide intermediate which caused chain scission and formation of decomposition products (Figure 4.36). For HNR vulcanizates, the number of cracks apparently decreased with increasing degrees of hydrogenation. The increase in the degrees of hydrogenation causes the decrease in the amounts of C=C bonds. Thus, there would be less amounts of C=C bonds available for ozone attack, resulting in less ozone and UV cracking on the rubber surface. In addition, reactions between ozone and saturated units are much slower than those between ozone and the C=C bond (Simma *et al.*,

2009) and reactions between UV radiation (320 nm or 288.9 kJ/mol) and C=C bonds are easier than those between UV and R-H bonds due to lesser bond dissociation energies, i.e., C=C (271.63 kJ/mol) < C-H (334.72 kJ/mol) < CH-H (414.22 kJ/mol) < CH₂-H (485.34 kJ/mol) (Stans, 1970; Walsh, 1998).

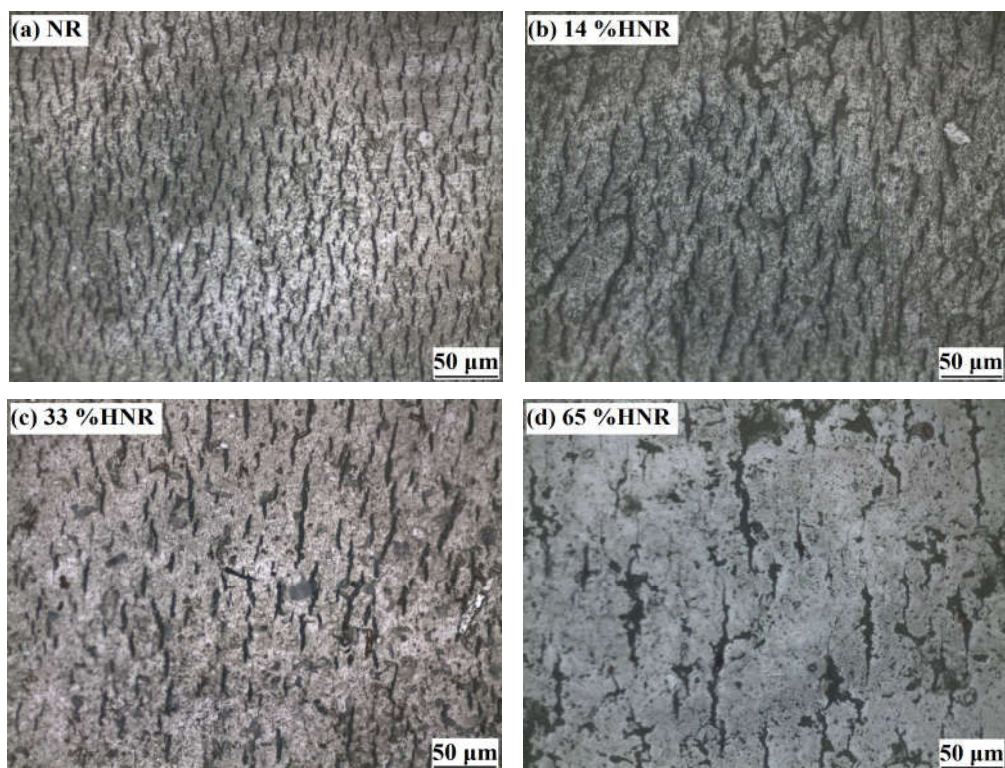


Figure 4.32 Optical photographs of cracks on surfaces of rubbers vulcanized by peroxide after ozone exposure; (a) NR, (b) 14 %HNR, (c) 33 %HNR, and (d) 65 %HNR

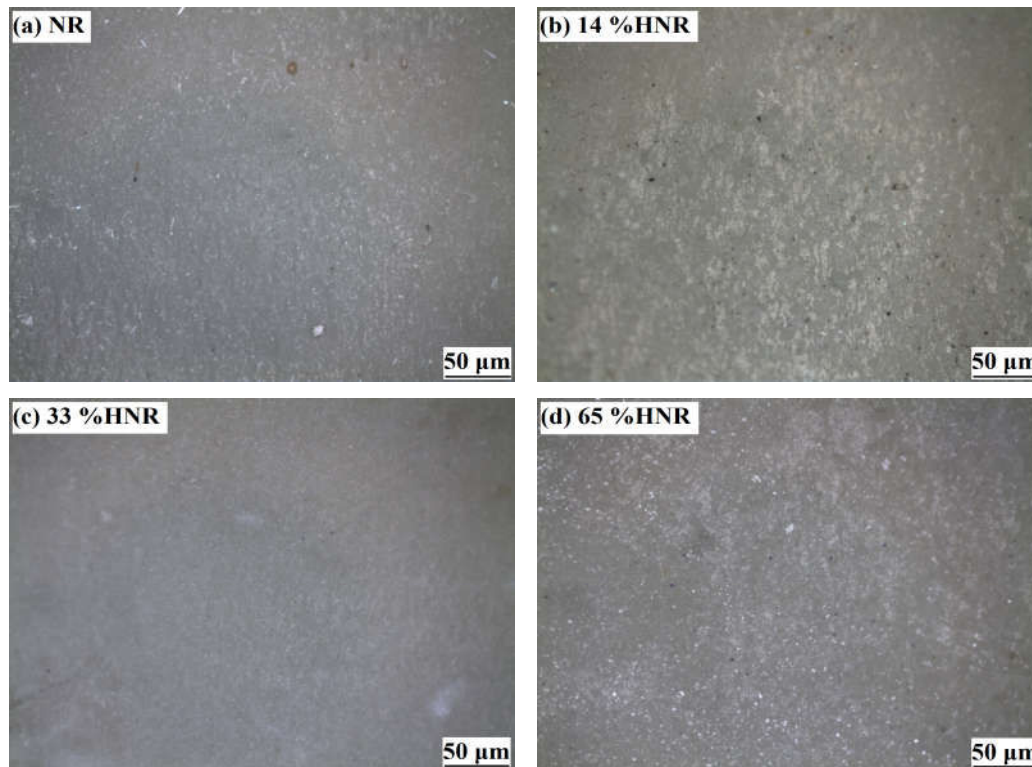


Figure 4.33 Optical photographs of cracks on surfaces of rubber vulcanized by sulfur after ozone exposure; (a) NR, (b) 14 %HNR, (c) 33 %HNR, and (d) 65 %HNR

Apparently, sulfur-vulcanized rubbers had greater ozone resistance than peroxide-cured rubbers due to lower unsaturated contents in the rubbers as evidenced by Raman spectra shown in Figure 4.37. Raman characteristic peaks of HNRs were shown in Table 4.9. The characteristic peak of C=C stretching was at 1664 cm^{-1} . From Table 4.10, it was noted that the amounts of unsaturated portions of uncured rubbers were high. After vulcanized with peroxide, the amounts of C=C bonds remained unchanged, implying that crosslinking reactions were less involved with C=C bonds. In contrast, the amounts of C=C bonds of sulfur-cured rubbers largely decreased after vulcanization, indicating that crosslinking reactions took place at C=C bonds.

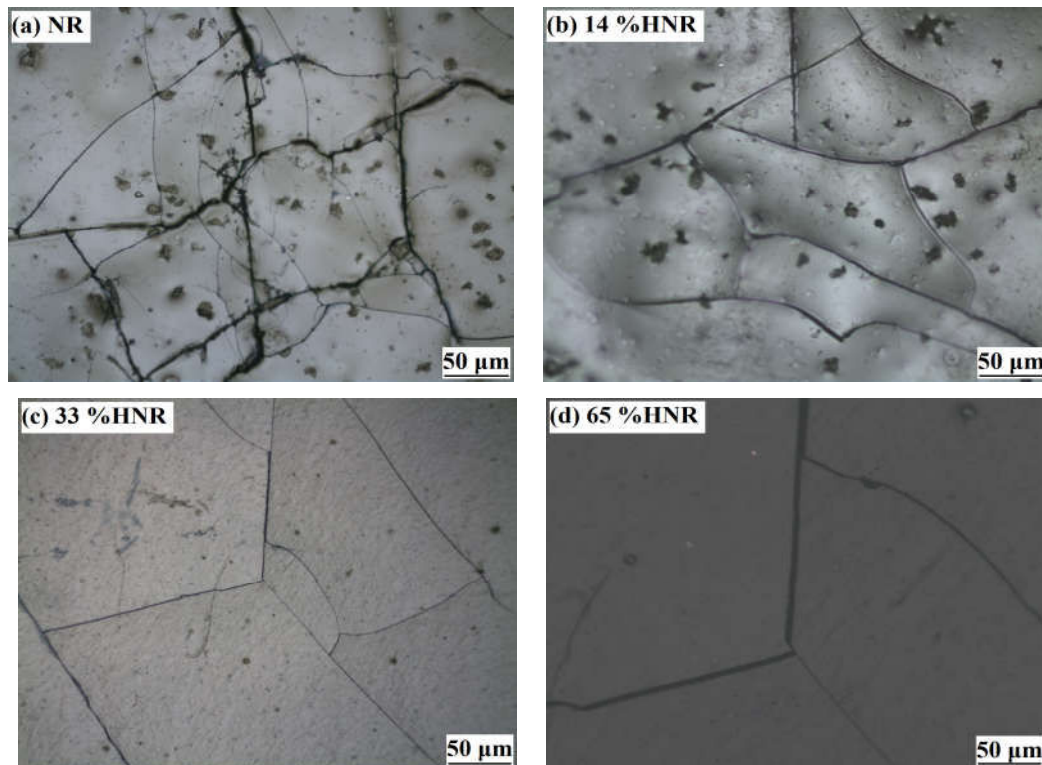


Figure 4.34 Optical photographs of cracks on surfaces of rubber vulcanized by peroxide after UV exposure; (a) NR, (b) 14 %HNR, (c) 33 %HNR, and (d) 65 %HNR

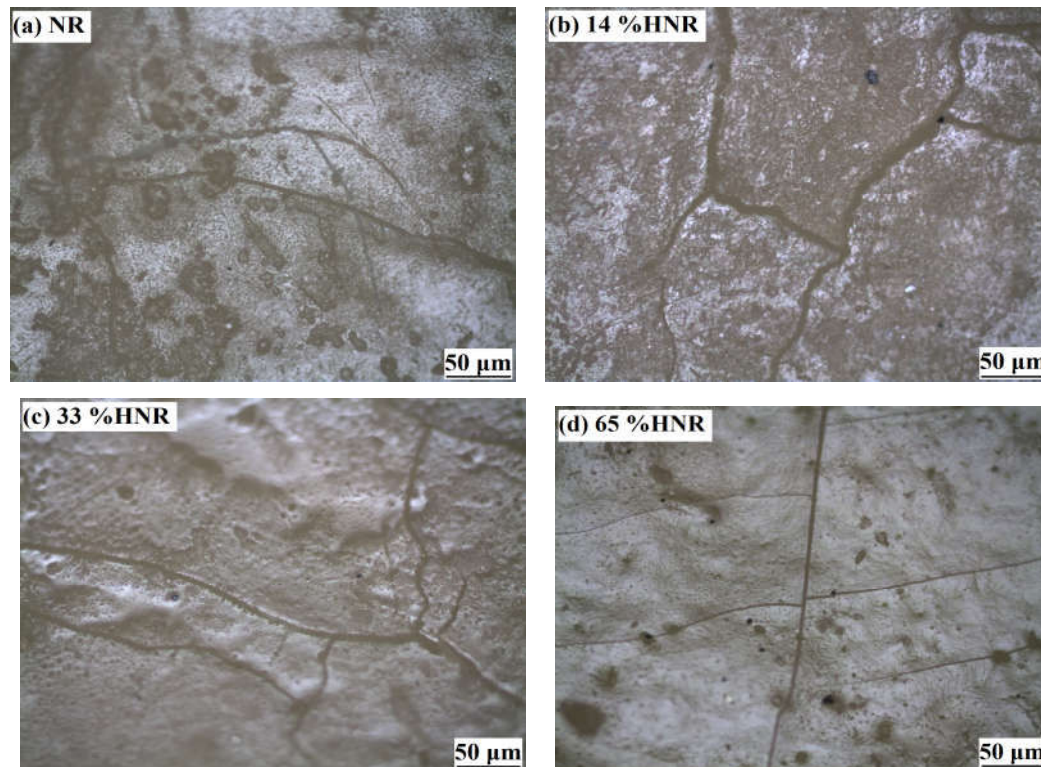


Figure 4.35 Optical photographs of cracks on surfaces of rubber vulcanized by sulfur after UV exposure; (a) NR, (b) 14 %HNR, (c) 33 %HNR, and (d) 65 %HNR

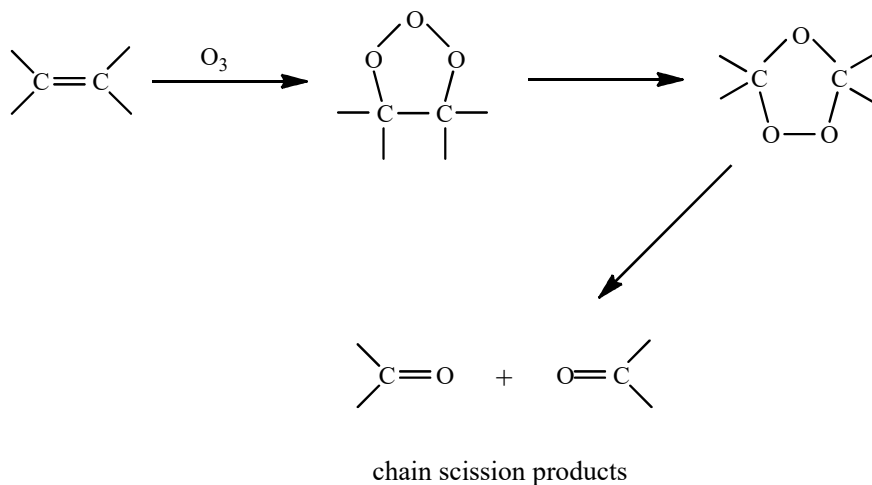


Figure 4.36 Mechanisms of ozone degradation in diene rubbers

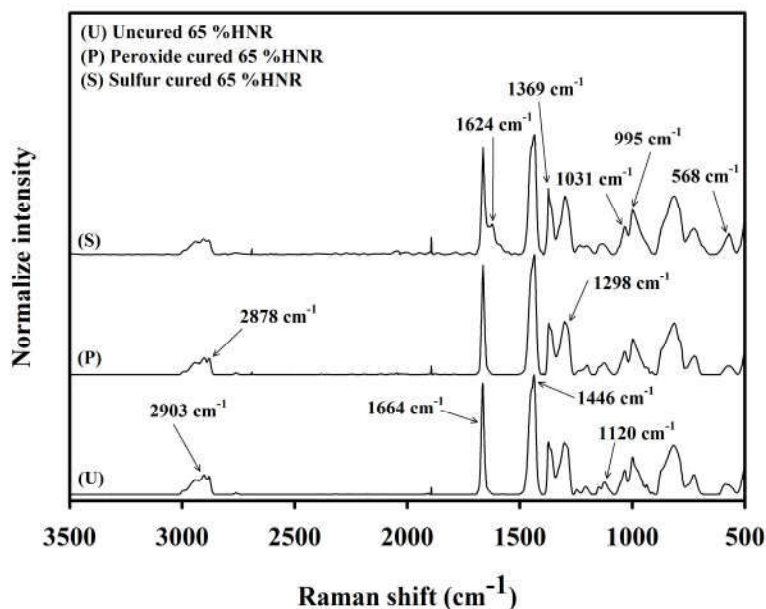


Figure 4.37 Raman spectra of 65 %HNR; (U) unvulcanized, (P) peroxide-vulcanized, and (S) sulfur-vulcanized

Table 4.9 Characteristic peak frequency of unvulcanized and vulcanized HNRs

Wave number (cm ⁻¹)	Assignments
568	S-S stretching
995	C-CH ₃ stretching
1031	CH ₃ rocking
1120	CH ₂ wagging
1298	CH bending
1369	CH ₂ deformation
1446	CH ₂ deformation asymmetric stretching
1624	C=C-C-S stretching
1664	C=C stretching
2878	CH ₂ symmetric stretching
2903	CH ₃ symmetric stretching

Table 4.10 Integral intensity of C=C bond stretching, $I_{C=C}$, at 1664 cm^{-1} of NR and HNRs vulcanized by peroxide and sulfur

Rubbers	Integral intensity (I), $I_{C=C}$ at 1664 cm^{-1} , (a.u.)		
	Uncured rubber	Peroxide cure	Sulfur cure
NR	1.93	1.90	1.17
14 %HNR	1.92	1.92	0.92
33 %HNR	1.08	1.02	0.44
65 %HNR	0.79	0.61	0.22

The Raman spectra peroxide-cured 65 %HNR before and after ozone exposure were illustrated in Figure 4.38. It was found that the amounts of C=C bonds decreased after ozone exposure as evidenced by the decrease in intensity at 1664 cm^{-1} . The integral intensity difference (ΔI_p), difference in peak integral at 1664 cm^{-1} before and after ozone/UV exposure, of NR and HNRs cured by peroxide and sulfur was shown in Table 4.11 and 4.12. It was noted that ΔI_p decreased with increasing degrees of hydrogenation. This was consistent well with optical photographs given in Figures 4.32-4.35, indicating that ozone and UV resistance of HNR vulcanizates was much better than that of the NR vulcanizates.

In addition, ΔI_p of sulfur-vulcanized rubbers was lower than that of peroxide-cured rubbers. This was due to lower unsaturated contents in the former.

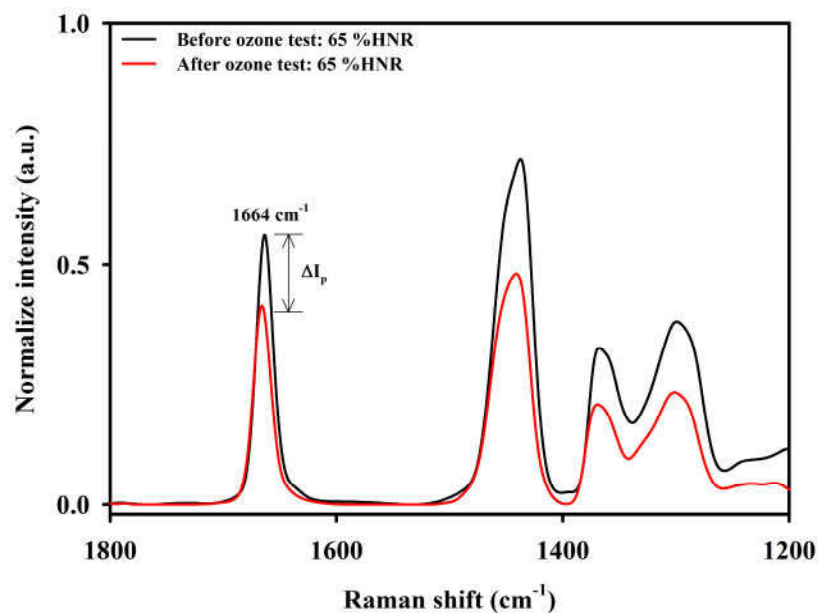


Figure 4.38 Raman spectra of peroxide-cured 65% HNR before (black line) and after (red line) ozone exposure

Table 4.11 Different integral intensity (ΔI_P) peak, $I_{C=C}$, at 1664 cm^{-1} of NR and HNRs vulcanized by peroxide and sulfur before and after ozone exposure

Rubbers	Different integral intensity (ΔI_P) peak, $I_{C=C}$, at 1664 cm^{-1} , (a.u.)	
	Peroxide cure	Sulfur cure
NR	-1.16	-0.83
14 %HNR	-1.33	-0.72
33 %HNR	-0.47	-0.35
65 %HNR	-0.23	-0.15

Table 4.12 Different integral intensity (ΔI_P) peak, $I_{C=C}$, at 1664 cm^{-1} of NR and HNRs vulcanized by peroxide and sulfur before and after UV exposure

Rubbers	Different integral intensity (ΔI_P) peak, $I_{C=C}$, at 1664 cm^{-1} , (a.u.)	
	Peroxide cure	Sulfur cure
NR	-1.51	-1.10
14 %HNR	-1.76	-0.87
33 %HNR	-0.89	-0.42
65 %HNR	-0.53	-0.20

4.3.3 Crosslink densities of HNR vulcanizates

Crosslink densities of NR and HNRs vulcanized by peroxide and sulfur were shown in Figure 4.39. It was seen that crosslink densities of sulfur-cured rubbers were higher than those of peroxide-cured rubbers. For HNR vulcanizates, crosslink densities increased with increasing hydrogenation levels. This may be due to initial gel, occurring during hydrogenation, present in the rubbers.

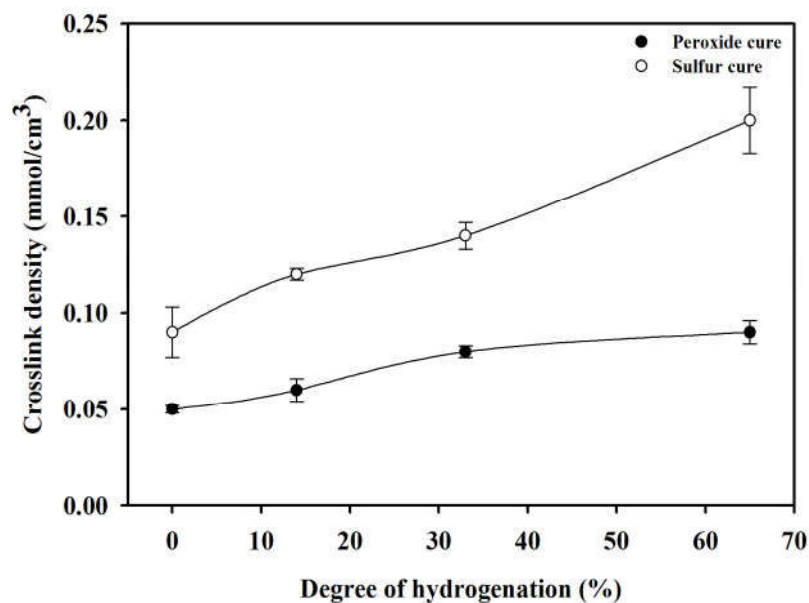


Figure 4.39 Crosslink densities versus degree of hydrogenation by peroxide and sulfur cure

4.3.4 Tensile properties of HNR vulcanizates

True stress - true strain curves of NR and HNRs cured by peroxide and sulfur were shown in Figures 4.40 and 4.41, respectively. At low elongation (< 200 % strain), 100 % Moduli, the stress required to stretched rubber to 100% strain, of HNR vulcanizates were greater than that for NR sample and the stress increased with increasing degrees of hydrogenation. Tensile strength or stress at break tended to increase whereas elongation at break decreased with increasing hydrogenation levels. As mentioned previously, hydrogenation transformed unsaturated, flexible, and elastic NR to partially saturated, stiff, and less elastic HNRs, therefore, HNR vulcanizates were stiffer and harder than NR vulcanizates, leading to higher modulus at low strain and lower elongation at break. Furthermore, larger gel contents present in higher HNR also helped increased the modulus of the rubber. However, tensile strength of vulcanizates was very low (≈ 0.1 MPa) due to strain rate was low (50 mm/min). Similar results were observed for NR and HNRs vulcanized by sulfur. However, the effect of hydrogenation degrees on stress at low strain was pronounced in sulfur-cured rubbers.

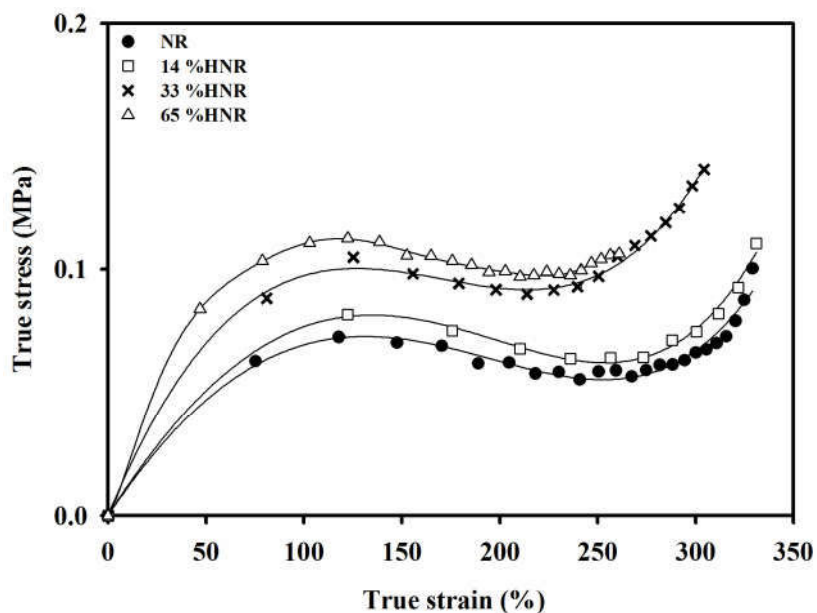


Figure 4.40 True stress - true strain curves of NR and HNRs vulcanized by peroxide

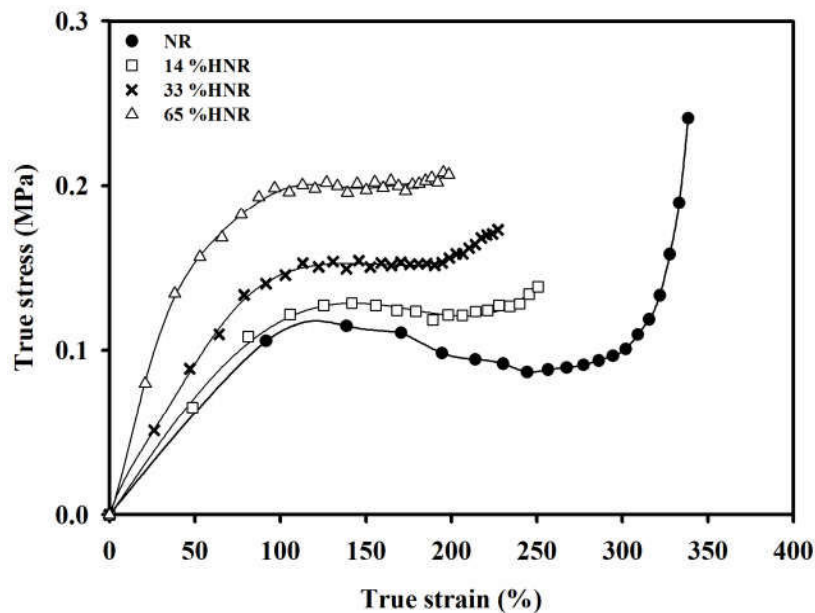


Figure 4.41 True stress - true strain curves of NR and HNRs vulcanized by sulfur

Sulfur-cured rubbers had higher moduli and tensile strength, but lower strain at break than peroxide-cured rubbers because of higher amounts of crosslinks.

4.4 Thermoplastic vulcanizates based on dynamically vulcanized HNR and PP blends

4.4.1 Mixing of TPVs

The TPVs were prepared from dynamic vulcanization of HNRs and PP blends using peroxide and sulfur as curing agents. 65 %HNRs was selected due to greater thermal resistance than 14 %HNR and 33 %HNR. Moreover, the chemical structure of 65 %HNR was similar to EPDM. The typical stages of the dynamic vulcanization in an internal mixer at 180 °C could be investigated from torque-time profile. Figure 4.42 showed time-dependent mixing torque of TPVs based on blends of NR/PP (70/30, 50/50) and 65 %HNR/PP (70/30, 50/50) vulcanized by peroxide and sulfur.

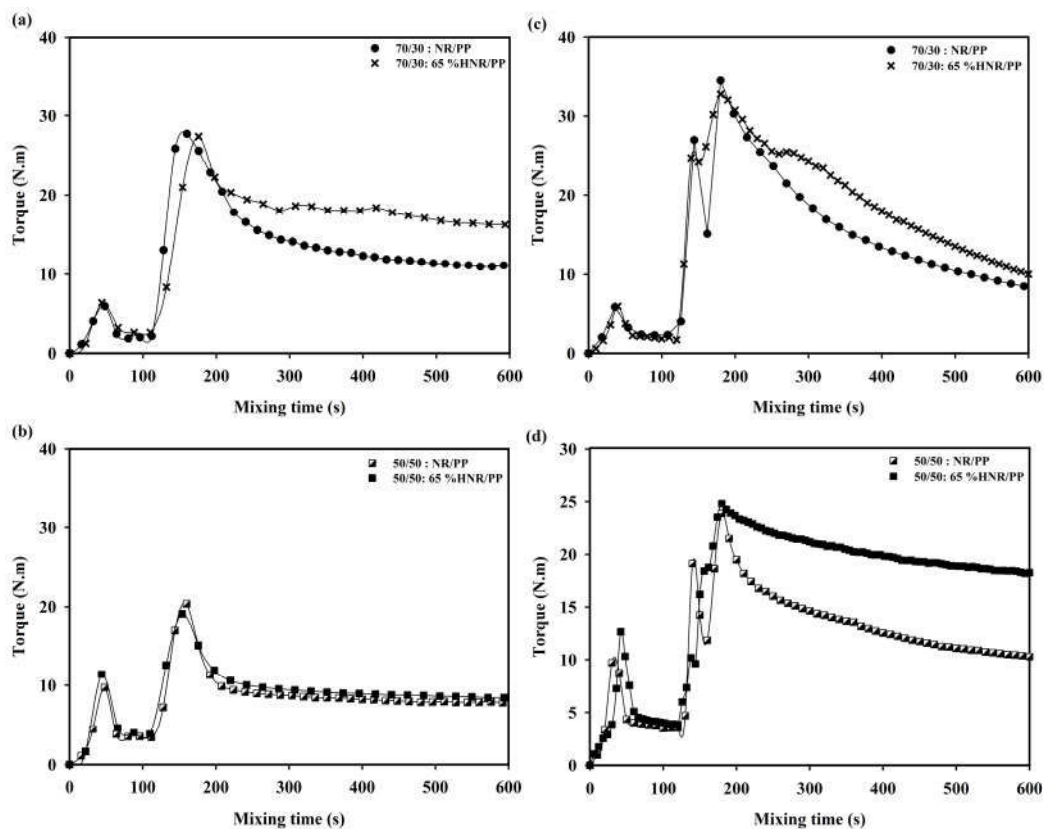


Figure 4.42 Mixing torque-time profiles of TPVs prepared from blends of NR/PP and 65 %HNR/PP at blend ratios 70/30 and 50/50 vulcanized with peroxide (left column) and sulfur (right column)

For all torque-time curves, when solid PP was first added, torque increased (peak 1) due to PP was not completely melt. After that, torque decreased due to PP was completely in molten state. When the rubber compound was added, mixing torque increased due to high viscosity rubber phase. At the same blend ratio, viscosities of NR and HNR compounds were about the same. For peroxide-cured systems, the increase in torque was only in one-step due to rapid crosslinking reactions initiated by free radicals generated from the decomposition of DCP. Crosslinking of NR and HNRs with peroxide involved hydrogen abstraction at allylic position of isoprene units to generate macroradicals followed by coupling of these macroradicals. After that the high viscosity crosslinked rubber phase was sheared and broken into small particles dispersed in PP matrix, resulting in a decrease in mixing

torque and finally reaching equilibrium state. Apparently, the difference in chemical structures between NR and 65 %HNR did not affect crosslinking with peroxide.

For sulfur-cured systems, after rubber compound was added, the increase in torque (peak 2) was observed, and then mixing torque decreased. This may be because of thermo-mechanically induced molecular destruction processes (Harrats *et al.*, 2005) and lower rate of sulfur vulcanization than peroxide cure due to the complexity of the number and variety of the ingredients used in the sulfur cure. After crosslinking took place, mixing torque increased (peak 3) to reach a maximum due to high viscosity crosslinked rubber phase, then decreased continuously with time because crosslinked rubber phase was deformed under intensive shear and broken into small particles dispersed throughout continuous PP phase. The decrease in torque was more pronounced in TPVs with higher rubber components and TPVs prepared from NR. Also, it could be seen that the difference in chemical structures between NR and 65 %HNR affected crosslinking with sulfur. This was because sulfur crosslinking involved reactions at C=C bonds. Hydrogenation caused C=C bonds in HNRs to decrease, leading to less C=C bonds available for crosslinking.

For TPVs with larger rubber portions, mixing torque was greater (Figure 4.43) due to high viscosity of rubber component.

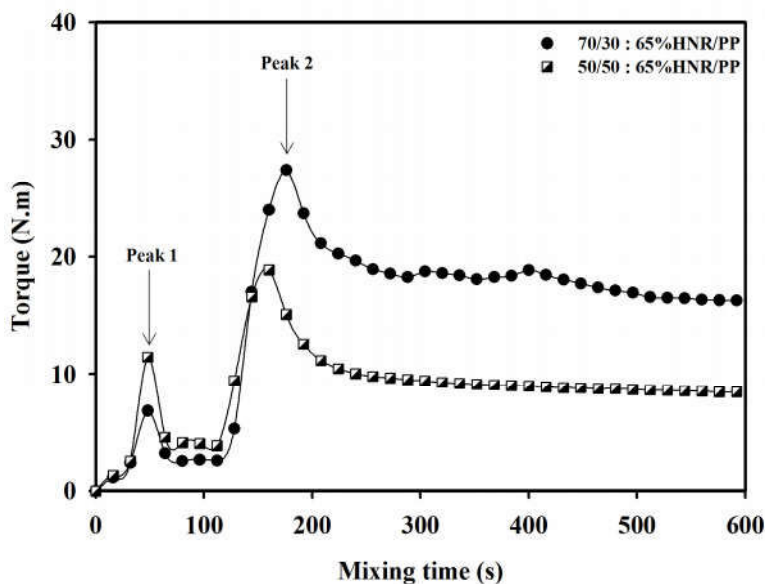


Figure 4.43 Mixing torque-time profiles of TPVs prepared from blends of 65 %HNR/PP at blend ratio 70/30 and 50/50 vulcanized with peroxide

4.4.2 Morphological characterization of TPVs by Raman mapping

The morphology of simple or physical blends of NR/PP and 65 %HNR/PP at blend ratio 50/50 characterized by Raman spectroscopic technique was shown in Figure 4.44, revealing co-continuous morphology of both rubber and PP phases. PP was characterized by peaks at 813 cm^{-1} and at 846 cm^{-1} corresponding to the CH_2 (rocking) and CH_3 (rocking), respectively. Characteristic peak of NR and HNR at 1664 cm^{-1} was assigned to stretching of C=C double bond. The intensity of this peak decreased in 65 %HNR. The absorption at 1434 cm^{-1} and 1452 cm^{-1} , attributed to the CH_3 symmetric bending and CH_2 twisting, respectively, increased in 65 %HNR. Therefore, characteristic frequencies in the range of $1434\text{-}1664\text{ cm}^{-1}$ for NR and 65 %HNR and $813\text{-}846\text{ cm}^{-1}$ for PP could be used to identify phase component in their blends. The Raman mapping of the distribution of the phase component in NR/PP and 65 %HNR/PP blends was also shown in Figure 4.44 (right). The colored image was constructed in the range of $813\text{-}846\text{ cm}^{-1}$ (blue), which represented characteristic frequencies of PP phase and $1434\text{-}1664\text{ cm}^{-1}$ (red), representing characteristic wave numbers of NR or 65 %HNR phase. The surface of these blends, it appears that NR/PP and 65 %HNR/PP blends seem to be continuous rubber phase morphology of the blends as shown in Figure 4.44. In this case, the blend system was nonreactive and phase inversion phenomenon not occurred.

The morphological maps of TPVs prepared from dynamically vulcanized blends of NR/PP and 65 %HNR/PP at 50/50 blend ratio cured by peroxide and sulfur were illustrated in Figures 4.45 and 4.46, respectively. Dispersed-continuous morphology was obvious in both cases. Crosslinked rubber particles were finely dispersed throughout thermoplastic PP matrix. These results were similar to those reported on PE/PP blends by Furukawa *et al.* (2006).

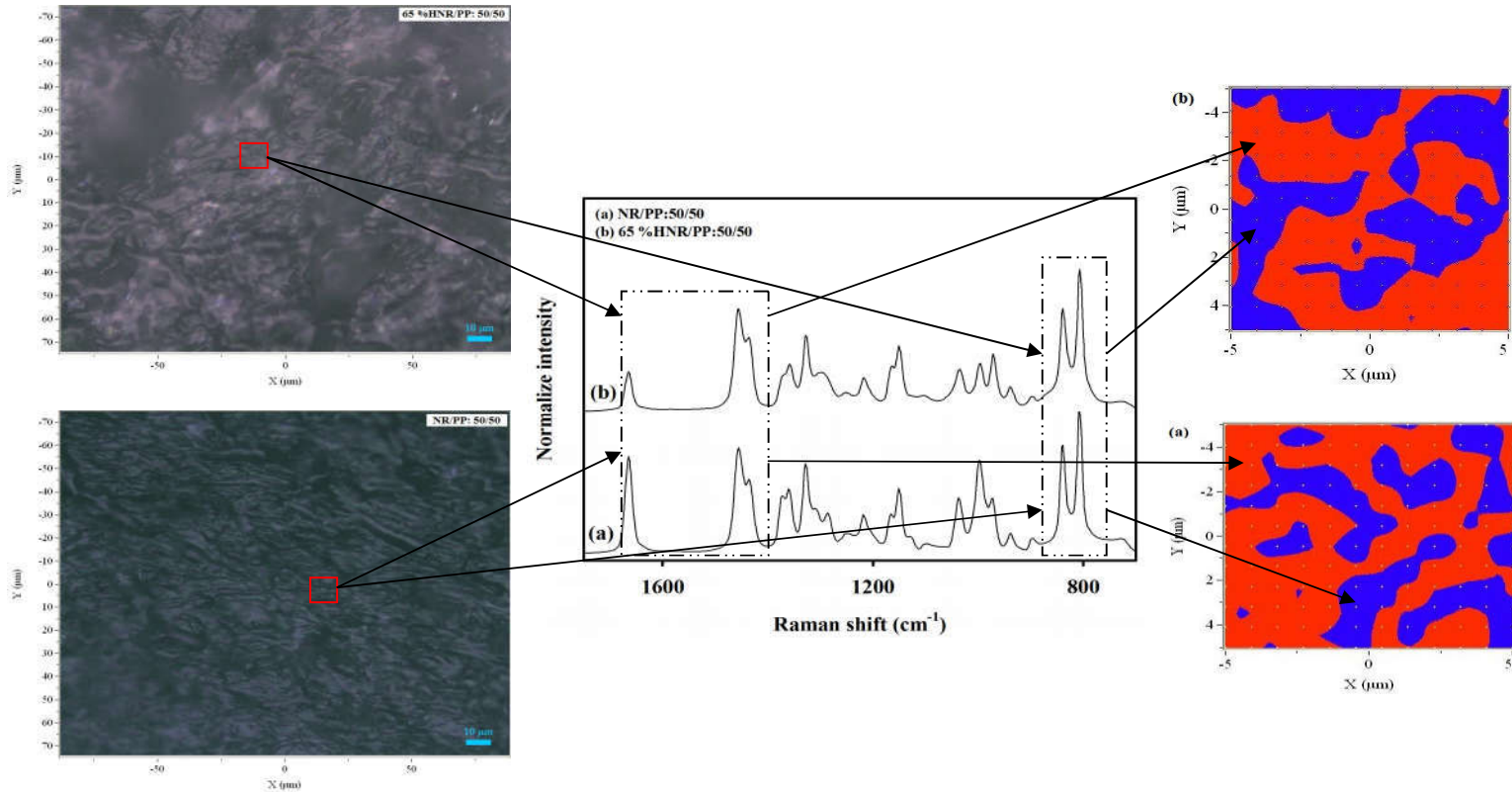


Figure 4.44 Morphology of simple blends; (a) NR/PP and (b) 65% HNR/PP at blend ratio of 50/50 (wt/wt%); Raman optical micrograph (left): rubber phase (white), PP phase (dark); Raman spectra (middle); and Raman mapping (right): PP phase (blue) and rubber phase (red)

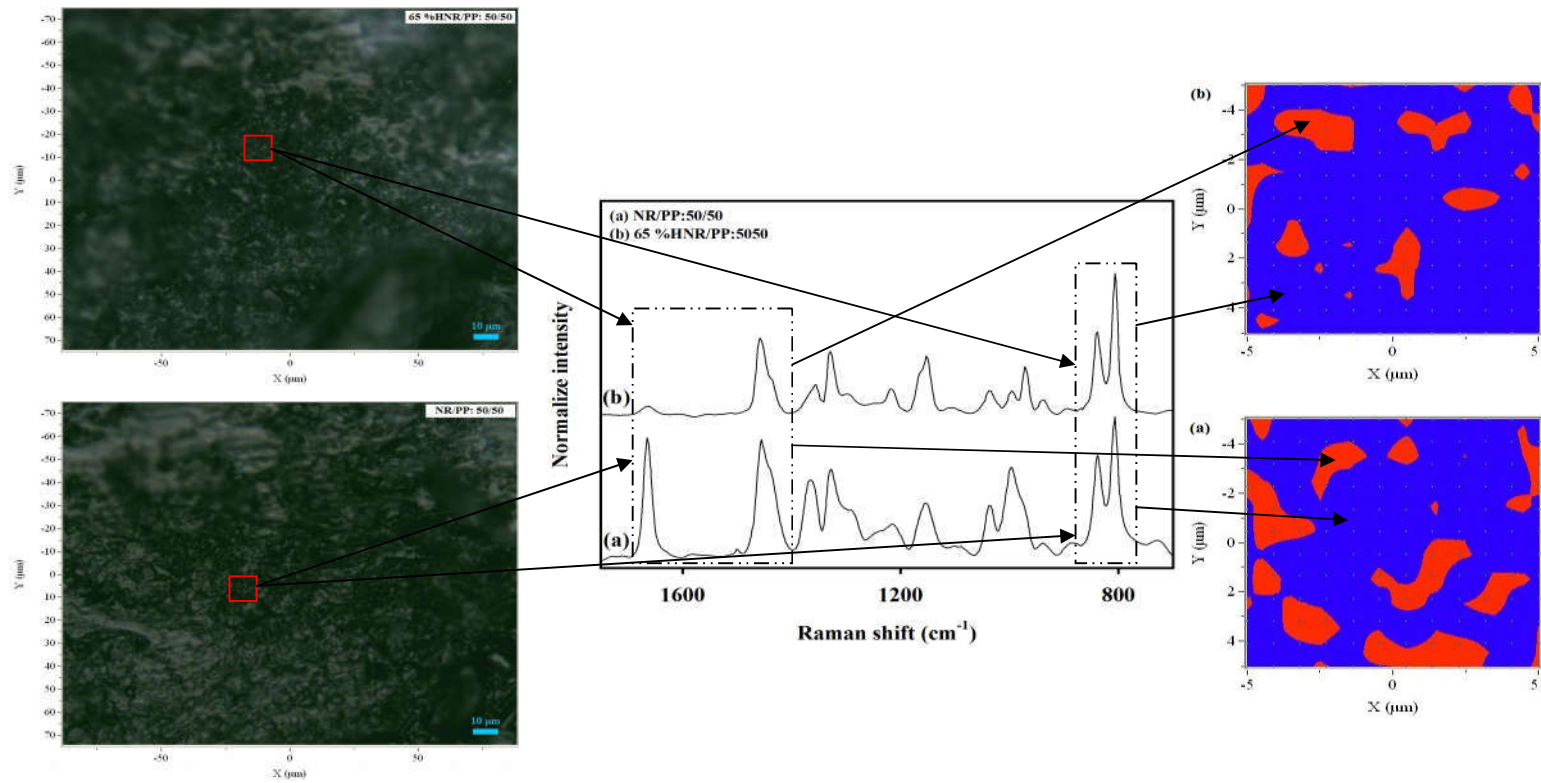


Figure 4.45 Morphology of TPVs prepared from dynamically vulcanized blends of (a) NR/PP and (b) 65 %HNR/PP at 50/50 blend ratio vulcanized by peroxide; Raman optical micrograph (left), rubber phase (white) and PP phase (dark); Raman spectra (middle); and Raman mapping (right), PP phase (blue) and rubber phase (red)

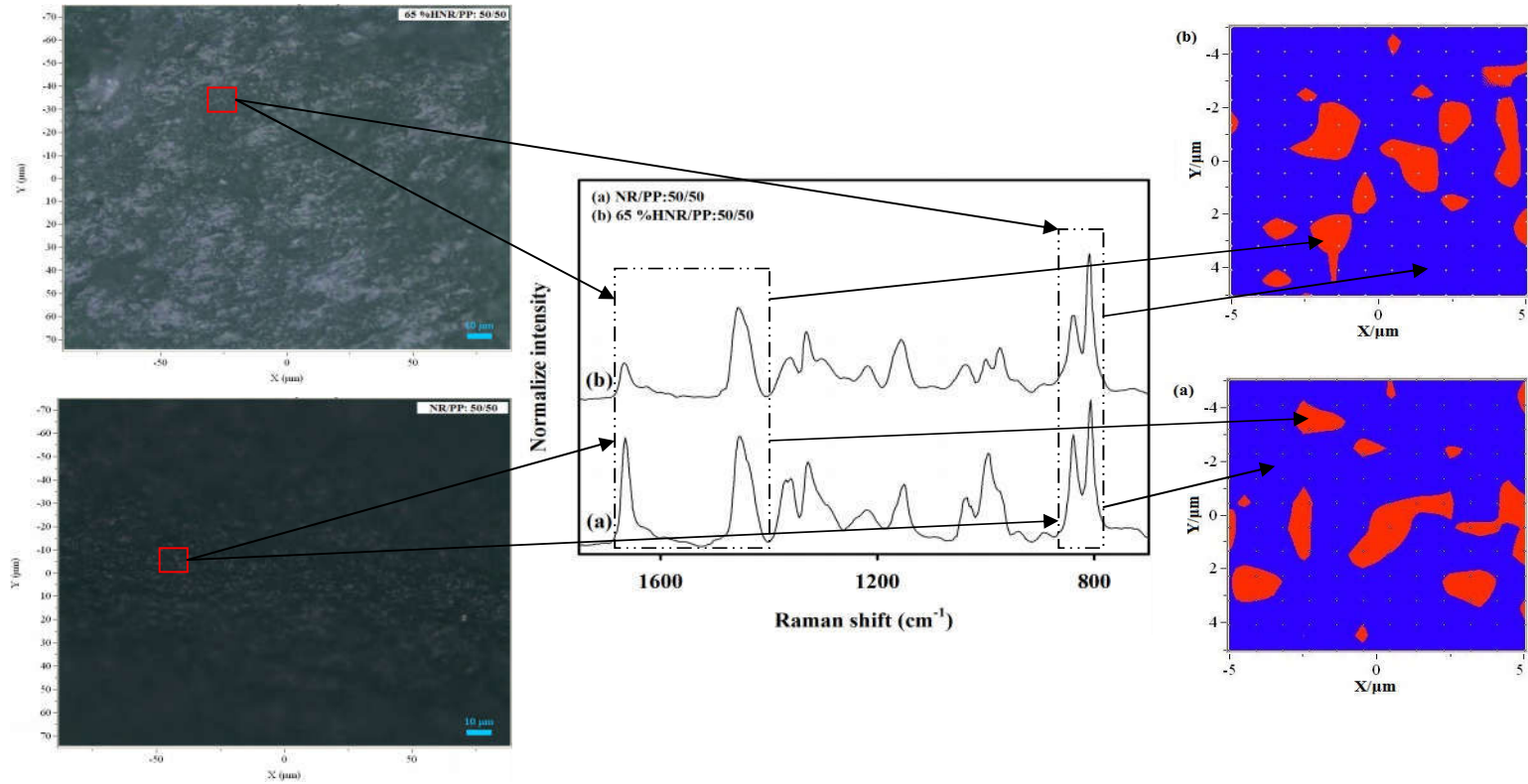


Figure 4.46 Morphology of TPVs prepared from dynamically vulcanized blends of (a) NR/PP and (b) 65 %HNR/PP at 50/50 blend ratio vulcanized by sulfur; Raman optical micrograph (left), rubber phase (white) and PP phase (dark); Raman spectra (middle); and Raman mapping (right), PP phase (blue) and rubber phase (red)

4.4.3 Phase size analysis by Raman mapping technique

The size of crosslinked rubber phase of TPVs was size dispersed in matrix PP phase was determined from Raman map (Figure 4.47) and compared with SEM micrograph (Figure 4.48). From Raman image, the range of particle size of crosslinked rubber was from 0.32 to 2.74 μm , while the values in the range of 0.44 to 1.95 μm were obtained from SEM method. The particle sizes of crosslinked rubber in TPVs measured by both techniques were in good correlation as shown in Figure 4.49.

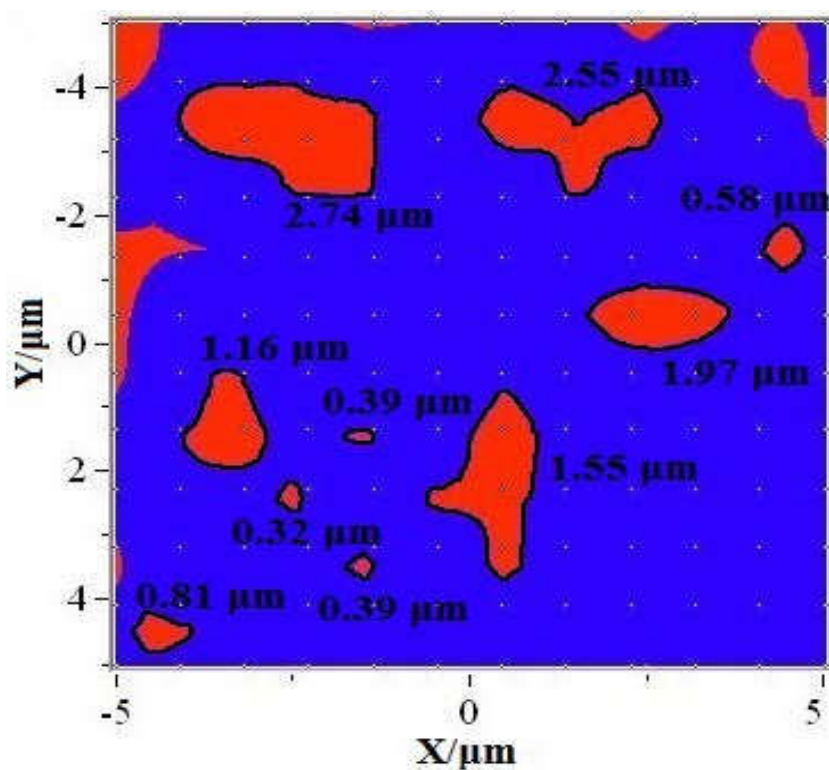


Figure 4.47 Raman maps of TPVs based on 50/50 of 65 %HNR/PP dynamically vulcanized blends cured by peroxide, revealing crosslinked rubber particles (red) dispersed in matrix PP (blue)

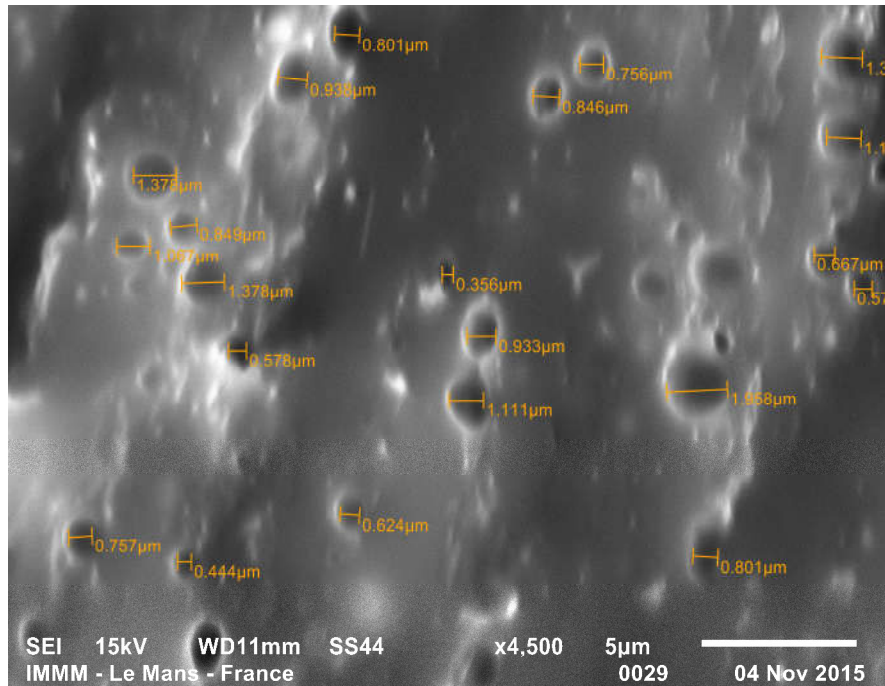


Figure 4.48 SEM micrograph of TPVs based on 50/50 of 65 %HNR/PP dynamically vulcanized blends cured by peroxide, revealing crosslinked rubber particles (dark hole) dispersed in PP matrix (magnification 4,500x)

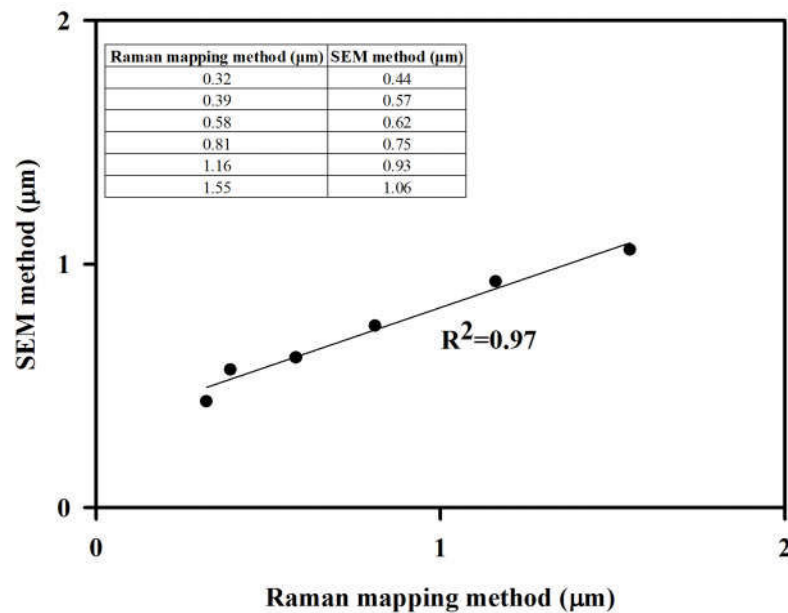


Figure 4.49 Correlation between of particle sizes of crosslinked rubber phase of TPVs measured by Raman mapping and SEM methods (50/50 of 65 %HNR/PP blend)

4.4.4 Determination of blend ratio by Raman spectroscopy

Raman spectroscopic technique could be employed to quantitatively determine the components of the TPVs. For NR/PP and HNR/PP blends, characteristic frequencies in the range of 813-846 cm^{-1} and 1434-1664 cm^{-1} , attributed to PP and NR or HNR, respectively, could be used to characterize the blends. The amount of each component could be calculated from equations (3.15) and (3.16). Figure 4.50 showed Raman spectra of TPVs based on dynamically cured 65 %HNR/PP blends vulcanized by peroxide at various blend ratios and Raman spectra of 65 %HNR/PP TPVs with blend ratios of 70/30 and 40/60 were shown in Figure 4.51. It was found that the increase in PP and rubber contents in TPVs led to the increase in intensity at 813-846 cm^{-1} for PP and at 1434-1664 cm^{-1} for 65 %HNR in their blends. The calculated blend ratios from Raman spectra were in good agreement with the nominal blend ratios (Table 4.13). Therefore, Raman spectroscopic technique can effectively be used to quantitatively determine blend ratios in simple blends or TPVs.

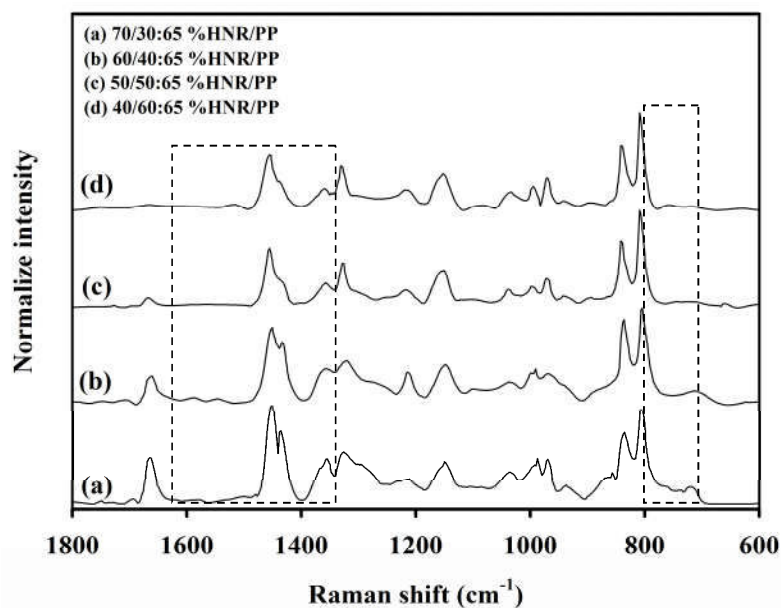


Figure 4.50 Raman spectra of TPVs based on 65 %HNR/PP blends cured by peroxide at blend ratios of (a) 70/30, (b) 60/40, (c) 50/50, (d) 40/60

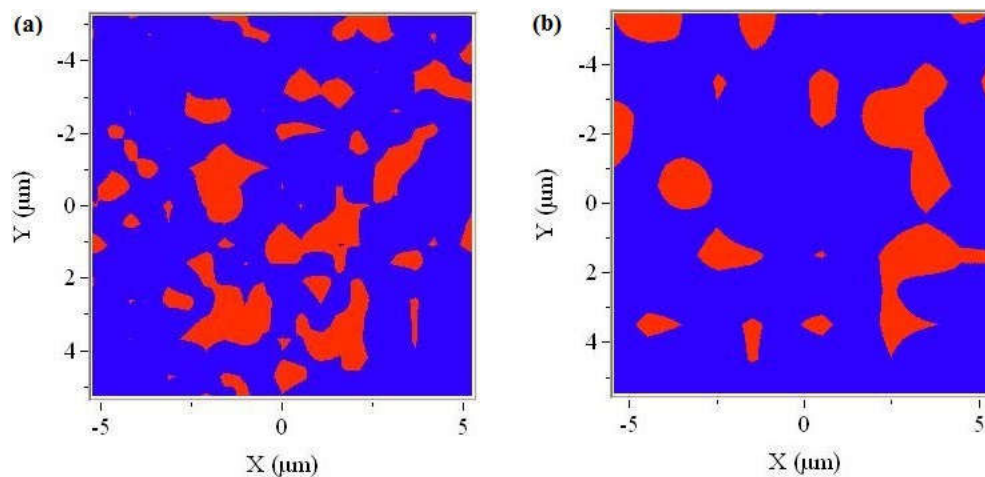


Figure 4.51 Raman maps of TPVs based on 65 %HNR/PP blends cured by peroxide with blend ratio (a) 70/30 and (b) 40/60 (PP phase (blue) and rubber phase (red))

Table 4.13 The content of each component of TPVs based on NR/PP and 65 %HNR/PP blends

Samples	The nominal blend ratio (%wt/%wt)		The blend ratio calculated from Raman spectra	
	Peroxide cure	Sulfur cure	Peroxide cure	Sulfur cure
NR/PP	70/30	70/30	72/28	69/31
	60/40	60/40	64/36	64/36
	50/50	50/50	52/48	51/49
	40/60	40/60	44/56	41/59
65 %HNR/PP	70/30	70/30	69/31	72/28
	60/40	60/40	59/41	64/36
	50/50	50/50	48/52	51/49
	40/60	40/60	39/61	42/58

4.4.5 Dynamic mechanical behavior of TPVs

Strain-dependent storage moduli of 65 %HNR vulcanizates and TPVs based on 65 %HNR/PP blends vulcanized by peroxide and sulfur at 70/30 and 50/50 blend ratios were shown in Figures 4.52 and 4.53, respectively. It was noted that storage modulus of sulfur- and peroxide-cured HNRs were lower than those of TPVs and were independent of the amplitudes of the strain. HNR vulcanizates exhibited only linear region on the dynamic mechanical behavior due to one phase nature, while linear and non-linear behaviors were observed for TPVs due to two-phase nature of the system. For TPVs, storage moduli were independent of strain amplitudes up to about 0.2. Further increase in strain amplitudes resulted in the decrease in storage modulus. TPVs with higher PP contents had higher storage modulus but modulus relaxed faster at high strain. The origin of non-linear region was probably due to the interfacial slippage between crosslinked rubber phase and PP matrix. The slopes of non-linear region for TPVs cured by peroxide were lower than those of sulfur-cured TPVs. This could be explained in terms of the increase in interfacial interactions between rubber and PP phases. Peroxide vulcanization involved hydrogen abstraction by free radicals from polymer chains to generate macroradicals followed by coupling of these macroradicals. Free radicals obtained from thermal decomposition of peroxide were able to abstract hydrogen atoms from rubber and PP to form macroradicals of these polymers, leading interfacial coupling of these two macroradicals. For sulfur-cured TPVs, interfacial interactions would rarely occur due to involvement of C=C bonds in crosslinking process.

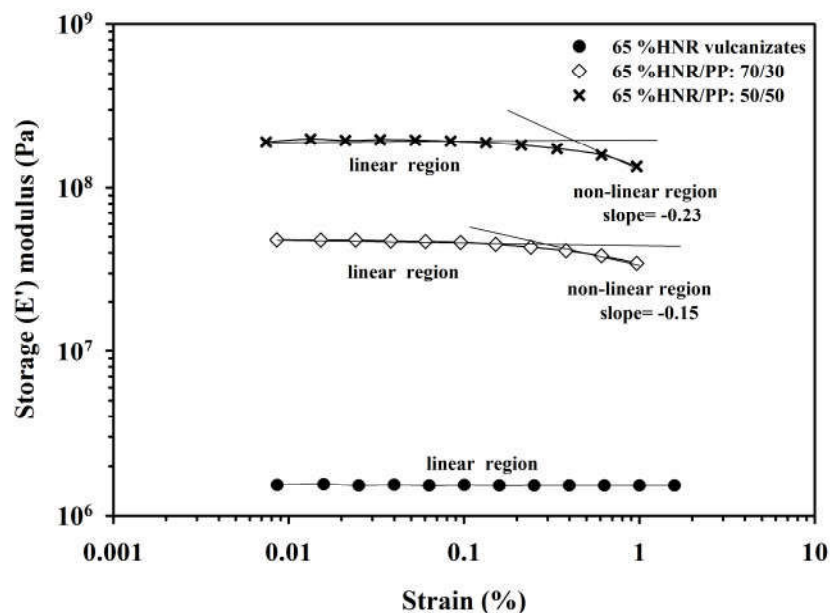


Figure 4.52 Strain-dependent storage modulus of 65 %HNR vulcanizates and TPVs based on 65 %HNR/PP blends vulcanized by peroxide at 70/30 and 50/50 blend ratios

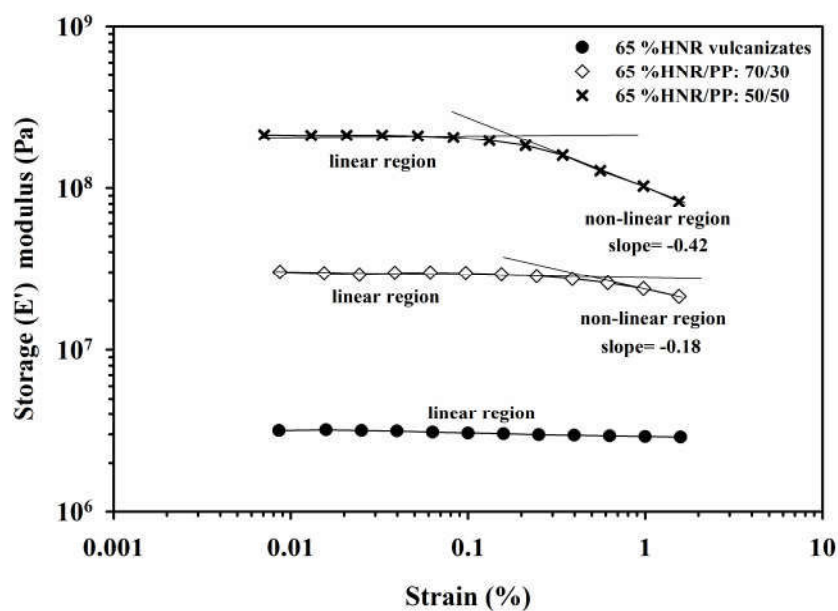


Figure 4.53 Strain-dependent storage modulus of 65 %HNR vulcanizates and TPVs based on 65 %HNR/PP blends vulcanized by sulfur at 70/30 and 50/50 blend ratios

4.4.6 Tensile properties of TPVs

True stress-true strain curves of HNR vulcanizate and peroxide-cured TPVs based on 65 %HNR/PP blends at various blend ratios were shown in Figure 4.54 and their tensile properties were shown in Figure 4.55. HNR vulcanizate had lowest strength and highest elongation at break. For TPVs, the increase in rubber contents resulted in the increase in elongation and the decrease in strength. This was because the strength of TPVs was governed by the hard phase PP. At the same rate of extension (50 mm/min), tensile strength of PP (the inset in Figure 4.54) was much greater than that of HNR vulcanizate. Therefore, strength of TPVs were mainly governed by the amount of hard thermoplastic phase.

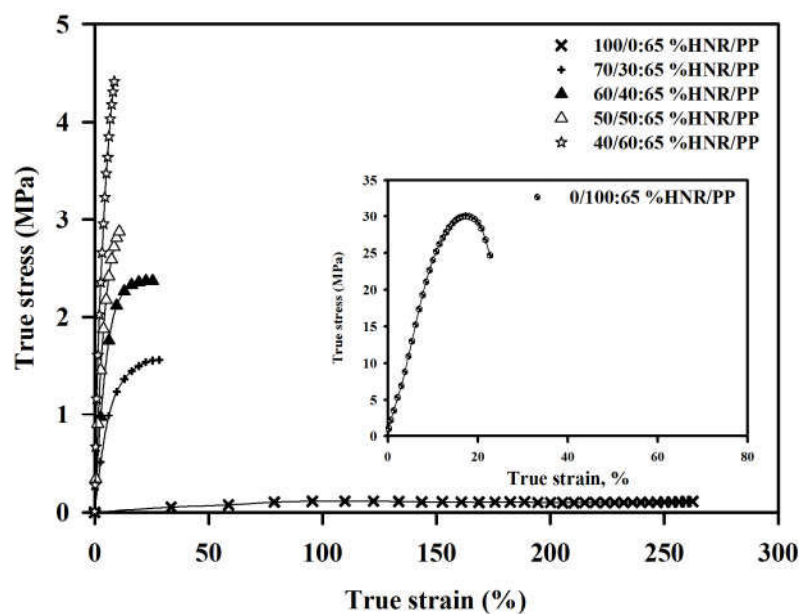


Figure 4.54 True stress-true strain curves of HNR vulcanizate and peroxide-cured TPVs based on 65% HNR/PP blends at various blend ratios

4.4.7 Fractured surface of TPVs

Fracture behavior of TPVs was largely affected by rubber contents. Figure 4.56 showed fractured surfaces of peroxide-cured TPVs based on 65 %HNR/PP blends at blend ratios of 70/30 and 50/50. It could be seen that the fractured surface of TPV with higher rubber content was rougher than that of TPV with lower rubber content, indicating the ductile failure with higher elongation. TPV with lower rubber content had smoother fractured surface, indicating brittle failure with low elongation.

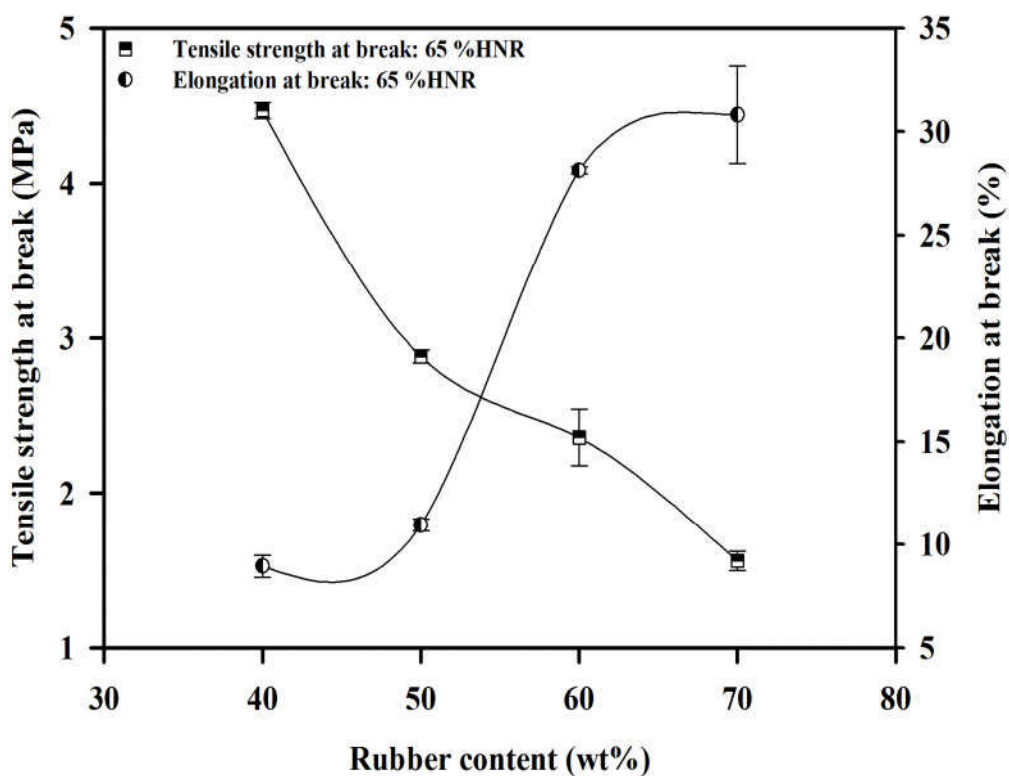


Figure 4.55 Tensile properties of peroxide-cured TPVs based on 65 %HNR/PP blends as a function of rubber contents

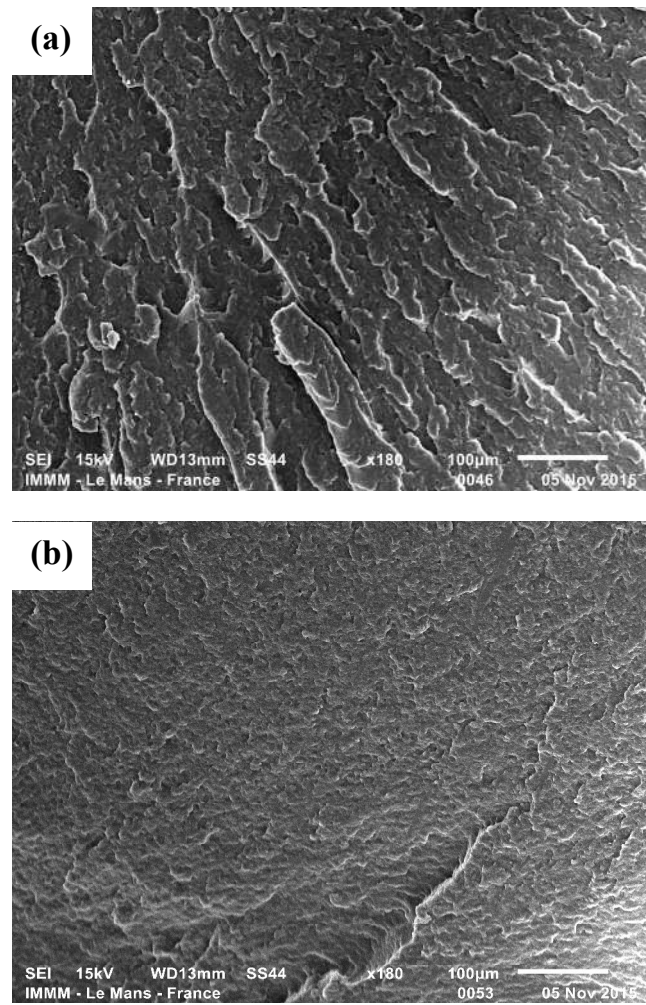


Figure 4.56 The fractured surfaces of peroxide-cured TPVs based on 65 %HNR/PP blends at blend ratio of (a) 70/30 and (b) 50/50

CHAPTER 5

CONCLUSIONS

1. Partially hydrogenated natural rubbers (HNRs) was prepared by non-catalytic hydrogenation of natural rubber latex (NRL) using diimide generated *in situ* from the reaction between hydrazine (N_2H_4) and hydrogen peroxide (H_2O_2).

2. Variations in moles of N_2H_4 and H_2O_2 in the range of 1.0-2.0 moles resulted in degrees of hydrogenation in the range of 10-18 %. High improvement in hydrogenation levels of HNRs was obtained when NRL particles were swollen in solvents by which toluene yielded slightly higher degrees of hydrogenation than hexane.

3. The increase in degrees of swelling of NRL could increase hydrogenation levels up to 42 %. TEM micrograph revealed that hydrogenation confined only at the swollen surface. After removal of toluene, particle size and particle size distribution of HNRL remained unchanged.

4. The increase in reaction volume could increase hydrogenation levels from 42 % to 65 %.

5. Crosslinking and *cis-trans* isomerization were side-reactions occurring during hydrogenation, leading the increase in gel contents and hardness with increasing degrees of hydrogenation of HNRs. Mooney viscosities of HNRs also increased with increasing degrees of hydrogenation due to gel present in rubbers. Stress relaxation of raw NR and HNRs were similar.

6. HNRs had greater thermal stability than NR and thermal stability increased with increasing degrees of hydrogenation. HNR vulcanizates had better resistance to ozone/UV than NR vulcanizates. Sulfur vulcanization provided rubbers with greater ozone/UV resistance than peroxide vulcanization. Furthermore, mechanical properties of sulfur-vulcanized rubbers were greater than those of peroxide-cured rubbers due to higher crosslink densities.

7. Raman spectroscopy was a powerful technique that could be employed to characterize phase morphology and to quantitatively determine blend

components of TPVs. Particle sizes of crosslinked rubber phase of TPVs measured by Raman spectroscopic technique were correlated well with those determined from SEM technique. Furthermore, the blend ratios of TPVs calculated from Raman spectra were in good agreement with the nominal blend ratios.

8. Strength properties of TPVs were mainly governed by the hard thermoplastic phase. Tensile strength of HNR/PP TPVs increased with increasing PP contents, while elongation decreased. For TPVs with high PP contents, fractured surface were smoother, indicating brittle fracture with low elongation. For TPVs with high rubber contents, fractured surfaces were rougher, indicating ductile failure with high elongation.

REFERENCES

- Aboulkas, A. and El Harfi, K. 2008. Study of the kinetics and mechanisms of thermal decomposition of Moroccan tarfaya oil shale and its kerogen. *Oil Shale*. 25, 426-443.
- Akiba, M. and Hashim, A.S. 1997. Vulcanization and crosslinking in elastomers. *Progress in Polymer Science*. 22, 475-521.
- Arayaprane, W. and Rempel, G.L. 2009. Synthesis and mechanical properties of diimide-hydrogenated natural rubber vulcanizates. *Journal of Polymer Science*. 114, 4066-4075.
- Barbillat, J. 1996. Raman imaging. In *Raman Microscopy: Development and Applications*. Turrell, G. and Corset, J., Eds. Elsevier-Academic Press. Amsterdam. pp. 175.
- Blaine, R.L. and Kissinger, H.E. 2012. Homer Kissinger and the Kissinger equation. *Thermochimica Acta*. 540, 1-6.
- Boyce, M. C., Kear, K., Socrate, S., and Shaw, K. 2001. Deformation of thermoplastic vulcanizates. *Journal of the Mechanics and Physics of Solids*. 49, 1073-1098.
- Bunce, S.J., Edwards, H.G.M., Johnson, A.F., Lewis, I.R. and Turner, P.H. 1993. Synthetic polyisoprenes studied by Fourier transform Raman spectroscopy. *Spectrochimica Acta*. 49, 775-783.
- Colthup, N. B., Daly, L. H., and Wiberly, H. E. 1975. *Introduction to Infrared and Raman Spectroscopy*, 2nd Edition, Academic Press, New York.
- Costa, F.R., Dutta, N.K., Choudhury, N.R. and Bhowmick, A.K. 2008. Current topics in elastomers research: Chapter 5 thermoplastic elastomers. CRC Press., USA.
- Daniel, L., Reger, S.R. and Goode, D.W.B. 2010. *Chemistry: principles and practice*. Third Edition. Cengage Learning, Inc., U.S.A.

- De Sarkar, M., De, P.P. and Bhowmick, A.K. 1997. Thermoplastic elastomeric hydrogenated styrene–butadiene elastomer: Optimization of reaction conditions, thermodynamics, and kinetics. *Journal of Applied Polymer Science*. 66, 1151–1162.
- De Sarkar, M., De, PP. and Bhowmick, A.K. 2000. Diimide reduction of carboxylated styrene–butadiene rubber in latex stage. *Polymer*. 41, 907–915.
- Drobny, J. G. 2007. *Handbook of thermoplastic elastomers* William Andrew, New York.
- Esmonde-White, F. W., and Morris, M. D. 2010. In *emerging Raman applications and techniques in biomedical and pharmaceutical fields; Raman imaging and Raman mapping*. Springer Inc., USA.
- Ferraro, J. R. 2003. *Introductory Raman spectroscopy*. 2nd Edition. Elsevier Academic Press Inc., USA.
- Flory, P.J. 1953. *Principles of polymer chemistry*. Cornell University Press, Ithaca, U.S.A., pp. 576-580.
- Furukawa, T., Sato, H., Kita, Y., Matsukawa, K., Yamaguchi, H., Ochiai, S., Siesler, H.W. and Ozaki, Y. 2006. Molecular structure, crystallinity and morphology of polyethylene/polypropylene blends studied by Raman mapping, scanning electron microscopy, wide angle x-ray diffraction, and differential scanning calorimetry. *Polymer Journal*, 38, 1127-1136.
- Gere, J.M. 2004. *Mechanics of Materials*. Sixth Edition. Thomson Learning, Inc, USA. pp. 1-19.
- Goharpey, F., Foudazi, R., Nazockdast, H. and Katbab, A.A. 2008. Determination of twin-screw extruder operational conditions for the preparation of thermoplastic vulcanizates on the basis of batch-mixer results. *Journal of Applied Polymer Science*. 107, 3840–3847.
- Greaves, D., Boxall, J., Mulligan, J., Montesi, A., Creek, J., Sloan, E.D. and Koh, C.A. 2008. Measuring the particle size of a known distribution using the focused beam reflectance measurement technique. *Chemical Engineering Science*. 63, 5410-5419.

- Han, S. J., Lohse, D. J., Radosz, M. and Sperling, L. H. 1998. Thermoplastic vulcanizates from isotactic polypropylene and ethylene-propylene-diene terpolymer in supercritical propane: synthesis and morphology. *Macromolecules*. 31, 5407-5414.
- Handt, J., Kunert, T. and Schmidt, R. 2006. Fragmentation and *cis-trans* isomerization of diimide in fs laser-pulses. *Chemical Physics Letters*. 428, 220–226.
- Harrats, C., Thomas, S., Groeninckx, G. and Radusch, H. J. 2005. Chapter 9 Phase morphology of dynamically vulcanized thermoplastic vulcanizates. *Micro-and nanostructured multiphase polymer blend systems: Phase morphology and interfaces*. CRC Press., USA.
- Harwood, H.J., Russell, D.B., Verthe, J.J.A. and Zymonas, J. 1973. Diimide as a reagent for the hydrogenation of unsaturated polymer. *Macromolecular Chemistry and Physics*. 163, 1-12.
- Healey, A.M., Hendra, P.J. and West, Y.D. 1996. A Fourier-transform Raman study of the strain-induced crystallization and cold crystallization of natural rubber. *Polymer*. 30, 4009-4024.
- Hendra, P. J., Jackson, K.D.O. 1994. Applications of Raman spectroscopy to the analysis of natural rubber. *Spectrochimica Acta*. 50A, 1987-1997.
- Hinchiranan, N., Charmondusit, K., Prasassarakich, P., and Rempel, G. L. 2006a. Hydrogenation of synthetic *cis*-1, 4-polyisoprene and natural rubber catalyzed by $[\text{Ir}(\text{COD})\text{py}(\text{PCy}_3)]\text{PF}_6$. *Journal of Applied Polymer Science*. 100, 4219–4233.
- Hinchiranan, N., Prasassarakich, P., and Rempel, G. L. 2006b. Hydrogenation of natural rubber in the presence of $\text{OsHCl}(\text{CO})(\text{O}_2)(\text{PCY}_3)_2$: Kinetics and mechanism. *Journal of Applied Polymer Science*. 100, 4499–4514.
- Hinchiranan, N., Lertweerasirikun, W., Poonsawad, W., Rempel, G. L., and Prasassarakich, P. 2009. Hydrogenated natural rubber blends: Aspect on thermal stability and oxidative behavior. *Journal of Applied Polymer Science*. 113, 1566–1575.
- Hudlicky, M. 1984. *Reductions in organic chemistry*. Ellis Horwood Limited, England.

- l'Abée, R., Goossens, H., van Duin, M., and Spoelstra, A. 2009. Sub-micrometer thermoplastic vulcanizates obtained by reaction-induced phase separation of miscible mixtures of poly(ethylene) and alkyl methacrylates. *European Polymer Journal*. 45, 503–514.
- Igathinathane, C., Pordesimo, L.O., Columbus, E.P., Batchelor, W.D. and Methuku, S.R. 2008. Shape identification and particles size distribution from basic shape parameters using ImageJ. *Computers and Electronics in Agriculture*. 63, 168-182.
- Jackson, K.D.O., Loadman, M. J. R., Jones, C. H. and Ellis, G. 1990. Fourier transform Raman spectroscopy of elastomers: an overview. *Specrochimica Acta*. 46A, 217-226.
- Jones, C.W. 1999. *Applications of Hydrogen Peroxide and Derivatives*. The Royal Society of Chemistry, Thomas Graham House, Science Park, Milton Road Cambridge CB4 0WF, UK.
- Koenig, J. L. 1999. *Spectroscopy of Polymers*, 2nd Edition, Elsevier Science, New York. pp. 256-258.
- Le, H. H., Heidenreich, D., Kolesov, I. S., Ilisch, S. and Radusch, H.J. 2010. Effect of carbon black addition and its phase selective distribution on the stress relaxation behavior of filled thermoplastic vulcanizates. *Journal of Applied Polymer Science*. 117, 2622–2634.
- Lee, U. 2012. Imaging modes. In *Raman Imaging: Techniques and Applications*. Zoubir, A., Ed. Springer, New York, USA. pp.1-6.
- Lee, Y.J., Moon, D., Migler, B.K. and Cicerone, M.T. 2011. Quantitative image analysis of broadband CARS hyperspectral images of polymer blends. *Journal of Analytical Chemistry*. 83, 2733-2739.
- Lin, X. 2005. *Hydrogenation of unsaturated polymers in latex Form*. Ph.D. Thesis, Waterloo University.
- Loan, L. D. 1972. Peroxide crosslinking reactions of polymers. *Pure and Applied Chemistry*. 30, 173-180.

- Li, Z. and Kontopoulou, M. 2009. Evolution of rheological properties and morphology development during crosslinking of polyolefin elastomers and their TPV blends with polypropylene. *Journal of Polymer Engineering and Sciences*. 49, 34-43.
- Mahittikul, A., Prasassarakich, P., and Rempel, G. L. 2007a. Noncatalytic hydrogenation of natural rubber latex. *Journal of Applied Polymer Science*. 103, 2885–2895.
- Mahittikul, A., Prasassarakich, P., and Rempel, G. L. 2007b. Diimide hydrogenation of natural rubber latex. *Journal of Applied Polymer Science*. 105, 1188–1199.
- Mark, J. E. 2007. *Physical properties of polymers handbook*. Second Edition. Springer Science and Business Media, LLC, New York, USA. pp. 430-431.
- McCreery, R. L. 2000. *Raman Spectroscopy for Chemical Analysis*. Wiley-Interscience, New York. pp. 15-16.
- Morris, H.R., Turner, J.F., Munro, B., Ryntz, R.A. and Treado, P.J. 1999. Chemical imaging of thermoplastic olefin (TPO) surface architecture. *Journal of Langmuir*. 15, 2961-2972.
- Nagdi, K. 1993. *Rubber as an engineering material: guideline for users*. Hanser., New York.
- Neon, G. S., Subramaniam, N., and Yahya, R. 1996. Hydrogenation of natural rubber using Nickel 2-Ethylhexanoate catalyst in combination with Triisobutylaluminum. *Journal of Applied Polymer Science*. 59, 63–70.
- Nicolini, A., de Campos Rocha, T. L. A., and Jacobi, M. A. M. 2008. Dynamically vulcanized PP/EPDM blends: Influence of curing agents on the morphology evolution. *Journal of Applied Polymer Science*. 109, 3093–3100.
- Overman, S.A. and Thomas, G. J. 1999. Raman markers of nonaromatic side chains in an α -helix assembly: Ala, Asp, Glu, Gly, Ile, Leu, Lys, Ser, and Val residues of phage *fd* subunits. *Biochemistry*. 38, 4018-4027.
- Paquette, L.A. 1991. *Organic reactions*. John Wiley & Sons, Inc., New Jersey.

- Pasto, D.J. and Taylor, R.T. 1991. Organic reactions, reduction with diimide. John Wiley & Sons, Inc., New Jersey.
- Phinyocheep, P., Pasiri, S., and Tavichai, O. 2002. Diimide hydrogenation of isoprene–styrene diblock copolymers. *Journal of Applied Polymer Science*. 87, 76–82.
- Prut, E.V., Erina, N.A., Karger-Kocsis, J. and Medintseva, T.I. 2008. Effects of blend composition and dynamic vulcanization on the morphology and dynamic viscoelastic properties of PP/EPDM blends. *Journal of Applied Polymer Science*. 109, 1212–1220.
- Rachapudy, H., Smith, G.G., Raju, V.R. and Graessley, W.W. 1979. Properties of amorphous and crystallizable hydrocarbon polymer. III. studies of the hydrogenation of polybutadiene. *Journal of Polymer Science*. 17, 1211-1222.
- Radusch, H. J. 2005. Phase morphology of dynamically vulcanized thermoplastic vulcanizates. Micro- and nanostructured multiphase polymer blend systems: Phase morphology and interfaces. pp. 295-330.
- Rylander, P.N. 1985. Hydrogenation methods. Academic press, INC., England.
- Rich, P.R. and Breton, J. 2002. Attenuated total reflection fourier transform infrared studies of redox changes in bovine cytochrome *c* oxidase: resolution of the redox fourier transform infrared difference spectrum of heme *a*3. *Biochemistry*. 41, 967-973.
- Samran, J., Phinyocheep, P., Daniel, P., Derouet, D., and Buzaré, J. Y. 2004a. Raman spectroscopic study of non-catalytic hydrogenation of unsaturated rubbers. *Journal of Raman Spectroscopy*. 35, 1073–1080.
- Samran, J., Phinyocheep, P., Daniel, P., and Kittipoom, S. 2004b. Hydrogenation of unsaturated rubbers using diimide as a reducing agent. *Journal of Applied Polymer Science*. 95, 16–27.
- Samran, J., Phinyocheep, P., Daniel, P., Derouet, D. and Buzaré, J.Y. 2004c. Spectroscopic study of di-imide hydrogenation of natural rubber. *Macromolecular Symposia*, 216, 131-143.
- Samran, J. 2005. A study of non-catalytic hydrogenation of natural rubber. Ph.D. Thesis, Mahidol University.

- Schmidt, P., Dybal, J., Scudla, J., Raab, M. and Kratochvil, J. 2002. Structure of polypropylene/polyethylene blends assessed by polarized PA-FTIR spectroscopy, polarized FT Raman spectroscopy and confocal Raman microscopy. *Journal of Macromolecular Symposia*. 184, 107-122.
- Simma, K., Rempel, G.L. and Prasassarakich, P. 2009. Improving thermal and ozone stability of skim natural rubber by diimide reduction. *Polymer Degradation and Stability*. 94, 1914–1923.
- Singha, N.K., Bhattacharjee, S. and Sivaram, S. 1997. Hydrogenation of diene elastomers, their properties and applications: A critical review. *Rubber Chemistry and Technology*. 70, 309-339.
- Slopiecka, K., Bartocci, P. and Fantozzi, F. 2011. Thermogravimetric analysis and Kinetic study of poplar wood pyrolysis. *Third International Conference on Applied Energy - 16-18 May 2011 - Perugia, Italy*, pp. 1687-1698.
- Smith, B.C. 2011. *Fundamentals of Fourier Transform Infrared Spectroscopy*, 2nd Edition. CRC Press, USA. pp. 5-7.
- Sperling, L. H. 2005. *Introduction to physical polymer science*. Fourth Edition. John Wiley & Sons. U.S.A. pp. 434-473.
- Stans, M.H. 1970. Bond dissociation energies in simple molecules. *NIST Special Publication*. 1, 58.
- Tanner, R.I. 2000. *Engineering rheology*, Second edition. Oxford University Press Inc., New York., U.S.A.
- Treloar, L.R.G. 1973. The elasticity and related properties of rubbers. *Reports on Progress in Physics*. 36, 755-826.
- Turrell, G., and Corset, J. 1996. *Raman microscopy: developments and applications*. Elsevier Academic Press Inc., USA.
- Van Duin, M. and Machado, A.V. 2005. EPDM-based thermoplastic vulcanisates: crosslinking chemistry and dynamic vulcanisation along the extruder axis. *Journal of Polymer Degradation and Stability*. 90, 340 – 345.
- Vennemann, N., Bokamp, K. and Broker, D. 2006. Crosslink density of peroxide cured TPV. *Journal of Macromolecular Symposia*. 245-246, 641–650.

- Walsh, R. 1998. Bond dissociation energies in organosilicon compounds. 23M. A. Brook, Silicon in Organic, Organometallic and polymer Chemistry. Wiley., New York.
- Xie, H.Q., Li, X.D. and Guo, J.S. 2003. Hydrogenation of nitrile-butadiene rubber latex to form thermoplastic elastomer with excellent thermooxidation resistance. *Journal of Polymer Science*. 90, 1026-1031.
- Xue, G. 1997. Fourier transform Raman spectroscopy and its application for the analysis of polymeric materials. *Progress in Polymer Science*. 22, 313-406.
- Yu, H., Zeng, Z., Lu, G. and Wang, Q. 2008. Processing characteristics and thermal stabilities of gel and sol of epoxidized natural rubber. *European Polymer Journal*. 44, 453–464.
- Yves, G. and Fontanille, M. 2008. *Organic and Physical Chemistry of Polymers*. John Wiley & Sons, Inc., Hoboken, New Jersey.
- Zoubir, A. 2012. *Raman imaging: techniques and applications*. Springer Inc., New York, USA.

APPENDICES

APPENDIX A

A.1 Effect of vulcanization systems on Raman spectra

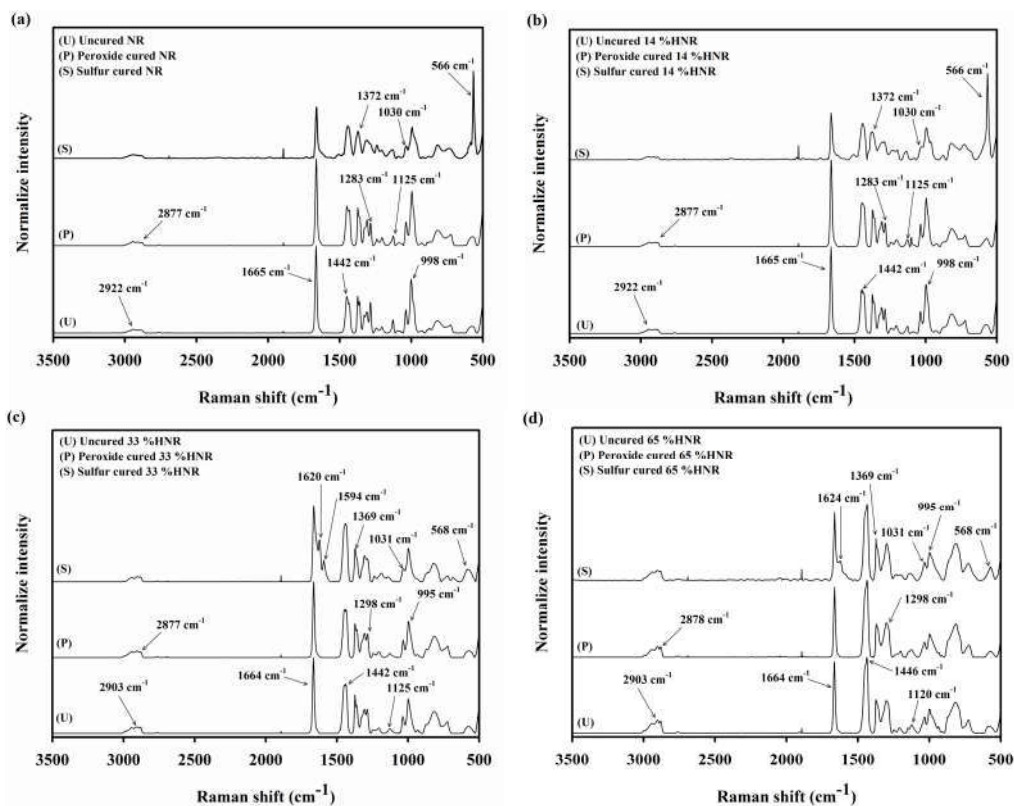


Figure A.1.1 Raman spectra of (a) NR, (b) 14 %HNR, (c) 33 %HNR, and (d) 65 %HNR, [U; Uncured, P; Peroxide cure, S; Sulfur cure]

A.2 Raman spectra of ozone and ultraviolet (UV) stability of HNR vulcanizates

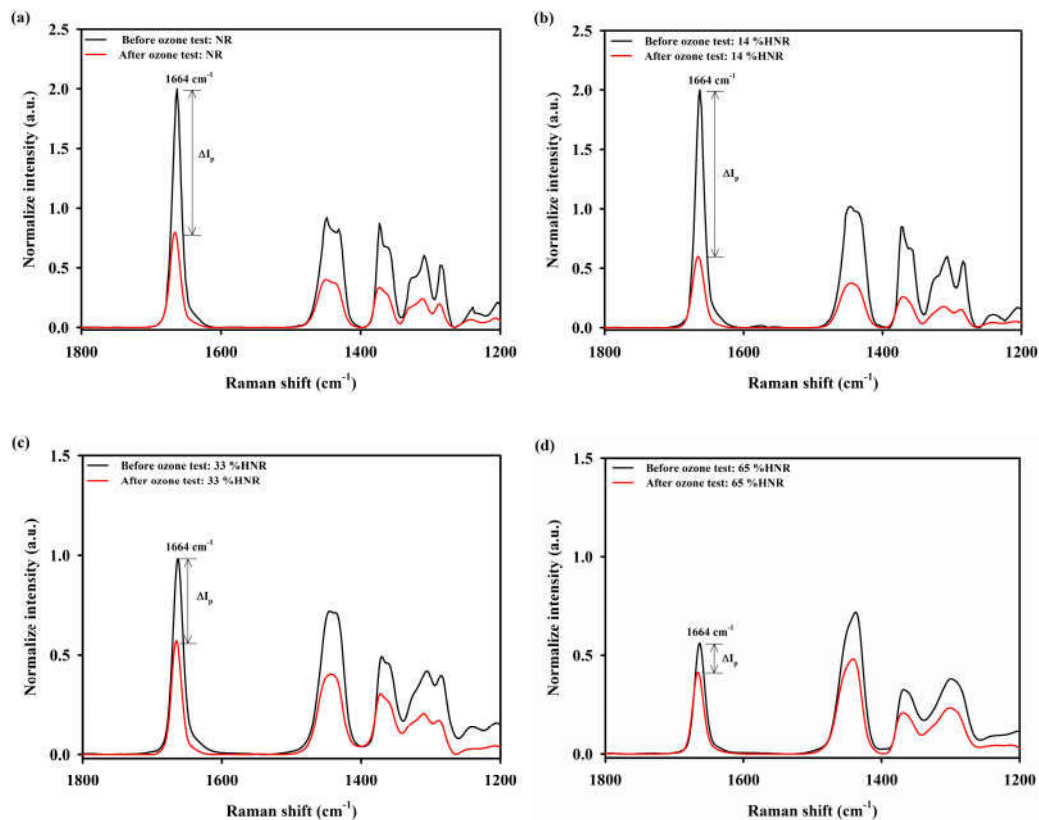


Figure A.2.1 Raman spectra before ozone (black line) and after ozone test (Red line) of rubber surface; (a) NR, (b) 14 %HNR, (c) 33 %HNR, and (d) 65 %HNR cured by peroxide

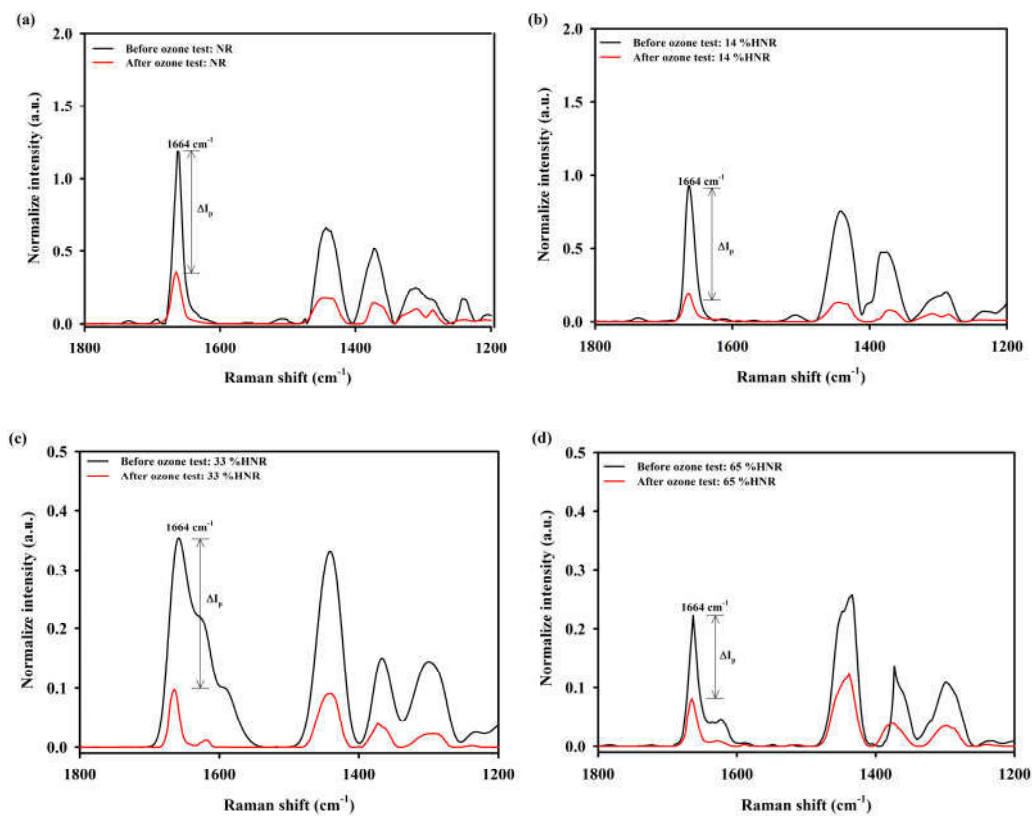


Figure A.2.2 Raman spectra before ozone (black line) and after ozone test (Red line) of rubber surface; (a) NR, (b) 14 %HNR, (c) 33 %HNR, and (d) 65 %HNR cured by sulfur

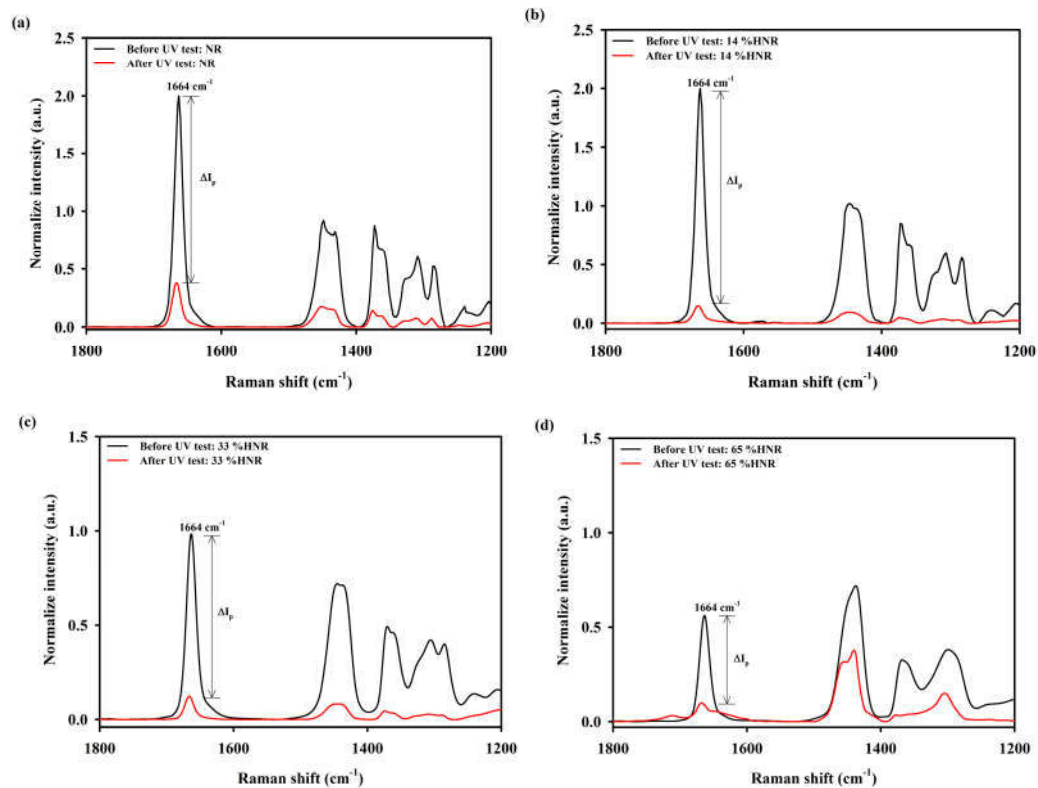


Figure A.2.3 Raman spectra before UV (black line) and after UV test (Red line) of rubber surface; (a) NR, (b) 14 %HNR, (c) 33 %HNR, and (d) 65 %HNR cured by peroxide

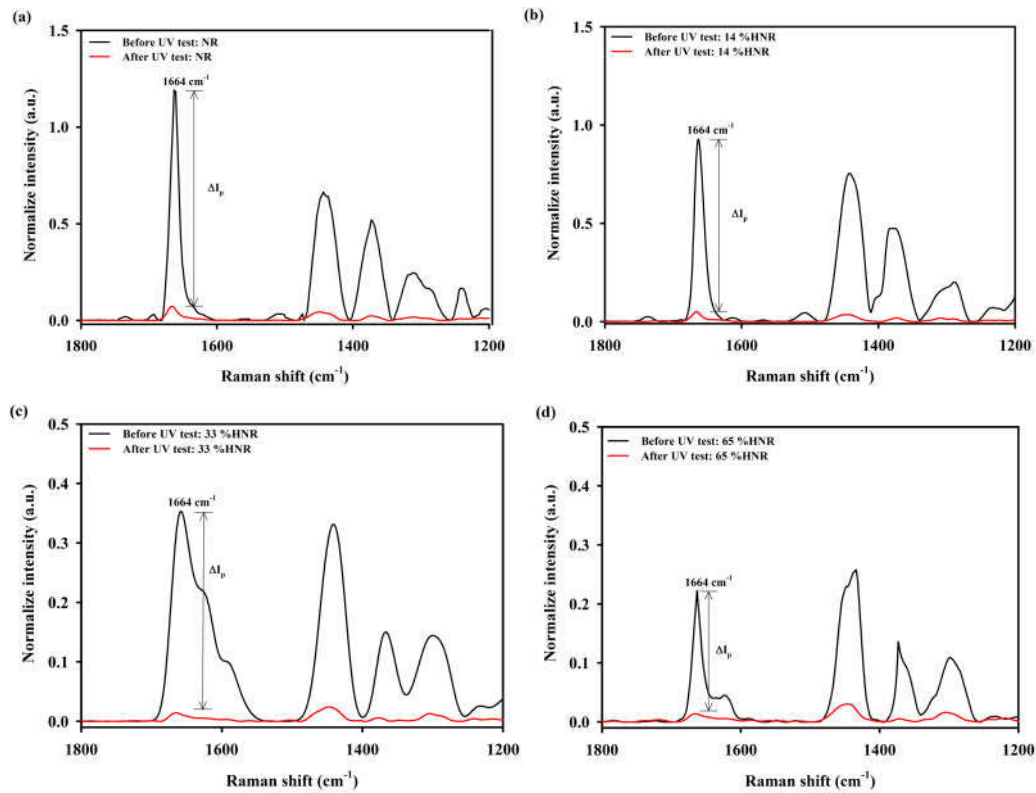


Figure A.2.4 Raman spectra before UV (black line) and after UV test (Red line) of rubber surface; (a) NR, (b) 14 %HNR, (c) 33 %HNR, and (d) 65 %HNR cured by sulfur

A.3 Mixing torque of thermoplastic vulcanizates based on dynamically vulcanized HNR and PP blends

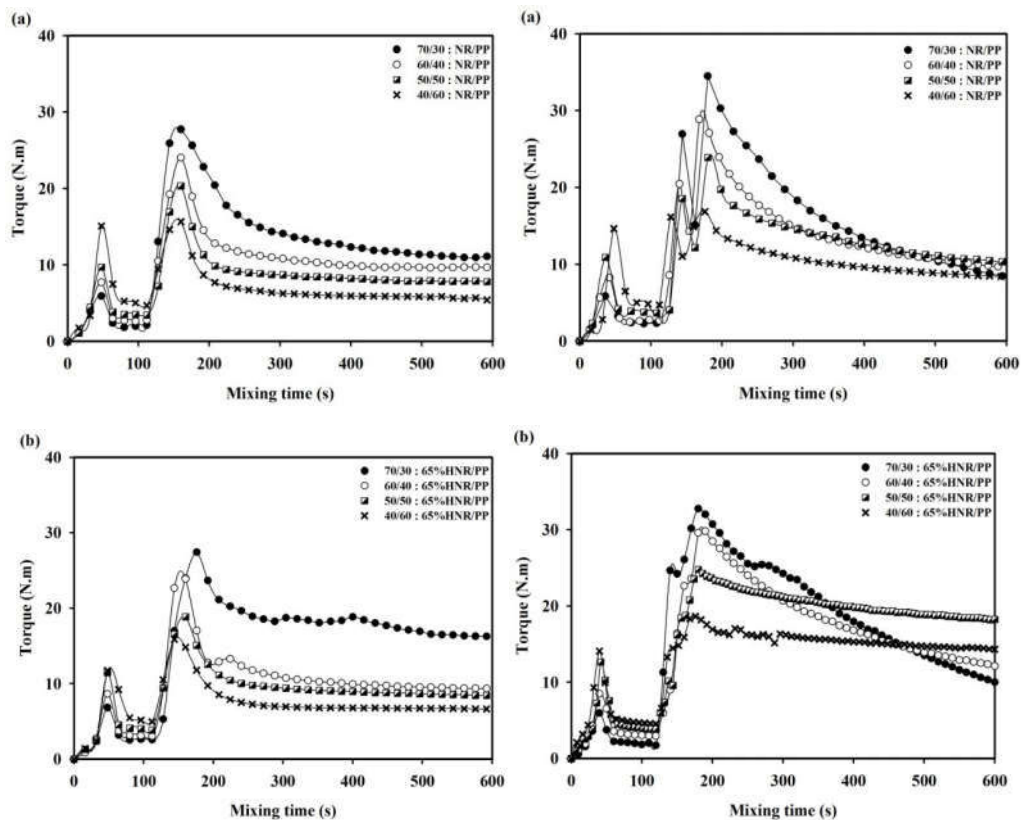


Figure A.3.1 Torque-time of (a) NR/PP, and (b) 65 %HNR/PP blends at 70/30, 60/40, 50/50, 40/60 (wt/wt%), peroxide cure (left column) and sulfur cure (right column)

A.4 Raman mapping of TPVs based on HNR/PP blends

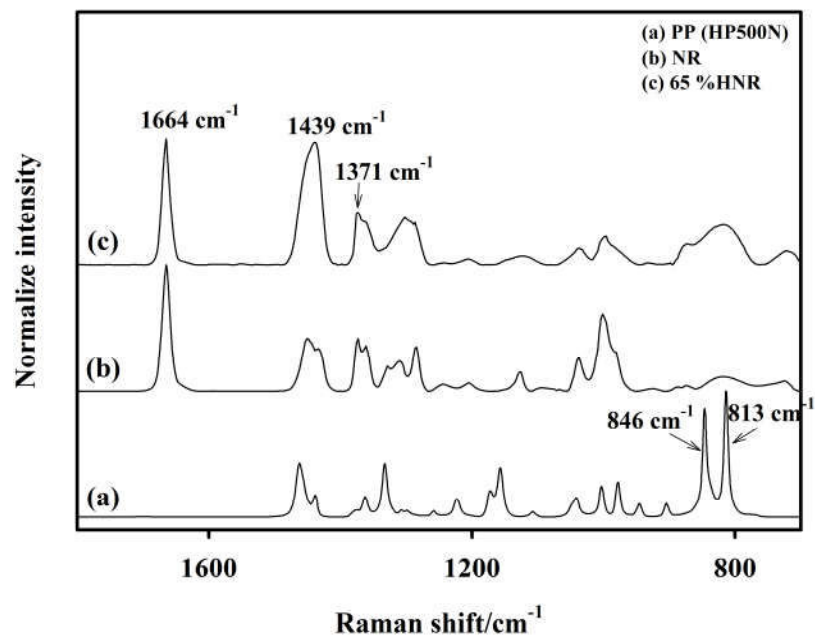


Figure A.4.1 Raman spectra of (a) PP (HP500N), (b) NR, (c) 65 % HNR

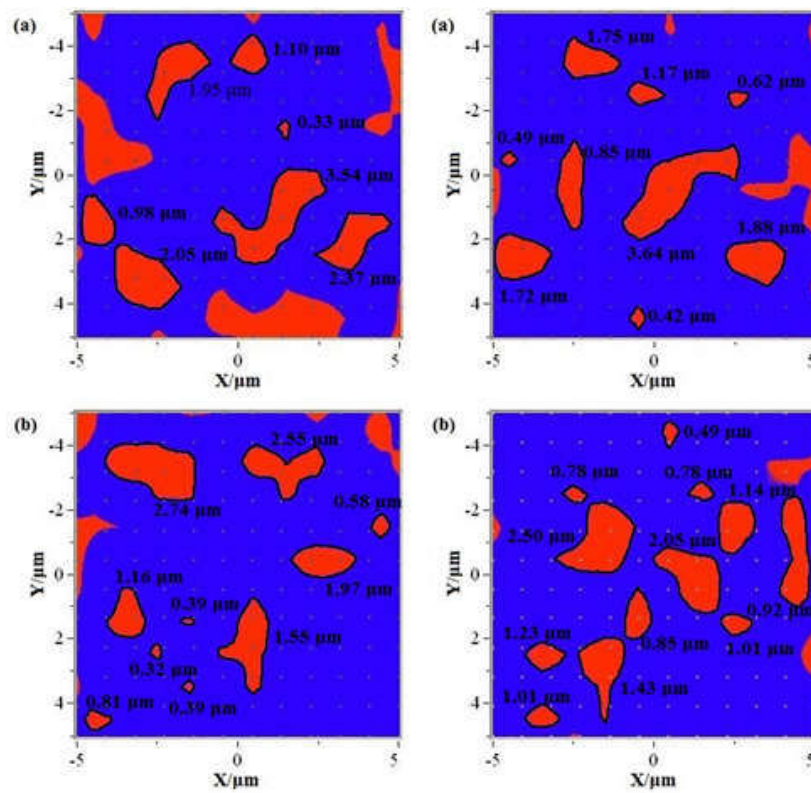


Figure A.4.1 The phase size of cross-linked rubber phase (red) dispersed in matrix PP phase (blue) of both peroxide cure (Left column) and sulfur cure (Right column) in TPVs based on (a) NR/PP and (b) 65 %HNR/PP at 50/50 wt/wt%. The phase size was calculated by using Raman mapping method

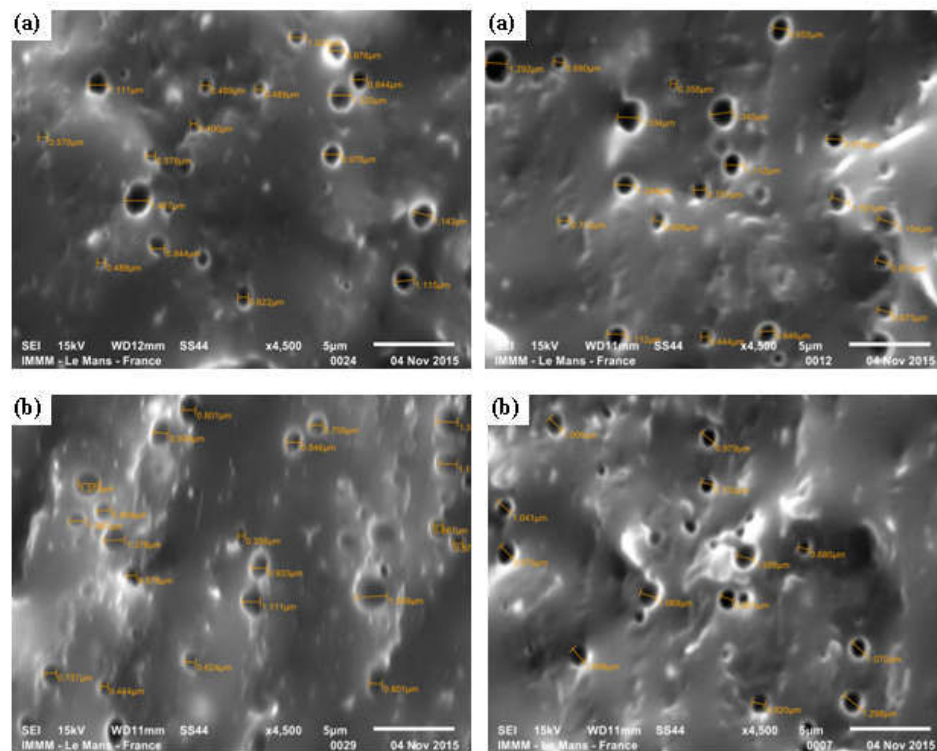


Figure A.4.2 The phase size of cross-linked rubber phase (dark hole) dispersed in matrix PP phase of both peroxide cure (Left column) and sulfur cure (Right column) in TPVs based on (a) NR/PP and (b) 65 %HNR/PP at 50/50 wt/wt% (magnification: 4,500x). The phase size was calculated by using SEM method

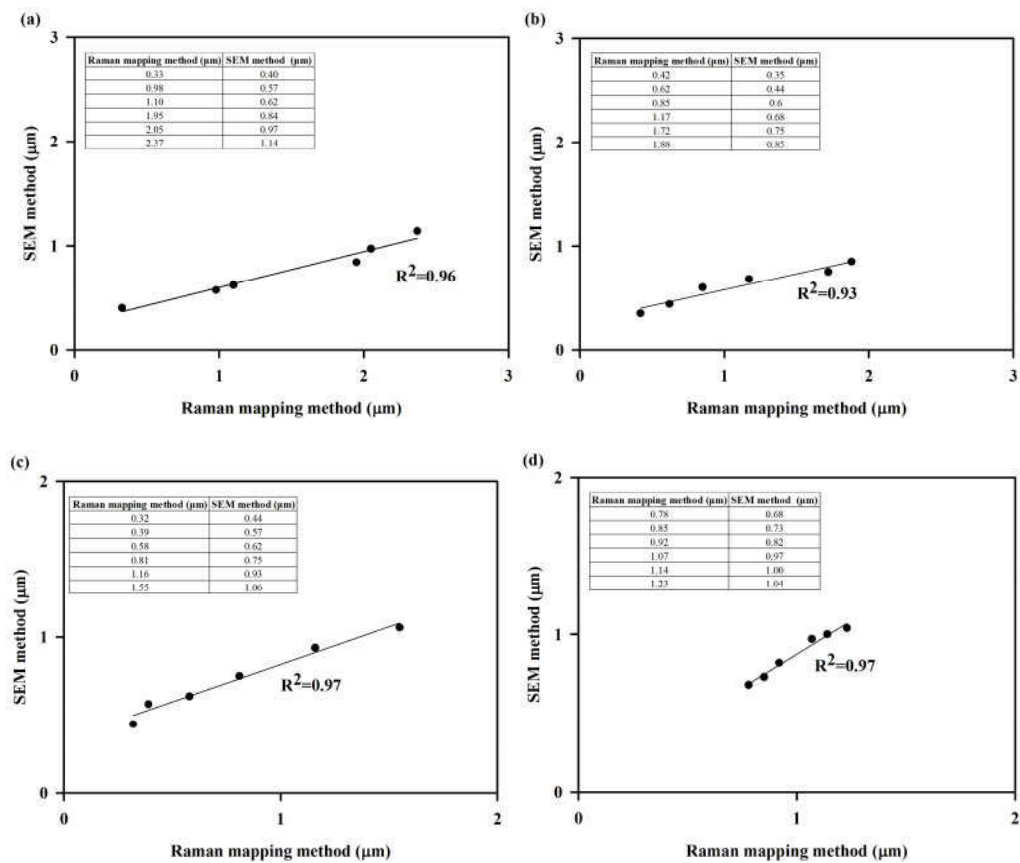


Figure A.4.3 Data correlation of phase size by using Raman mapping method versus SEM method of TPVs in peroxide cure (Left column,) and sulfur cure (Right column) base on NR/PP (a, b) and 65 %HNR/PP (c, d) at 50/50 (wt/wt%)

A.5 Determination of blend ratio by Raman spectroscopy

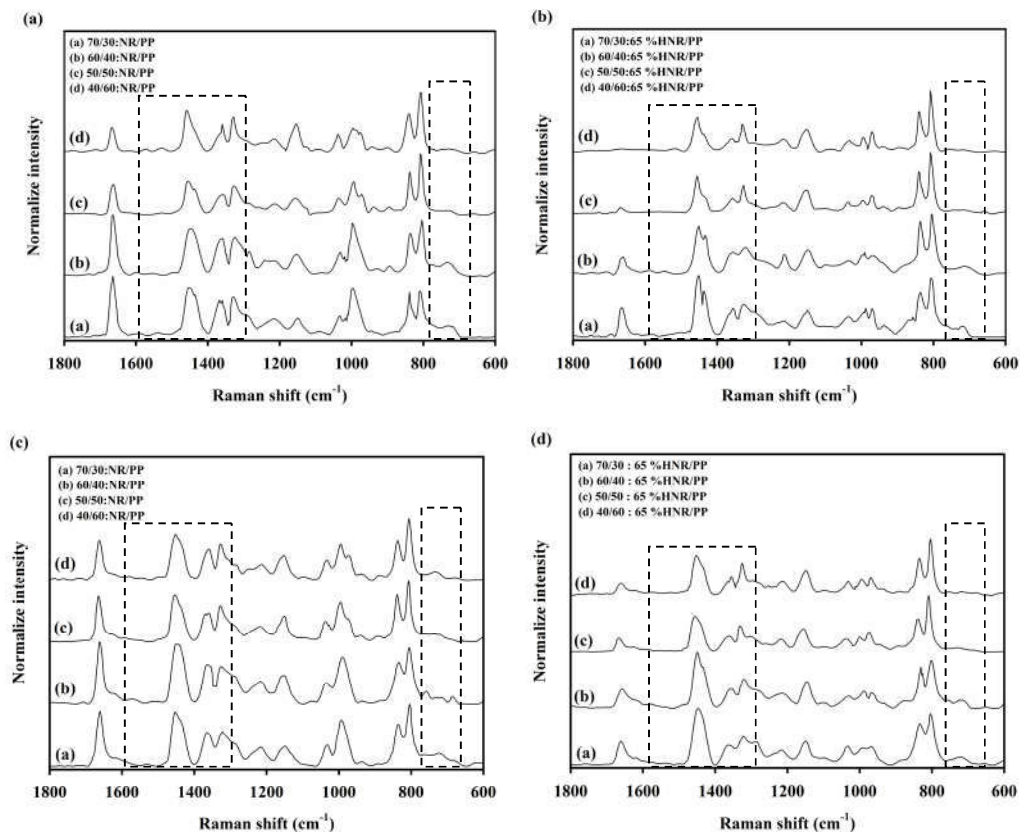


Figure A.5.1 Raman spectrum of TPVs (peroxide cure) based on (a) NR/PP, (b) 65 %HNR/PP and TPVs (sulfur cure) based on (c) NR/PP, (d) 65 %HNR/PP. The blends ratio of TPVs at 70/30, 60/40, 50/50 and 40/60 (wt/wt%)

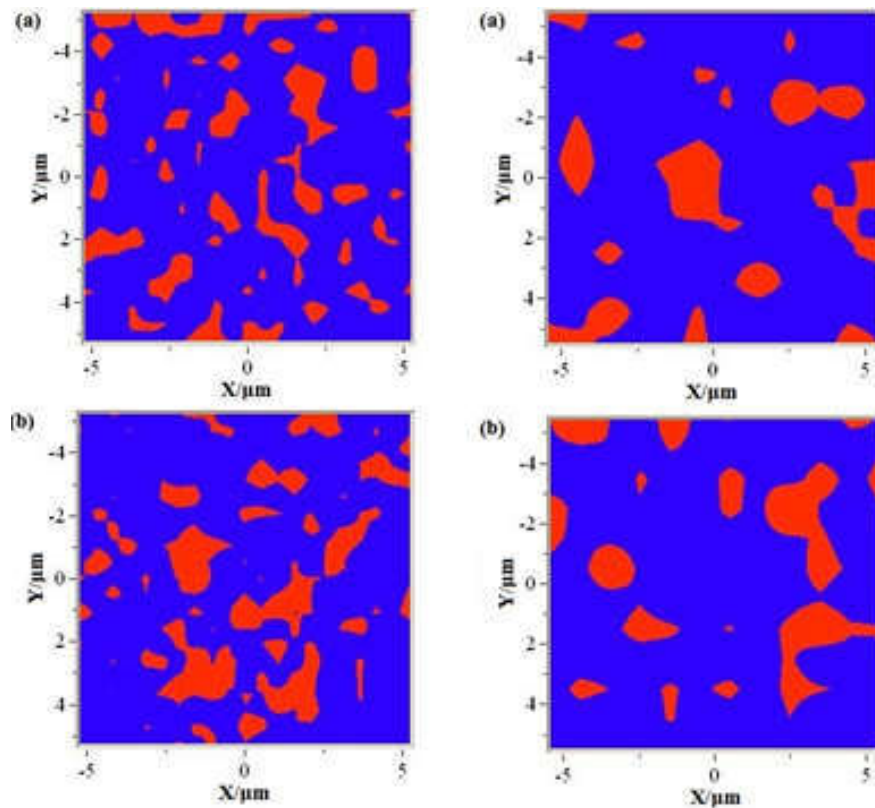


Figure A.5.2 Raman mapping of the blends ratio at 70/30 (wt/wt%) (Left column), at 40/60 (wt/wt%) (Right column) of TPVs (peroxide cure) based on (a) NR/PP, (b) 65 %HNR/PP: [PP phase (blue), rubber phase (red)].

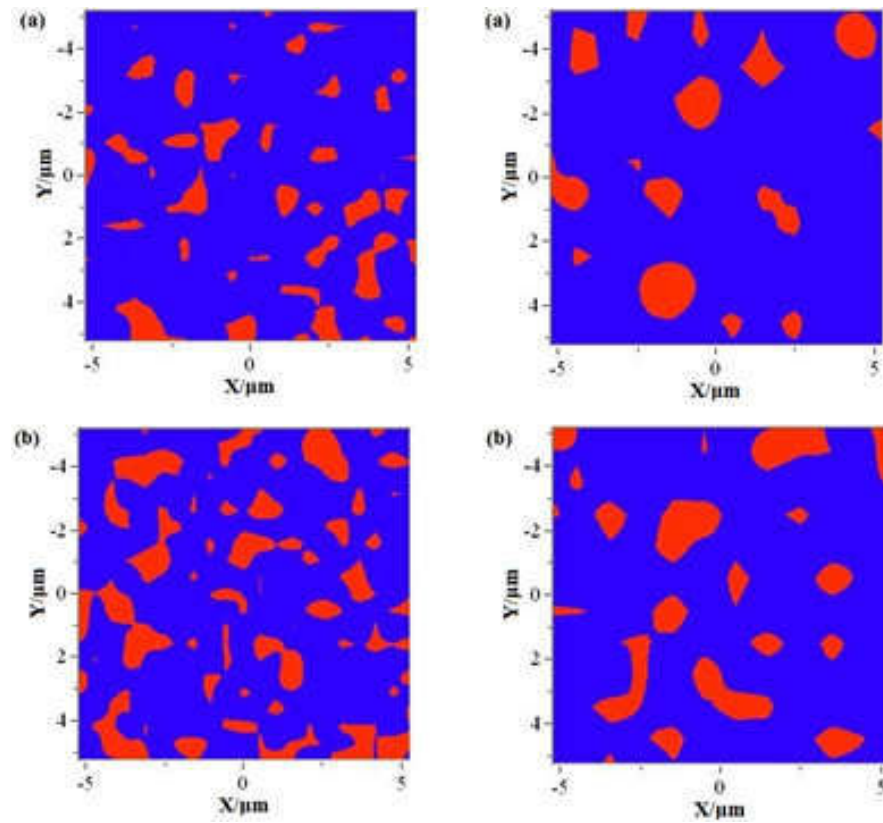


Figure A.5.3 Raman mapping of the blends ratio at 70/30 (wt/wt%) (Left column), at 40/60 (wt/wt%) (Right column) of TPVs (sulfur cure) based on (a) NR/PP, (b) 65 %HNR/PP: [PP phase (blue), rubber phase (red)]

A.6 Dynamic properties of TPVs based on HNR/PP blends

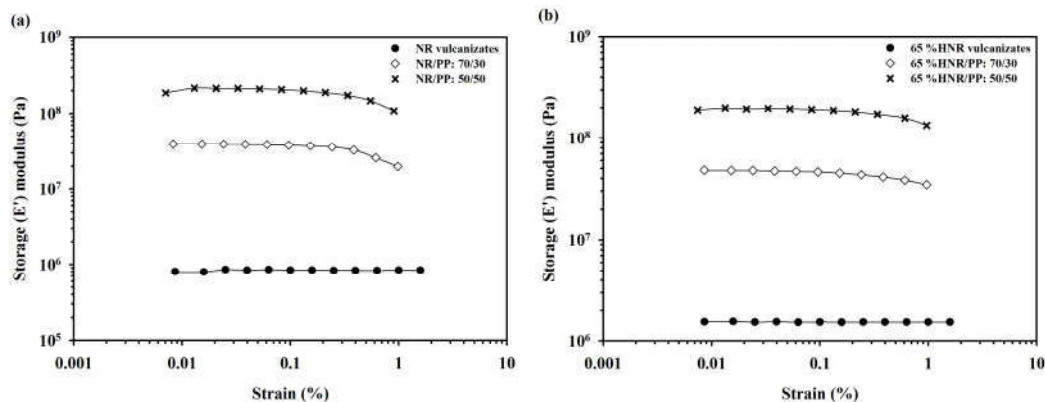


Figure A.6.1 Dynamic strain sweep of (a) NR vulcanizates and NR/PP blends at 70/30, 50/50 (wt/wt%) and (b) 65 %HNR vulcanizates and 65 %HNR/PP blends at 70/30, 50/50 (wt/wt%) in peroxide cure

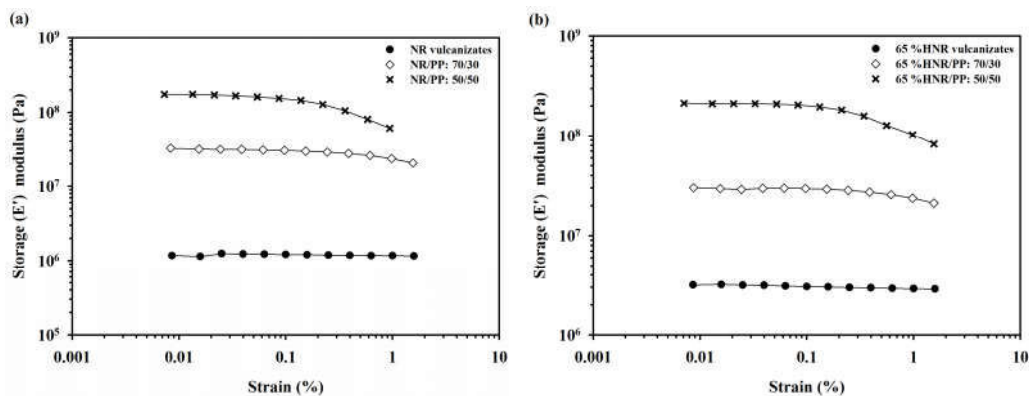


Figure A.6.2 Dynamic strain sweep of (a) NR vulcanizates and NR/PP blends at 70/30, 50/50 (wt/wt%) and (b) 65 %HNR vulcanizates and 65 %HNR/PP blends at 70/30, 50/50 (wt/wt%) in sulfur cure

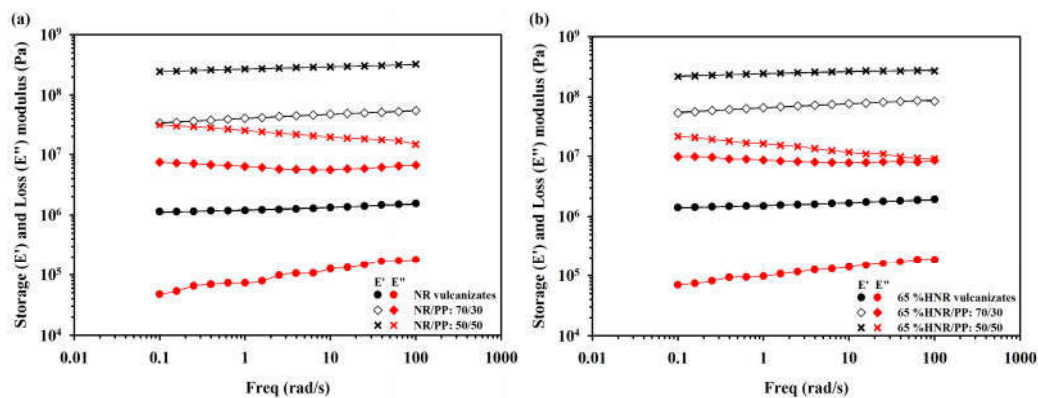


Figure A.6.3 Dynamic frequency sweep of (a) NR vulcanizates and NR/PP blends (b) 65 %HNR vulcanizates and 65 %HNR/PP blends. The blend ratio at 70/30, 50/50 (wt/wt%) in peroxide cure

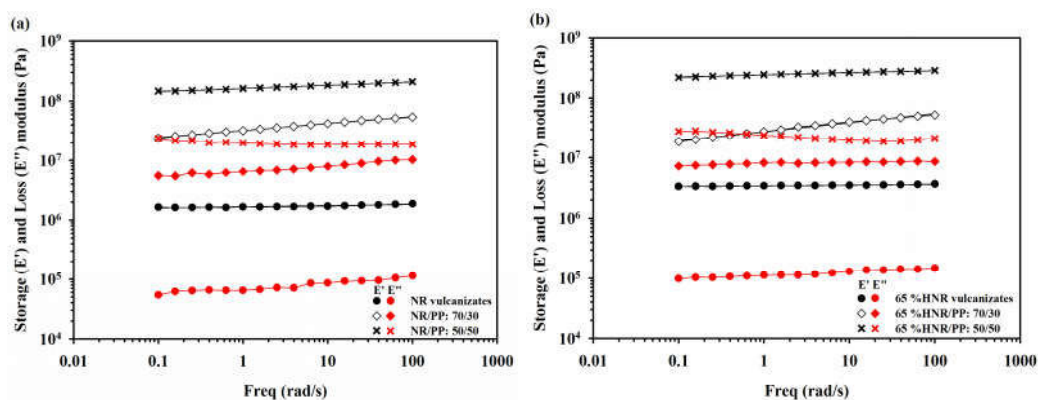


Figure A.6.4 Dynamic frequency sweep of (a) NR vulcanizates and NR/PP blends (b) 65 %HNR vulcanizates and 65 %HNR/PP blends. The blend ratio at 70/30, 50/50 (wt/wt%) in sulfur cure

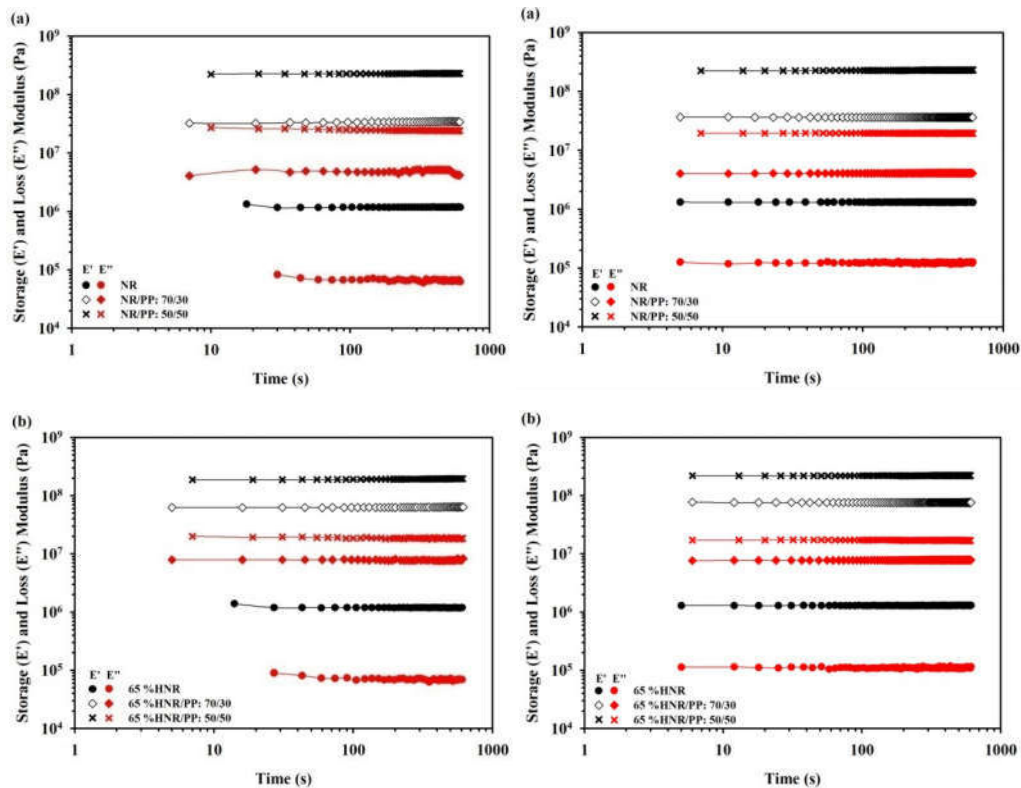


Figure A.6.5 Dynamic time sweep at frequency =1 rad/s (Left column) and frequency =10 rad/s (Right column) of (a) NR vulcanizates and NR/PP blends (b) 65 %HNR vulcanizates and 65 %HNR/PP blends. The blend ratio at 70/30, 50/50 (wt/wt%) in peroxide cure

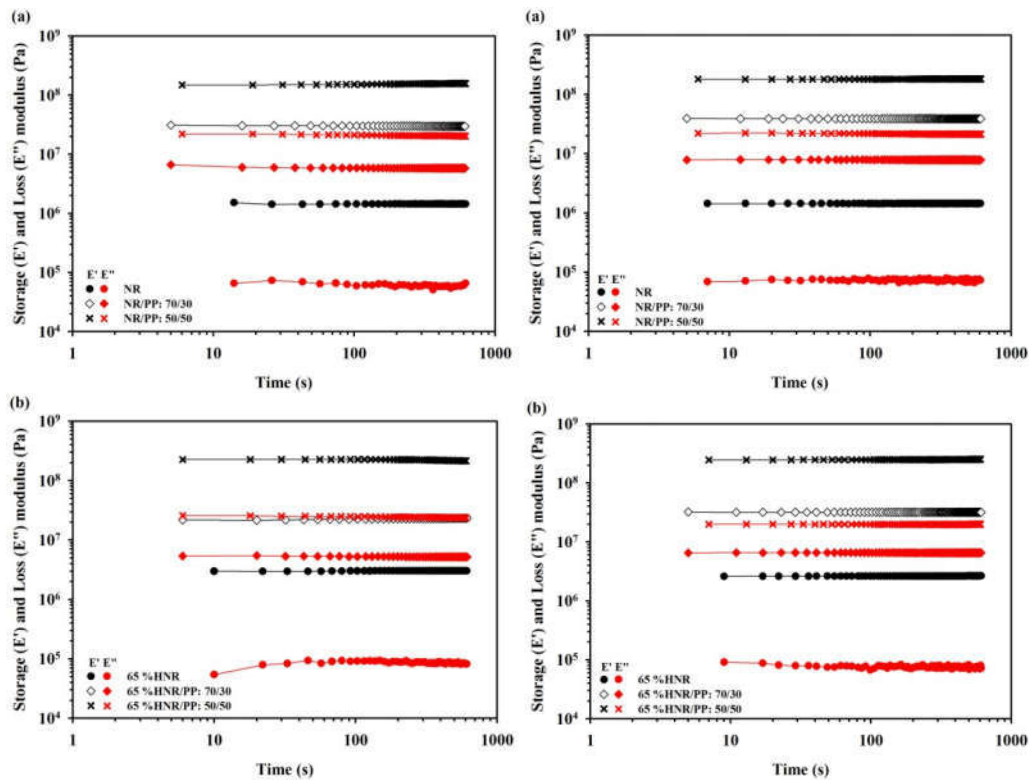


Figure A.6.6 Dynamic time sweep at frequency =1 rad/s (Left column) and frequency =10 rad/s (Right column) of (a) NR vulcanizates and NR/PP blends (b) 65 %HNR vulcanizates and 65 %HNR/PP blends. The blend ratio at 70/30, 50/50 (wt/wt%) in sulfur cure

A.7 Tensile properties of TPVs based on HNR/PP blends

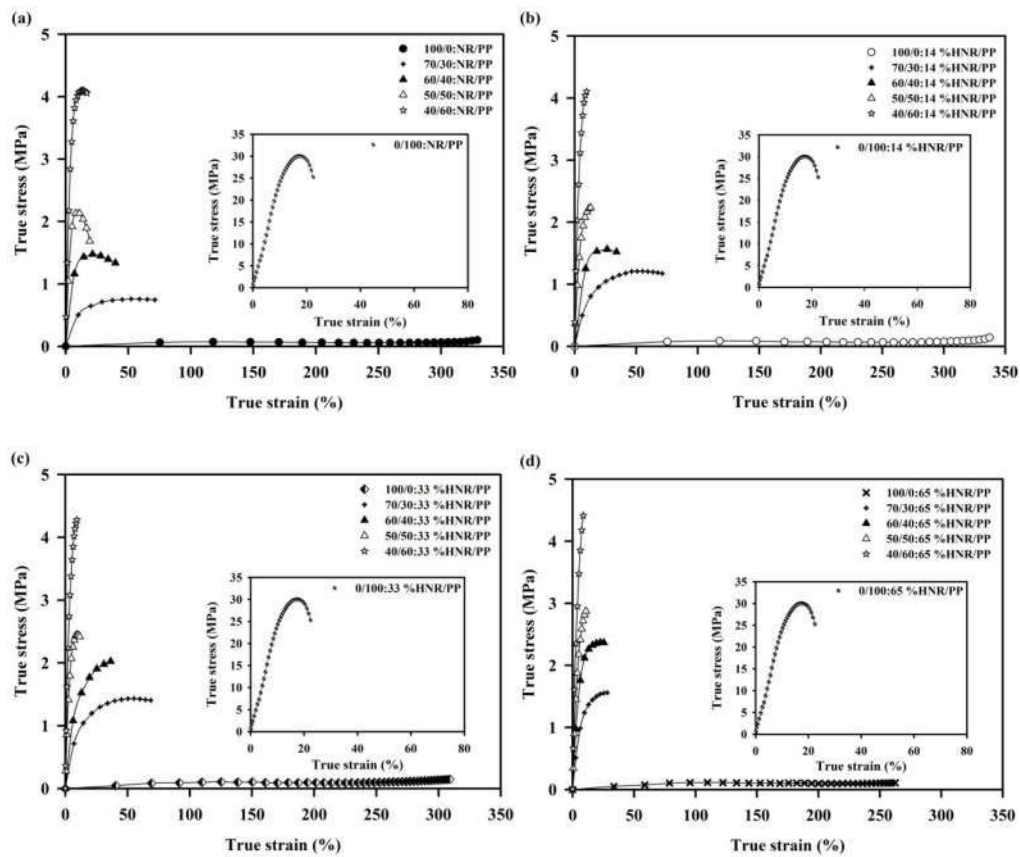


Figure A.7.1 True stress-strain curve of (a) NR/PP, (b) 14 %HNR/PP, (c) 33 %HNR/PP and (d) 65 %HNR/PP blends at 100/0, 70/30, 60/40, 50/50, 40/60, 0/100 (wt/wt%), peroxide cure

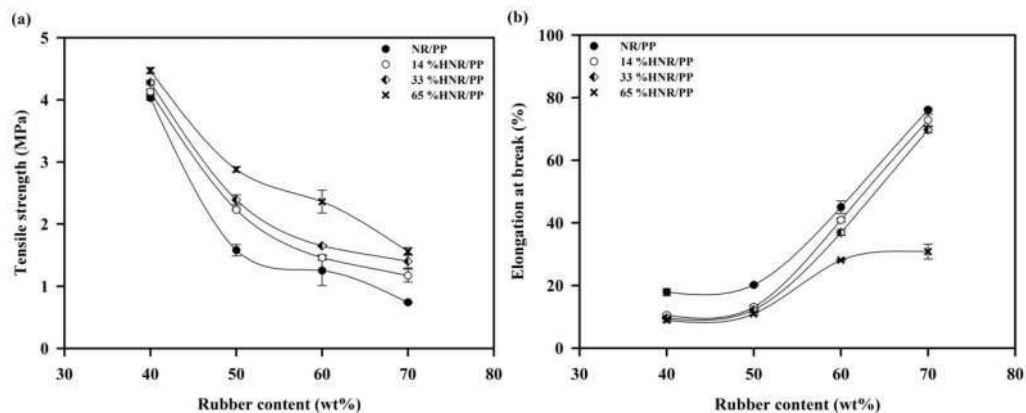


Figure A.7.2 Rubber contents of NR/PP, 14 %HNR/PP, 33 %HNR/PP and 65 %HNR/PP blends on (a) tensile strength (MPa) and (b) elongation at break (%) in peroxide cure

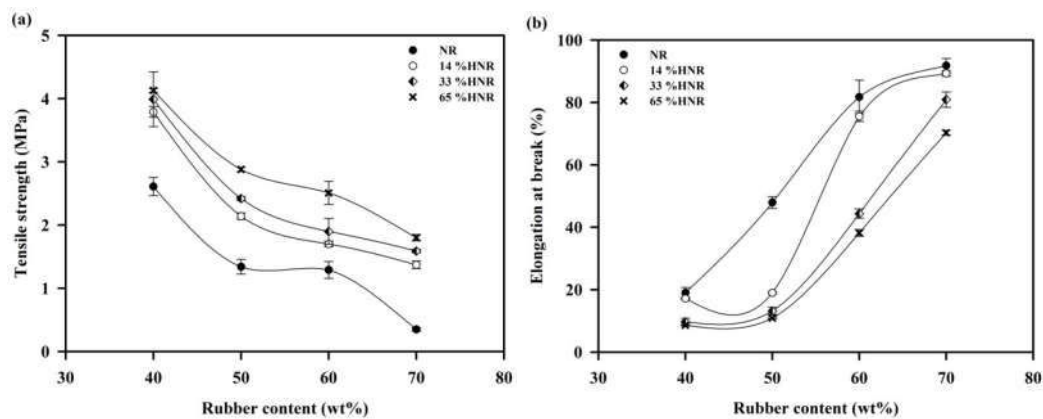


Figure A.7.3 Rubber contents of Rubber contents of NR/PP, 14 %HNR/PP, 33 %HNR/PP and 65 %HNR/PP blends on (a) tensile strength (MPa) and (b) elongation at break (%) in sulfur cure

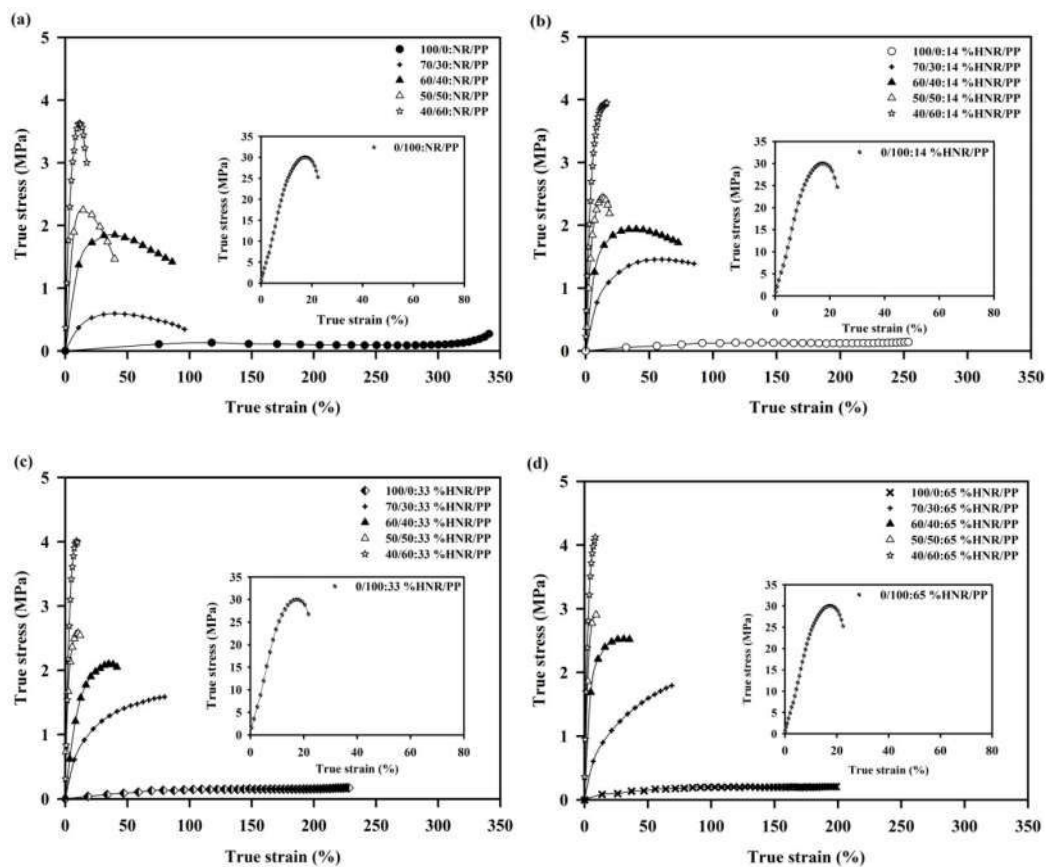


Figure A.7.4 True stress-strain curve of (a) NR/PP, (b) 14 %HNR/PP, (c) 33 %HNR/PP and (d) 65 %HNR/PP blends at 100/0, 70/30, 60/40, 50/50, 40/60, 0/100 (wt/wt%), sulfur cure

A.8 Fracture surface of TPVs based on HNR/PP blends

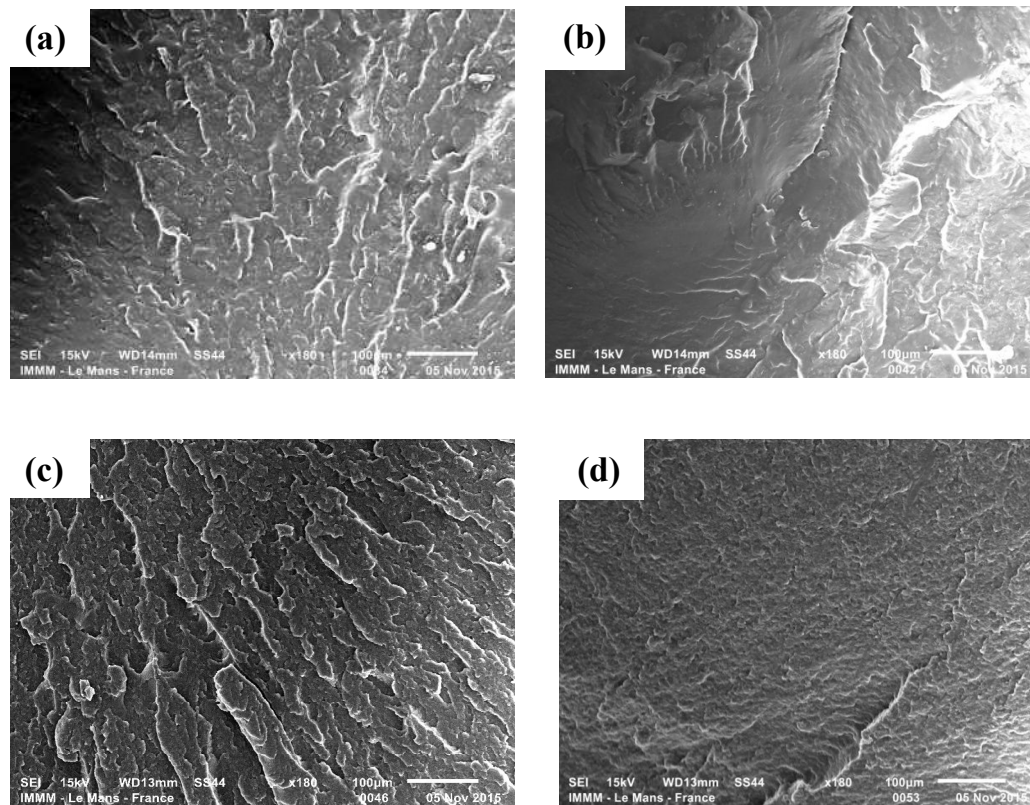


Figure A.8.1 The fracture surface morphology of TPVs: (a) NR/PP at 70/30 wt/wt%, (b) NR/PP at 50/50 wt/wt%, (c) 65% HNR/PP at 70/30 wt/wt% and (d) 65 %HNR/PP at 50/50 wt/wt% in peroxide cure

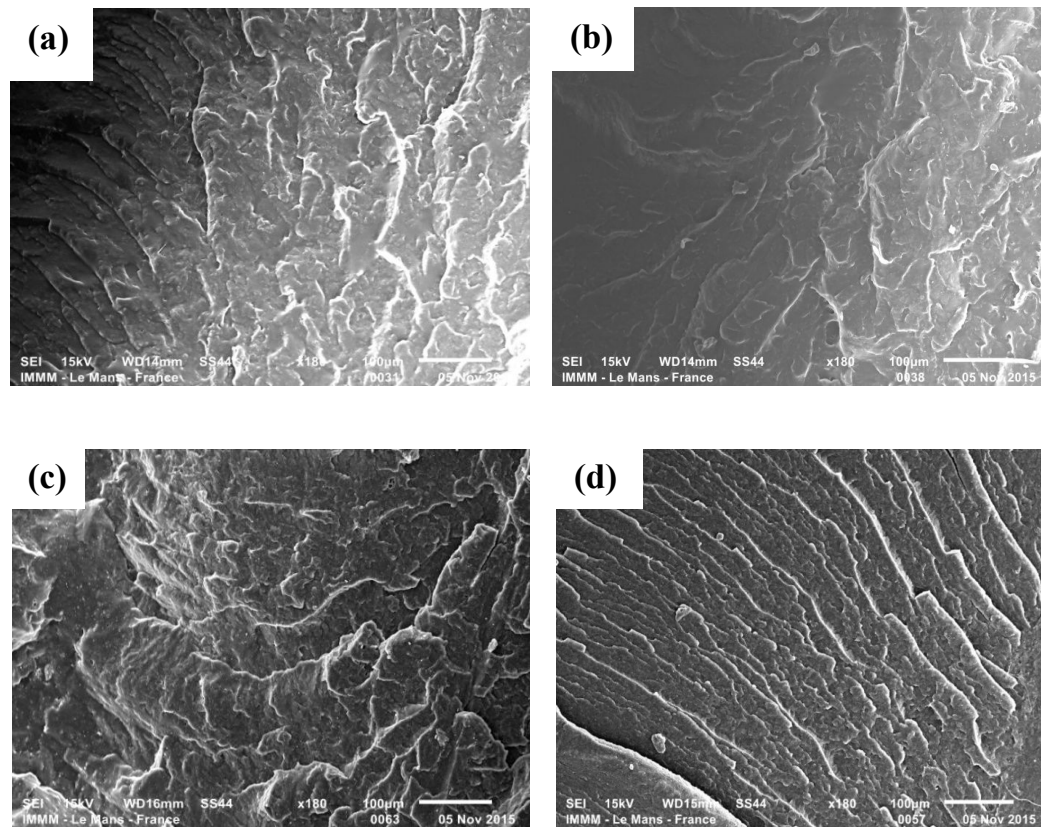
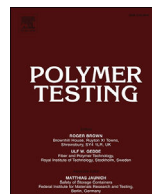


Figure A.8.2 The fracture surface morphology of TPVs: (a) NR/PP at 70/30 wt/wt%, (b) NR/PP at 50/50 wt/wt%, (c) 65% HNR/PP at 70/30 wt/wt% and (d) 65 %HNR/PP at 50/50 wt/wt% in sulfur cure

APPENDICES**APPENDIX B**

Raman investigation of thermoplastic vulcanizates based on hydrogenated natural rubber/polypropylene blends (Polymer Testing Journal)



Material Characterisation

Raman investigation of thermoplastic vulcanizates based on hydrogenated natural rubber/polypropylene blends



Korn Taksapattanakul ^{a, b, 1}, Tulyapong Tulyapitak ^b, Pranee Phinyocheep ^c, Polphat Ruamcharoen ^d, Jareerat Ruamcharoen ^e, Fabienne Lagarde ^a, Mathieu Edely ^a, Philippe Daniel ^{a, *}

^a Institut des Molécules et des Matériaux du Mans, IMMM –UMR-CNRS 6283, Université du Maine, Avenue Olivier Messiaen, 72085 Le Mans France

^b Department of Rubber Technology and Polymer Science, Faculty of Science and Technology, Prince of Songkla University, Pattani Campus, 94000 Thailand

^c Department of Chemistry, Faculty of Science, Mahidol University, 10400 Thailand

^d Rubber and Polymer Technology Program, Faculty of Science and Technology, Songkhla Rajabhat University, 90000 Thailand

^e Division of Chemistry, Department of Science, Faculty of Science and Technology, Prince of Songkla University, Pattani Campus, 94000 Thailand

ARTICLE INFO

Article history:

Received 21 July 2016

Received in revised form

30 September 2016

Accepted 11 November 2016

Available online 12 November 2016

Keywords:

Raman spectroscopy

Thermoplastic elastomers

Thermoplastic vulcanizates

Hydrogenated natural rubber

Polymer blends

ABSTRACT

Raman spectroscopy including mapping technique appears as a powerful technique for the characterization of polymer blends like thermoplastic elastomers (TPEs) and thermoplastic vulcanizates (TPVs). The Raman spectra of polymers blends such as natural rubber/polypropylene (NR/PP) and 65% hydrogenated natural rubber/polypropylene (65%HNR/PP) were identified and the phase distribution was determined. The study was driven for the same type of blends in TPEs state and TPVs state obtained after to 2 different processes, either peroxide cure or sulfur cure. The morphology of TPEs and TPVs obtained by Raman spectroscopy were compared and confirmed using scanning electronic microscopy.

Raman mapping shows that the phase morphology of NR/PP, 65%HNR/PP, were characterized as continuous rubber phase morphology of the thermoplastic elastomers (TPEs) and a fine dispersion of cross-linked rubber phase in a continuous matrix of the thermoplastic vulcanizates (TPVs). Raman spectroscopy is demonstrated to be a reference to determine the content ratio of each component in the TPVs. Moreover, Raman mapping could be used to calculate the phase size of cross-linked rubber phase dispersed in the thermoplastic vulcanizates (TPVs).

© 2016 Elsevier Ltd. All rights reserved.

1. Introduction

Thermoplastic vulcanizates (TPVs) constitute a special class of Thermoplastic Elastomers (TPEs) resulting from elastomer cross-linking and generating a fine dispersion of cross-linked elastomer particles in a continuous matrix of thermoplastics. The vulcanization of the elastomer phase has been carried out under dynamic shear during mixing (dynamic vulcanization) by sulfur and accelerator, peroxide vulcanization systems [3]. TPVs offer properties of cross-linked rubber, coupled with the processability of

thermoplastics. There may be several combinations of rubbers, like Ethylene-propylene-diene-rubber (EPDM), natural rubber (NR), with plastics, like PP, to form TPEs and TPVs. Polypropylene (PP) was used because of its high melting point and high crystallinity, resulting in good TPV properties even at high temperatures. EPDM can be also used because of its stability against high temperatures and ozone as same as hydrogenated natural rubber (HNR), thus giving to the corresponding TPVs good heat and ozone resistance. Due to the process of dynamic vulcanization used, the production of TPVs has been carried out under high temperature (melt temperature of plastic). Natural rubber (NR) can be degraded under high temperature due to the unsaturation of C=C double bonds within the isoprene backbone. Hydrogenation of natural rubber helps to improve the thermal and oxidative stability, since the radical-susceptible C=C bonds are replaced by saturated C–C bonds. With almost complete saturation, the backbone structure of natural rubber is changed from *cis*-1,4-polyisoprene to an

* Corresponding author. Institut des Molécules et des Matériaux du Mans, IMMM –UMR CNRS 6283, Université du Maine, Le Mans 72085 France.

E-mail address: philippe.daniel@univ-lemans.fr (P. Daniel).

¹ Permanent address. Department of Rubber Technology and Polymer Science, Faculty of Science and Technology, Prince of Songkla University, Pattani Campus, 94000 Thailand.

alternating ethylene-propylene copolymer. Therefore, the thermoplastic vulcanizates (TPVs) based on blends of hydrogenated natural rubber (HNR) and polypropylene (PP) were investigated. Hydrogenated natural rubber (HNR) was prepared by the chemical modification of natural rubber via non-catalytic hydrogenation reaction.

Raman mapping techniques can characterize distribution of polymer components in multiphase systems. Actually Raman spectroscopy provides the potential of fast determination with little or no sample preparation and also without the classical use of stains or dyes samples [1,2]. Moreover, Raman spectroscopy has the advantage to produce a strong signal especially in systems with non polar bonds like for instance C=C bond in the case of NR [2]. Additionally Raman spectroscopy is a non-destructive method and a fingerprint technique.

Numerous studies have been done on the Raman mapping of multilayer polymer blends based on polystyrene, polypropylene and poly (styrene-ethylene/propylene) diblock copolymer [4], IR/HNBR blends [5], PET/HDPE polymer blends [6], polypropylene/polyethylene blends [7], thin film of thermoplastic olefin (TPO) of chlorinated Polyolefin (CPO), ethylene-propylene rubber (EPR) and polypropylene (PP) [8], polypropylene/polyethylene/ethene-propenecopolymer, polybutyleneterephthalate/polycarbonate/low density polyethylene, and styrene-co-acrylonitrile/styrene-co-maleicanhydrate/poly-2,6-dimethylphenylene oxide [9], polystyrene/micro-diamonds composite (PS/C) [10].

However, thermoplastic vulcanizates based on hydrogenated natural rubber/polypropylene blends investigated by Raman spectroscopy such as Raman mapping, with calculation of blends ratio, determination of particle size of cross-linked rubber phase dispersed in the thermoplastic vulcanizates (TPVs), has not yet been reported up to our knowledge.

In this work, Raman spectroscopy and Raman mapping were used (1) to characterize the structure of the blends TPEs and TPVs in the 50/50 content ratio, (2) to study the rubber and plastic phase distribution also in the 50/50 content ratio for both blends TPEs and TPVs (3) to determine the content ratio of polypropylene (PP) and natural rubber (NR), hydrogenate natural rubber (65%HNR) in the blends for different ratio contents and finally (4) to calculate the phase size of cross-linked rubber phase dispersed in the thermoplastic vulcanizates (TPVs).

2. Experimental

2.1. Materials

Natural rubber latex (NRL) with 60% dry rubber content (DRC) was purchased from Yala latex Co. Yala, Thailand. Hydrogenated natural rubber (HNR) with a degree of hydrogenation equal to 65% was prepared by using hydrazine monohydrate ($N_2H_4 \cdot H_2O$) (the assay is 35%, commercial grade, Lanxess Deutschland GmbH, Germany) and hydrogen peroxide (H_2O_2) (the assay is 50%, standard, Thai peroxide co. ltd. Thailand) via non-catalytic hydrogenation. Polypropylene was obtained from HP500N, Homopolymer, Lyon-dell Basell co. USA.

The chemicals for the vulcanization were purchased according to the following: sulfur (vulcanizing agent, Siam Chemicals Co. Ltd. Thailand), Stearic acid (activator, Imperial Chemical Co. Ltd. Thailand), Zinc oxide (activator, Global Chemical Co. Ltd. Thailand), Tetramethylthiuram disulfide (TMTD) (accelerator or as a sulfur donor, Flexsys Co. Ltd. Belgium), 2-mercaptobenzothiazole (MBT) (accelerator, Flexsys American LP Co. Ltd. USA), Dicumyl peroxide (DCP) (curing agent, Wuzhou International Co. Ltd. China), Triallyl cyanurate (TAC) (co-agent, Fluka Chemie, Buchs, Switzerland).

2.2. Preparation of thermoplastic elastomers and thermoplastic vulcanizates

For the preparation of TPEs and TPVs, the grade of PP which was used is characterized by a melt flow rate of 12 g/10 min at 230 °C under 2.16 kg load. Additionally the average molecular weight of this PP grade has been reported in literature to be in the range of 2.38×10^5 – 2.60×10^5 g/mol and polydispersity in the range of 3.3–6.9 [11–14]. The degree of crystallinity of PP HP500N, used in this work, has been previously reported and calculated according to the classical relation:

$$\% \chi C = \Delta H_f / \Delta H_f^0$$

where ΔH_f is an enthalpy of fusion of PP crystals and ΔH_f^0 is the enthalpy of fusion of 100% crystalline PP. These values were then reported in literature to be 45.4%–46.3% and 57.4–58.7% [15–18] depending of the value of ΔH_f^0 used in calculation [19,20].

Note that the blending process probably induce a decreasing in the percentage of crystallinity as it was observed in other blends like PP-thermoplastic polyurethane [18], PP-polyolefine elastomer [21], or also PP-chloroprene rubber [22].

Then for preparing thermoplastic elastomers (TPEs), PP was melt for 3 min in the internal mixer before adding rubber. Two polymers were mixed in the internal mixer (fill factor = 0.8) until the constant torque is obtained. The mixing time for each batch was 10 min at a constant rotor speed of 80 rpm. The temperature setting of the mixer is 180 °C. For the blends without chemicals, they were removed immediately from the mixer and passed through the two-roll mill to get sheets.

The preparation of NR and HNR compounds was performed using an internal mixer (fill factor = 0.8). The mixing was performed at room temperature (30 °C) and at a constant rotor speed of 60 rpm. NR and HNR were masticated for 2 min and then the chemicals were added. The mixing time for each batch took 10 min.

For the vulcanization process peroxide or sulfur were used. The formulation used for the preparation of the rubber compounds is given in Table 1.

For preparing thermoplastic vulcanizates (TPVs), PP was melt for 3 min in the internal mixer before adding rubber compounds. The temperature setting of the mixer is 180 °C. Two polymers were mixed in the internal mixer (fill factor = 0.8) until the constant torque is obtained. The mixing time for each batch took 10 min. The TPVs were removed immediately from the mixer and passed through the two-roll mill to get sheets. TPEs and TPVs samples were pressed for 5 min in a compression molding press at a temperature of 190 °C and at a pressure of 12.5 MPa. Subsequently, the samples were cooled down under pressure to room temperature.

Note that considering the sample preparation method, where compression molding was used with very low shear rate, together with a 1–2 mm samples thickness, a skin-core effect can't be observed.

2.3. Raman spectroscopy and Raman mapping

In this study, Raman spectra of the samples were recorded with a Xplora-Horiba spectrometer. The experiment was performed at room temperature under microscope (Olympus BX 40) using a long distance work objective with a magnification $\times 50$. The simple spectrograph was adjusted with a 1200 lines per mm grating. The samples were illuminated with a laser light at 785 nm. The frequency range studied was 400–3500 cm^{-1} with 50 accumulations and an acquisition time of 2 s per spectrum. The lateral resolution is

Table 1
Formulation of the rubber compounds, TPEs and TPVs preparation.

Ingredients	TPEs	TPVs	
		Peroxide cure	Sulfur cure
NR (phr ^a)	-	100	100
HNR (phr ^a)	-	100	100
DCP (phr ^a)	-	1.0	-
TAC (phr ^a)	-	0.6	-
Sulfur (phr ^a)	-	-	1.50
TMTD (phr ^a)	-	-	0.65
MBT (phr ^a)	-	-	0.40
Zinc oxide (phr ^a)	-	-	5.00
Stearic acid (phr ^a)	-	-	1.00
NR/PP (wt/wt%)	50/50	70/30, 60/40, 50/50, 40/60	70/30, 60/40, 50/50, 40/60
HNR/PP (wt/wt%)	-	-	-

^a phr, parts per hundred of rubber by weight.

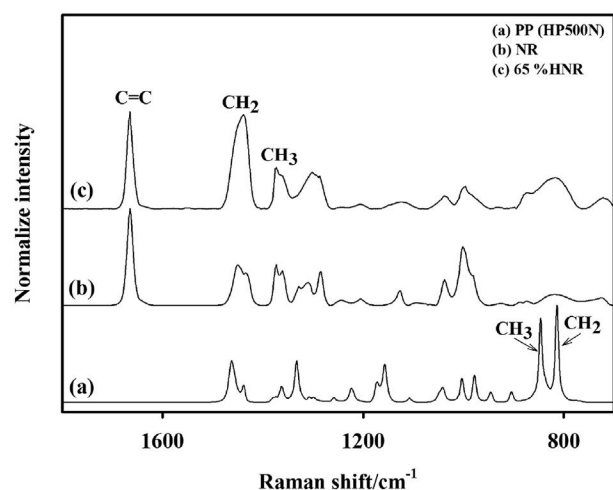


Fig. 1. Raman spectra of polymer: (a) polypropylene (PP, HP500N), (b) natural rubber (NR), (c) hydrogenated natural rubber (HNR) at 65% HNR.

depending of the entrance slit (100 μm in our case), the selected objective and the grating. Then Raman mapping in this study was recorded by means of scanning a sample surface ($10 \times 10 \mu\text{m}^2$) by step size of 0.9 μm in both X- and Y-axes (point to point), which is lower than the lateral resolution in these conditions. The confocal pinhole conjugated to microscope was adjusted to 500 μm in this experiment and gives the depth resolution which can be estimated in these conditions to 1 μm . Labspec 6 software (from Horiba) was used to operate the mapping system and record the spectral data.

Because Raman scattering is not only qualitative technique but can bring quantitative information, the content ratio of NR/PP and 65%HNR/PP blends can be calculated using Eq. (1), Eq. (2) as following:

$$\text{PP content (\%)} = \left[\frac{I_{(813-846)}}{I_{(813-846)} + I_{(1434-1664)}} \right] \times 100 \quad (1)$$

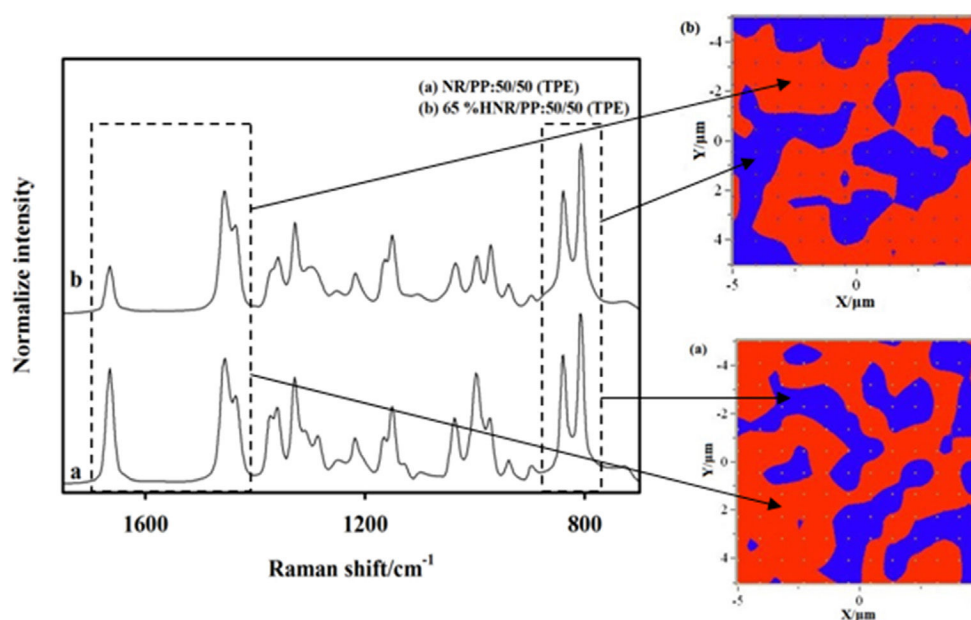


Fig. 2. Raman spectrum and Raman mapping of TPEs based on (a) NR/PP, (b) 65%HNR/PP. All containing 50 wt% rubbers, Raman mapping: PP phase (blue) and rubber phase (red). (For interpretation of the references to colour in this figure legend, the reader is referred to the web version of this article.)

$$\text{NR or 65 \%HNR content (\%)} = \left[\frac{I_{(1434-1664)}}{I_{(813-846)} + I_{(1434-1664)}} \right] \times 100 \quad (2)$$

where $I_{(813-846)}$ are the integrated intensities of the Raman spectra peaks of PP phase at 813–846 cm^{-1} , $I_{(1434-1664)}$ are the integrated intensities of the Raman spectra peaks of NR or HNR phase at 1434–1664 cm^{-1} .

2.4. Scanning electron microscopy (SEM)

The samples were taken from the tensile dumbbell test. The samples were frozen in liquid nitrogen and fractured. The dispersed rubber phase was extracted using toluene for 120 h and stirred at room temperature. The dry samples were coated with gold. Jeol (JSM-6510LV) scanning electron microscopy was used and operated at 15 kV.

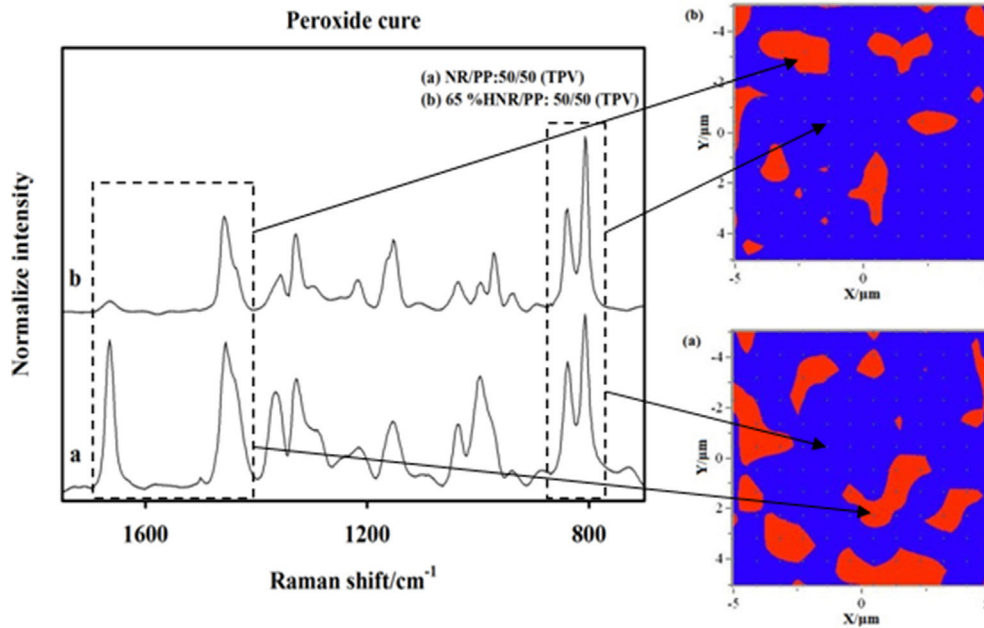


Fig. 3. Raman spectrum and Raman mapping of TPVs (peroxide cure) based on (a) NR/PP, (b) 65%*HNR*/PP. All containing 50 wt% rubbers, Raman mapping: PP phase (blue) and rubber phase (red). (For interpretation of the references to colour in this figure legend, the reader is referred to the web version of this article.)

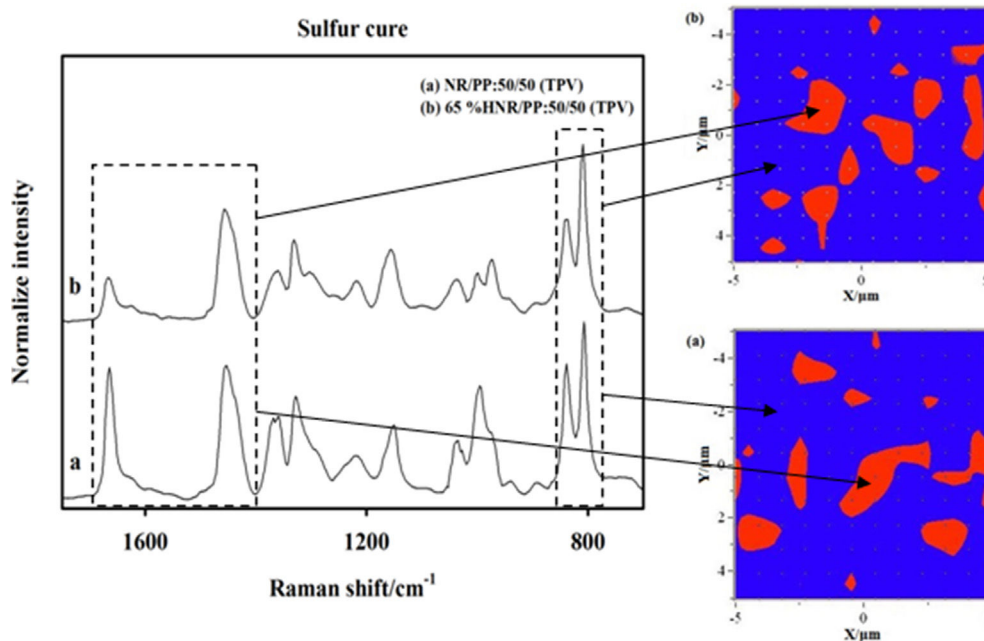


Fig. 4. Raman spectrum and Raman mapping of TPVs (sulfur cure) based on (a) NR/PP, (b) 65%*HNR*/PP. All containing 50 wt% rubbers, Raman mapping: PP phase (blue) and rubber phase (red). (For interpretation of the references to colour in this figure legend, the reader is referred to the web version of this article.)

2.5. Phase size analysis

The phase sizes of cross-linked rubber phase dispersed in the thermoplastic vulcanizates (TPVs) were calculated by using Raman mapping and compared with scanning electron microscopy. For Raman mapping, ImageJ software (Open source image processing program designed for scientific multidimensional images) was used to calculate the phase size [23,24].

3. Results and discussion

3.1. Raman spectrum of pure polymer

In order to have spectral reference [25–30], it was firstly recorded Raman scattering for the natural rubber (NR), hydrogenated natural rubber (65%HNR), polypropylene (PP, HP500N). Results are exhibited in Fig. 1.

Polypropylene was clearly characterized by Raman spectroscopy. The spectra of PP contain some well-known group frequencies (involving CH₂, CH₃ groups). Fig. 1 shows that polypropylene (PP) was clearly characterized by bands at 813 cm⁻¹ and at 846 cm⁻¹ corresponding to the CH₂ (rocking) and CH₃

(rocking) respectively.

Raman spectra of natural rubber (NR) show in particular the typical band at 1664 cm⁻¹ corresponding to the stretching of the C=C double bond. Logically intensity of this band decreased in the hydrogenated natural rubber (65%HNR). Reversely the scattering at 1334 cm⁻¹, which is attributed to the CH₃ sym bending, and the one at 1452 cm⁻¹ which is CH₂ twisting, increase in the hydrogenated natural rubber (65%HNR).

3.2. Morphology characterization by raman mapping and SEM for 50/50 polymers blends

This part of the study was focused on one type of blend with a content ratio of 50/50. As a consequence of the good knowledge of the reference spectra of pure compounds, the characteristic Raman peaks at 1434–1664 cm⁻¹ for natural rubber (NR) and hydrogenated natural rubber (65%HNR), at 813–846 cm⁻¹ for polypropylene (PP) can be used to identify phase component in their blends as illustrated in Figs. 2–4. By comparison between Fig. 2 and Figs. 3–4, it is evidently observed that the Raman spectra look different between two components of TPEs and TPVs and are identifiable as NR, 65%HNR, and PP phase component in the TPEs and TPVs.

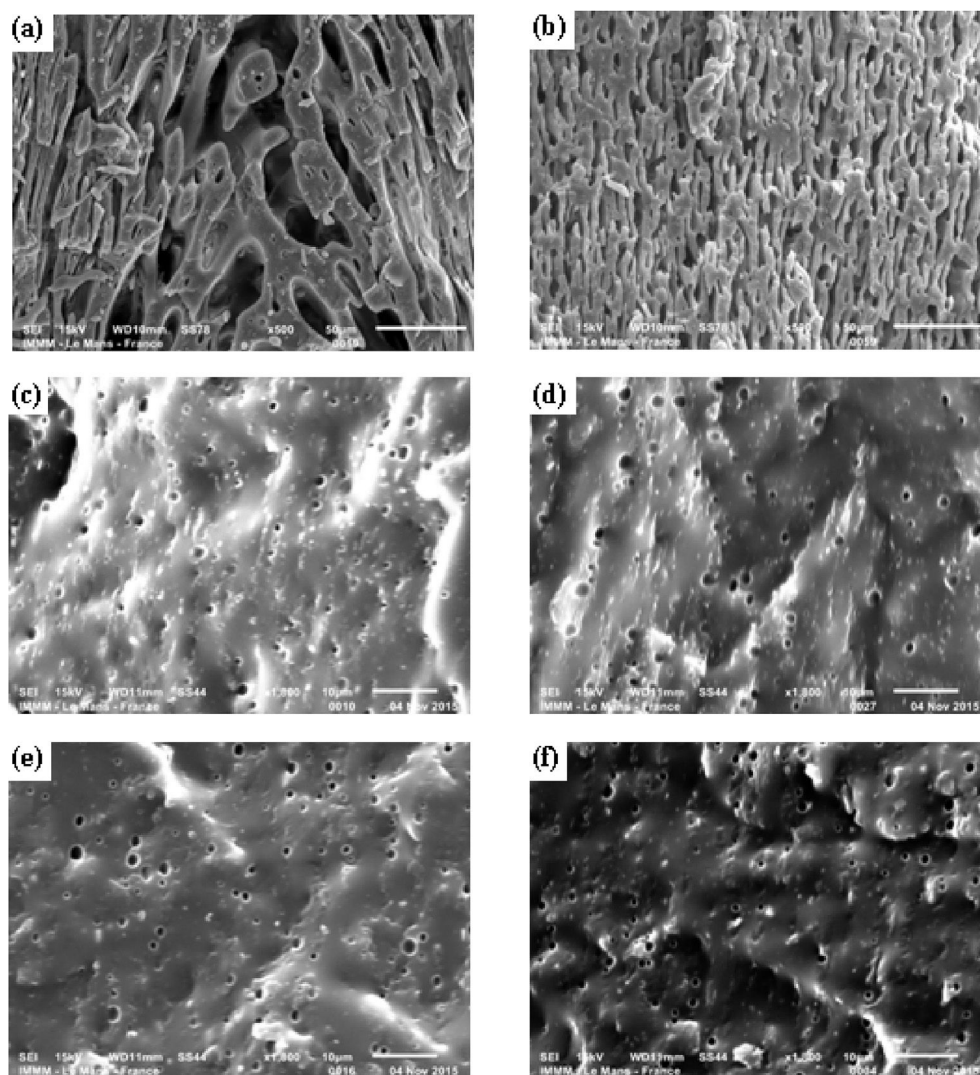


Fig. 5. SEM images of TPEs based on (a) NR/PP, (b) 65%HNR/PP (magnification: 500×) and TPVs based on (c, e) NR/PP, (d, f) 65%HNR/PP (magnification: 1,800×) by peroxide cure [(c), (d)] and sulfur cure [(e), (f)]. All containing 50 wt% rubbers, rubber phase (dark hole).

The Raman mapping of the distribution of the phase component for this typical 50/50 ratio in the TPEs and TPVs is shown in also shown Figs. 2–4 (a,b). The images were built considering the intensities of typical Raman lines of each component, namely: (i) the 813–846 cm^{-1} range (in blue on the figure), which represent characteristic Raman peaks of PP phase, and (ii) at 1434–1664 cm^{-1} (in red in the figure), which represent characteristic Raman peaks of NR or 65%HNR phase, for NR/PP, 65%HNR/PP blends.

From Fig. 2 (a, b), at the surface of these blends, it appears that NR/PP, 65%HNR/PP blends seem to be a continuous rubber phase (red) morphology in the PP matrix (blue) of the thermoplastic elastomers (TPEs). This result is confirmed by using SEM as shown in Fig. 5 (a, b). Actually the morphology of rubber phase (dark hole) seems to be a continuous phase in the PP matrix of thermoplastic elastomers. In this TPEs case, the blend system was nonreactive and phase inversion phenomenon [31] not occurred. Also, after processing in the internal mixing with relatively high mixing intensity, there is no change in the continuous morphology type. The non-cross-linked elastomer phase could be deformed further by the application of shear stresses, but the continuous morphology remains unchanged.

For TPVs of both peroxide and sulfur cure, it was shown that a fine dispersion of cross-linked rubber phase (red) was generated in a continuous matrix of PP (blue), as shown in Figs. 3–4 (a, b). This morphology is also obtained by using SEM, then it was shown that

the cross-linked rubber phase (dark hole) was dispersed in a continuous matrix of PP, as shown in Fig. 5(c–f).

These results can be compared to the work of Furukawa et al. [32] who studied the morphology of polyethylene (PE) and polypropylene (PP) blends by using Raman mapping where they especially investigate the Raman mapping of the metallocene polyethylene (MEPE)/polypropylene (PP) blends and show the dispersion of each component in polymer blends.

In this TPVs case, the cross-linking reaction in the rubber phase is initiated and phase inversion phenomenon was occurred. Harrats et al. [31] studied the morphology transformation during the dynamic vulcanization of polymer blends. It was found that the co-continuous of rubber-thermoplastic blends for TPEs before cross-linked and shows that after phase inversion, the cross-linked rubber dispersed in thermoplastic matrix for TPVs. Thus, the morphology of the TPEs and TPVs were obtained by using Raman spectroscopy, Raman mapping and compared with SEM technique. It is then proved that Raman spectroscopy and Raman mapping could be used to study the morphology of the TPEs and TPVs. Consequently this study was done in fixed conditions for some parameters like temperature, time, etc ... and their effect on the distribution and size of PP and Rubber phases was not investigated. Actually as previously mentioned the main goal of this work was dedicated to the usefulness of the Raman spectroscopy for such blends. Note that the effect of these parameters was previously

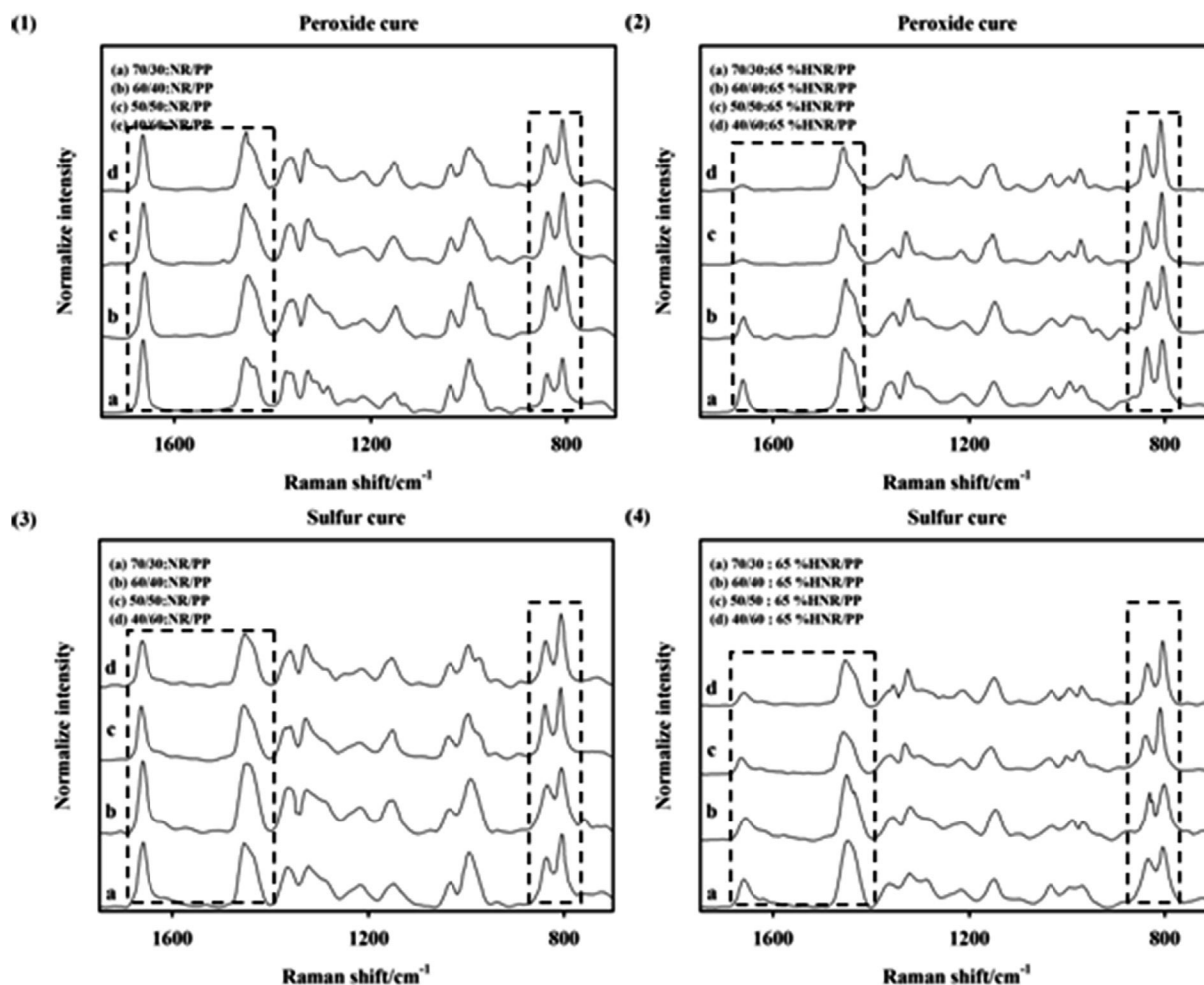


Fig. 6. Raman spectrum of TPVs (peroxide cure) based on (1) NR/PP, (2) 65%HNR/PP and TPVs (sulfur cure) based on (3) NR/PP, (4) 65%HNR/PP. The blends ratio of TPVs at (a) 70/30 (wt/wt%), (b) 60/40 (wt/wt%), (c) 50/50 (wt/wt%), (d) 40/60 (wt/wt%).

reported in vulcanized thermoplastic elastomer recently [33,34].

3.3. Determination of the blends ratio by raman spectroscopy

In addition to the previous study dedicated to one type of blend different ratio contents between NR or 65%HNHR, and PP content in the TPVs of both peroxide cure and sulfur cure were confirmed by using Raman spectra of TPVs. As previously mentioned the content ratio of NR/PP and 65%HNHR/PP blends were calculated using Eq. (1) and Eq. (2). The Raman spectra of NR/PP and 65%HNHR/PP of TPVs are shown in Fig. 6(1–4) and Raman mapping in Figs. 7–8. It was found that the increase in the PP content and the increase in the rubber content in the TPVs led respectively to an increase in the scattering at $813\text{--}846\text{ cm}^{-1}$ for PP and an increase in the absorption at $1434\text{--}1664\text{ cm}^{-1}$ for natural rubber (NR) and hydrogenated natural rubber (65%HNHR) in their blends. As a comparison of content ratio (Table 2) between calculations method and Raman spectra, it was established that Raman spectroscopy can be used as a reference method to calculate the content ratio in their blends. The nominal concentrations are then fully confirmed.

3.4. Phase size analysis by raman mapping and SEM method

The phase size of cross-linked rubber phase dispersed in matrix PP phase of both peroxide cure and sulfur cure in TPVs was calculated by using Raman mapping method and compared with SEM method. The range size for phase diameter in cross-linked rubbers was estimated from $0.32\text{--}3.64\text{ }\mu\text{m}$ by using Raman mapping method and $0.35\text{--}1.29\text{ }\mu\text{m}$ diameter by using SEM method. As also noticed by Markwort and Kip [9] who studied the morphology of three other ternary polymer blends by confocal laser line scanning Raman imaging technique, it is found that the heterogeneities in composition and morphology are on a rather large scale equal to or larger than $1\text{ }\mu\text{m}$. In most cases, fully cross-linked rubbers of $0.5\text{--}3.0\text{ }\mu\text{m}$ diameter were dispersed in thermoplastic matrix. Moreover, the phase size was obtained by using Raman mapping

method and SEM method. It was shown a linear data correlation between both methods with a correlation coefficient value (R^2) within the range $0.93\text{--}0.97$. Thus, Raman mapping could be used to calculate the phase size of cross-linked rubber phase dispersed in matrix PP phase in TPVs. The difference of maximum phase size of cross-linked rubber phase in TPVs was calculated by using Raman mapping method and SEM method, it may be due to (1) the selection of position test on the samples test, (2) cross-linked rubber phase dispersed in the TPVs could not be control and it's random to disperse in PP matrix of TPVs and (3) the effect of sample preparation for testing, in which the Raman mapping method did not sample preparation. For SEM method, the samples were frozen in liquid nitrogen and fractured, and the dispersed cross-linked rubber phase was extracted.

4. Conclusion

Raman spectroscopy and especially mapping configuration appear to be a powerful technique for the characterization and the study of morphology of polymer blends. The Raman spectra of two components in the blends were identifiable as NR, 65%HNHR, PP

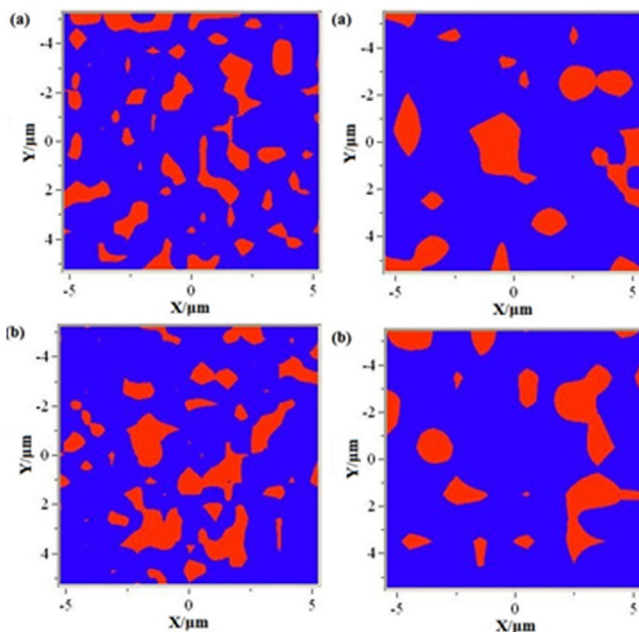


Fig. 7. Raman mapping of the blends ratio at 70/30 (wt/wt%) (Left column), at 40/60 (wt/wt%) (Right column) of TPVs (peroxide cure) based on (a) NR/PP, (b) 65%HNHR/PP: [PP phase (blue), rubber phase (red)]. (For interpretation of the references to colour in this figure legend, the reader is referred to the web version of this article.)

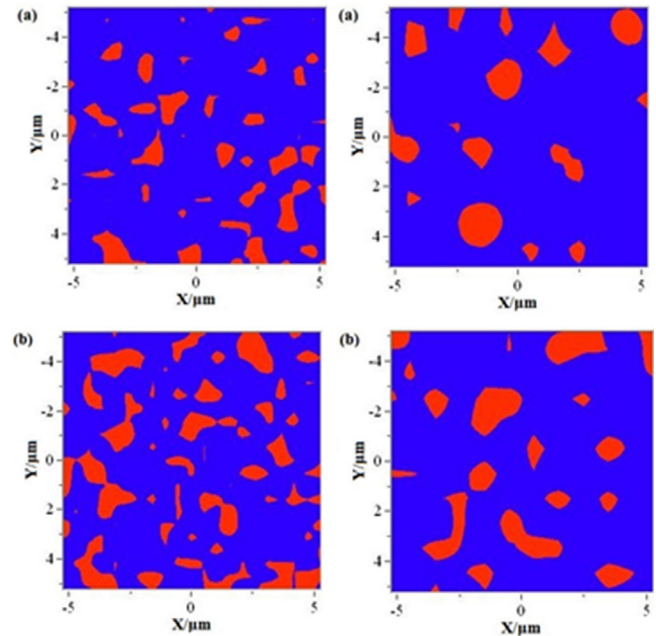


Fig. 8. Raman mapping of the blends ratio at 70/30 (wt/wt%) (Left column), at 40/60 (wt/wt%) (Right column) of TPVs (sulfur cure) based on (a) NR/PP, (b) 65%HNHR/PP: [PP phase (blue), rubber phase (red)]. (For interpretation of the references to colour in this figure legend, the reader is referred to the web version of this article.)

Table 2

Content ratio of TPVs based on NR/PP, 65%HNHR/PP blends.

Samples	Calculated content ratio (wt/wt%)		Experimental content ratio obtained with Raman data (%)	
	Peroxide cure	Sulfur cure	Peroxide cure	Sulfur cure
NR/PP	70/30	70/30	72/28	69/31
	60/40	60/40	64/36	64/36
	50/50	50/50	52/48	51/49
	40/60	40/60	44/56	41/59
65%HNHR/PP	70/30	70/30	69/31	72/28
	60/40	60/40	59/41	64/36
	50/50	50/50	48/52	51/49
	40/60	40/60	39/61	42/58

phase component. Due to the contrast between two components in each blends, the blends compositions in the thermoplastic elastomers (TPEs) and thermoplastic vulcanizates (TPVs) could be determined. Raman mapping was shown that the phase morphology of NR/PP, 65%HNBR/PP, were characterized as continuous rubber phase morphology of the thermoplastic elastomers (TPEs) and a fine dispersion of cross-linked rubber phase in a continuous matrix of the thermoplastic vulcanizates (TPVs). The morphology of TPEs and TPVs obtained by Raman spectroscopy, were compared with SEM with consistent results. Additionally a comparison between nominal content ratio and calculated ratio using Raman are fully consistent and shows that this vibrational spectroscopy could be used to calculate the content ratio in the TPVs. Moreover, Raman mapping could be used to calculate the phase size of cross-linked rubber phase dispersed in thermoplastic vulcanizates (TPVs).

References

- [1] F.R. Costa, N.K. Dutta, N.R. Choudhury, A.K. Bhowmick, *Current Topics in Elastomers Research: Chapter 5-thermoplastic Elastomers*, CRC Press, 2008.
- [2] L.R. Lewis, H.G.M. Edwards, *Handbook of Raman Spectroscopy: from the Research Laboratory to the Process Line*, CRC Press, 2001.
- [3] J.M. Chalmers, R.J. Meier, *Molecular Characterization and Analysis of Polymers*, Elsevier, 2008.
- [4] Y.J. Lee, D. Moon, B.K. Migler, M.T. Cicerone, Quantitative image analysis of broadband CARS hyperspectral images of polymer blends, *Anal. Chem.* 83 (7) (2011) 2733–2739.
- [5] W. Smitthipong, R. Gadiou, L. Vidal, P. Wagner, M. Nardin, 3D Raman images of rubber blends (IR-HNBR), *Vib. Spectrosc.* 46 (1) (2008) 8–13.
- [6] S. Huan, W. Lin, H. Sato, H. Yang, J. Jiang, Y. Ozaki, H. Wu, G. Shen, R. Yu, Direct characterization of phase behavior and compatibility in PET/HDPE polymer blends by confocal Raman mapping, *J. Raman Spectrosc.* 38 (3) (2007) 260–270.
- [7] P. Schmidt, J. Dybal, J. Scudla, M. Raab, J. Kratochvil, Structure of polypropylene/polyethylene blends assessed by polarised PA-FTIR spectroscopy, polarised FT Raman spectroscopy and confocal Raman microscopy, *Macromol. Symp.* 184 (2002) 107–122.
- [8] H.R. Morris, J.F. Turner, B. Munro, R.A. Ryntz, P.J. Treado, Chemical imaging of thermoplastic olefin (TPO) surface architecture, *Langmuir* 15 (1999) 2961–2972.
- [9] L. Markwort, B. Kip, Micro-Raman imaging of heterogeneous polymer systems: General applications and limitations, *J. Appl. Polym. Sci.* 61 (2) (1996) 231–254.
- [10] M. Pastorczyk, M. Wiatrowski, M. Lodzinski, U. Ulanski, Confocal Raman microscopy in 3-dimensional shape and composition determination of heterogeneous systems, *J. Mol. Struct.* 744 (SI) (2005) 997–1003.
- [11] M. Khalil, P. Hébraud, A. Mcheik, H. Mortada, H. Lakis, T. Hamieh, Elongational flow-induced crystallization in polypropylene/talc nanocomposites, *Phys. Procedia* 55 (2014) 259–264.
- [12] M. Yousfi, S. Livi, J. Duchet-Rumeau, Ionic Liq. A new way Compat. Thermoplast. blends, 255, 2014, pp. 513–524.
- [13] M. Yousfi, S. Livi, A. Dumas, J. Crepin-Leblond, M. Greenhill-Hooper, J. Duchet-Rumeau, Compatibilization of polypropylene/polyamide 6 blends using new synthetic nanosized talc fillers: morphology, thermal, and mechanical properties, *J. Appl. Polym. Sci.* 131 (13) (2014), <http://dx.doi.org/10.1002/app.40453>.
- [14] B. Fiorentino, R. Fulchiron, V. Bounor-Legare, J.C. Majeste, J.C. Leblond, J. Duchet-Rumeau, Chemical modification routes of synthetic talc: Influence on its nucleating power and on its dispersion state, *Appl. Clay Sci.* 109 (2015) 107–118.
- [15] C.Z. Liao, H.M. Wong, K.W.K. Yeung, S.C. Tjong, The development, fabrication, and material characterization of polypropylene composites reinforced with carbon nanofiber and hydroxyapatite nanorod hybrid fillers, *Int. J. Nanomedicine* 9 (2014) 1299–1310, <http://dx.doi.org/10.2147/IJN.S58332>.
- [16] Z. Lin, Z. Guan, Z. Zhang, K. Mai, The effect of thermal history of polyamide 6 on the crystallization and melting behavior of beta-nucleated polypropylene/polyamide 6 blends, *Thermochim. Acta* 543 (2012) 59–65, <http://dx.doi.org/10.1016/j.tca.2012.05.003>.
- [17] Y. Chen, C. Xu, L. Cao, Y. Wang, X. Cao, PP/EPDM-based dynamically vulcanized thermoplastic olefin with zinc dimethacrylate: Preparation, rheology, morphology, crystallization and mechanical properties, *Polym. Test.* 31 (6) (2012) 728–736, <http://dx.doi.org/10.1016/j.polymertesting.2012.05.010>.
- [18] E.G. Bajsic, V.O. Bulatovic, V. Rek, The influence of filler treatment on the properties of TPU/PP Blends: I. Thermal properties and stability, *Polym. Eng. Sci.* 55 (8) (2015) 1920–1930, <http://dx.doi.org/10.1002/pen.24033>.
- [19] B. Wunderlich, *B. Macromolecular Physics*, vol. 3, Academic Press, New York, 1980, p. 63.
- [20] L. Mandelkern, R. Alamo, *Thermodynamic quantities governing melting*, in: J.E. Mark (Ed.), *Physical Properties of Polymer Handbook*, second ed., Springer, New York, 2007, pp. 165–186.
- [21] G.Y. Liu, G.X. Qiu, Study on the mechanical and morphological properties of toughened polypropylene blends for automobile bumpers, *Polym. Bull.* 70 (3) (2013) 849–857, <http://dx.doi.org/10.1007/s00289-012-0880-1>.
- [22] H. Salmah, B.N. Azra, M.D. Yusrina, H. Ismail, A comparative study of polypropylene/(chloroprene rubber) and (recycled polypropylene)/(chloroprene rubber) blends, *J. Vinyl Addit. Technol.* 21 (2) (2015) 122–127, <http://dx.doi.org/10.1002/vnl.21390>.
- [23] C. Igathinathane, L.O. Pordesimo, E.P. Columbus, W.D. Batchelor, S.R. Methuku, J. Shape identification and particles size distribution from basic shape parameters using Image, *Comput. Electron. Agric.* 63 (2) (2008) 168–182.
- [24] D. Greaves, J. Boxall, J. Mulligan, A. Montesi, J. Creek, E.D. Sloan, C.A. Koh, Measuring the particle size of a known distribution using the focused beam reflectance measurement technique, *Chem. Engineering Sci.* 63 (22) (2008) 5410–5419.
- [25] E. Andreassen, *Polypropylene: An A-Z*, Kluwer Publishers, Dordrecht, 1999.
- [26] P.J. Hendra, K.D.O. Jackson, Applications of Raman-spectroscopy to the analysis of natural-rubber, *Spectrochim. Acta* 50 (11) (1994) 1987–1997.
- [27] A.M. Healey, P.J. Hendra, Y.D. West, A Fourier-transform Raman study of the strain-induced crystallization and cold crystallization of natural rubber, *Polymer* 30 (18) (1996) 4009–4024.
- [28] K.D.O. Jackson, M.J.R. Loadman, C.H. Jones, G. Ellis, Fourier-transform Raman spectroscopy of elastomers - an overview, *Spectrochim. Acta* 64 (2) (1990) 217–226.
- [29] S.J. Bunce, H.G.M. Edwards, A.F. Johnson, I.R. Lewis, P.H. Turner, Synthetic polyisoprenes studies by Fourier-transform Raman-spectroscopy, *Spectrochim. Acta* 49 (5–6) (1993) 775–783.
- [30] J. Samran, P. Phinyocheep, P. Daniel, D. Derouet, J.Y. Buzare, Raman spectroscopic study of non-catalytic hydrogenation of unsaturated rubbers, *J. Raman Spectrosc.* 35 (12) (2004) 1073–1080.
- [31] C. Harrats, S. Thomas, G. Groeninckx, H.J. Radusch, Phase Morphology of Dynamically Vulcanized Thermoplastic Vulcanizates. Micro-and Nanostructured Multiphase Polymer Blend Systems: Phase Morphology and Interfaces, CRC Press, 2005.
- [32] T. Furukawa, H. Sato, Y. Kita, K. Matsukawa, H. Yamaguchi, S. Ochiai, H.W. Siesler, Y. Ozaki, Molecular structure, crystallinity and morphology of polyethylene/polypropylene blends studied by Raman mapping, scanning electron microscopy, wide angle X-Ray diffraction, and differential scanning calorimetry, *Polym. J.* 38 (2006) 1127–1136.
- [33] S. Shahbikian, P.J. Plasticization and morphology development in dynamically vulcanized thermoplastic elastomers (Chapter 3), in: C.K. Das (Ed.), *Thermoplastic Elastomers – Synthesis and Applications*, Intech, 2015, p. 2015.
- [34] H. Wu, M. Tian, L. Zhang, H. Tian, Y. Wu, N. Ning, T.W. Chan, New understanding of morphology evolution of thermoplastic vulcanizate (TPV) during dynamic vulcanization, *ACS Sustain. Chem. Eng.* 3 (1) (2015) 26–32, <http://dx.doi.org/10.1021/sc500391g>.

APPENDICES

APPENDIX C

Curriculum Vitae

Mr. Korn Taksapattanakul

Student ID: 5520330101

Tel.: +669-18472196

E-mail: kornpolymer@gmail.com

**1. Education Background:**

- **Bachelor of Science: Physics (second class honors) (2005 – 2009)**
 - Division of Physics, Department of Science, Faculty of Science and Technology, Prince of Songkla University, Pattani, Thailand
 - GPA: 3.35
 - Thesis: Mechanical property of EPDM/PP blend carbon fibers reinforced
Advisor: Mr. Somchai Kopoonpat
- **Master of Science: Polymer Physics (2009 – 2011)**
 - Division of Physics, Department of Science, Faculty of Science and Technology Prince of Songkla University, Pattani, Thailand
 - GPA: 3.51
 - Thesis: Compression properties of natural rubber – asphalt – aggregated blends
Advisor: Associate Professor Dr. Sombat Puttajukr
Co-advisor: Assistant Professor Dr. Thoranit Navarat

2. Scholarships and Prize:

- Human resource development in science project (Science Achievement Scholarship of Thailand, SAST) (B.Sc, M.Sc. – Ph.D.)
- Highest mark in Physics, Science, Prince of Songkla University, by Prof. Dr. TAB Foundation, 2009.
- The financial support from Prince of Songkla University graduate thesis grant for Ph.D. research.

3. Apprenticeship:

- March-May, 2008, Apprentice in R&D section, The National Metal and Materials Technology Center (MTEC), National Science and Technology Development Agency (NSTDA), Pathum Thani, Thailand

4. List of Presentations:

- Chelae, F., and Kopoonpat, S. “Mechanical property of EPDM/PP Blend carbon fibers reinforced”, The 4th Conference on Science and Technology for Youth, Bangkok international trade and exhibition centre, Bangkok, Thailand on 20 – 21 March 2009. (Oral presentation)
- Chelae, F., Puttajukr, S., and Navarat, T. “Compression Properties of Natural Rubber – Asphalt - Aggregate blends”, The 6th Conference on Science and Technology for Youth, Bangkok international trade and exhibition centre, Bangkok, Thailand on 18 – 19 March 2011. (Oral presentation)
- Taksapattanakul, K., Tulyapitak, T., Phinyocheep, P., and Ruamcharoen, P. “*In situ* Hydrogenation of Natural Rubber from Oxidation, Reaction of Hydrazine Monohydrate ($N_2H_4 \cdot H_2O$) by Hydrogen Peroxide (H_2O_2)”, The 8th Conference on Science and Technology for Youth, Bangkok international trade and exhibition centre, Bangkok, Thailand on 22 – 23 March 2013. (Oral presentation)
- Taksapattanakul, K., Tulyapitak, T., Phinyocheep, P., Ruamcharoen, P., Ruamcharoen, J., and Daniel, P. “Hydrogenated natural rubber (HNR) as a potential replacement for ethylene – propylene – diene – monomer (EPDM) rubber”, The 6th Sci-Tech Grad Symposium 2016, Faculty of Science and Technology, Prince of Songkla University. Pattani, Thailand, on 23 May 2016. (Oral presentation)
- Korn Taksapattanakul, Tulyapong Tulyapitak, Pranee Phinyocheep, Polphat Ruamcharoen, Jareerat Ruamcharoen and Phillippe Daniel. “Rheological properties of hydrogenated natural rubber”, The International Rubber Conference 2016, Kitakyushu, Japan on 24-28 October 2016. (Oral presentation)

5. List of Publications:

- Chelae, F., Puttajukr, S., and Navarat, T. 2011. Compression Properties of Natural Rubber – Asphalt – Aggregate blends. The Proceedings of the 6th Conference on Science and Technology for Youths: 2011. 132 – 142.
- Taksapattanakul, K., Tulyapitak, T., Phinyocheep, P., and Ruamcharoen, P. 2013. *In situ* Hydrogenation of Natural Rubber from Oxidation, Reaction of Hydrazine Monohydrate ($N_2H_4 \cdot H_2O$) by Hydrogen Peroxide (H_2O_2). The Proceedings of the 8th Conference on Science and Technology for Youths: 2013. 94 – 102.
- Korn Taksapattanakul, Tulyapong Tulyapitak, Pranee Phinyocheep, Polphat Ruamcharoen, Jareerat Ruamcharoen and Phillippe Daniel. Rheological properties of hydrogenated natural rubber. The proceedings of IRC 2016 Kitakyushu, Japan
- Korn Taksapattanakul, Tulyapong Tulyapitak, Pranee Phinyocheep, Polphat Ruamcharoen, Jareerat Ruamcharoen, Fabienne Lagarde, Mathieu Edely, Philippe Daniel. Raman investigation of thermoplastic vulcanizates based on hydrogenated natural rubber/polypropylene blends. Polymer Testing, Volume 57, February 2017, Pages 107–114.

6. Extra-curricular activities:

- The 4th Human Resource Development in Science Project (Science Achievement Scholarship of Thailand ,SAST) of Science Camp, 23-25 October 2008, Faculty of Science, Mahidol University, Thailand
- The 4th Conference on Science and Technology for Youth, Bangkok international trade and exhibition centre, Bangkok, Thailand, on 20 – 21 March 2009
- The 6th Conference on Science and Technology for Youth, Bangkok international trade and exhibition centre, Bangkok, Thailand, on 18 – 19 March 2011

- The 1st Human Resource Development in Science Project (Science Achievement Scholarship of Thailand ,SAST) of Graduate Camp, 16-17 May 2013, Asia Hotel, Phayathai Road Ratchathewi, Bangkok, Thailand
- The 8th Conference on Science and Technology for Youth, Bangkok international trade and exhibition centre, Bangkok, Thailand, on 22 – 23 March 2013
- The 6th Sci-Tech Grad Symposium 2016, Faculty of Science and Technology, Prince of Songkla University. Pattani, Thailand, on 23May 2016
- Taksapattanakul, K., Tulyapitak, T., Phinyocheep, P., Ruamcharoen, P., Ruamcharoen, J., and Daniel, P. “Hydrogenated natural rubber (HNR) as a potential replacement for ethylene – propylene – diene – monomer (EPDM) rubber”, TechnoBiz Communications Co., Ltd. (TechnoBiz) and China United Rubber Corporation (CURC) jointly organizing 3rd Edition of GRTE 2016 - Global Rubber, Latex & Tire Expo 2016 during 9-11 March 2016 at Bangkok International Trade & Exhibition Center (BITEC) in Bangkok, Thailand. (Poster Presentation)

Thèse de Doctorat

korn TAKSAPATTANAKUL

Etude et caractérisation de thermoplastiques vulcanisés à base de caoutchouc naturel hydrogéné et de polypropylène Thermoplastic Vulcanizates Based on Hydrogenated Natural Rubber/Polypropylene Blends

Résumé

L'préparation du caoutchouc naturel hydrogéné (HNR) par réaction avec l'hydrazine et le peroxyde d'hydrogène et le latex de caoutchouc naturel a été intéressée. L'influence de conditions de réaction, types et volume de solvants, volume du réactionnel, l'quantité d'hydrazine et de peroxyde d'hydrogène sur le degré d'hydrogénation du caoutchouc naturel a été étudiée. Le structure et détermination du degré d'hydrogénation des caoutchoucs naturel hydrogénés a été analysée par résonance magnétique nucléaire (RMN), transformée de fourier infrarouge (FTIR) et spectroscopie Raman. Un degré d'hydrogénation de 18 % a été obtenu à 1.0 - 2.0 du la molaire de d'hydrazine et de peroxyde d'hydrogène, température optimale de 50°C et le temps de réaction de 24h. Afin d'améliorer le degré d'hydrogénation, des solvants tels que le toluène et le hexane et l'effet de le volume du réactionnel ont été étudiée, ce qui a permis d'obtenir des degrés d'hydrogénation élevés (proches de 65% avec le toluène). D'autre part, des mesures de tailles de particules de latex ont montré que l'hydrogénation du caoutchouc naturel n'avait pas d'effet sur latex de caoutchouc naturel. Un résultat également intéressant concerne le détermination du taux de gel. Ce gel augmente avec le degré d'hydrogénation, prouvant que des réactions de réticulation ont eu lieu. Néanmoins aucun effet de degré d'hydrogénation sur le température de transition vitreuse n'est détecté. L'dureté et viscosités Mooney augmentent, en lien avec l'augmentation du taux de gel. Par ailleurs, l'résistance thermique du caoutchouc naturel hydrogéné est considérablement améliorée lorsque le degré d'hydrogénation augmente. Le partie suivante est consacrée à l'vulcanisation du caoutchouc. Deux types de réticulation ont été utilisés : au soufre et au peroxyde. Les élastomères HNR réticulés montrent une meilleure résistance à l'ozone et l'UV que le NR réticulé. De plus, cette résistance à l'ozone et l'UV est plus élevée pour le réticulation au soufre, comparée à le réticulation au peroxyde. Une bonne corrélation entre les images de microscopie optique et les résultats des analyses Raman est obtenue. L'préparation et l'étude de mélanges HNR/PP obtenus par vulcanisation dynamique en utilisant du peroxyde et du soufre comme agents de réticulation. Un degré d'hydrogénation de 65% a été choisi, et différentes ratio HNR/PP ont été étudiés, et comparés avec des mélanges NR/PP. L'morphologie des mélanges a été caractérisée par spectroscopie Raman, ce qui a permis d'obtenir des images cartographie Raman indiquant de façon précise le localisation et l'distribution des phases de caoutchouc et de PP. Une bonne corrélation entre le cartographie Raman et les images de microscopie électronique à balayage (SEM) est obtenue. Ainsi il apparaît que les particules de caoutchouc sont dispersées dans une phase continue de PP, ceci à la fois pour le HNR et le NR. L'étude des propriétés mécaniques a montré que celles-ci étaient gouvernées principalement par la phase continue de PP.

Mots clés

Non-catalytique l'hydrogénation, caoutchouc naturel hydrogéné, spectroscopie Raman, thermoplastiques vulcanisés

Abstract

The non-catalytic hydrogenation of natural rubber latex (NRL) was carried out by using diimide generated *in situ* from the reaction between hydrazine (N_2H_4) and hydrogen peroxide (H_2O_2). The effects of mole ratios of $[C=C]:[N_2H_4]:[H_2O_2]$, reaction conditions, solvent types, solvent volumes and reaction scale-up on the hydrogenation levels were investigated. Nuclear magnetic resonance (NMR), Fourier transform infrared (FTIR), and Raman spectroscopic techniques were employed to investigate the chemical structure of the hydrogenated natural rubber (HNRs) and to quantify the hydrogenation levels. It was found that variations in moles of N_2H_4 and H_2O_2 in the range of 1.0-2.0 moles resulted in degrees of hydrogenation in the range of 10-18%. Little improvement in hydrogenation levels of HNRs was obtained when NRL particles were swollen in solvents by which toluene yielded better results than hexane. The increase in toluene volume resulted in the increase in hydrogenation levels up to 42%. TEM micrographs revealed that swelling mainly occurred at the surface of NRL particles, implying that hydrogenation reaction confined largely at the surface of NRL particles. After removal of toluene, particle size and particle size distribution of partially hydrogenated NRL remained unchanged. To further improve degrees of hydrogenation, the reaction volume was extended and 65% hydrogenation levels were obtained. Therefore, 14%HNR, 33%HNR, and 65%HNR were successfully prepared under suitable reaction conditions. However, crosslinking and *cis-trans* isomerization were side-reactions occurring during hydrogenation. Gel and *trans* contents increased with increasing hydrogenation levels, leading to the increase in hardness of HNRs. Mooney viscosities of HNRs increased with increasing degrees of hydrogenation due to the increased gel contents. Mooney torque relaxation of NR and HNRs were similar. Thermogravimetric analysis revealed that HNRs had greater thermal stability than NR and thermal stability increased with increasing degrees of hydrogenation. HNR vulcanizates were much better resistant to ozone and UV than cured NR. Sulfur-vulcanized rubbers had greater ozone resistance than peroxide-cure rubbers due to less amounts of carbon-carbon double bonds present in rubbers. In addition, modulus at low strain and tensile strength of sulfur-cured rubbers were higher than those of peroxide-cured rubbers, but lower elongation due to higher crosslink densities. Also, modulus at low strain and tensile strength increased with increasing hydrogenation levels of HNRs, in contrast to strain at break. Thermoplastic vulcanizates (TPVs) from blends of HNR and Polypropylene (PP) were prepared via dynamic vulcanization using peroxide and sulfur as curing agents. The effects of blend ratios on mechanical properties of TPVs were investigated. Tensile strength increased with increasing PP portions, but breaking strain decreased. Morphology of TPVs was characterized with Raman mapping and scanning electron microscope (SEM). The phase sizes of crosslinked rubber obtained from both techniques were correlated well.

Key Words

Non-catalytic hydrogenation, Hydrogenated natural rubber, Raman spectroscopy, Thermoplastic vulcanizates